DFT modelling of Methane Oxidation with H_2O_2 over Heterogeneous Catalysts

Adam Thetford

Thesis submitted for the Degree of PhD

September 2012

Acknowledgments

I would like to thank my supervisor, Dr David J. Willock for his support with my research and my scientific development. I would also like to thank Graham J. Hutchings and the members of the Dow methane challenge.

I would like to like thank Kara and people I know in office 1.95.

I would to thank my parents for their continuing support.

I would like to thank the Materials Chemistry Consortium for the time of the Hector supercomputer and ACCRA for use of the Merlin cluster and support with use and problems with it.

Finally, I would like to thanks Dow and the EPRSC for funding for my PhD.

Papers published

Direct catalytic conversion of methane to methanol in an aqueous medium by using copper-promoted Fe-ZSM-5, *Angewandte Chemie International ed*., 2012, **50**, 5129.

The decomposition of H_2O_2 over the components of Au/TiO2 catalysts, *Proceedings of the Royal Society A: Mathematical, Physical and Engineering Sciences*, 2011, **467,** 1885.

Involvement of Surface-Bound Radicals in the Oxidation of Toluene Using Supported Au-Pd Nanoparticles, *Angewandte Chemie International Edition*, 51, **2012**, 5981

Catalytic and Mechanistic Insights of the Low-Temperature Selective Oxidation of Methane over Cu-Promoted Fe-ZSM-5, *Chemistry - A European Journal*, 18, **2012**, 15735

DECLARATION

This work has not been submitted in substance for any other degree or award at this or any other university or place of learning, nor is being submitted concurrently in candidature for any degree or other award.

Signed …… (candidate)

Date ……

STATEMENT 1

This thesis is being submitted in fulfilment of the requirements for the degree of PhD

Signed …… (candidate)

Date ……

STATEMENT 2

This thesis is the result of my own independent work/investigation, except where otherwise stated.

Other sources are acknowledged by explicit references. The views expressed are my own.

Signed …… (candidate)

Date ……

STATEMENT 3

I hereby give consent for my thesis, if accepted, to be available for photocopying and for inter-library loan, and for the title and summary to be made available to outside organisations.

Signed …… (candidate)

Date ……

Table of Contents

Summary

DFT methods were used to study the mechanism of methane oxidation using H_2O_2 over a TiO_2 supported Au and Fe-ZSM-5 catalyst to produce CH_3OH. DFT+U was employed to improve the model of the oxide surface, framework and framework metal centre in CHA and MFI structures. The catalysts were modelled in VASP. Au_{10} clusters were used to produce a preliminary mechanism, which was tested on the different design catalysts. The Au_{10} clusters were supported on TiO_2 to model small clusters and extended Au, Pd and PdO surfaces were used to model larger clusters. The mechanism is tested on $[Fe_2O_2]^{2+}$ which is in the zeolite extra-framework in both the CHA structure and MFI structure with two Al ions in the framework as counter ions. H_2O_2 is found to spontaneously break the HO – OH bond in the presence of Au_{10} clusters, Au(111) surface and Pd(111) surface. CH_3OOH is produced via OOH formed from H_2O_2 and a radical methyl on the Au(111) and Pd(111) surfaces. Fe_2O_2 as an extra-framework species is modified with water to produce an active site. The active site was then further modified with H_2O_2 to produce a $Fe^{4+} = O$ which is used to break a C – H bond in methane. The mechanism on the metal/oxide was shown to differ from the mechanism in the zeolite. The formation of the C – O bond in CH_3OOH is the most important step on the metal/oxide whereas this is low energy or spontaneous in the zeolite. CH_4 directly producing CH_3OOH has a barrier of 50 kJ mol^{-1} on the modified Fe_2O_2 in the Al-MFI structure.

1. Introduction

This thesis will focus on DFT modelling of methane oxidation to methanol, using hydrogen peroxide as an oxidant. This reaction is done in the presence of two catalysts: Au and Pd supported on TiO_2 and Fe-ZSM-5, which are both modelled with VASP.

The aim of this thesis is to investigate the mechanism for methane and H_2O_2 interactions with the catalysts to produce methanol. The mechanism is investigated by finding a series structures of both the catalysts and the reactants interacting with the catalysts and locating the barriers and transition states between each minimum. This involved the interactions of H_2O_2 and CH_4 with a catalyst to produce CH_3OH.

$$CH_4 + H_2O_2 \xrightarrow{\text{catalyst}} CH_3OH + H_2O$$

This reaction using a Au/TiO_2 catalyst has been shown to produce CH_3OH in aqueous conditions at a low temperature (70°C). However as the products are produced on the surface of the catalysts mechanistic information is difficult to obtain from experimental results, other than products made during the reaction that move into the liquid phase and how different conditions affect the reaction. This is where this work is used by producing a model for the catalyst which can be compared to experiment work.

The decomposition of H_2O_2 is important to reaction as in the experimental work H_2O_2 is required to produce CH_3OH. There are two possible initial steps for the decomposition: HO – OH bond breaking and HOO – H bond breaking, with the latter predicted to be the active species for this reaction.

Methane has to have a C – H bond broken but this is normally considered to occur at higher temperatures so to break the C – H bond at low temperatures, a low energy barrier will be required to identify the active site on the catalyst.

The modelling results of this thesis have been compared to experimental results from the group of Professor Graham Hutchings as part of the DOW methane challenge, STEM results from the group of Dr. Chris Kiely as part of the same project and

EXAFS results from within DOW. The experimental work discussed in thesis was performed by Ceri Hammond, Michael M. Forde and Mohd Hasbi Ab Rahim with the first two doing the experimental work in Chapter 6 and the last the experimental work in Chapters 4 and 5. Comparing the experimental and modelling result should allow for identification of an active site to be made and a mechanism to be produced.

The Au cluster models are mainly compared to the ADF-STEM results for size, shape and composition of the cluster. The Fe-ZSM-5 models are compared to the EXAFS result for the co-ordination of the Fe and Al centres in the zeolite. The reactor results show the intermediates that are present in the reaction and therefore indicate a possible path for the reaction.

2. Literature Review

This thesis focuses on methane activation and oxidation to methanol via H_2O_2. The mechanism of the reaction for the oxidation of methane is studied on Au supported on TiO_2 and in zeolites with MFI (Mordenite framework inverted) and CHA (Chabazite) structures used. This is compared to experimental work done by the group of Professor G.J. Hutchings. This literature review will mainly focus on previous computational results and will be separated into three sections: C – H bond activation, catalytic reactions utilising H_2O_2 and Au supported by various metal oxides.

2.1. C – H bond activation

C – H bond activation has been studied extensively but this section will focus on alkanes and especially methane. Three different types of materials are discussed metal and metal oxide surfaces, zeolites and biological Fe containing materials.

A direct synthetic route for the oxidation of methane has long been sought after. Methane oxidation has been traditionally done by the synthetic gas process (syngas i.e. a mixture of H_2 and CO). This produces CO_2 and CO but not methanol or other partially oxidised carbon products. At present the syngas method is the most commercially viable procedure.

In the last 20 years numerous reviews have appeared on methane and alkane oxidation[1–7].

Transfer of a hydrogen atom from an alkane has been achieved on several different metal (M) and metal oxide surfaces. Au, Ng and Liao[8] investigated C – H dissociations on the M(111) which were made from a two layer M_{10} cluster with M = Ru, Os, Rh, Ir, Pd, Pt, Cu, Ag and Au. Their work shows methane poorly binding with all the M(111) clusters but this is to be expected as it is a saturated molecule and also methane has a long M – CH_4 distances indicating only a small interaction with the cluster. The CH_3 binds strongly to the M(111) clusters with the Ru hollow site having the strongest binding energy of -193 kJ mol^{-1} and Ag and Au hollow sites having the weakest binding energies of -40 kJ mol^{-1} and -37 kJ mol^{-1} respectively. The C – H bond dissociation with CH_4 producing CH_3 product and a hydrogen atom

on the Ru and Rh clusters have the lowest activation energies of 60 kJ mol^{-1} and 61 kJ mol^{-1}. Au and Ag have the highest activation energies of 137 kJ mol^{-1} and 149 kJ mol^{-1}, indicating on the cluster methane C – H is easiest on Ru and Rh, which would be expected.

Zhang, Song and Wang[9] investigated dehydrogenation of CH_4 on Rh(111), Rh(110) and Rh(100) surface. They found CH_4 adsorbs over four sites on Rh(111): the top, bridging, fcc and hcp sites with adsorption energies of -12.1 kJ mol^{-1}, -9.7 kJ mol^{-1}, -10.5 kJ mol^{-1} and -10.5 kJ mol^{-1}. CH_3 and a hydrogen atom have a co-adsorption energy of -627.3 kJ mol^{-1} with a barrier of 79.4 kJ mol^{-1} for the hydrogen atom transfer to the surface from CH_4. CH_4 over the Rh(110) surface on a top site has an adsorption energy of -60.4 kJ mol^{-1} and CH_3 and a hydrogen atom have an co-adsorption energy of -694.9 kJ mol^{-1} with a barrier for formation from CH_4 of 67.3 kJ mol^{-1}. CH_4 over the Rh(100) surface has an adsorption energy of -15.9 kJ mol^{-1} and CH_3 and hydrogen atom have an co-adsorption energy of -652.6 kJ mol^{-1} with a barrier for formation from CH_4 of 62.4 kJ mol^{-1}. They conclude that methane dehydrogenation on a Rh(100) surface would be the probable reaction pathway based on the activation energies. The adsorption energy for CH_4 also shows a strong binding with the Rh(110) which is not shown in other systems.

Mayernick and Janik[10] investigated methane oxidation to CO_2. They studied CeO_2 (111), $Pd_xCe_{1-x}O_2$ (111), PdO (100) surfaces and compared to Pd metal surface using a Pd(111) surface. A free energy barrier of 152 kJ mol^{-1} is required on PdO (100) for hydrogen abstraction and to form the radical methyl. All the surfaces show the formation of a methyl radical from homolytic cleavage of a C-H bond from methane with a hydrogen abstraction. This is shown in Figure 2.1. with images of methyl and methane on Pd(111)(d,e,f), CeO_2(111)(a,b,c) and Pd_xCe_1-$_xO_2$(111) (g,h). The result for the methane activation on PdO(100) at 63 kJ mol^{-1} is shown to be better than the barrier on CeO_2 (111) at 178 kJ mol^{-1} and the same barrier on Pd(111) at 86 kJ mol^{-1} but $Pd_xCe_{1-x}O_2$ (111) has a lower barrier at 17 kJ mol^{-1}, which is attributed to the Pd^{4+} in $Pd_xCe_{1-x}O_2$ (111) with only Pd^{2+} in Pd(100). They conclude that the C – H activation is the limiting step for further oxidation.

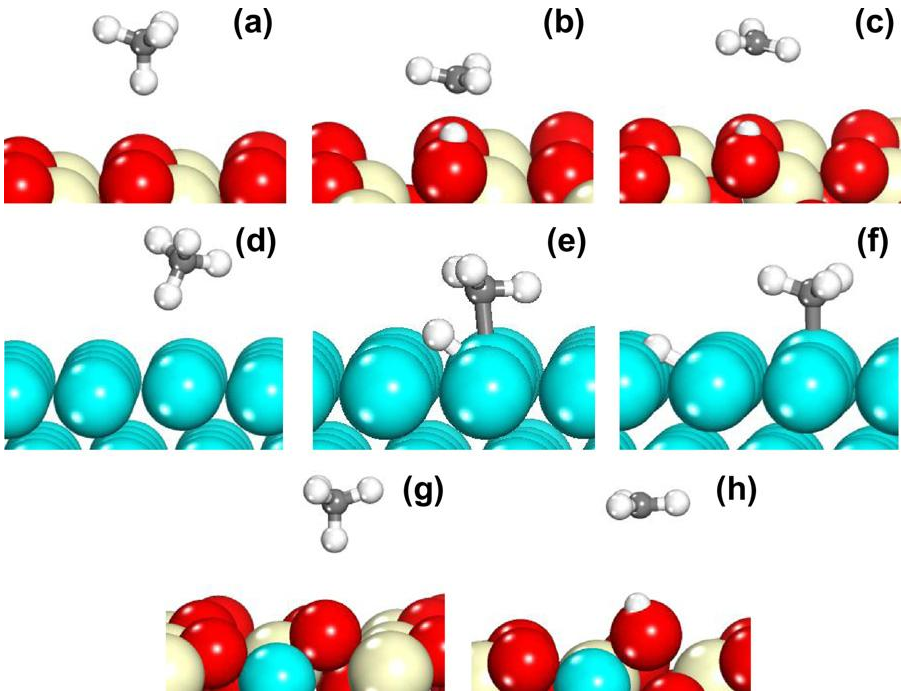

Figure 2.1. Initial (a,d,g), transition (b,e), and final (c,f,h) states for methane activation on $CeO_2(111)$ (a,b,c), Pd(111) (d,e,f), and $Pd_xCe_{1-x}O_2(111)$ (g,h). Ce is displayed as tan (light), Pd as light blue (gray), O as red (dark), C as gray, and H as white.[10]

Methane activation has been studied on framework and extra-framework species in zeolites. Broclawik *et al.*[11] investigated Ga in a ZSM-5 structure modelled as an $[Al(OH)_4]GaO$ cluster. CH_4 can transfer a hydrogen atom to the oxygen atom connected to the Ga atom. The CH_4 has a binding energy of -21 kJ mol^{-1} and the CH_3 and the hydrogen atom has a binding energy of -235 kJ mol^{-1}. The barrier for the dissociation of CH_4 is 120 kJ mol^{-1} to form the CH_3 and hydrogen atom.

Fellah and Onal[12] have used DFT to investigate, the C – H bond activation in ZSM-5 on extra-framework metals and metal oxides in the form of an individual metal atom and metal oxide (MO), M = Ag, Au, Cu, Rh and Ru. With the metal oxides the hydrogen atom from the CH_4 transfers to the oxygen atom of the MO leaving a radical methyl. With the metals, the hydrogen atom from CH_4 transfers to an oxygen atom in the framework and the methyl binds to the metal, which are both shown in Figure 2.2. The activation energy is the lowest for Au in the lone metals at 105 kJ mol^{-1} with Rh at 142 kJ mol^{-1}, Cu and Ru at 151 kJ mol^{-1} and Ag at 155 kJ mol^{-1}. The metals with the oxygen atom in the MO form reduce the activation energy in all

cases, which most noticeably for Ag, Cu and Au at 17 kJ mol^{-1}, 21 kJ mol^{-1} and 37 kJ mol^{-1} respectively. Only the Au metal and the Ag and Cu oxides have end points more favourable that the starting structure.

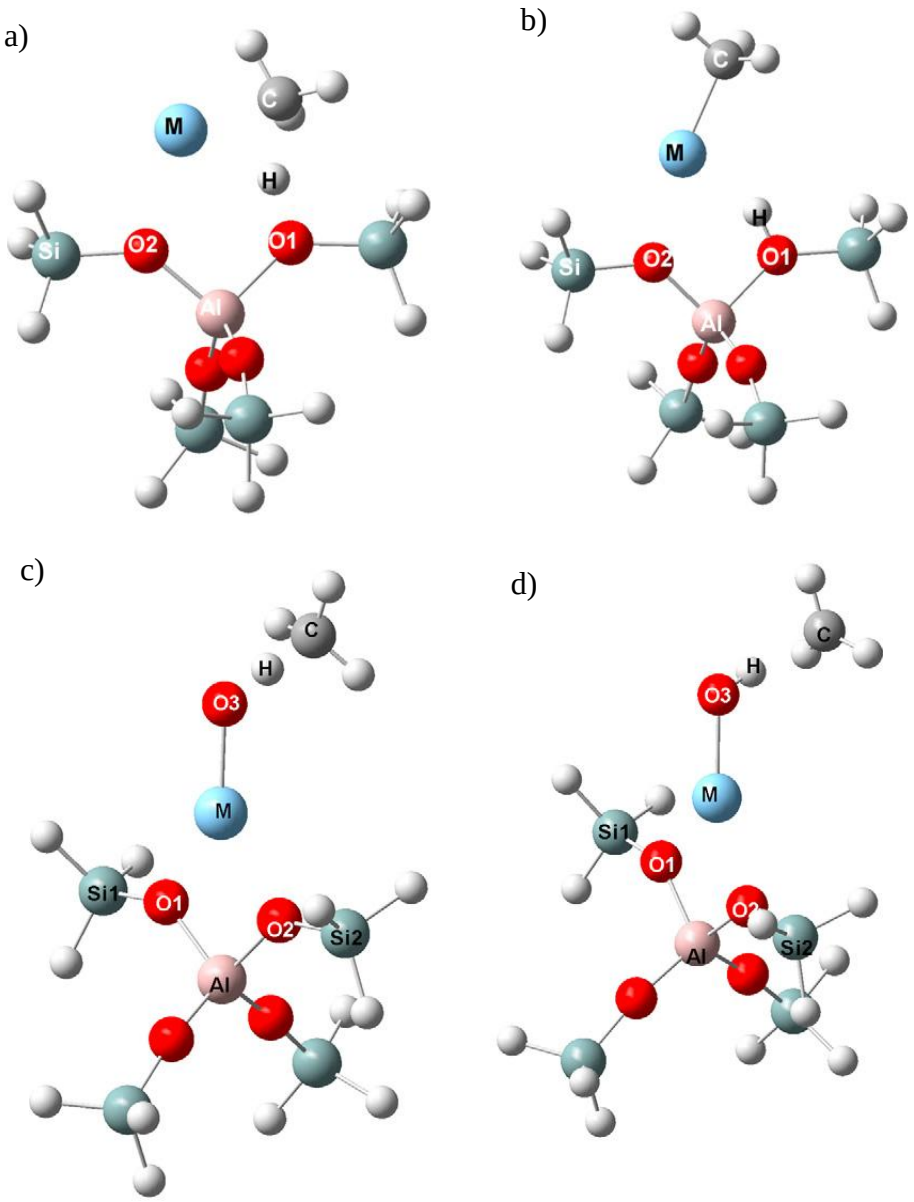

Figure 2.2. (a) Transition state geometry and (b) equilibrium geometry for C‑H bond activation of methane on M-ZSM-5, (c) Transition state geometry and (d) equilibrium geometry for C‑H bond activation of methane on MO-ZSM-5 cluster (M = Ag, Au, Cu, Rh and Ru).[12]

Zhou *et al.*[13] investigated C – H bond dissociation in ZSM-5 with extra-framework $Mo_2O_5^{2+}$ and MoO_2^{+}. These show C – H bond cleavage barriers of 266 kJ mol^{-1} for

the and 159 kJ mol^{-1} for the MoO_2^+ indicting the Mo(VI) of the $Mo_2O_5^{2+}$ has a higher energy barrier to overcome to the Mo(V) of the MoO_2^+.

Shaik, Kumar and de Visser[14] investigated C – H bond activation by the cytochrome P450 enzymes. The active species in these enzymes are a $Fe^{IV} = O$ in a porphyrin which gets reduced to a Fe^{III}. A radical rebound mechanism was found to produce the corresponding alcohol of the alkane, which is shown Figure 2.3. This involves the transfer of a hydrogen atom from the alkane to form a hydroxyl group and an alkyl radical. The second step is the alkyl radical binding with the hydroxyl group to the form the alcohol. The hydrogen abstraction step is the highest energy step with methane having the TS energy of 108 kJ mol^{-1}.

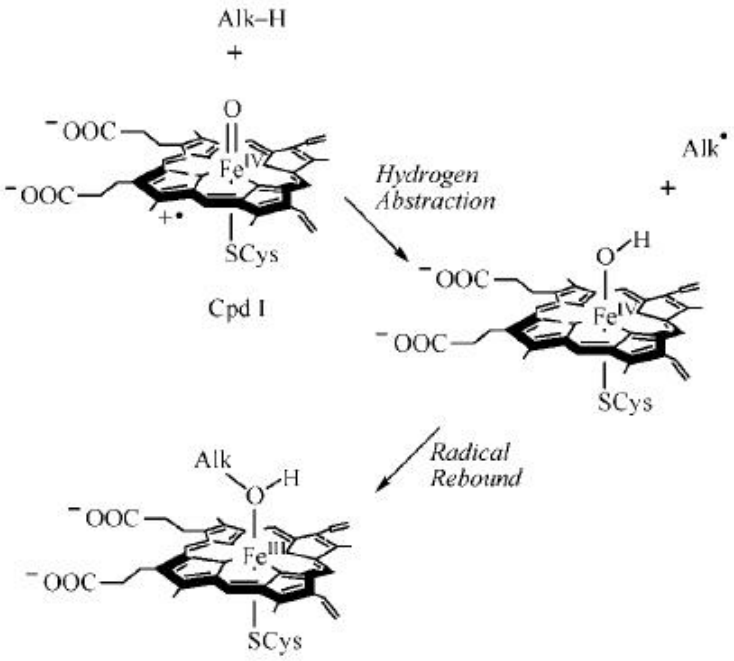

Figure 2.3. The Groves Rebound Mechanism of Alkane (Alk-H) Hydroxylation by Iron-Oxo Species.[14]

Rinaldo *et al.*[15] investigated intermediates for oxygen activation in methane monooxygenase. The Fe – Fe distances are given for different structures, the longest values found are for the superoxide and peroxide species on the Fe dimer. The O_2 molecule is shown to cleave across the Fe dimer to form a Fe_2O_2 diamond in the species indicated to activate methane with the mechanism in shown in Figure 2.4.

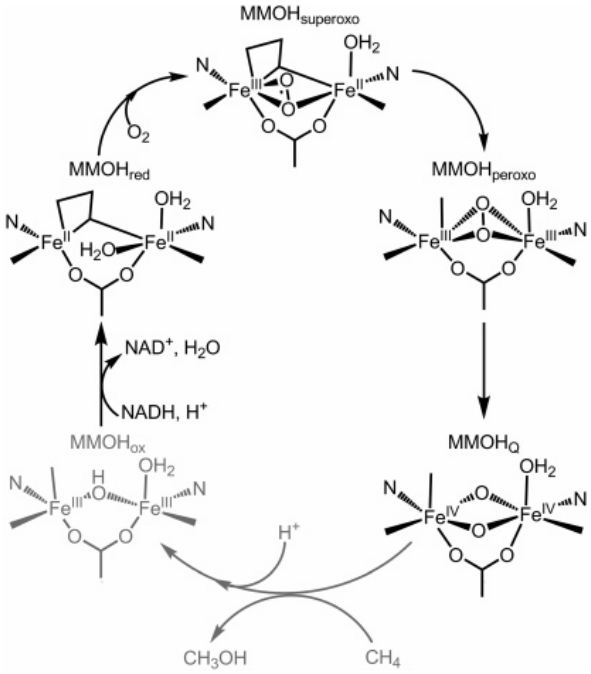

Figure 2.4. The catalytic cycle of MMOH. The part of the cycle corresponding to activation of dioxygen is shown in black while the oxidation of the substrate (hydroxylation of methane into methanol *in vivo*) is in light gray. [15]

2.2. Utilising H_2O_2 as oxidant

H_2O_2 has been used as a green oxidant as it readily reacts to donate O producing water, so many studies have been done into its viability as a oxidant of alkane with most the recent work investigating its involvement in epoxidation reactions. These have been done mainly in zeolites, of which TS-1 is the most common. TS-1 is a Ti atom containing MFI structure. Reactions with H_2O_2 have additionally been studied on surfaces with a recent review done 2007 on various aspects of zeolite and surface studies[16].

Huang and Lin[17] investigated the reactions of H_2O_2 on a rutile TiO_2 (110) surface and an anatase TiO_2 (101) surface. The two structures are shown in Figure 2.5. H_2O_2 decomposes to give OOH and a hydrogen atom but direct decomposition into two hydroxyl groups was not shown. H_2O_2 has a binding energy of -78 kJ mol^{-1} to a rutile TiO_2 (110) surface. A hydrogen atom can be transferred to form η_1-OOH which has a binding energy of -80 kJ mol^{-1}, with a barrier of 9 kJ mol^{-1}. The η_2-OOH forms from H_2O_2 with a binding energy of -85 kJ mol^{-1} and a barrier of 42 kJ mol^{-1}.

On the anatase TiO_2 (101) surface, H_2O_2 has a binding energy of -75 kJ mol^{-1}. A hydrogen atom can be transferred to form η_1-OOH which has a binding energy of -74 kJ mol^{-1}, with a barrier of 48 kJ mol^{-1}. The η_2-OOH forms from η_1-OOH with a binding energy of -87 kJ mol^{-1} and a barrier of 3 kJ mol^{-1}.

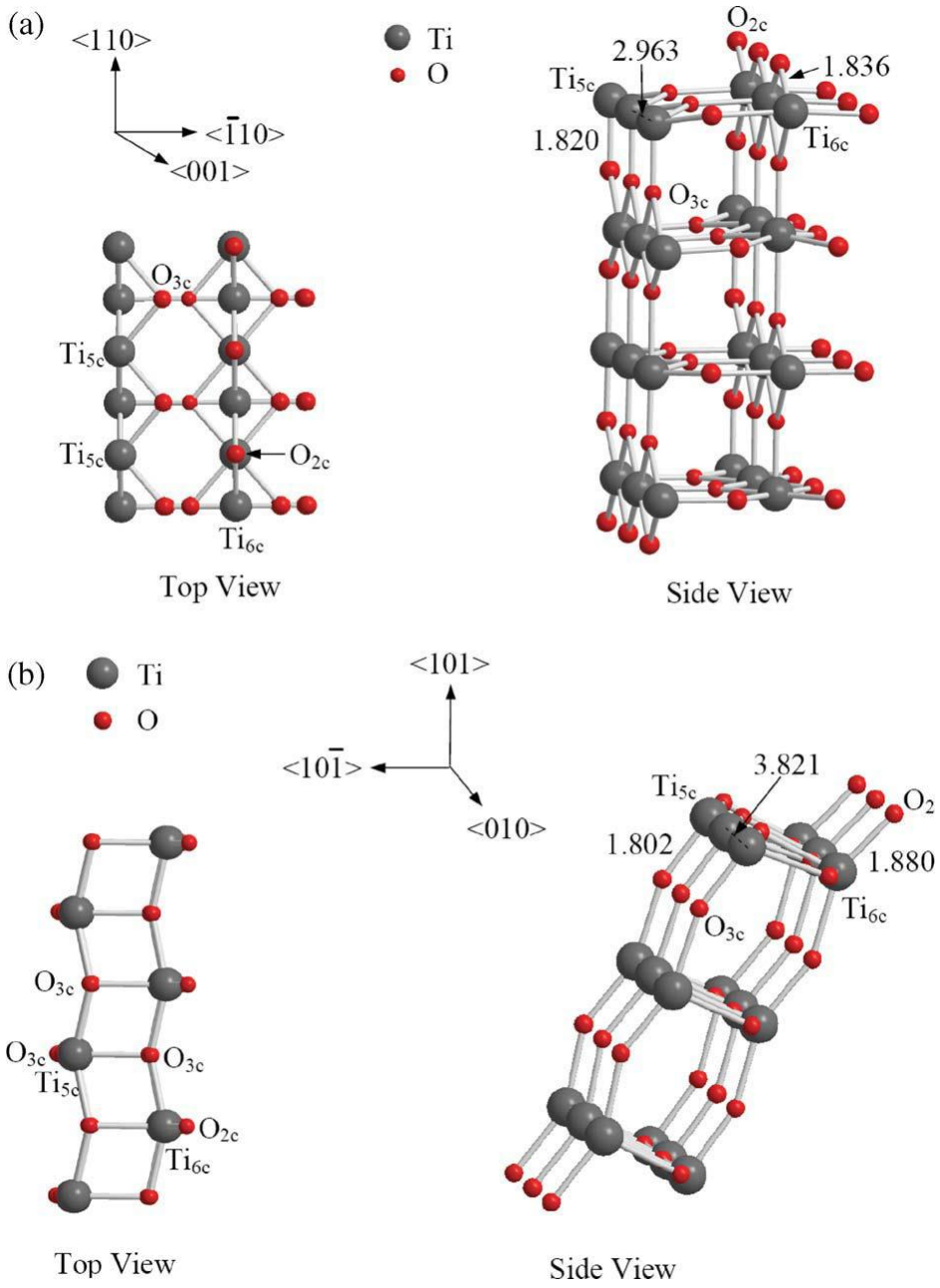

Figure 2.5. The geometry of the optimized surface with the PW91 method: (a)TiO_2-rutile (110) (b)TiO_2-anatase (101).[17]

Kirillova *et al.*[18] investigated alkane oxidation with H_2O_2 by Vanadate anions. The mechanism was studied on a divanadate system and the production of OOH and OH radicals. This is done by the transfer of hydrogen atoms, H_2O_2 replacing H_2O and the

loss of OH and OOH. The first hydrogen atom transfer to produce OOH requires a free energy barrier of 28 kJ mol^{-1}. The lowest energy path goes through multiple V – OH rather than V ═ O, V ═ O is slightly more energetic.

Kuznetsov *et al*[19] investigated the interaction of H_2O_2 with Al^{3+} and the oxidation of hydrocarbons by epoxidation. They studied the interaction of H_2O_2 and decomposition into OOH and OH radicals. H_2O_2 has a $\Delta H^{\ddagger}$ of 77 kJ mol^{-1} to adsorb to Al^{3+} and remove the H_2O present on the Al^{3+} centre. OOH and OH forming from H_2O_2 have an 8 kJ mol^{-1} difference in formation energy with the formation of OOH the higher in energy. They investigated two mechanisms using OOH to form an epoxide and also stating that OH radicals can react directly via the Sharpless mechanism. The Sharpless mechanism is shown in Figure 2.6. The first mechanism is the Sharpless-type with the ethene forming a π-bonded system with the adsorbed OOH in the transition step and has a $\Delta H^{\ddagger}$ of 31 kJ mol^{-1} and 38 kJ mol^{-1}. This producing to an OH group and an epoxide with an adsorption energy of -264 kJ mol^{-1} and -271 kJ mol^{-1}. The second mechanism is the Momoun-type forming a cyclic system with ethene and the OOH in the transition step and has a $\Delta H^{\ddagger}$ of 91 kJ mol^{-1}. This forms an OH group and an epoxide with an adsorption energy of -34 kJ mol^{-1}.

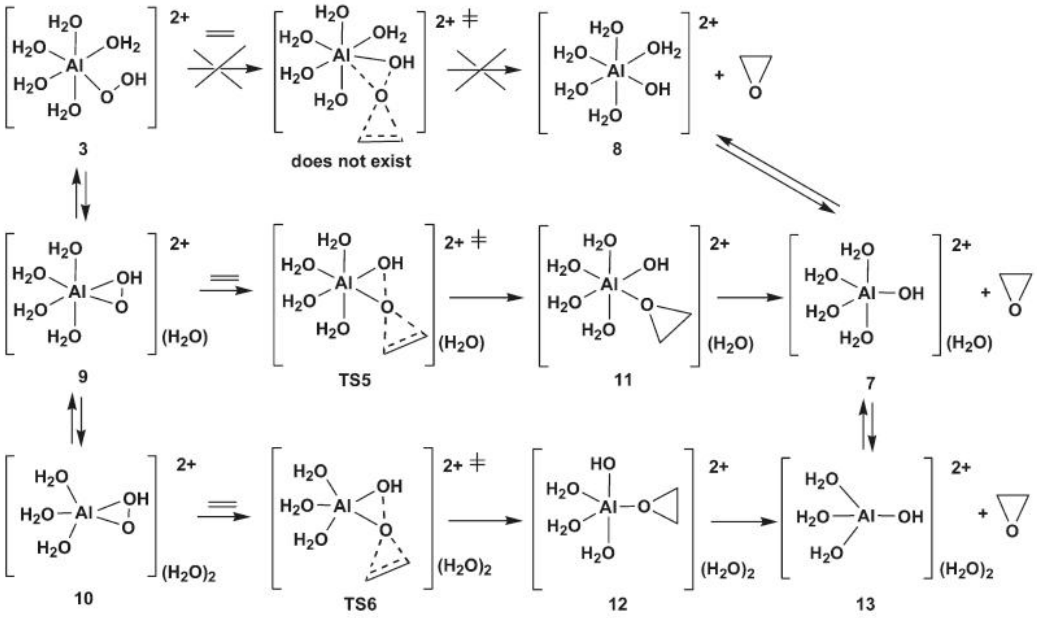

Figure 2.6. Sharpless mechanisms of ethylene epoxidation with complexes 9 and 10.[19]

Sinclair and Catlow[20] investigated partial oxidation in titanosilicate catalysts. A Ti^{IV} has several active sites produced around it including Ti = O, TiOH and $Ti(OH)_2$ bound silicates. Ti – OOH bound as η_1 is 33 kJ mol^{-1} more stable than the η_2, which meant the η_1 was used to study as the reactive surface species. The formation of the OOH species on TiOH has a barrier of 56 kJ mol^{-1} and on the $Ti(OH)_2$, a barrier of 48 kJ mol^{-1}.

To *et al.*[21] investigated the properties of Ti and H_2O_2 in TS-1 using a QM/MM approach. The binding energies of H_2O_2 and H_2O were compared on both tripodal and tetrapodal Ti centres with H_2O binding more strongly to the tetrapodal Ti centre, -60 kJ mol^{-1} compared to -40 kJ mol^{-1} for H_2O_2 on the same site. On the tripodal site similar results have been found for both H_2O_2 and H_2O with binding energies of -43 kJ mol^{-1} and -42 kJ mol^{-1} respectively. Transfer of one of the hydrogen atoms to the TiOH site in the tripodal system gives binding energies of -58 kJ mol^{-1} and -53 kJ mol^{-1} for the η_1 and η_2 complexes respectively with both becoming unfavourable with the loss of water from the complex. Loss of an addition hydrogen atom is very unfavourable at 453 kJ mol^{-1}.

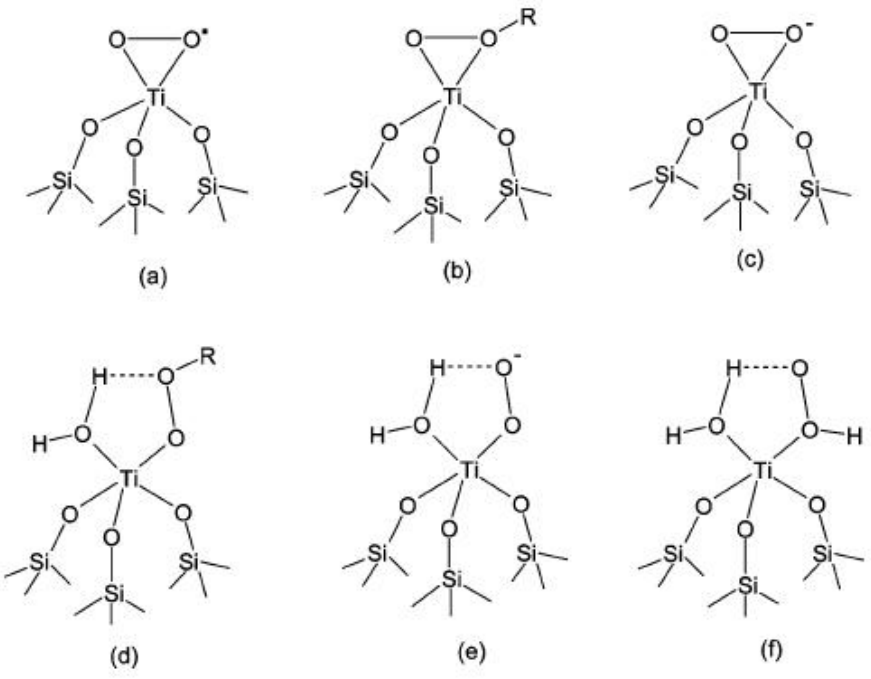

Figure 2.7. Postulated models for Ti-peroxo species: (a) Ti-$\eta^2(O_2\cdot)$, (b) Ti-η^2(OOR), (c) Ti-$\eta^2(O_2^-)$, (d) Ti-η^1(OOR), (e) Ti-$\eta^1(O_2^-)$, and (f) Ti-η^1(O(H)OH). [21]

Wells, Delgass and Thomson[22] investigated epoxidation using H_2O_2 in defective and non-defective TS-1. The defective structure has a Si vacancy forming four silinol groups. On the non-defective structure, Ti – H_2O_2 has a binding energy of -23 kJ mol^{-1} and Ti – OOH has binding energies of 27 kJ mol^{-1} and 25 kJ mol^{-1}. On the defective structure, Ti – OOH has a binding energy of -38 kJ mol^{-1}. For epoxidation the activation energy is 39 kJ mol^{-1} on the defective structure and 84 kJ mol^{-1} on the non-defective structure.

Wells *et al.*[23] investigated propylene epoxidation formation using H_2O_2 and TS-1. The employed a QM/MM approach. They studied 5 mechanisms previously proposed involving a framework, extra-framework or defective Ti site in QM region of the TS-1 structure all completed at the same level of theory (BPW91,LANL2DZ). Mechanism 1 is the mechanism proposed by Sinclair and Catlow[20]. Mechanism 2 was proposed by Vayssilov and van Santen[24]. Mechanism 3 was proposed by Munakata *et al*[25]. Mechanisms 4 and 5 are defect silanol nests (4 is partial and 5 is full). Mechanism 6 is a gas phase reaction, which is noncatalytic. All mechanisms involve active oxygen species, of which 1, 4 and 5 are hydroperoxy. Energies for these are shown in Table 2.1.

Mechanism	Step	Energy barrier / kJ mol^{-1}
1	Hydroperoxy formation	31
	Epoxidation	36
2	Epoxidation	80
3	1st peroxo formation step	89
	2nd peroxo formation step	30
	Epoxidation	5
4	Hydroperoxy formation	64
	Epoxidation	54
5	Hydroperoxy formation	42
	Epoxidation	26
6	Epoxidation	88

Table 2.1. Energies for each step in mechanism 1 – 6 proposed for propylene epoxidation[23]

The epoxidation step in mechanism 3 has the lowest energy but the formation of the reactive oxygen species has the highest energy and is comparable to the epoxidation step in the gas phase. Mechanism 1 has the lowest energy hydroperoxy formation and lowest activation energy for the reaction.

Antonova *et al*[26] investigated alkene epoxidation with H_2O_2 by Ti-Polyoxometalates. H_2O_2 can interact with a TiOH site to form a TiOOH or TiOO with the hydrogen atom on an oxygen atom on the $[PTi(OH)W_{11}O_{39}]^{4-}$. There is 6 kJ mol^{-1} difference between the two structures with the TiOO the more favourable but with the small difference both structures would be expected to be present with a barrier of 68 kJ mol^{-1} to interconvert between TiOOH and TiOO. The TiOOH forms an epoxide with a barrier of 77 kJ mol^{-1} which is 7 kJ mol^{-1} lower than the TiOO pathway with the pathway having to go through TiOOH to make the TiOO.

2.3. Oxide Supported Gold cluster

In the 1980s gold was found to be able to catalyses oxidation reactions[27,28] and various studies have investigated the structure of the active sites and the catalytic activity[29–34]. A review has recently been done about the reactions Au has been used for[35] and a review of computational results with supported Au clusters has also recently appeared[36].

Howard and Willock[37,38] investigated the activation of O_2 by Au_{10} on Fe_2O_3 (0001). This study uses DFT+U and the PBE functional with a U value of 4 eV. The Au_{10} cluster is made up of a layer of 7 (base) and layer of 3 (top) to give a [7,3] arrangement. The Au_{10} cluster adsorbs on two sites, one over a Fe atom has a binding energy of -88 kJ mol^{-1} and one over an oxygen atom has a binding energy of -86 kJ mol^{-1}. The Fe site is the favoured of the two but only by 2 kJ mol^{-1}. O_2 binds to an isolated Au_{10} cluster with a binding energy of -84 kJ mol^{-1} to the (100) face on the base of the cluster and -34 kJ mol^{-1} on the (111) face. The O_2 on the (111) face has an O – O distance of 1.41 Å and the O_2 on the (100) face has an O – O distance of 1.35 Å, which are both longer than the expected O – O distance for an isolated O_2 molecule of 1.23 Å. When the Au_{10} is on the Fe_2O_3 (0001) surface the O_2 binds to the (111) face with a binding energy of -108 kJ mol^{-1} and binds to the (100) face with a binding energy of -130 kJ mol^{-1}. The O_2 on the (111) face has an O – O distance of 1.48 Å and the O_2 on the (100) face has an O – O distance of 1.50 Å, these are longer than with the isolated Au_{10} indicating a stronger charge transfer which is supported by the Bader charges and the density of states (DOS).

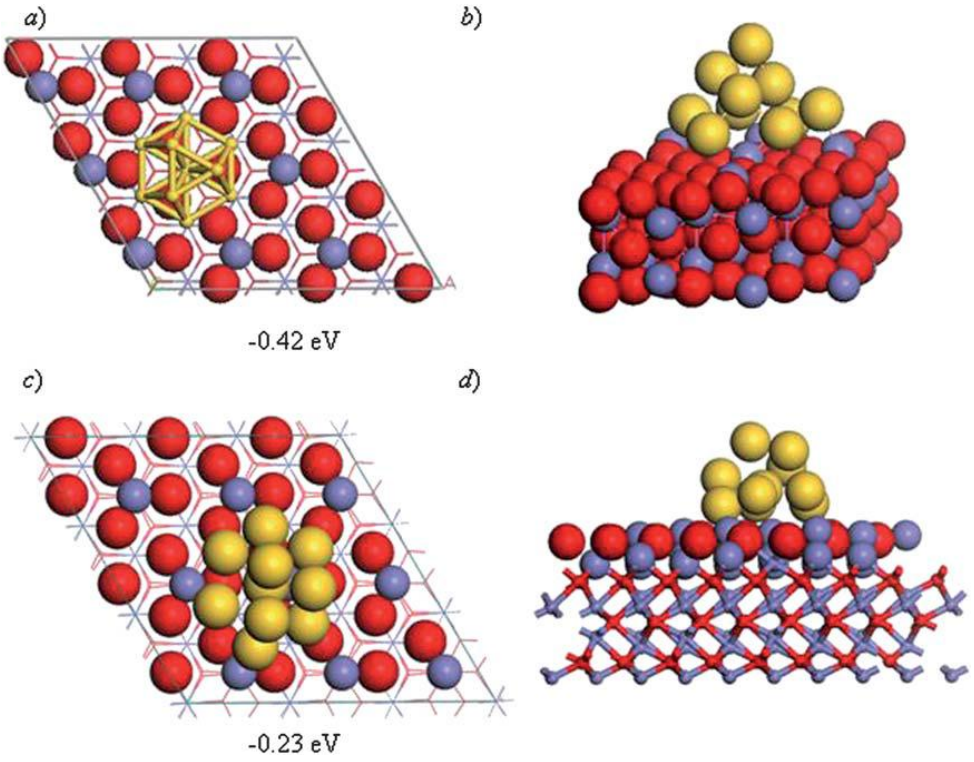

Figure 2.8. $Au_{10}(7,3)$ on α-$Fe_2O_3(0001)$ surface a) starting orientation with (100) face edges aligned with surface O atoms, b) The relaxed structure after optimisation from starting point in (a) for 3 layer slab model. c) Plan and d) side view of $Au_{10}(7,3)$ relaxed structure on α-$Fe_2O_3(0001)$ surface using the 4l slab, atoms free to move during optimisation are shown as spheres in this case. Values shown in (a) and (c) are the relaxed adsorption energy per Au atom. Atom colours: Au; yellow, Fe; blue and O; red.[37]

Pulido, Boronat and Corma[39] investigated the adsorption of Au clusters supported on a graphene sheet. The graphene sheet has a vacancy in it and the Au clusters are adsorbed to it. A single Au atom has a binding energy of -332 kJ mol^{-1}, a Au_5 cluster has a binding energy of -520 kJ mol^{-1}, a Au_6 cluster has a binding energy of -483 kJ mol^{-1}, a Au_{19} cluster has a binding energy of -396 kJ mol^{-1} and a Au_{39} cluster has a binding energy of -412 kJ mol^{-1}. These calculations are all preformed with the PW91 functional. The dispersion interactions are poorly modelled with DFT so a dispersion correction is added and the binding energies increase to -355 kJ mol^{-1}, -599 kJ mol^{-1}, -565 kJ mol^{-1}, -500 kJ mol^{-1} and -523 kJ mol^{-1} for Au_1, Au_5, Au_6, Au_{19} and Au_{39}. The Bader charges on the Au bound to the graphene sheet are 0.317 e for Au_1, 0.499 e for Au_5, 0.438 e for Au_6, 0.346 e for Au_{19} and 0.314 e for Au_{39}. These correlate with the binding energies both with general trend.

Teng *et al*[40] investigated the adsorption of Au atoms onto a CeO_2(111) surface. Au adsorbs to the top site of a surface oxygen atom or hollow site of CeO_2 with a binding energy of -104 kJ mol^{-1} and -88 kJ mol^{-1} respectively. Binding for 2 – 10 Au atoms are in Table 2.2 with m-n-l in the table referring to the number of Au atom in each layer with the binding energy per Au atom below.

Number of Au atoms	**First row m-n-l for layers of Au atom and second row binding energies per Au atom in cluster / kJ mol^{-1}**						
2	1-1	2-0					
	-193	-170					
3	3-0a	3-0a	2-1				
	-193	-193	-220				
4	4-0	3-1a	3-1b	2-2			
	-196	-212	-214	-211			
5	5-0	4-1	3-2a	3-2b	2-3		
	-217	-216	-229	-223	-222		
6	6-0a	6-0b	6-0c	6-0d	4-2	3-3	
	-228	-224	-221	-223	-228	-217	
7	7-0	6-1	5-2	4-3	3-4		
	-233	-229	-226	-231	-228		
8	8-0a	8-0b	7-1	6-2	5-3a	5-3b	4-4
	-233	-231	-233	-232	-232	-236	-233
9	9-0	7-2	6-3a	6-3b	6-3c	5-4	
	-230	-233	-229	-238	-236	-237	
10	10-0	7-3	6-3-1a	6-3-1b	6-3-1c		
	-233	-234	-236	-248	-246		

Table 2.2. Energies for each Au cluster configuration.

The Au atoms adsorb with increasing adsorption energy per Au atom for fewer Au atoms on the surface for 1 – 5 Au, which would indicate the Au – Au interactions are stronger than Au – O interaction in this case.

Roldan *et al*[41] investigated O_2 activation by Au_5 clusters on MgO(401) surface. Using the PW91 functional, the Au_5 cluster has a binding energy of -360 kJ mol^{-1} to the MgO(401) surface. The Au_5^- cluster has a binding energy of -445 kJ mol^{-1} to the MgO(H^+) surface, where the presence of the H^+ is to make an overall neutral system. O_2 has a binding energy of -79 kJ mol^{-1} to Au_5/MgO and -89 kJ mol^{-1} to Au_5/MgO(H^+). There is an O – O distance of 1.31 Å and a Bader charge of -0.52 e for O_2/Au_5/MgO and an O – O distance of 1.44 Å and a Bader charge of -1.02 e for O_2/Au_5/MgO(H^+). This indicates that there is more electron transfer in the O_2/Au_5/MgO(H^+) system.

Lopez and Norskov[42] investigated the interface of Au on TiO_2(110). Four different amounts of Au are adsorbed to the surface 0.17 ML, 0.33 ML, 1 ML and 2 ML. The lowest coverage has the strongest adsorption energy of -150 kJ mol^{-1}. This would correspond with one Au atom per two unit cells of TiO_2(110). The d-band filling shows a reduced filling for the lowest coverage and the largest shift in the d-band centre from the free Au, -1.17 eV to -2.34 eV.

TiO2	**Au_7 (2D)**	**Au_7 (3D)**
Vacancy	-50	26
H_{cap}	-84	10
Stoichiometric	-114	-16
OH_{tr}	-226	-200
OH_{tr} + H_2O_{tr}	-230	-204
O_{tr} + H_{cap}	-220	-233
O_{tr} + H_{cap} + H_2O_{tr}	-230	-232

Table 2.3. Binding energies for Au_7 on TiO_2 with different defects with structures shown in Figure 2.9.

Wang and Hammer[43] investigated Au_7 supported by TiO_2(110). A 2D and 3D Au_7 cluster was adsorbed to the TiO_2(110) surface, with the binding energies shown in Table 2.3.

This shows that the Au_7 cluster binds more strongly on alkaline surfaces with the charge reducing by 0.49 e on the alkaline surfaces but only 0.23 e to 0.26 e on the stoichiometric and reduced surfaces.

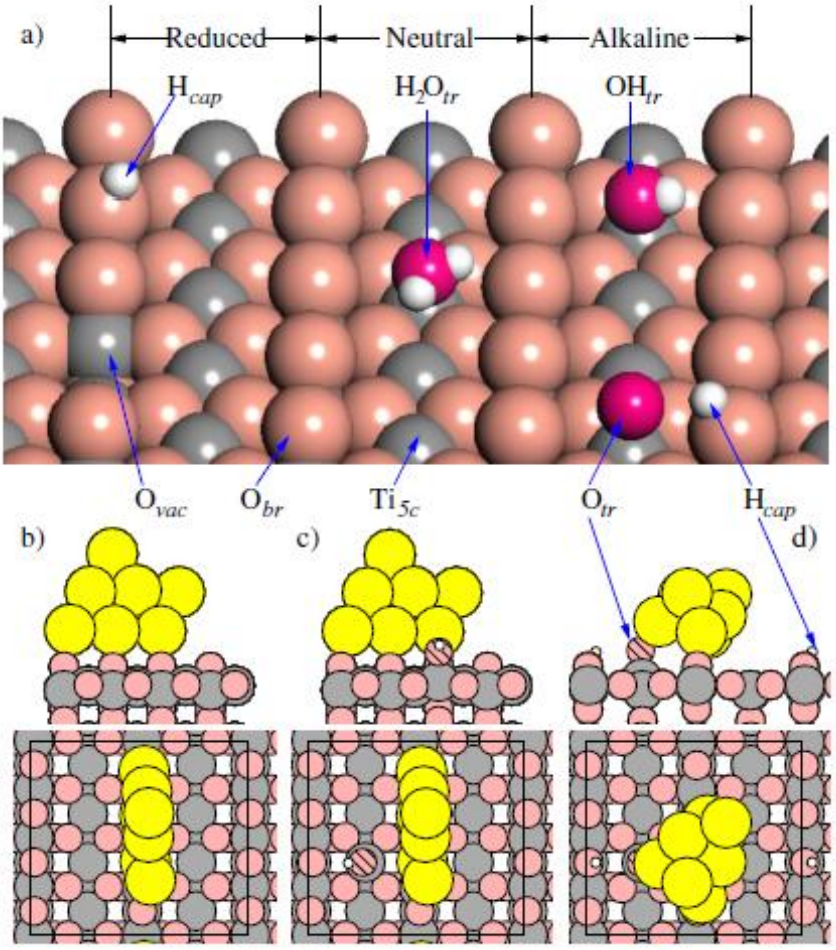

Figure 2.9. (a) Schematic of the rutile TiO_2(110) surface. Most stable structures of Au_7 on (b) stoichiometric TiO_2 and alkaline TiO_2 with (c) intact or (d) dissociated OH_{tr}.[43]

Ammal and Heyden[44] investigated Au_n and Pt_n clusters with n = 2, 3 on TiO_2 (110) with and without an oxygen vacancy using a hybrid DFT functional and comparing to the PBE functional. Au_2 on TiO_2(110) has a binding energy of -94 kJ mol^{-1} with a Bader charge of 0.1 e. Au_3 on TiO_2(110) has a binding energy of -162 kJ mol^{-1} with

a Bader charge of 0.59 e. These results were obtained as a periodic lattice. If a cluster model is used PBE gives a different result for Au_2 (-120 kJ mol^{-1}, 0.35 e) and Au_3 (-244 kJ mol^{-1}, 0.79 e) and when PBE0 is used these result differ more: Au_2 (-115 kJ mol^{-1}, 0.33 e) and Au_3 (-276 kJ mol^{-1}, 0.82 e). PBE0 energies indicate stronger bonding to the surface than PBE. This same pattern is shown for a TiO_2 with an oxygen vacancy with larger binding energies (Au_3, -298 kJ mol^{-1}, PBE0) but the Bader charges are all negative for PBE results in the periodic lattice but for the embedded cluster method showing the same pattern as PBE0 but producing more negative results.

Wanbayor and Ruangpornvisti[45] investigated the adsorption of Au, Pd and Pt onto anatase TiO_2 (001) surface, which are shown in Figure 2.10. With a 0.5 mono-layer coverage giving binding energies of -146 kJ mol^{-1} for the Au, -134 kJ mol^{-1} for the Pd and -256 kJ mol^{-1} for the Pt. All bind to the O_{2c} and Ti_{5c} of the TiO_2 surface. The Au – O distance is 2.46 Å and the Au – Ti distance is 2.52 Å. The Pd – O distance is 2.23 Å and the Pd – Ti distance is 2.66 Å. The Pt – O distance is 2.06 Å and the Pt – Ti distance is 2.62 Å. The Au atom has the longest M – O distance but the shortest M – Ti distance meaning the Au must favour binding to the Ti whereas Pt and Pd have shorter M – O distances but longer M – Ti distances. In the case of Pt the M – O distance is the shortest indicating Pt favours M – O bonds, which accounts for the stronger binding energy as the M – O are so short. This is not the case with Pd as the M – Ti is the longest but the M – O distances are not the shortest, as would be expected if more strongly bonded, as the metal is the smallest of the three.

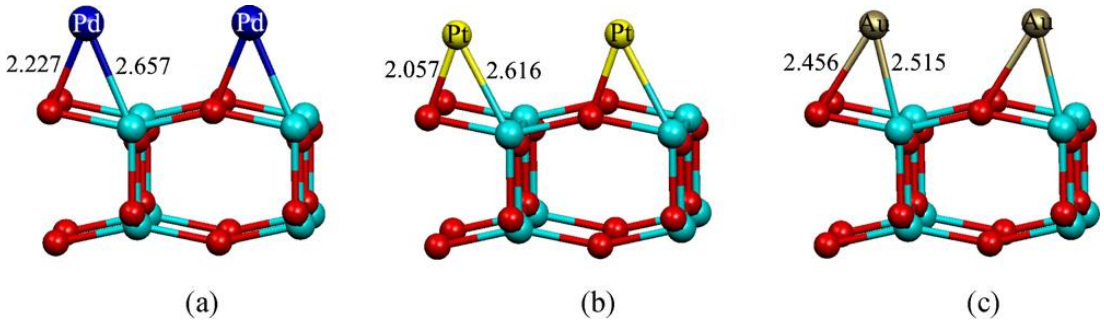

Figure 2.10. The structures of anatase TiO_2 (001)-supported (a) Pd, (b) Pt and (c) Au. Bond distances are in Å.[45]

Hernandez and Sanz[46] used classical molecular dynamics to study a Au cluster on rutile TiO_2(110). This allows a larger cluster to be studied than with DFT. They

studied a Au_{145} cluster which shows a consistent Au – Au distance of 2.90 Å but no consistent Au – Ti and Au – O distances, indicating these fluctuate in a short time scale and the Au cluster moves around the surface, which would agree with the small clusters having high mobility.

This chapter has discussed various types of C – H activation with it leading to a complex with metal cations and formation of radical species. Metal surfaces tend to not be as good at breaking the C – H as metal oxides with some metal oxides showing promising results. Fe containing enzymes have been found to be good at cleaving C – H bonds and forming the alcohol. Oxidant activation has been shown to be most effective in TS-1 with TiO_2 not being as active despite Ti centres being the active site in both. Al cations are also effective for H_2O_2 activation.

References

1. H. Schwarz, *Angewandte Chemie (International ed. in English)*, 2011, **50**, 10096–115.

2. T. J. Hall, J. S. J. Hargreaves, G. J. Hutchings, R. W. Joyner, and S. H. Taylor, *Fuel Processing Technology*, 1995, **42**, 151–178.

3. L. Yuliati and H. Yoshida, *Chemical Society reviews*, 2008, **37**, 1592–602.

4. R. Burch and M. J. Hayes, *Journal of Molecular Catalysis A: Chemical*, 1995, **100**, 13–33.

5. H. Heinemann and J. Carberry, *Catalysis Reviews*, 2002, **44**, 1–58.

6. A. P. E. York, T. Xiao, and M. L. H. G. Ã, *Topics in Catalysis*, 2003, **22**, 345–358.

7. B. Christian Enger, R. Lødeng, and A. Holmen, *Applied Catalysis A: General*, 2008, **346**, 1–27.

8. C. Au, C. Ng, and M. Liao, *Journal of Catalysis*, 1999, **185**, 12–22.

9. B. Wang, L. Song, and R. Zhang, *Applied Surface Science*, 2012, **258**, 3714–3722.

10. A. D. Mayernick and M. J. Janik, *Journal of Catalysis*, 2011, **278**, 16–25.

11. E. Broclawik, H. Himei, M. Yamadaya, M. Kubo, A. Miyamoto, and R. Vetrivel, *The Journal of Chemical Physics*, 1995, **103**, 2102–2108.

12. M. F. Fellah and I. Onal, *Catalysis Today*, 2011, **171**, 52–59.

13. D. Zhou, Y. Zhang, H. Zhu, D. Ma, and X. Bao, *Journal of Physical Chemistry C*, 2007, **111**, 2081–2091.

14. S. Shaik, D. Kumar, and S. P. de Visser, *Journal of the American Chemical Society*, 2008, **130**, 10128–40.

15. D. Rinaldo, D. M. Philipp, S. J. Lippard, and R. A. Friesner, *Journal of the American Chemical Society*, 2007, **129**, 3135–47.

16. S. Bordiga, F. Bonino, A. Damin, and C. Lamberti, *Physical Chemistry Chemical Physics : PCCP*, 2007, **9**, 4854–78.

17. W. Huang, P. Raghunath, and M. C. Lin, *Journal of Computational Chemistry*, 2011, **32**, 1065–1081.

18. M. V Kirillova, M. L. Kuznetsov, Y. N. Kozlov, L. S. Shul'pina, A. Kitaygorodskiy, A. J. L. Pombeiro, and G. B. Shul'pin, *ACS Catalysis*, 2011, 1511–1520.

19. M. L. Kuznetsov, Y. N. Kozlov, D. Mandelli, A. J. L. Pombeiro, and G. B. Shul'pin, *Inorganic Chemistry*, 2011, **50**, 3996–4005.

20. P. E. Sinclair and C. R. A. Catlow, *Journal of Physical Chemistry B*, 1999, **103**, 1084–1095.

21. J. To, A. A. Sokol, S. A. French, and C. R. A. Catlow, *Journal of Physical Chemistry C*, 2008, **112**, 7173–7185.

22. D. H. Wells, W. N. Delgass, and K. T. Thomson, *Journal of the American Chemical Society*, 2004, **126**, 2956–62.

23. D. H. Wells, A. M. Joshi, W. N. Delgass, and K. T. Thomson, *Journal of physical chemistry. B*, 2006, **110**, 14627–39.

24. G. N. Vayssilov and R. A. van Santen, *Journal of Catalysis*, 1998, **175**, 170–174.

25. H. Munakata, Y. Oumi, and A. Miyamoto, *The Journal of Physical Chemistry B*, 2001, **105**, 3493–3501.

26. N. S. Antonova, J. J. Carbó, U. Kortz, O. A. Kholdeeva, and J. M. Poblet, *Journal of the American Chemical Society*, 2010, **132**, 7488–97.

27. G. J. Hutchings, *Journal of Catalysis*, 1985, **96**, 292–295.

28. M. Haruta, N. Yamada, T. Kobayashi, and S. Iijima, *Journal of Catalysis*, 1989, **115**, 301–309.

29. M. Valden, X. Lai, and D. Goodman, *Science*, 1998, **281**, 1647–50.

30. D. C. Meier and D. W. Goodman, *Journal of the American Chemical Society*, 2004, **126**, 1892–9.

31. M. S. Chen and D. W. Goodman, *Science*, 2004, **306**, 252–5.

32. M. Haruta, *Catalysis Today*, 1997, **36**, 153–166.

33. K. Okazaki, S. Ichikawa, Y. Maeda, M. Haruta, and M. Kohyama, *Applied Catalysis A: General*, 2005, **291**, 45–54.

34. P. Landon, P. J. Collier, A. J. Papworth, C. J. Kiely, and G. J. Hutchings, *Chemical communications*, 2002, 2058–9.

35. A. S. K. Hashmi and G. J. Hutchings, *Angewandte Chemie (International ed. in English)*, 2006, **45**, 7896–936.

36. R. Coquet, K. L. Howard, and D. J. Willock, *Chemical Society Reviews*, 2008, **37**, 2046–76.

37. K. L. Howard and D. J. Willock, *Faraday Discussions*, 2011, **152**, 135.

38. A. F. Carley, D. J. Morgan, N. Song, M. W. Roberts, S. H. Taylor, J. K. Bartley, D. J. Willock, K. L. Howard, and G. J. Hutchings, *Physical Chemistry Chemical Physics : PCCP*, 2011, **13**, 2528–38.

39. A. Pulido, M. Boronat, and A. Corma, *New Journal of Chemistry*, 2011, **35**, 2153.

40. B.-T. Teng, F.-M. Wu, W.-X. Huang, X.-D. Wen, L.-H. Zhao, and M.-F. Luo, *ChemPhysChem*, 2012, **13**, 1261–71.

41. A. Rolda, J. M. Ricart, F. Illas, and G. Pacchioni, *Journal of Physical Chemistry C*, 2010, **114**, 16973–16978.

42. N. Lopez and J. K. Nørskov, *Surface Science*, 2002, **515**, 175–186.

43. J. Wang and B. Hammer, *Physical Review Letters*, 2006, **97**, 5–8.

44. S. C. Ammal and A. Heyden, *The Journal of Chemical Physics*, 2010, **133**, 164703.

45. R. Wanbayor and V. Ruangpornvisuti, *Applied Surface Science*, 2012, **258**, 3298–3301.

46. N. Hernandez and J. Sanz, *Catalysis Today*, 2007, **128**, 230–234.

3. Theory and Methodology

This chapter discusses the theory that is used in this thesis including DFT methods, Bader charge analysis, density of states, vibrational frequency analysis and implementation of the codes used.

3.1. Density Functional Theory

Density functional theory (DFT) is the method chosen for this work. This is because it is a faster method than the higher order wavefunction methods but can study bond breaking unlike fast non-quantum mechanical methods which is key to this work. This section discusses the basics of the theory behind DFT. More details are discussed in Density-Functional Theory of Atoms and Molecules by R. G. Parr and W. Yang[1]. In addition to this there is a book by R. Dronskowski, Computational Chemistry of Solid State Materials[2] which discusses more of DFT in the solid state. Finally there is a paper by J. Hafner[3] which relates to the implementation in Vienna ab-intio simulation program (VASP). A further book by R. M. Martin[4] discusses DFT but going into more detail of electronic structure methods.

The basics of DFT come from quantum mechanics which uses the time-independent Schrödinger equation, shown in equation 3.1.

$$\hat{H}\Psi = E\Psi \tag{3.1}$$

where E is the electronic energy, $\hat{H}$ is the Hamiltonian operator and Ψ is the wave function. $\hat{H}$ is made up of kinetic energy part, $\hat{T}$, and a potential energy part, $\hat{V}$, which can be further divided into nucleus – electron interaction and electron – electron interaction potential energy. This is for an isolated N-electron system shown in equation 3.2.

$$\hat{H} = \hat{T} + \hat{V}_{ne} + \hat{V}_{ee} = \sum_{i=1}^{N}\left(-\frac{1}{2}\nabla_i^2\right) + \sum_{i=1}^{N} v(\boldsymbol{r}_i) + \sum_{i<j}^{N}\frac{1}{r_{ij}} \tag{3.2}$$

DFT

DFT uses the single particle electron density as a fundamental variable. This is derived from the Hohenberg-Kohn theorem[5], which states the ground state electron density $n_0(r)$ will minimise the functional for the energy;

$$E[n(r)] = F[n(r)] + \int n(r)V_{ext}(r)d^3r \tag{3.3}$$

where $F[n(r)]$ is an unknown functional and the E is the ground state energy E_0 at its minimum. Kohn and Sham[6] produced a possible form for $F[n(r)]$ as;

$$F[n(r)] = T_s[n(r)] + \frac{e^2}{2}\iint \frac{n(r)n(r')}{|r-r'|}d^3rd^3r' + E_{xc}[n(r)] \tag{3.4}$$

where $T_s[n(r)]$ is the kinetic energy for non-interacting electrons, $\frac{e^2}{2}\iint \frac{n(r)n(r')}{|r-r'|}d^3rd^3r'$ is the electron – electron interaction and $E_{XC}[n(r)]$ is the exchange-correlation energy. $T_s[n(r)]$ can be rewritten by defining the electron density as a set of single particle wavefunctions, Ψ_i;

$$n(r) = \sum_i |\Psi_i(r)|^2 \tag{3.5}$$

$$T_s[n(r)] = -\frac{\hbar^2}{2m_e}\sum_i \Psi_i(r)\nabla^2\Psi_i(r)d^3r \tag{3.6}$$

When $E[n(r)]$ is minimised with respect to $n(r)$ with a constant number of electrons, a set of equations are produced from this;

$$\left(-\frac{\hbar^2}{2m_e}\nabla^2 + V_{eff}(r)\right)\Psi_i(r) = \varepsilon_i\Psi_i(r) \tag{3.7}$$

where V_{eff} is the effective potential for each i;

$$V_{eff} = V_{ext}(r) + e^2\int \frac{n(r')}{|r-r'|}d^3r' + V_{xc}(r) \tag{3.8}$$

where;

$$V_{xc}(r) = \frac{\delta E_{xc}}{\delta n(r)} \tag{3.9}$$

This allows $T_s[n(r)]$ to be written as a Schrödinger-like equation for single particle Kohn-Sham orbitals;

$$\hat{H}_{KS}|\Psi_i\rangle = \varepsilon_i|\Psi_i\rangle \tag{3.10}$$

However this leaves the exchange-correlation energy, $E_{XC}[n(r)]$ as an unknown part as the form of $F[n(r)]$ is unknown. A number of approximations can be used to find $E_{XC}[n(r)]$. The simplest of these is the local density approximation (LDA), in which E_{XC} is defined as;

$$E_{xc}^{LDA} = \int n(r)\varepsilon_{xc}\big(n(r)\big)\, d^3r \tag{3.11}$$

Where $\varepsilon_{XC}\big(n(r)\big)$ is exchange-correlation energy per unit volume, which can be calculated by various method including quantum Monte Carlo[7] and parameterisation[8].

The General Gradient Approximation (GGA) is a further method. This works by adding a gradient term of the electron density resulting in;

$$E_{xc}^{GGA} = \int n(r)\varepsilon_{xc}\big(\mathrm{n(r)}, \nabla n(r)\big) d^3\, r \tag{3.12}$$

This is the method used mainly in this thesis with two parameterisations used; Perdew, Burke and Ernzerhof (PBE)[9] and Revised Perdew, Burke and Ernzerhof (RPBE)[10]. Another commonly used functional is by Perdew and Wang[11] (PW91).

The last type of functional discussed here is hybrid GGA, which combines the GGA functional and with the exact exchange (Hartree-Fock)[12,13];

$$E_{xc}^{hybrid} = \alpha(E_x^{HF} - E_x^{GGA}) + E_{xc}^{GGA} \tag{3.13}$$

The coefficient α determined by semi-empirical methods and E_x^{HF} is the Hartree-Fock exchange[12,13].

This method was first proposed by Becke[14] who noted from work by Harris[15] that the limits of the adiabatic connection integral for the exact exchange-correlation energy can be approximated;

$$E_{xc} = \int_0^1 U^{\lambda} d\lambda = \frac{1}{2}U^0 + \frac{1}{2}U^1 \tag{3.14}$$

λ = 0 is the exchange only limit and is well described by Hartree-Fock theory and λ = 1 is the local part of the electron interactions formed because of the correlation. Becke proposed the half and half functional because of this.

$$E_{xc} = \frac{1}{2}E_x^{HF} + \frac{1}{2}E_{xc,\lambda=1}^{DFT} \tag{3.15}$$

Several hybrid functionals have been developed since including PBE0[16,17], HSE06[18,19] and B3LYP[20], which are used in this work. The equation to calculate E_{xc} for B3LYP is as follows;

$$E_{xc} = E_{xc}^{LDA} + 0.2(E_x^{HF} - E_{xc}^{LDA}) + 0.72\Delta E_x^{B88} + 0.81\Delta E_x^{PW91} \tag{3.16}$$

Hybrid functionals tend to offer the best results but are slow for periodic systems as they perform poorly with planewaves, so GGA functionals are favoured in this work.

DFT+U

DFT tends to poorly describe strongly correlated systems with d or f orbitals. DFT+U corrects this by adding a Hubbard Hamiltonian for the Coulomb repulsion and exchange interactions.

The method for applying DFT+U in this thesis was proposed by Dudarev *et al.*[21] where E_{DFT+U} is calculated by

$$E_{DFT+U} = E_{DFT} + \frac{(\bar{U} - \bar{J})}{2}\sum_{\sigma}\left[\left(\sum_j \rho_{jj}^{\sigma}\right) - \left(\sum_{j,l} \rho_{jl}^{\sigma}\rho_{lj}^{\sigma}\right)\right] \tag{3.17}$$

Where U is a spherically averaged Hubbard parameter which can be described as an on-site coulombic interaction and J represents the screened exchange. ρ_{jj}^{σ} is the on-site density matrix of the electron with the U value applied. This makes the DFT+U method a DFT method with semi-empirical penalty function as the value of U and J are chosen. The actual values of U and J do not affect the result, because only the difference between U and J has meaning as $(\bar{U} - \bar{J})$ is in the expression.

3.2. Geometry Optimisers

In calculating the optimum structure a geometry optimiser is required, and for this work two are used: a conjugate-gradient algorithm[22,23] and a residual minimisation scheme-direct inversion in the iterative subspace[24] (RMM-DIIS).

A conjugate-gradient algorithm is used to optimise structures in this work. This works by finding the minimum by the steepest decent in a three step process; initial, trial and corrector steps with the trial and corrector steps repeated in a loop until convergence is achieved. In the initial step the steepest descent is calculated from the calculated forces and the stress tensors and the ions positions are changed accordingly. The second step is a trial step and the third step, a corrector step. These two steps are repeated until a minimum energy configuration can be found or one within the required cut-off. A new gradient is calculated after the first step and every subsequent step, which are preconditioned and conjugated to the previous search vector.

A residual minimisation scheme-direct inversion in the iterative subspace (RMM-DIIS) is a quasi-Newton method. The inverse of the hessian matrix is approximated and improved in each step with the search vector determined by the forces and stress tensor. This method will optimise more rapidly but fails if too far from the stationary point so is not desirable for the structural optimisations as the stationary point may not be easily obtained but is good for electronic optimisations as the structure is not changed.

The conjugate gradient method is used to optimise the configuration of ions in the cell. The RMM-DIIS method is used to optimise the electronic structure on the bands in a stationary point calculation. The conjugate gradient method has a cut-off of 10^{-5} and the RMM-DIIS method has a cut-off of 10^{-4}.

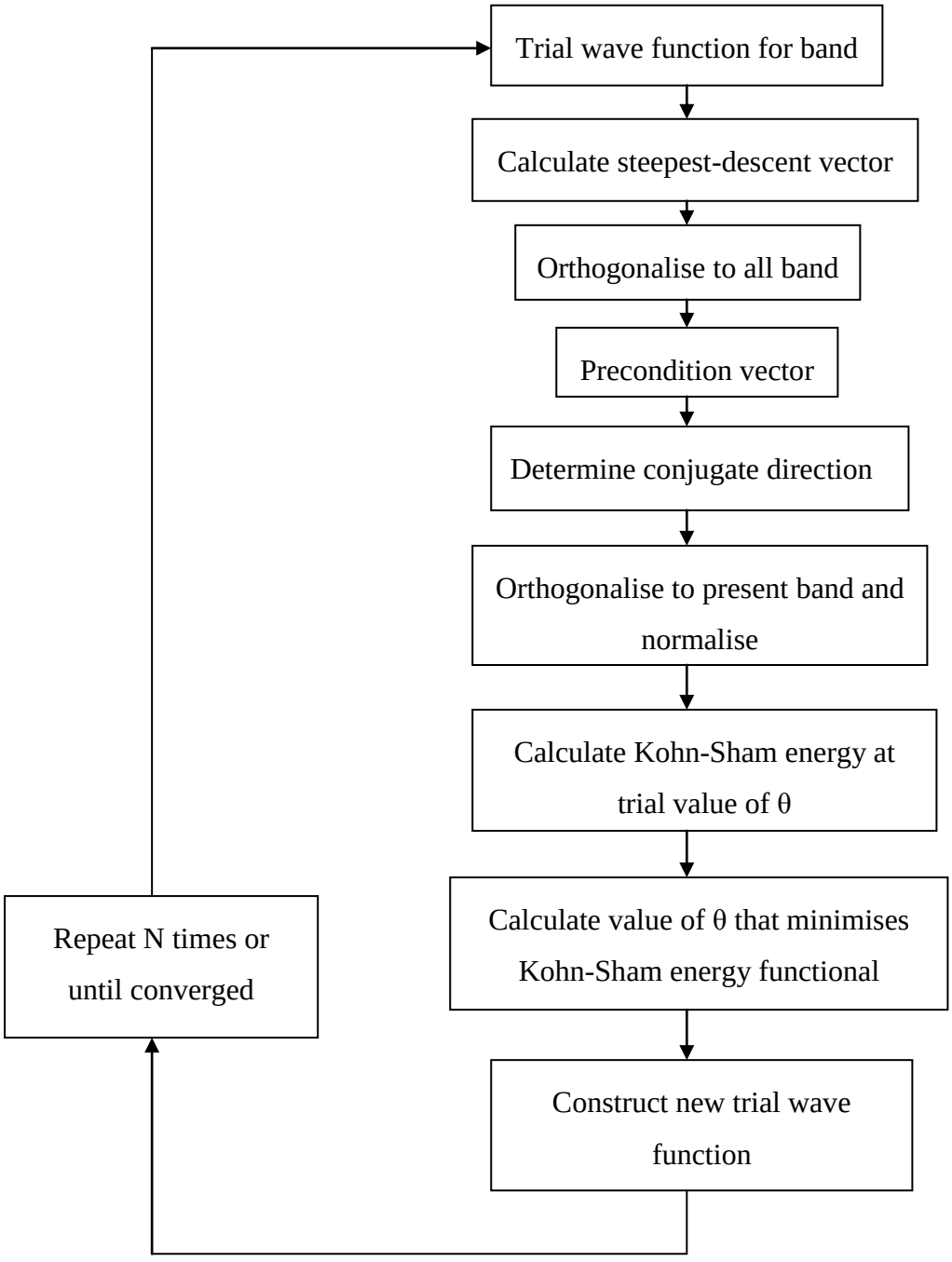

Figure 3.1. Flow diagram for update of a single band in the conjugate-gradient method.[25]

3.3. Vibrational frequency analysis

To calculate a vibrational frequency, a harmonic oscillator is used as a model, which has a time period is given by;

$$T = 2\pi\sqrt{\frac{\mu}{k}} \tag{3.18}$$

Where k is the force constant and μ is the reduced mass. This gives the time period of a bond stretch of a simple diatomic. This equation can be altered to give the time period in cm^{-1} as this is most common unit used for bond stretches and bends.

$$\bar{\upsilon} = \frac{1}{2\pi c}\sqrt{\frac{k}{\mu}} \tag{3.19}$$

Where $\bar{\upsilon}$ is the vibrational frequency. Diagonalisation of the mass-weight hessian matrix will give the force constant indirectly and elements of this matrix are defined as;

$$H_{i,j} = \frac{\delta^2 E}{\delta x_i \delta x_j} \tag{3.20}$$

This can be rewritten by calculating the gradient at a small increment and recalculating the gradient after a decrement and calculating the second derivative from the difference.

$$H_{i,j} = \frac{\left(\frac{\delta E}{\delta x_i}\right)_{+0.5\Delta x_j} - \left(\frac{\delta E}{\delta x_i}\right)_{-0.5\Delta x_j}}{\Delta x_j} \tag{3.21}$$

Due to the matrix being symmetric, it has to be re-defined to reduce errors;

$$H_{i,j} = \frac{1}{2}\left(\frac{\left(\frac{\delta E}{\delta x_i}\right)_{+0.5\Delta x_j} - \left(\frac{\delta E}{\delta x_i}\right)_{-0.5\Delta x_j}}{\Delta x_j} + \frac{\left(\frac{\delta E}{\delta x_j}\right)_{+0.5\Delta x_i} - \left(\frac{\delta E}{\delta x_j}\right)_{-0.5\Delta x_i}}{\Delta x_i}\right) \tag{3.22}$$

Diagonalisation of this matrix gives the force constant.

The matrix has to be mass weighted to for diagonalisation to give a value that can be used to calculate the vibrational frequency with the diagonalisation supplying the value ε which equates to $\sqrt{\frac{k}{\mu}}$,

$$H_{i,j}^{m} = \frac{H_{i,j}}{\sqrt{M_i \cdot M_j}} \tag{3.23}$$

So the vibrational frequencies can be calculated by;

$$\bar{\upsilon}_i = \frac{1}{2\pi c}\sqrt{\varepsilon_i} \tag{3.24}$$

3.4. Nudged Elastic Band method

The Nudged Elastic Band[26,27] (NEB) method is used to find a barrier between any two structures in a reaction co-ordinate by the lowest energy path between then. In this method the reaction path is described by two fixed end points, $\vec{P}_0$ and $\vec{P}_M$. These are separated by a series of points, $\vec{P}_1$,..., $\vec{P}_{M-1}$, each of the points being a structure on the reaction co-ordinate. These structures are connected by harmonic springs, which prevent the structures obtaining the nearest local minimum configuration. However with just the springs the structures tend to move toward the local minima and the get the shape of the barrier wrong. The NEB method solves this by projecting out the perpendicular component of the force from the spring and the parallel component of the force acting on each on the structures. The force on structure i is defined as;

$$F_i = \vec{F}_{i||}^{s} + \vec{F}_{i\perp}^{l} \tag{3.25}$$

Where the parallel component is;

$$F_{i||}^{s} = \left(k_{i+1}\left|\vec{P}_{i+1} - \vec{P}_i\right| - k_i\left|\vec{P}_i - \vec{P}_{i-1}\right|\right)\hat{\eta}_i \tag{3.26}$$

Where k_i is the spring constant between structure *i* and *i-1* and $\hat{\eta}_i$ is the normalised local tangent at structure *i*. $\vec{F}_{i\perp}^{l}$ is the component perpendicular to the tangent $\hat{\eta}_i$ at structure *i*.

One of the considerations to be taken is how the structures on the reaction path are found. In simple cases a linear approach can be used, which changes the structure by a uniform distance between each step and is calculated using Equation 3.27.

$$s_i = s_0 + \frac{i}{N}(s_N - s_0) \tag{3.27}$$

where s_i is the $3N_{atoms}$vector for the position of structure i with s_0 the start structure, s_N the end structure, N the number of atoms in all structures and i the number of structures.

However this fails for more complex systems. Two methods were used to resolve these problems: The first method is called a late centre, which involves treating the whole molecule as a group until a defined point and then splitting an atom off with linear path to study the desired barrier. This is used in this work to study hydrogen atom transfer reactions, which is mostly used with C – H bond activation in methane. The other method is a two group approach[28], which has each group centred on an atom each side of the bond that will break. This is used when the bond is breaking in the middle of the molecule or when the system is complex. The interpolation of the group, G, is defined by the distance to a nominated central atom with the other atoms in the group constrained between the distance in the start structure and in the end structure and moving smoothly between them. The adjustment of the interpolation is calculated by;

$$s_{ij} = s_{j0} + \frac{i}{N}(s_{jN} - s_{j0}) - r_{jci} + \frac{i}{N}(d_{jcN} - d_{jc0})\hat{r}_{jci}, \qquad j \in G \tag{3.28}$$

Where s_{ij} is a three component vector belonging to atom *j* in structure *i*. r_{jci} is a vector between the group centre and atom *j* after the linear interpolation to structure *i* has been preformed. d_{jc0} and d_{jcN} are the distances between the group centre and atom *j* at start and end points.

To calculate the relative reaction co-ordinate, each structure is compared to the start structure and the distance moved, $D_{i,}$ is obtained and divided by the distance moved to get to the end structure from the start structure, $D_{N,}$ to normalise the valves calculated, D_i/D_N.

$$D_i = \sqrt{\sum_{j=1}^{3Nat} (s_{ij} - s_{0j})^2} \tag{3.29}$$

Where s_{ij} is Cartesian co-ordinate *j* in structure *i* for N_{at} atoms.

This reaction co-ordinate is used all barrier plots between a start and end which will be defined for each plot.

3.5. Eigenvector following method

Eigenvector following can be used for two reasons, either to support a transition state (TS) found by vibrational frequency analysis or to follow the eigenvector of a bond stretch to obtain a barrier for cleavage of that bond. Eigenvector following works by producing a series of structures along the eigenvector.

The TS is found by finding a single negative mode that matches with the chemical process that the barrier is showing. The eigenvector of the negative mode will move across the maximum or saddle point showing the shape of the barrier.

Following the eigenvector can be used to follow a bond stretching mode to find a possible maximum or saddle point. This is used on a positive mode at a minimum and if done in both directions will produce a Morse curve with a barrier at the longest extent of the bond as the transferred section of the molecule forms a new stable product.

3.6. Density of States

To analyse the electronic structure for system modelled in VASP, density of states (DOS) per unit energy (E) is used.

$$D = \frac{1}{V} . \frac{N(E, E + \Delta E) - N(E)}{\Delta E} = \frac{1}{V} . \frac{dN}{dE} \tag{3.30}$$

$$D = \frac{1}{V} . \frac{dN_s}{dE} = \frac{1}{2\pi^2} \left(\frac{2me}{\hbar^2} \right)^{3/2} . E^{1/2} \tag{3.31}$$

For a periodic systems the DOS (D) is calculated by the inverse of the volume of the cell (V) multiplied by the differential of the state with respect to the unit energy. The DOS is the number of available states, at 0 K states with energies below the Fermi level are filled and above this they are empty states.

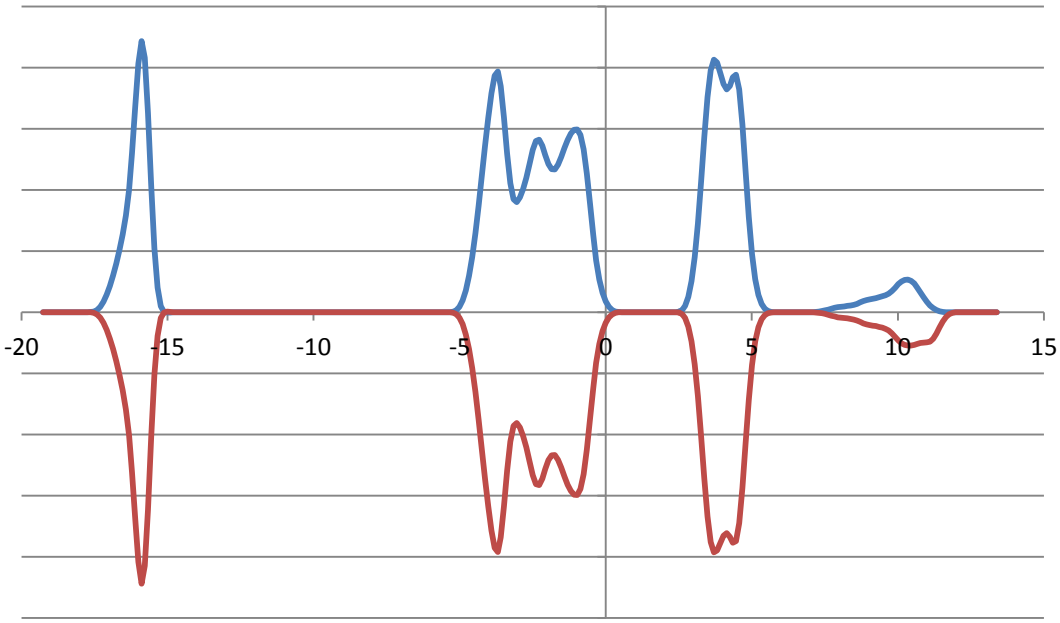

Figure 3.2. Spin unrestricted DOS plot for TiO_2

3.7. Bader Charge Analysis

Calculations in this work use density functional theory which obtains a charge density. Bader[29] devised a method a calculate charges on individual atoms. This is done by dividing the space into regions using surfaces that run though the minima in the charge density, which is a point in a dividing surface that the gradient of the charge density has no component to the normal of that surface. The charge of an ion is obtained by integrating the charge density in a region with a nucleus present and adding appropriate adjacent regions.

The algorithm used in this work was developed by Henkelman *et al.*[30], which is a fast, grid based method for decomposition of the charge density. This method uses steepest ascent trajectories but these are constrained to the grid points and used to define the Bader regions. A grid point is defined as (*i*,*j*,*k*), and from this point a steepest ascent move is made in the direction that maximises the charge density gradient defined as $\nabla\rho$, calculated along the directions $\hat{r}$, using;

$$\nabla\rho(i,j,k)\cdot\hat{r}(di,dj,dk)=\frac{\Delta\rho}{|\Delta\vec{r}|} \tag{3.32}$$

Where *di*, *dj*, *dk* are assigned the values [-1,0,1] but excluding *di* = *dj* = *dk* = 0. The change in charge density is defined as;

$$\Delta\rho = \rho(i + di, j + dj, k + dk) - \rho(i, j, k) \tag{3.33}$$

And the distance is defined as;

$$|\Delta\vec{r}| = |\vec{r}(i + di, j + dj, k + dk) - \vec{r}(i, j, k)| \tag{3.34}$$

Where $\vec{r}(i, j, k)$ is the vector in Cartesian co-ordinates to the grid point (*i*,*j*,*k*), $\vec{r}(di, dj, dk)$ is the steepest ascent step which maximises the positive values of $\nabla\rho(i, j, k)$. When no positive values are found the grid point (*i*,*j*,*k*) can be considered a maximum in the charge density. When this is done for all grid points, the partitioning is complete, all Bader regions are defined and charges on the atoms can be assigned.

3.8. Implementation of VASP

VASP[31,32] (Vienna *ab initio* Simulation Package) was developed by Professor J Hafner and group and has been used to study metal oxides and reactions in and on them. VASP implements DFT using planewaves in a periodic system with projector augmented wave[33,34] (PAW-PP) pseudopotentials.

PAW-PP contains the wave function for the valence electrons and the nodes for the wave function for the core electrons in which the core electrons are kept frozen in the calculation. This is to limit the number of planewaves used to model the system. In this work the cut-off for the planewaves is set to 400 eV.

In VASP the Kohn-Sham equations are solved self-consistently by diagonalisation an iterative matrix and a Broyden[35] mixing method. Generalised Gradient Approximation, GGA functionals are used with both the PBE[9] (Perdew, Burke and Ernzerhof) and RPBE[10] (Revised Perdew, Burke and Ernzerhof) functionals.

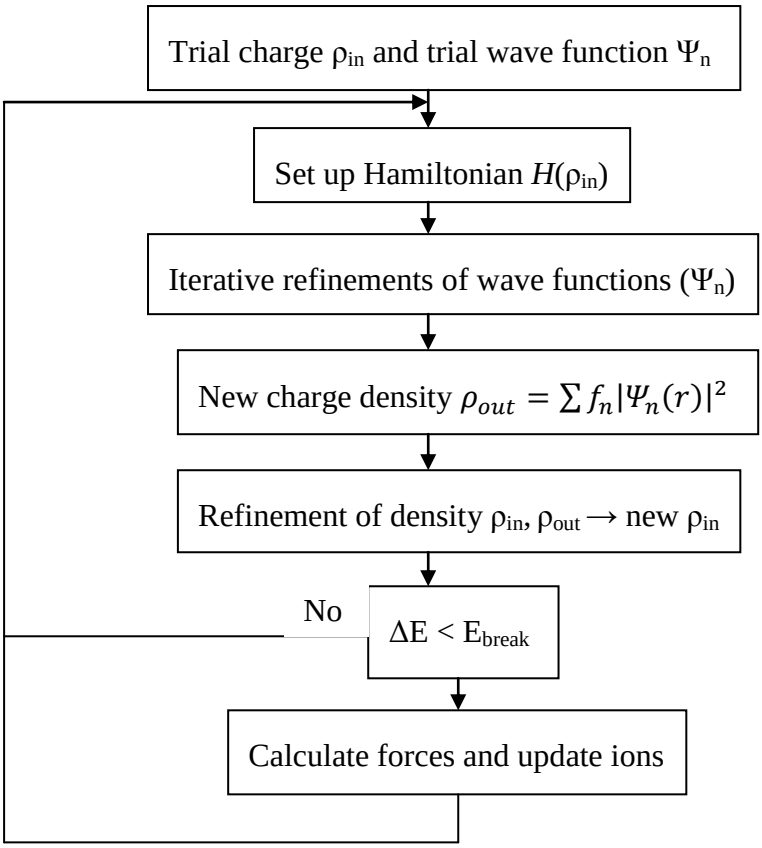

Figure 3.3. Self-consistent scheme

The mixing is used to aid convergence in a DFT calculation. An example of a self-consistent scheme is shown in figure 3.3.

A k-point sampling grid is calculated using a Monkhorst-Pack[36] scheme centred on the Γ-point. The number of k-points in the irreducible Brillouin zone required is dependent on the size of the cell with the cells over a certain size requiring only the Γ-point as the k-points are used in calculated properties in reciprocal space. Several different numbers of k-points are used for this work with 3 × 3 × 1 used for the TiO_2 surfaces, the Γ-point used for the MFI structure and 3 × 3 × 3 is used for the CHA structure.

3.9. Implementation of Gaussian

Gaussian[37] was developed by Professor J. Pople and group and has been used to study molecules and the π orbitals. Gaussian implements DFT and Wavefunction methods with Gaussian basis sets.

Gaussian uses a basis set of Gaussian functions to produce the orbitals. The DFT functionals used in Gaussian are mainly hybrids but GGA and LDA functionals can be used, As basis sets are used, hybrid functionals are fast and do not have the disadvantages that have are present in the VASP code with planewaves. B3LYP was used for all Gaussian calculations in this work.

3.10. Energy calculations

The binding energy of an adsorbing molecule can be calculated by several methods. The binding energies in this work are calculated by subtracting the energy for both the slab (a surface or bulk whichever is appropriate for the given case) and the energy of the isolated adsorbate in the same cell as the slab (without the slab present) from the energy of the molecule and the slab in the same cell.

$$E_b = E_{ab} - (E_{slab} - E_{abs}) \tag{3.35}$$

Where E_b is the binding energy, E_{ab} is the total energy of the adsorbate and slab in the same cell, E_{slab} is the total energy of the slab and E_{abs} is the total energy of the isolated adsorbate.

The surface energy can be calculated when a surface has been cut to ascertain the stability of the surface, which is done by subtracting the bulk energy from the slab energy and dividing by twice the surface area.

$$E_s = \frac{E_{slab} - E_{bulk}}{2s} \tag{3.36}$$

$$s = |a||b| \sin\gamma \tag{3.37}$$

Where E_s is the surface energy, E_{slab} is the total slab energy, E_{bulk} is the total bulk energy, s is the surface area, a and b are the lengths of the a and b vector is the cell and γ is the angle between a and b.

3.11. Lattice parameters

The lattice parameters are taken from the experimental values which come from the Materials Studio database or from reference papers if not present. In this work this was done for PdO as it was not in the materials studio database. The lattice parameters are optimised for the DFT functional used by finding cell volume with the lowest energy, which is done by plotting a series of energies for a known cell volumes. These are fitted using a quadratic function to obtain a minimum energy and cell volume. An example plot of energy against cell volume is shown in figure 3.4.

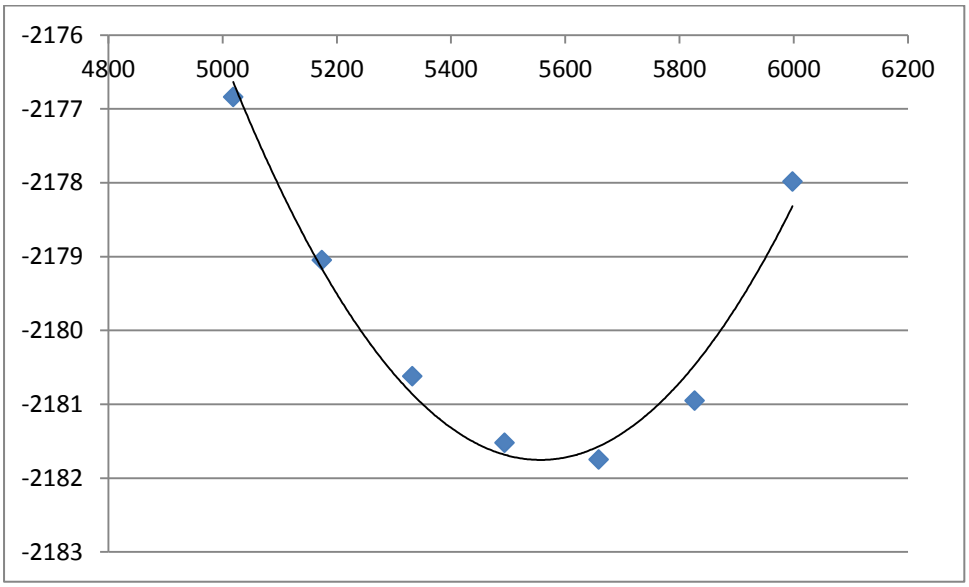

Figure 3.4. A plot of energy against cell volume in a MFI structure zeolite.

The bulk modulus can be calculated to be compared with experimental results to check if the result is reliable. The bulk modulus is calculated using volume multiplied by the second differential of the energy with respect to the volume.

$$K = V\frac{\partial^2 E}{\partial V^2} \tag{3.38}$$

where K is the bulk modulus, E is the energy and V is the cell volume.

3.12. Calculating U values with TiO_2

TiO_2 like most transition metal oxide has errors in DFT calculations due to it being a strongly correlated system. Originally a U value of 4.2 eV was chosen from work by Morgan and Watson[38–40] and is used for other studies[41–43], which is used is Chapter 4

sections 2 and 3. The U value is applied to the Ti d band to correct the error in the electronic structure of TiO_2. However when a Au_{10} cluster adsorbs of the rutile TiO_2(110) surface, the Au_{10} fails to wet the surface, which would be expected as ADF-STEM results show Au clusters wetting the surface. A different U value has been used by Nishi *et al.*[44], with the U values applied to both the Ti d band and O p band with a value of 8 eV applied to both.

The U values were tested by setting the U value on the Ti d band with a series of integer values between 0 eV and 9 eV with the J value set to 0 eV as only the difference U – J matters. The U value of O p band (U_p) is tested in the same way but for each of the Ti d band U values (U_d). This is done for both the anatase and rutile structures of TiO_2. To obtain the correct U value, the band gap is compared to the experimental found band gap for both the rutile[45] at 3.05 eV and anatase[46] at 3.20 eV. A plot of band gap against U value is shown in figure 3.5.

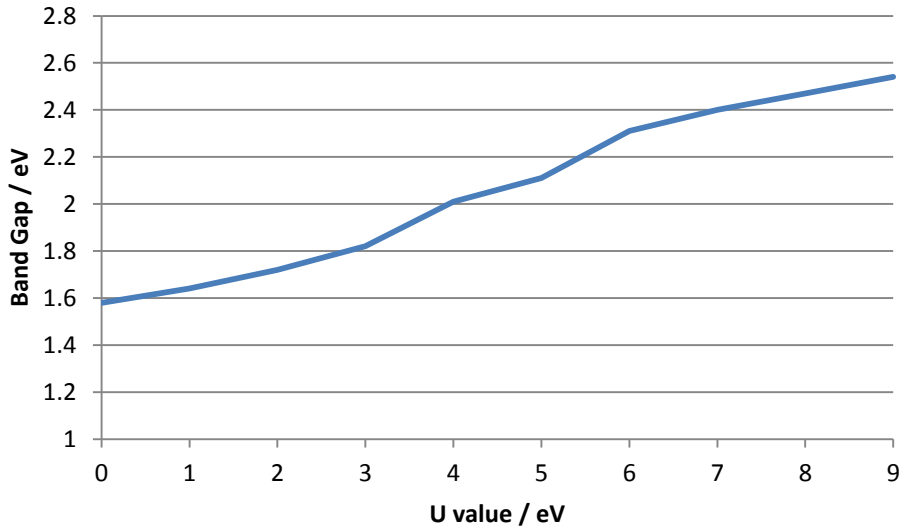

Figure 3.5. A plot of band gap against U value.

This plot shows the band gap increasing linearly with U value but the band gap is still less than would be expected from the experiment results. The experimental band gap would be achieved at a U value of approximately 13 eV assuming a linear extrapolation but this would be an unphysical U value. Figure 3.6. shows the DOS plot for U = 0, 3, 6 and 9 with the U value only applied to the Ti d band.

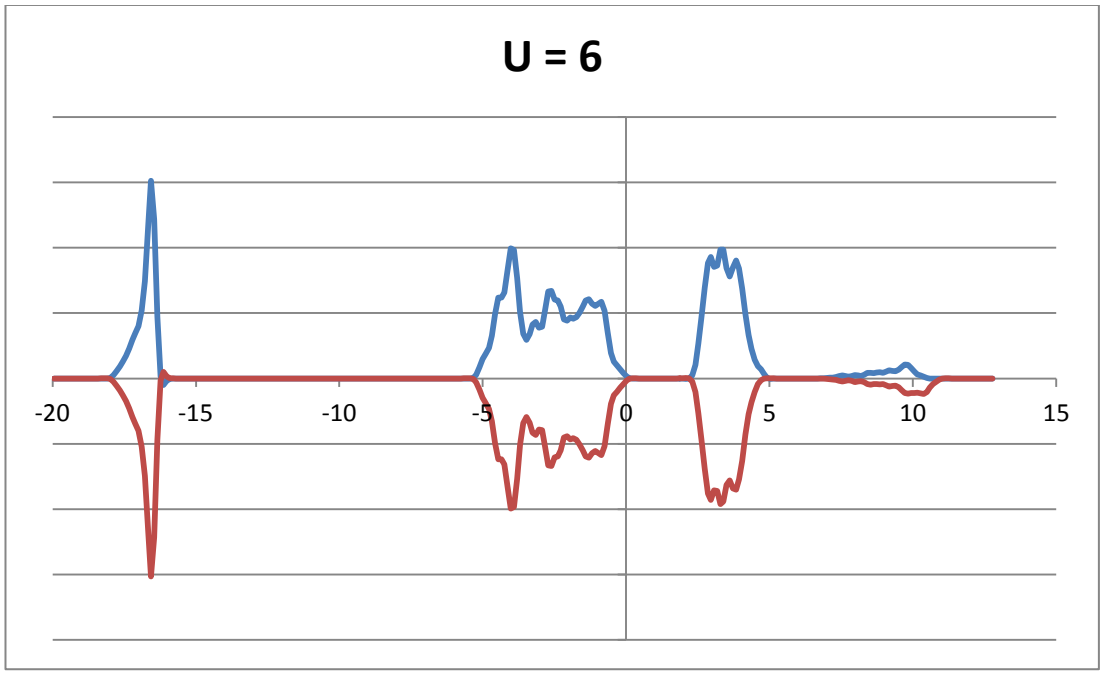

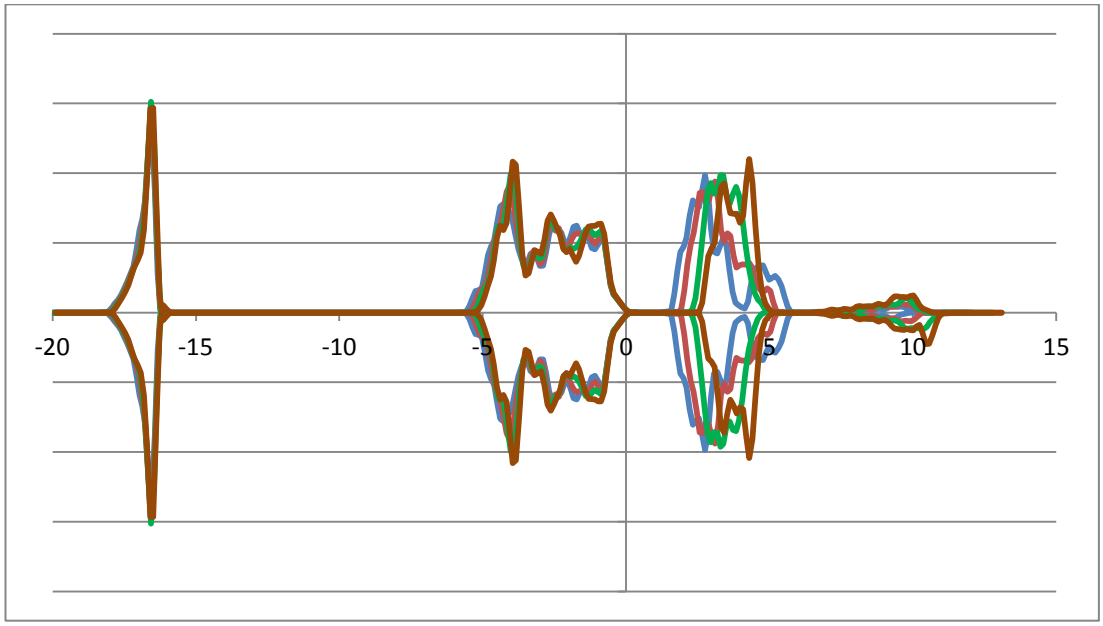

Figure 3.6. DOS plots for TiO_2 rutile structure with the U value of 6 and for U values of 0 (blue), 3 (red), 6 (green) and 9 (brown) overlaid.

The DOS plots show a shift in Ti d band and the O p band, which the partial DOS for U = 0 and 9 with the O 2p band shown in figure 3.7. and the Ti 3d band is shown in figure 3.8. This indicates that the DOS changes significantly with U value with the largest effect above the Fermi level.

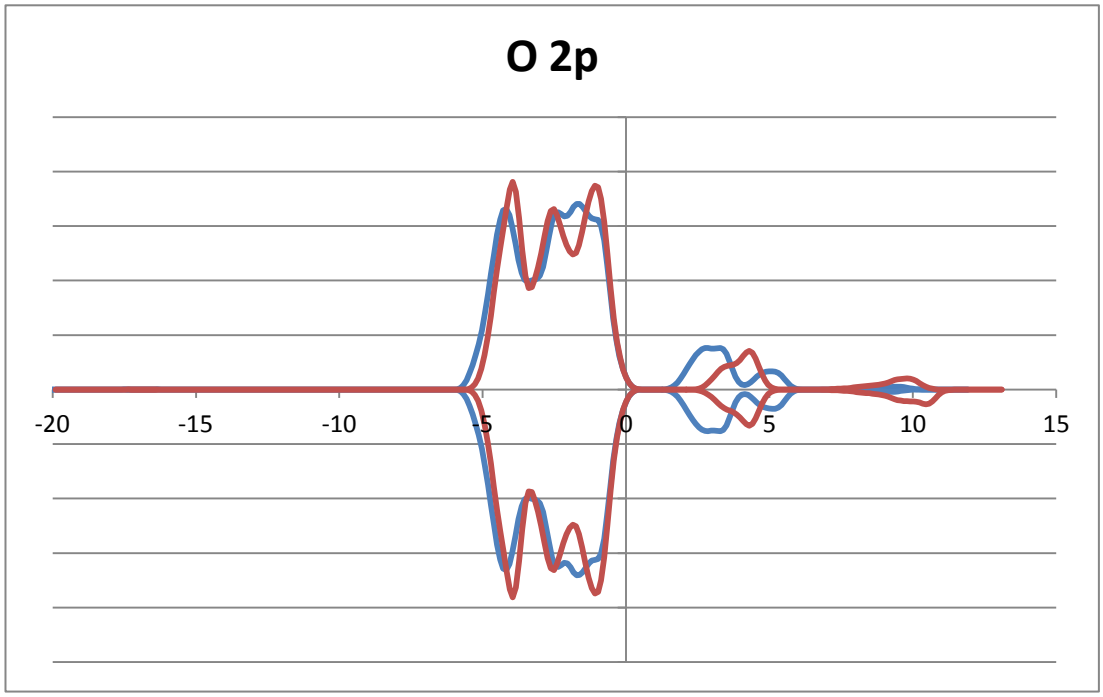

Figure 3.7. DOS plots for TiO_2 rutile structure with the U value of 0 (blue) and 9 (red) for the O 2p band.

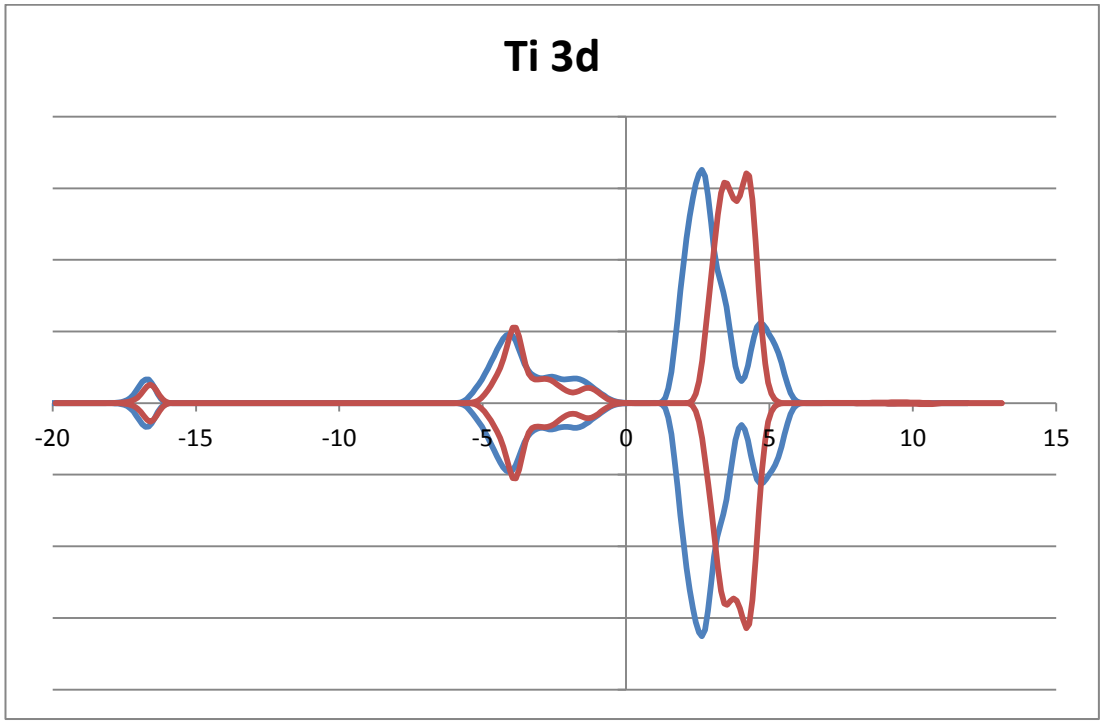

Figure 3.8. DOS plots for TiO_2 rutile structure with the U value of 0 (blue), 9 (red) for the Ti 3d band.

When the U_p value is applied to O p band for each U_d, the band gap increases with both U_d and U_p value with a value 8 for both U values showing the best band gap for both rutile and anatase structure at 2.94 eV for the rutile and 3.15 eV for the anatase. The DOS are shown in figure 3.9. for the rutile structure and 3.10. for the anatase structure.

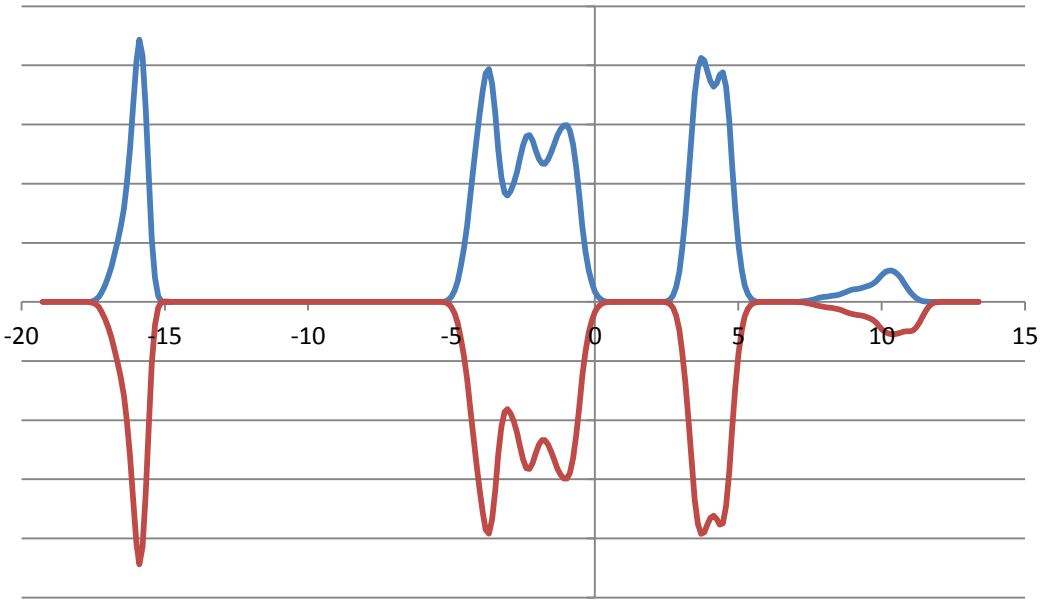

Figure 3.9. DOS plot of rutile structure with $U_d = 8$ and $U_p = 8$.

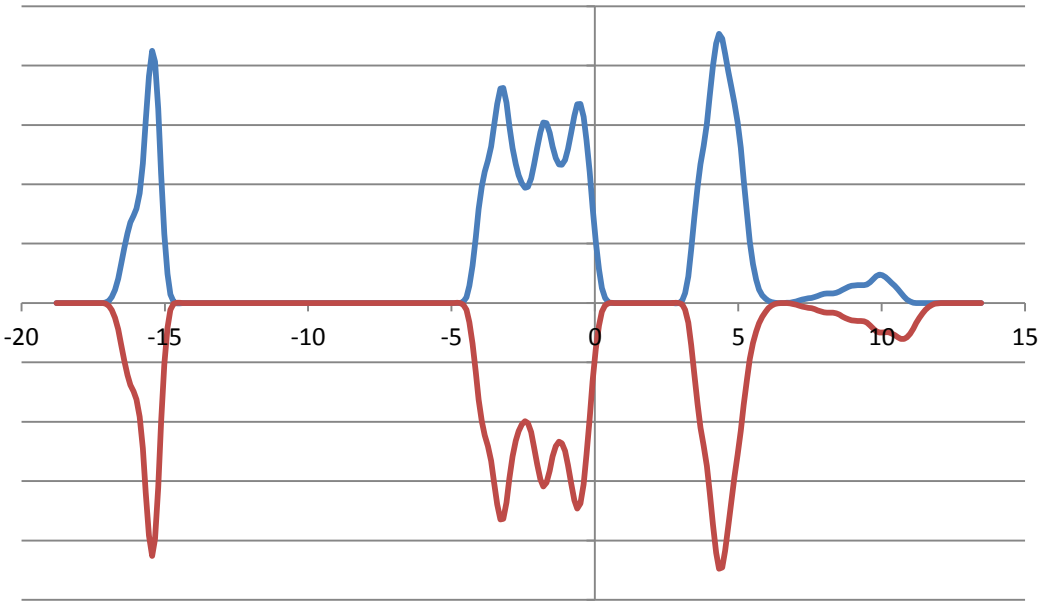

Figure 3.10. DOS plot of anatase structure with $U_d = 8$ and $U_p = 8$.

3.13. PdO bulk and calculating the U value

There have been several examples of work to show the bulk unit cell of this material[47–49] and my work has used these. The PdO bulk unit cell is triclinic made up of Pd at (0, 0, 0) and (0.5, 0.5, 0. 5) and O at (0, 05, 0.25) and (0, 0.5, 0.75). (see figure 3.11).

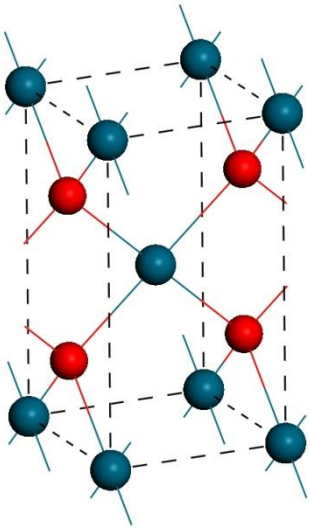

Figure 3.11. Bulk structure of PdO.

The parameters used in this were 9×9×9 k-points with a planewave cutoff of 400 eV. Initially the geometry was optimised with GGA-DFT with the PBE function. A number of other standard and hybrid methods were used in a single point calculation as some of these are very computational expensive. The methods tested were PBE0, HSE06, B3LYP and GGA+U. These were compared to the standard PBE using the DOS with the experiment band gap expected to be around is approximately 0.7eV[50]. Using the PBE function the unit cell had dimensions a = 3.075 and c = 5.538 which is 5.6% different from the experimentally derived structure.

The following DOS are all single point calculations from the bulk unit cell of PdO optimised with the PBE functional. This was done due to the PBE0 and HSE06 calculation requiring a large amount of computer time for the just the single point, making a geometry optimisation too computationally expensive.

The calculations that were performed are as follows PBE0, HSE06, B3LYP, PBE, PBE+U_d (U_d = 0-9) and PBE+U (U_d = 6,7 , U_p = 0-9). PBE+U is a GGA+U using the

PBE functional. U_d is the GGA+U applied to the 4d orbital on Pd, U_p is the GGA+U applied to the 2p orbital on O.

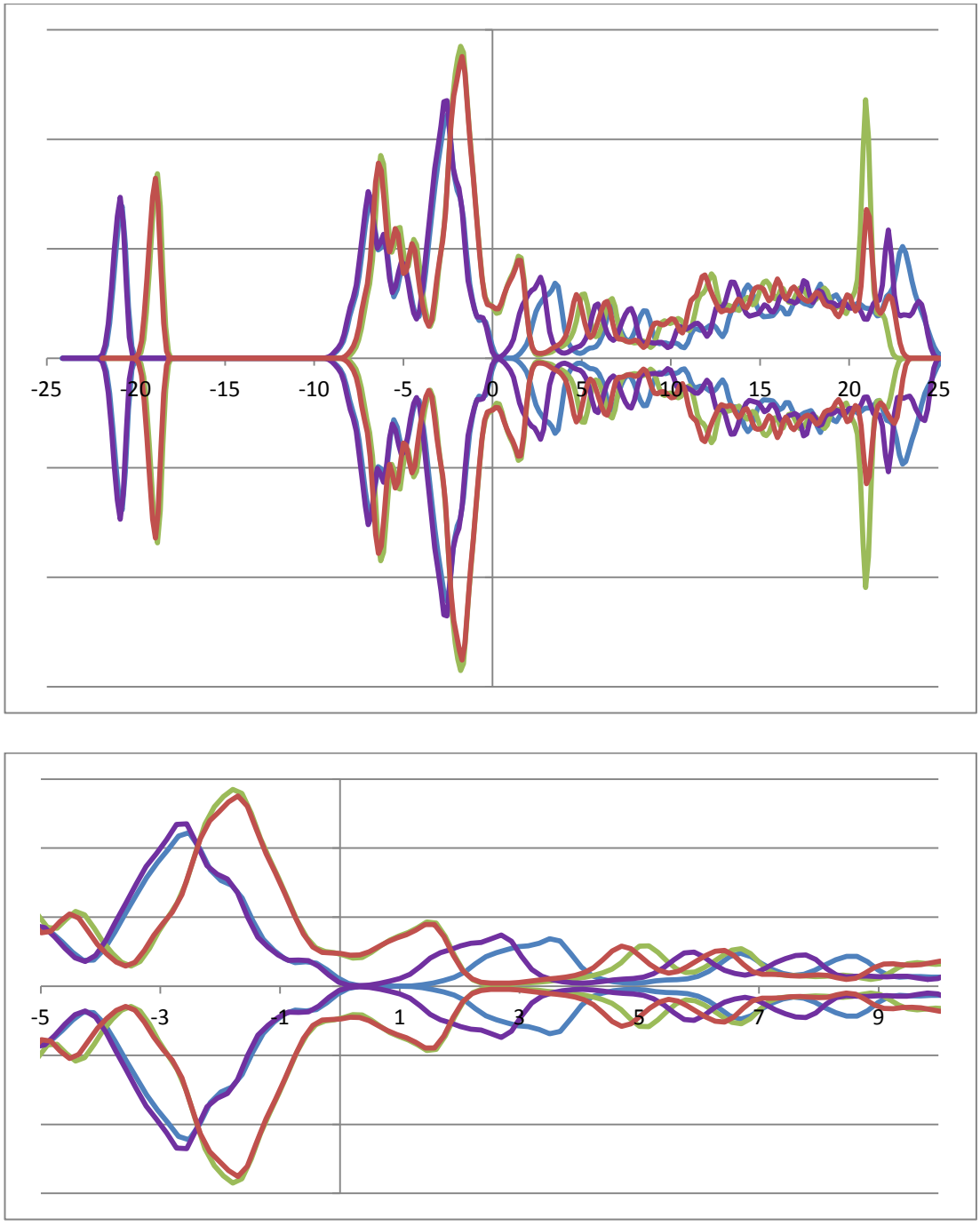

Figure 3.12 DOS plot for PdO bulk comparing PBE (red line), B3LYP (green line), HSE06 (purple line) and PBE0 (blue line).

Initial work found PBE geometry to be within 5.6% to the experimental result.[47–49]

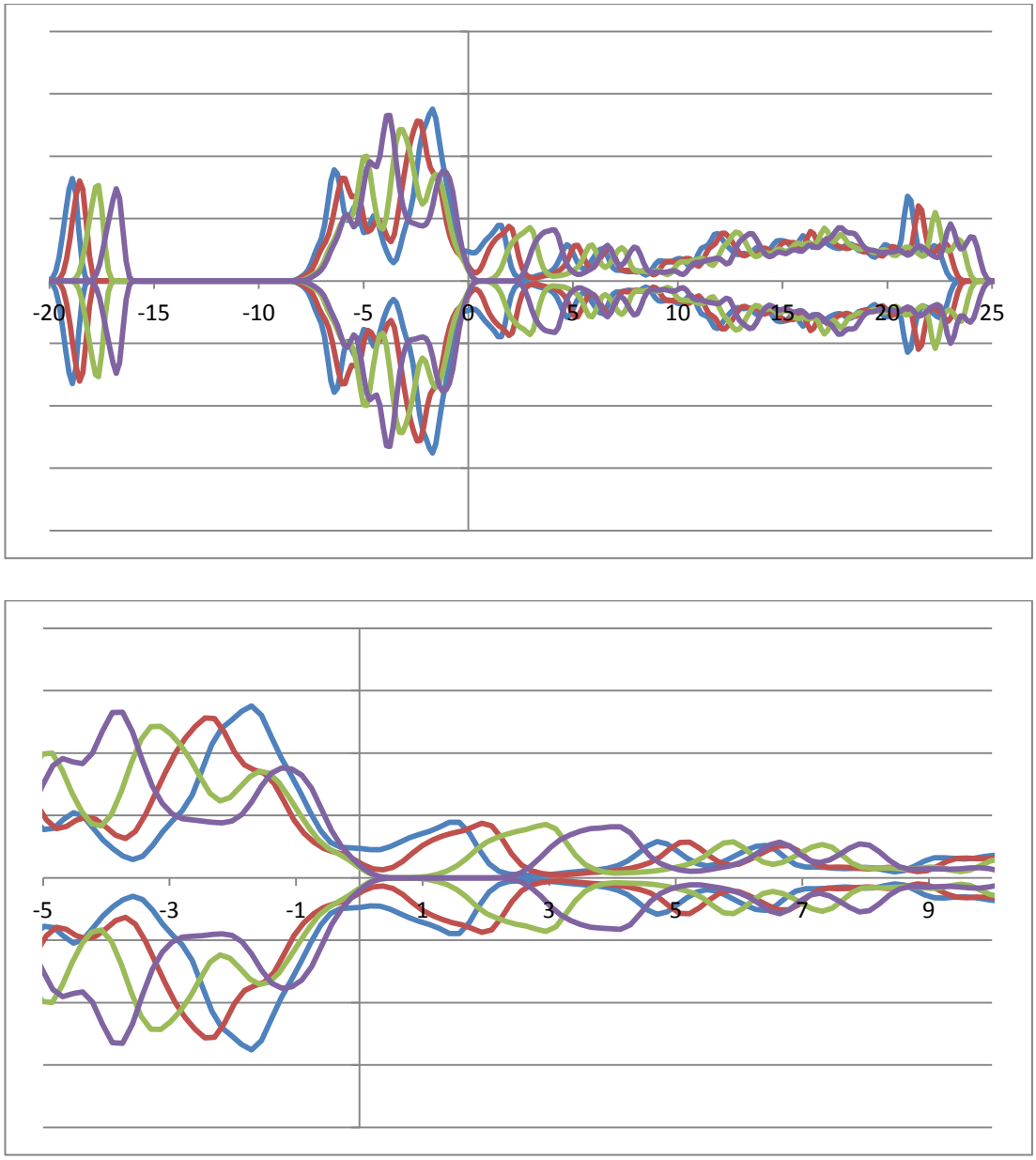

Figure 3.13. DOS plot for PdO bulk using PBE+U method with U = 0 (blue line), 3 (red line), 6 (green line) and 9 (purple line).

PBE failed to model the band gap and shows a metallic like state, the same being true for the B3LYP hybrid functional. PBE0 and HSE06 both show a band gap with HSE06 showing the approximately correct 0.7 eV band gap.

A GGA+U with a PBE functional were employed to give a better answer than PBE functional in standard DFT without the high computational cost. A series of U values were implemented between 0 and 9 with an interval of 1. It was found that the band gap increases linearly with U_d value for the values tested. This however is not the case with U_p as only negligible changes to the character of the DOS were seen.

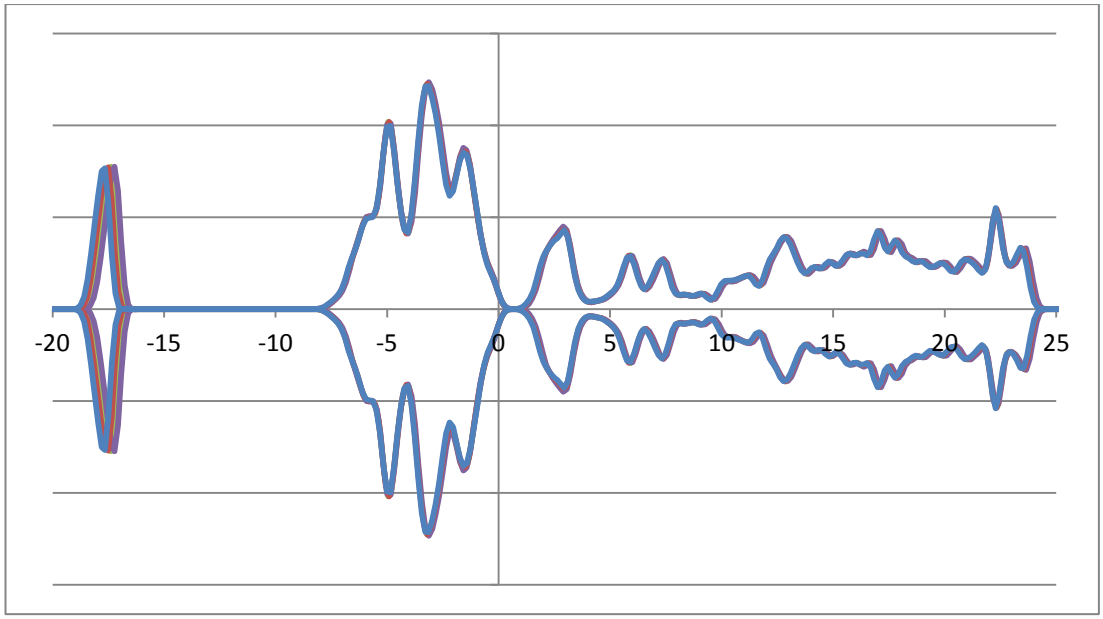

Figure 3.14. DOS plot for PdO bulk using PBE+U method with U_d = 6 and U_p = 0 (blue line), 3 (red line), 6 (green line) and 9 (purple line).

Whereas the U_d can affect the size of the band gap, it also changes the character of the DOS from the PBE0 and PBE functionals.

3.14. Analysis of electronic states

These methods were developed to have a different way of looking at the reactivity and electronic structure of the materials studied with the code VASP. Plane-wave basis sets can be used to obtain the density of states which will give the same information via the band filling and centre of the band on the valence electrons.

Method

The density of states is analysed in two ways[51–53]. The first is calculating the first moment of the states, sometimes referred to as the band centre. The second is calculating the fraction the band is filled, this also can be used on α and β spins.

Band Centre

The energy of the band centre is calculated using equation 3.39.

$$E_c = \frac{\int_{-\infty}^{\infty} B.E.dE}{\int_{-\infty}^{\infty} B.dE} \tag{3.39}$$

This calculates the band centre E_c using the normalised integral of the density of state, B is the band energies for the DOS, which multiplied by the energy of each state, E over all energies used by valance states. Equation 3.39 has an exact solution but as the form of the equation applying to the DO is only given as a series of values a numeric solution is required as shown as equation 3.40.

$$E_b = \frac{\sum_{N}^{N_k} \frac{\Delta E}{2} (N_s + (N + \Delta E)_s).E}{\sum_{N}^{N_k} \frac{\Delta E}{2} (N_s + (N + \Delta E)_s)} \tag{3.40}$$

The integrals are solved by a composite trapezium rule, N_s is the number of states in the DOS at each E being the energy of those states starting with the lowest and increasing by ΔE to obtain the next N_s until N_k is reached at which it is considered that no states are beyond this, ΔE is set by VASP with the NEDOS tag.

This method of integration is used because the DOS is produced as a series of finite points so using a higher order method would increase the size of ΔE lowering the accuracy as only a finite number are known.

Band Filling

The band filling, E_b is calculated by equation 3.41.

$$E_b = \frac{\int_{-\infty}^{E_f} B.dE}{\int_{-\infty}^{\infty} B.dE} \tag{3.41}$$

In equation 3.40 the integral of the DOS is calculated up to the Fermi level, E_f and normalised over all energies. The Fermi level is set to zero in the plots. As before the DOS is defined numerically so a numerical method has to be used shown in equation 3.42.

$$E_b = \frac{\sum_N^{N_f} \frac{\Delta E}{2} (N_s + (N + \Delta E)_s)}{\sum_N^{N_k} \frac{\Delta E}{2} (N_s + (N + \Delta E)_s)} \tag{3.42}$$

Electron Spin

With a spin polarised calculation separate DOS are calculated for α and β spins so both the band centre and band filling can be obtained for each spin independently. With the band filling the difference between fillings of α and β spins gives the number of unpaired electrons, using the number of electron in the band, N_e and the number of unpaired electrons can be found, shown in equation 3.43.

$$N_u = |\alpha - \beta|.\frac{N_e}{2} \tag{3.43}$$

Benchmarking

Benchmarking is required to see how analysis can work and test for the systems it is required for. The systems to be tested are bulk transition metals as these are simple bulk metals with known electronic structures and have a known series of results.

Small molecules as with metal lattices have known electronic structures and can be compared to molecular orbitals produced by an orbital based program.

Benchmarking with bulk 1st and 2nd row transition metals

	s ratio	p ratio	d ratio	s electron	p electron	d electron	tot electron	POTCAR value
Sc	0.938	0.491	0.236	1.877	2.944	2.357	7.178	3
Ti	0.460	0.154	0.226	0.920	0.922	2.260	4.102	4
V	0.456	0.253	0.305	0.913	1.519	3.046	5.478	5
Cr	0.461	0.273	0.386	0.923	1.635	3.855	6.413	6
Fe	0.425	0.246	0.568	0.851	1.475	5.676	8.002	8
Co	0.426	0.238	0.671	0.851	1.426	6.710	8.987	9
Ni	0.399	0.228	0.771	0.798	1.369	7.707	9.874	10
Cu	0.387	0.208	0.882	0.774	1.249	8.825	10.848	11
Zn	0.394	0.131	0.798	0.787	0.788	7.985	9.560	12

Table 3.1. Electronic structures of 1st row transition metals, Mn is not included as bulk structure was not readily available.

The band filling is compared to the number of electrons in the valance band stated in the setup pseudopotential file on the calculations shown in table 3.1. and table 3.2. With ratio of filling used to calculate the expected number of electrons in each orbital. Most calculations produced the number of valence electrons with reasonable accuracy with a few cases with larger errors occur. 1st row transition metals show the best fit with the exception of Zn which the d-band DOS of which is shown in Figure 3.15. This is most likely due to the d-band peak for the expected full band being very sharp allowing for a large error than expected and a large amount of low states beyond the Fermi level.

	s ratio	p ratio	d ratio	s electron	p electron	d electron	tot electron	POTCAR value
Y	0.988	0.949	0.226	1.976	5.696	2.257	9.930	11
Zr	0.807	0.814	0.202	1.614	4.884	2.017	8.515	12
Nb	0.048	0.972	0.525	0.096	5.831	5.247	11.174	11
Mo	0.017	0.335	0.440	0.034	2.011	4.402	6.447	6
Tc	0.039	0.844	0.495	0.079	5.064	4.954	10.096	13
Ru	0.429	0.256	0.593	0.858	1.537	5.931	8.326	8
Rh	0.753	0.472	0.774	1.506	2.830	7.741	12.078	9
Pd	0.323	0.169	0.799	0.645	1.013	7.993	9.651	10
Ag	0.340	0.165	0.912	0.680	0.991	9.124	10.794	11
Cd	0.405	0.120	0.847	0.810	0.721	8.470	10.001	12

Table 3.2. Electronic structures of 2nd row transition metals.

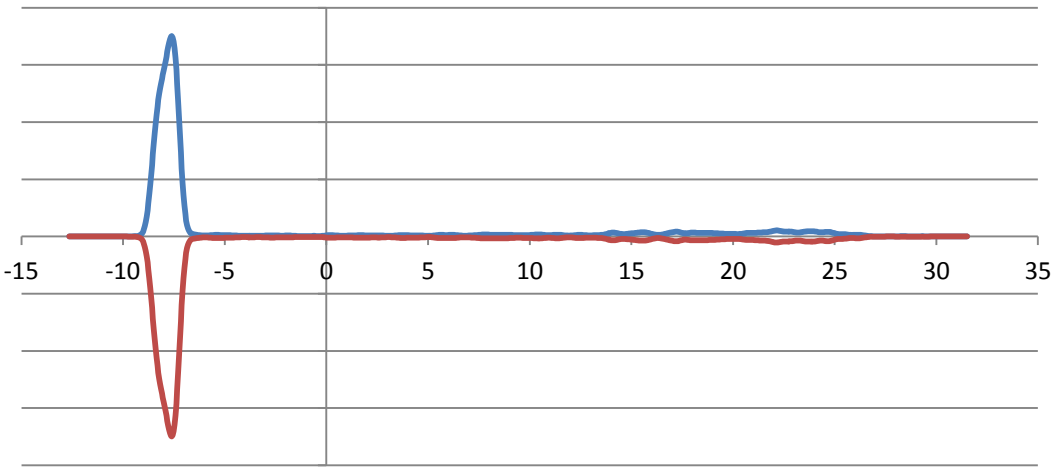

Figure 3.15. Density of states of d-band of bulk Zn metal.

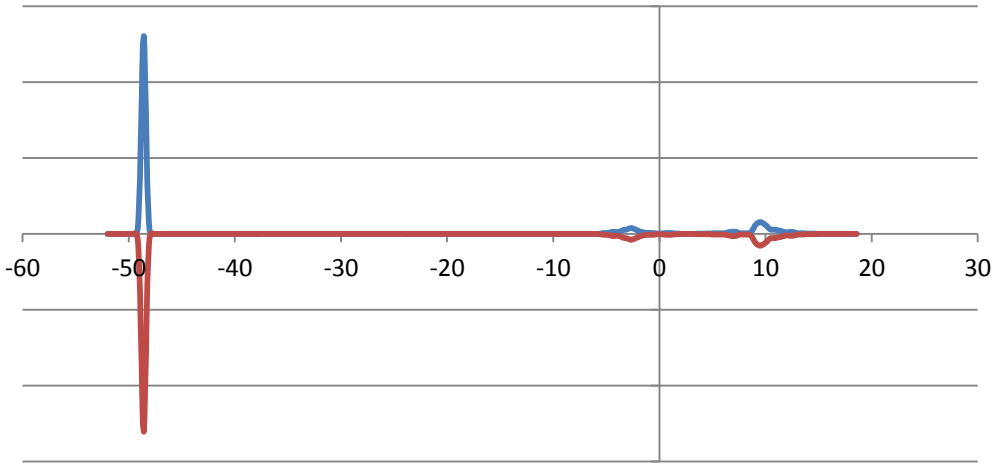

Figure 3.16. DOS of s-band of bulk Zr metal showing extra filled 3s orbital.

The states at higher energy are most likely present because of the next d-band exchanging character with it. This is shown with several other elements. Y and Zr show two orbitals within the s band with the lower s orbital at -48 eV which would be expected to be the core rather the valence electrons. This results in the wrong number of electrons being calculated in the s band if only one s orbital is taken into account, shown in Figure 3.16. In the case of Sc bulk metal, the model produces too many electrons but this can be seen the DOS plots shown in Figures 3.17., 3.18. and 3.19.

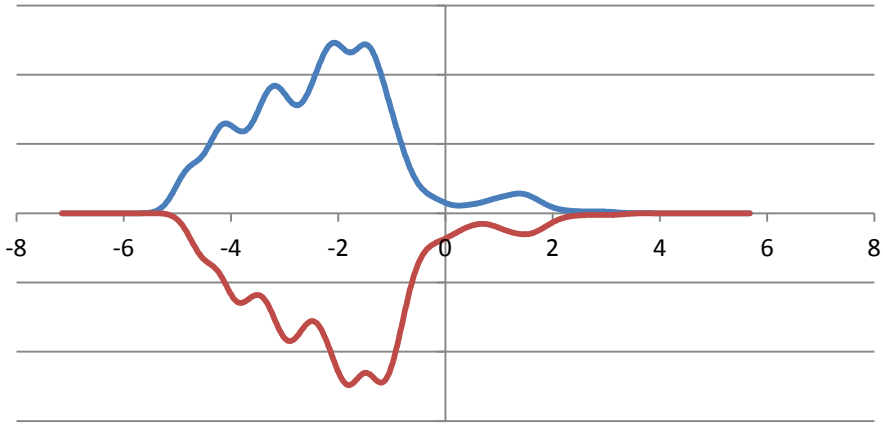

Figure 2.17. DOS of s-band of bulk Sc metal

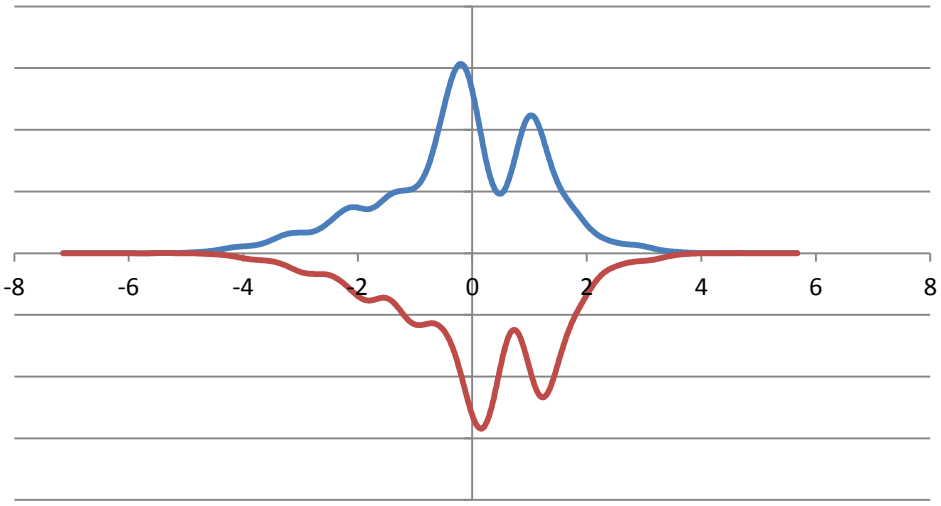

Figure 3.18. DOS of p-band of bulk Sc metal

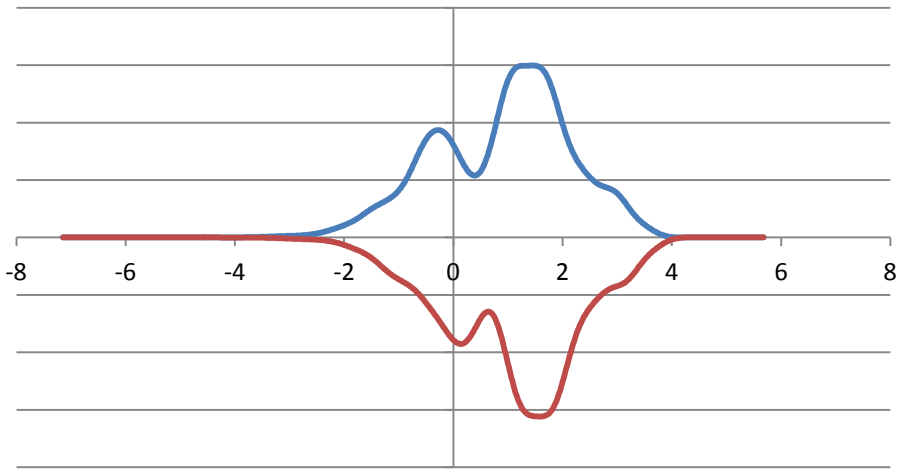

Figure 3.19. DOS of d-band of bulk Sc metal

The other part of the code gives the centre of the band, which can show the reactivity of the metal, in this case the bulk material. The d-band is looked at in particular as this would show how reactive the metal is compared to other bulk metals. These are shown in table 3.3. and table 3.4.

Metals	s / eV	p /eV	d / eV
Sc	3.357	6.849	2.815
Ti	3.518	7.578	2.585
V	4.185	6.864	3.302
Cr	3.705	7.046	2.368
Fe	3.879	7.291	1.435
Co	3.506	7.441	0.557
Ni	3.945	7.317	0.118
Cu	3.149	6.708	-1.472
Zn	7.302	14.841	2.766

Table 3.3. s, p and d band centre for 1st row transition elements. Mn is not including for the same reason as before.

Metals	s / eV	p / eV	d / eV
Y	-38.253	-20.681	1.350
Zr	-33.754	-19.228	3.413
Nb	1.377	-28.051	0.252
Mo	9.666	5.077	0.892
Tc	11.337	-28.884	1.409
Ru	3.919	7.467	0.431
Rh	-2.710	1.016	-1.881
Pd	5.168	8.396	-0.618
Ag	3.177	6.495	-3.233
Cd	2.477	8.486	-5.725

Table 3.4. s, p and d band centre for 2nd row transition elements.

The band centre shows how close the centre of the orbital is to the Fermi level with the results closer to it having the most states near the Fermi level. This would indicate the most reactive element in the metallic state, with the result closest to zero.

As expected certain groups are more reactive than other such as Pd being more reactive than Ag.

Benchmarking with small molecules

In addition to the bulk metal isolated molecule have been studied. These are used to check if singlet, doublet and triplet states are correctly produced.

Molecule	**Spin**
C_2H_6	-0.180
CH_3	1.181
CH_4	0.013
Cl_2	0.125
F_2	-0.194
H_2O_2	-0.274
HCl	0.441
HF	0.589
N_2	-0.001
NH_3	-0.308
O_2	0.724
C_4H_9OOH	-0.517
C_4H_9OO	1.337
C_4H_9O	1.208

Table 2.5. Spin of set of molecules some neutral and some radical**.**

The spin values show a large error as it would be expect to produce no spin for methane, ethane and any system with no dipole but this can be affected by the value set in the MAGMOM tag, shown in table 3.6.

MAGMOM value (C, 4H)	**Spin**
Not set	0.796
0 0 0 0 0	0.013
1 1 1 1 1	0.719
1 -1 -1 -1 -1	-0.627

Table 3.6. Spin on methane under different starting parameters.

References

1. R. G. Parr and Y. Weitao, *Density-Functional Theory of Atoms and Molecules*, Oxford University Press, USA, 1994.

2. R. Dronskowski and R. Hoffmann, *Computational Chemistry of Solid State Materials*, Wiley, 2008.

3. J. Hafner, *Journal of Computational Chemistry*, 2008, **29**, 2044–2078.

4. R. M. Martin, *Electronic Structure: Basic Theory and Practical Methods*, Cambridge University Press, 2004.

5. P. Hohenberg and W. Kohn, *Phys. Rev.*, 1964, **136**, B864–B871.

6. W. Kohn and L. J. Sham, *Phys. Rev.*, 1965, **140**, A1133–A1138.

7. D. M. Ceperley and B. J. Alder, *Phys. Rev. Lett.*, 1980, **45**, 566–569.

8. A. Zunger and J. P. Perdew, *Phys. Rev. B*, 1981, **23**, 5048.

9. J. P. Perdew, K. Burke, and M. Ernzerhof, *Phys. Rev. Lett.*, 1996, **77**, 3865–3868.

10. B. Hammer, L. B. Hansen, and J. K. Norskov, *Phys. Rev. B*, 1999, **59**, 7413–7421.

11. J. P. Perdew, J. A. Chevary, S. H. Vosko, K. A. Jackson, M. R. Pederson, D. J. Singh, and C. Fiolhais, *Phys. Rev. B*, 1992, **46**, 6671–6687.

12. V. Fock, *Zeitschrift für Physik A Hadrons and Nuclei*, 1930, **61**, 126–148.

13. J. C. Slater, *Phys. Rev.*, 1951, **81**, 385–390.

14. A. D. Becke, *The Journal of Chemical Physics*, 1993, **98**, 1372–1377.

15. J. Harris, *Phys. Rev. A*, 1984, **29**, 1648–1659.

16. C. Adamo and V. Barone, *Chemical Physics Letters*, 1998, **298**, 113–119.

17. C. Adamo and V. Barone, *The Journal of Chemical Physics*, 1999, **110**, 6158–6170.

18. J. Heyd, G. E. Scuseria, and M. Ernzerhof, *The Journal of Chemical Physics*, 2003, **118**, 8207–8215.

19. J. Heyd, G. E. Scuseria, and M. Ernzerhof, *The Journal of Chemical Physics*, 2006, **124**, 219906.

20. P. J. Stephens, F. J. Devlin, C. F. Chabalowski, and M. J. Frisch, *Journal of Physical Chemistry*, 1994, **98**, 11623–11627.

21. S. L. Dudarev, G. A. Botton, S. Y. Savrasov, C. J. Humphreys, and A. P. Sutton, *Physical Review B*, 1998, **57**, 1505–1509.

22. M. P. Teter, M. C. Payne, and D. C. Allan, *Phys. Rev. B*, 1989, **40**, 12255–12263.

23. D. M. Bylander, L. Kleinman, and S. Lee, *Phys. Rev. B*, 1990, **42**, 1394–1403.

24. P. Pulay, *Chemical Physics Letters*, 1980, **73**, 393.

25. C. Payne, M. P. Teter, D. C. Allen, T. A. Arias, and J. D. Joannopoulos, *Review of Modern Physics*, 1992, **64**, 1045.

26. G. Mills, H. Jonsson, and G. K. Schenter, *Surface Science*, 1995, **324**, 305–337.

27. G. Mills and H. Jónsson, *Phys. Rev. Lett.*, 1994, **72**, 1124–1127.

28. A. Thetford, G. J. Hutchings, S. H. Taylor, and D. J. Willock, *Proceedings of the Royal Society A: Mathematical, Physical and Engineering Sciences*, 2011, **467**, 1885–1899.

29. R. F. W. Bader, *Atoms in Molecules: A Quantum Theory*, Oxford University Press, USA, 1994.

30. G. Henkelman, A. Arnaldsson, and H. Jónsson, *Computational Materials Science*, 2006, **36**, 354–360.

31. G. Kresse and J. Hafner, *Phys. Rev. B*, 1994, **49**, 14251–14269.

32. G. Kresse and J. Hafner, *Phys. Rev. B*, 1993, **47**, 558–561.

33. G. Kresse and D. Joubert, *Phys. Rev. B*, 1999, **59**, 1758–1775.

34. P. E. Blöchl, *Phys. Rev. B*, 1994, **50**, 17953–17979.

35. D. D. Johnson, *Phys. Rev. B*, 1988, **38**, 12807–12813.

36. H. J. Monkhorst and J. D. Pack, *Phys. Rev. B*, 1976, **13**, 5188–5192.

37. M. J. Frisch, G. W. Trucks, H. B. Schlegel, G. E. Scuseria, M. A. Robb, J. R. Cheeseman, J. A. Montgomery Jr., T. Vreven, K. N. Kudin, J. C. Burant, J. M. Millam, S. S. Iyengar, J. Tomasi, V. Barone, B. Mennucci, M. Cossi, G. Scalmani, N. Rega, G. A. Petersson, H. Nakatsuji, M. Hada, M. Ehara, K. Toyota, R. Fukuda, J. Hasegawa, M. Ishida, T. Nakajima, Y. Honda, O. Kitao, H. Nakai, M. Klene, X. Li, J. E. Knox, H. P. Hratchian, J. B. Cross, V. Bakken, C. Adamo, J. Jaramillo, R. Gomperts, R. E. Stratmann, O. Yazyev, A. J. Austin, R. Cammi, C. Pomelli, J. W. Ochterski, P. Y. Ayala, K. Morokuma, G. A. Voth, P. Salvador, J. J. Dannenberg, V. G. Zakrzewski, S. Dapprich, A. D. Daniels, M. C. Strain, O. Farkas, D. K. Malick, A. D. Rabuck, K. Raghavachari, J. B. Foresman, J. V Ortiz, Q. Cui, A. G. Baboul, S. Clifford, J. Cioslowski, B. B. Stefanov, G. Liu, A. Liashenko, P. Piskorz, I. Komaromi, R. L. Martin, D. J. Fox, T. Keith, M. A. Al-Laham, C. Y. Peng, A. Nanayakkara, M. Challacombe, P. M. W. Gill, B. Johnson, W. Chen, M. W. Wong, C. Gonzalez, and J. A. Pople, .

38. B. J. Morgan and G. W. Watson, *Surface Science*, 2007, **601**, 5034–5041.

39. B. J. Morgan and G. W. Watson, *The Journal of Physical Chemistry C*, 2009, **113**, 7322–7328.

40. B. J. Morgan and G. W. Watson, *Journal of Physical Chemistry C*, 2010, **114**, 2321–2328.

41. S. Chrétien and H. Metiu, *Journal of Physical Chemistry C*, 2011, **2**, 4696–4705.

42. C. Di Valentin, G. Pacchioni, and A. Selloni, 2009, 20543–20552.

43. E. Finazzi, C. Di Valentin, G. Pacchioni, and A. Selloni, *The Journal of chemical physics*, 2008, **129**, 154113.

44. S.-G. Park, B. Magyari-Köpe, and Y. Nishi, *Physical Review B*, 2010, **82**, 1–9.

45. D. C. Cronemeyer, *Phys. Rev.*, 1952, **87**, 876–886.

46. C. J. Howard, T. M. Sabine, and F. Dickson, *Acta Crystallographica Section B*, 1991, **47**, 462–468.

47. J. Rogal, K. Reuter, and M. Scheffler, *Phys. Rev. B*, 2004, **69**, 75421.

48. D. B. Rogers, R. D. Shannon, and J. L. Gillson, *Journal of Solid State Chemistry*, 1971, **3**, 314–316.

49. K. C. Hass and A. E. Carlsson, *Physical Review B*, 1992, **46**, 4246–4249.

50. M. A. Khan, R. Ahuja, S. Auluck, and B. Johansson, *Physical Review B*, 1994, **50**, 2128–2132.

51. J. R. Kitchin, J. K. Norskov, M. A. Barteau, and J. G. Chen, *The Journal of Chemical Physics*, 2004, **120**, 10240–10246.

52. A. Ruban, B. Hammer, P. Stoltze, H. L. Skriver, and J. K. Norskov, *Journal of Molecular Catalysis A: Chemical*, 1997, **115**, 421–429.

53. B. Hammer and J. K. Norskov, *Surface Science*, 1995, **343**, 211–220.

4. Supported Au and Pd catalysts.

The direct synthesis of H_2O_2 and the oxidation of methane can be studied on isolated and oxide supported Au clusters. In this chapter, the adsorption and dissociation of the reactants (CH_4, H_2, O_2, H_2O_2) on isolated Au_{10} clusters will be discussed, together with catalytic reaction mechanisms. TiO_2 surfaces will be investigated with adsorbed H_2O_2 and up to a monolayer of H_2O, which is the experimental solvent and the interactions of CH_4 and H_2O_2 with Au_{10} supported on TiO_2 will be studied. Finally, the effect of changing the DFT+U parameters on the calculated properties of the TiO_2 surface will be discussed. All unless otherwise stated are coloured Au in yellow, Pd in blue, C in grey, O in red and H in white.

4.1. Isolated Au_{10}

0.5 nm diameter clusters are found to be active for supported Au catalysts for CO oxidation. For example, the group of C. Kiely[1] has used ADFSTEM to show bilayer clusters of this size, containing approximately 10 atoms, are active for CO oxidation and a combined experimental and theoretical study[2] has given insight into the mechanism and the energetics of different small [3]cluster sizes. The small size of the cluster means calculations on the isolated clusters are computationally inexpensive, and they can supported on oxide surfaces without requiring large unit cells using periodic boundary conditions.

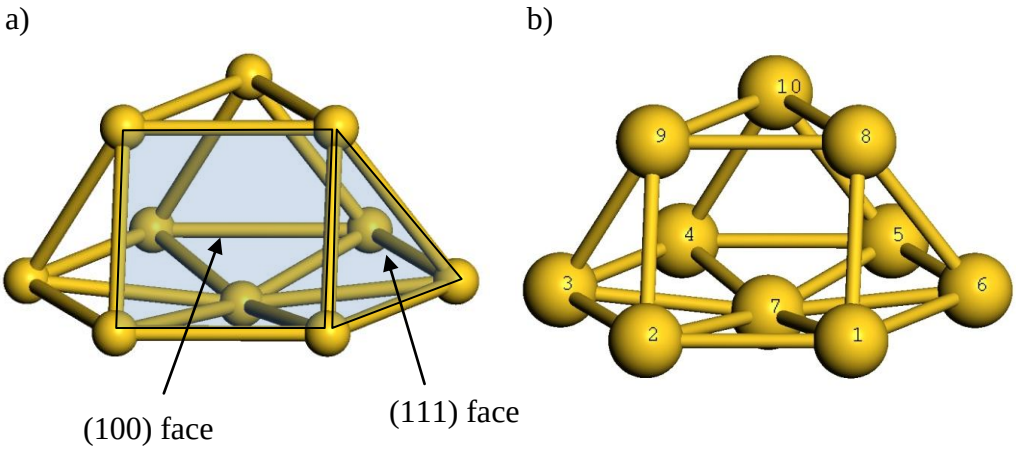

Figure 4.1. Au_{10} cluster showing a) highlighted faces with miller indexes, and b) labelled Au atoms.

The Au_{10} cluster is obtained from the fcc bulk structure of Au. It is cut from two (111) index planes with 7 atoms in one plane and 3 atoms in the other plane. These are arranged in a [7,3] configuration as shown in Figure 4.1. Au_{10} has three (100) faces and four (111) faces assuming that the layer with the 7 atoms is in contact with the support and so not available to adsorbates. The cluster has C_{3v} symmetry with the C_3 axis through atom 7 and the (111) face of atoms 8, 9, and 10 as labelled in figure 4.1.1. and $3\sigma_v$ between a (100) face and the opposite (111) face.

The structure in Figure 4.1. was optimised using the RPBE functional but a similar geometry is obtained using the PBE functional. When the structure is optimised, the atom in the 7 position repositions out of the plane away from the bulk of the cluster. The average Au – Au distance between nearest neighbours is 2.79 Å, which is shortened compared to the optimised bulk Au lattice nearest neighbour distance of 2.98 Å.

The d-state PDOS shows a similar result for the Au_{10} cluster and the bulk Au unit cell as shown in figure 4.2. The bulk Au unit cell and the Au_{10} cluster both have the highest occupied states about 1 eV below the Fermi level, E_{fermi}. The d-band for the Au bulk is wider than that for the Au cluster. Both PDOS have been normalised to show on the same plot.

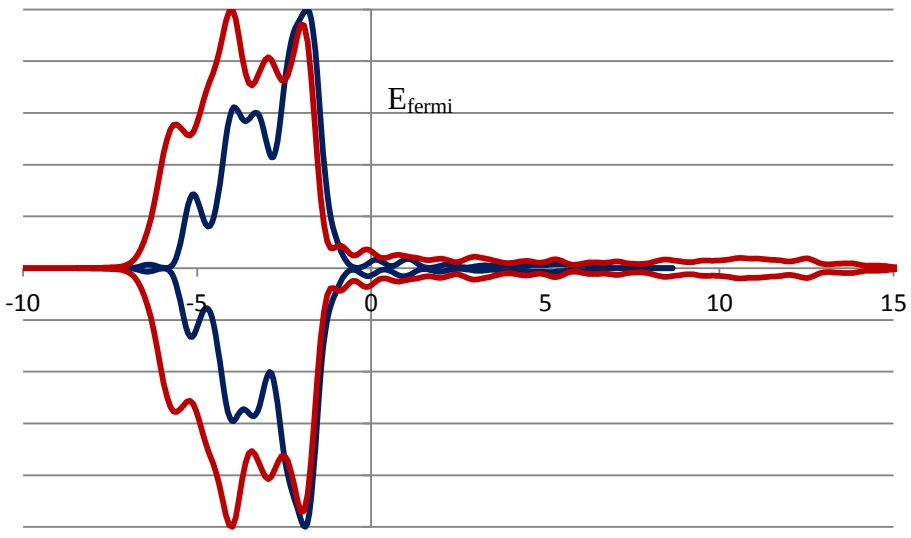

Figure 4.2. Density of states of d-band of an isolated Au_{10} cluster. The blue line is for the Au_{10} cluster and the red line is for the Au bulk.

The Bader charges on the cluster as shown in Table 4.1. has the base of the cluster (atoms 1 – 6) with small negative charges, and the top (atoms 8 – 10) and central (atom 7) with positive changes. Atoms 2 and 8 don't fit with this and have the opposite changes to the rest of the same symmetry identical positions.

Atom Number	Charge in electron charge
1	-0.0465
2	0.004
3	-0.0253
4	-0.0091
5	-0.0309
6	-0.0251
7	0.0989
8	-0.0113
9	0.0341
10	0.0113

Table 4.1. Bader Charges of Au atoms in an Au_{10} cluster position labelled with numbers from figure 4.1.

CH_4

CH_4 shows a negligible interaction with the Au_{10} cluster. CH_4 has an adsorption energy of -5 kJ mol^{-1} and moves away from the cluster to a final position at about 3 Å away from the nearest Au atom during geometry optimisation and would be expected to have a low interaction energy at this distance but at closer distance the adsorption becomes more unfavourable.

C-H bond cleavage can be studied by the NEB method. The end points of the barrier with CH_4 in a local minimum and CH_3 and H adsorbed to the cluster in another local minimum are shown in Figure 4.3. The poor interaction of CH_4 is confirmed by the molecule and the cluster having no charge transfer between them, which is found by Bader analysis. With CH_3 and H, the lone hydrogen has a Bader charge of -0.61e, the CH_3 has a Bader charge of -0.17e and the cluster in this case has a Bader charge of

0.78e. This means the hydrogen is partially hydride in nature. The cluster can be considered to be Au_{10}^{+} so the cluster has an overall positive charge and all the atoms are in the range between -0.5e and 0.4e. The Au atoms in positions 1 and 6 have the highest positive charges (1; 0.38e, 6; 0.40e) due to the CH_3 attached to atom 6 and H bridging between the two. The Au – C distance between the cluster and methyl is 2.10 Å and Au – H distances are 1.72 Å and 1.98 Å. This with the Bader charge information shows a bond must exist between the Au_{10} cluster and both the methyl and the hydrogen atom but no bond exists between the methyl and hydrogen atom due to the molecule having to be negatively charged which would be highly unfavourable.

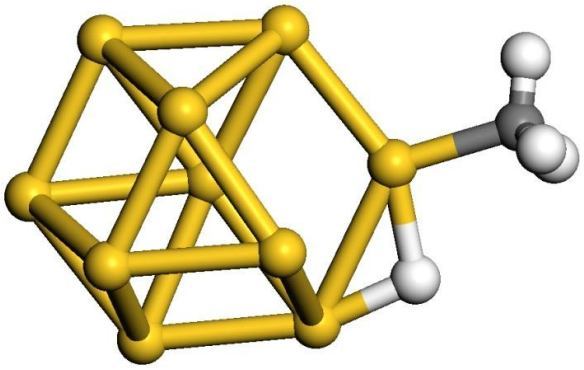

Figure 4.3. Au_{10} cluster with a hydrogen atom and a methyl group. Au is yellow, C is grey and H is white.

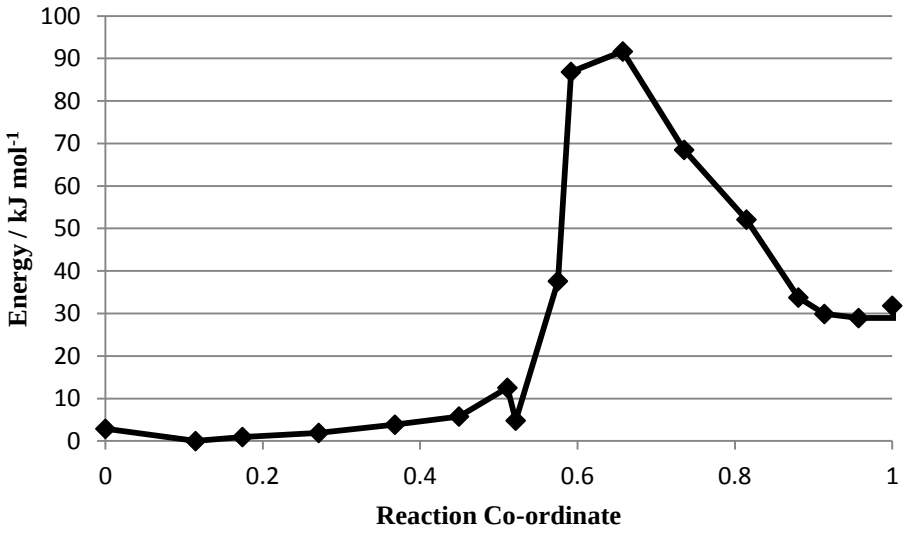

Figure 4.4. Reaction co-ordinate of cleavage of C-H bond in CH_4 on Au_{10} cluster.

The C – H bond cleavage reaction barrier shown in Figure 4.4. has a barrier of 92 kJ mol^{-1} proceeding from CH_4 to CH_3 but only 60 kJ mol^{-1} in the reverse direction. These are both large barriers so the reaction would be slow. CH_3 and a hydrogen atom has an adsorption energy of +37 kJ mol^{-1} on the base of the cluster but +95 kJ mol^{-1} on the top. The d-band centre shows a shift of 0.25 eV further from the Fermi level for the dissiocated CH_3 and H atom adsorbed on the cluster compared to CH_4 and the isolated cluster so more energy would required to activate further molecules on the Au cluster.

H_2

H_2 shows no interaction with the Au_{10} cluster. H_2 has a binding energy of +4 kJ mol^{-1} and moves away from the cluster to a final position at about 3 Å away from the nearest Au atom during geometry optimisation. It would be expected to have a negligible interaction energy at this distance but at closer distance the adsorption becomes more unfavourable.

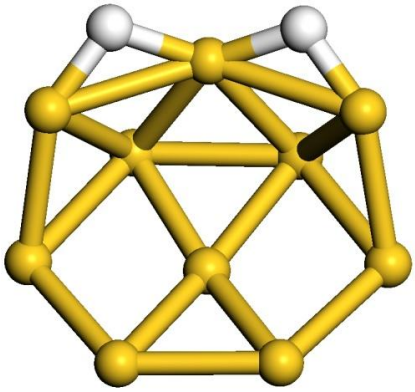

Figure 4.5. Au_{10} cluster with two hydrogen atoms. Au is yellow and H is white.

H_2 can be cleaved into two hydrogen atoms on the Au_{10} cluster with a binding energy of -82 kJ mol^{-1}. H_2 has a 0.42e charge from Bader analysis at 3Å away from the nearest Au atom. This is compared to hydrogen atoms at 1.73 Å from the Au_{10} cluster shown in figure 4.5. These have a charge of -0.60e and -0.81e for each hydrogen atom. This would indicate the hydrogen atoms are bound to the cluster and are hydride in nature. The barrier to H_2 cleavage is 56 kJ mol^{-1} and the reverse barrier is 142 kJ mol^{-1} as shown in figure 4.6.

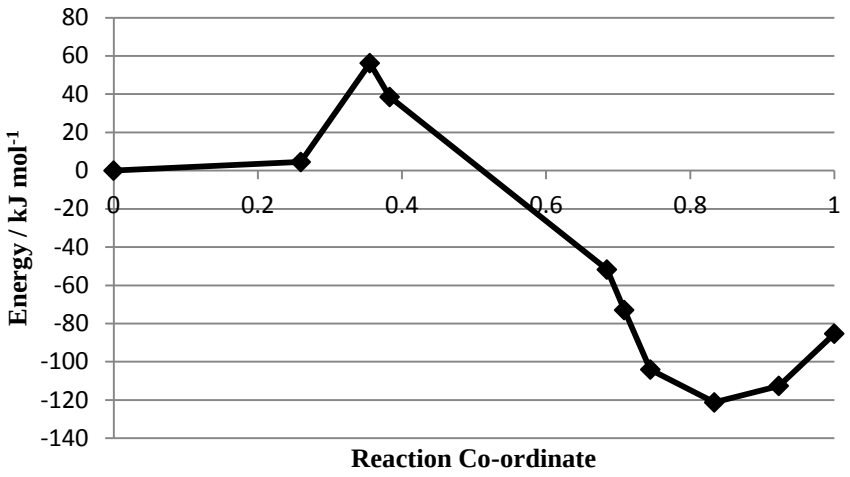

Figure 4.6. Barrier for cleavage of H_2 to produce two hydrogen atoms.

The d-band centre shows a shift from the Fermi level of 0.64 eV between adsorbed H_2 and two hydrogen atom adsorbed which would indicate a reduction in activity of the Au_{10} cluster.

O_2

O_2 will adsorb around the base on the cluster with a binding energy of -49 kJ mol^{-1}, a Au – O bond length of 2.1 Å and an O – O bond distance at 1.33 Å. The O – O distance increases from 1.25 Å found for an isolated O_2, which would indicate a superoxide species. The Bader analysis has O_2 with a charge of -0.64e which further supports the idea that the O_2 is a superoxide. The spin density of the O_2-Au_{10} system shows a change from the triplet state found for ground state O_2 and a diagram of this is shown in figure 4.7.

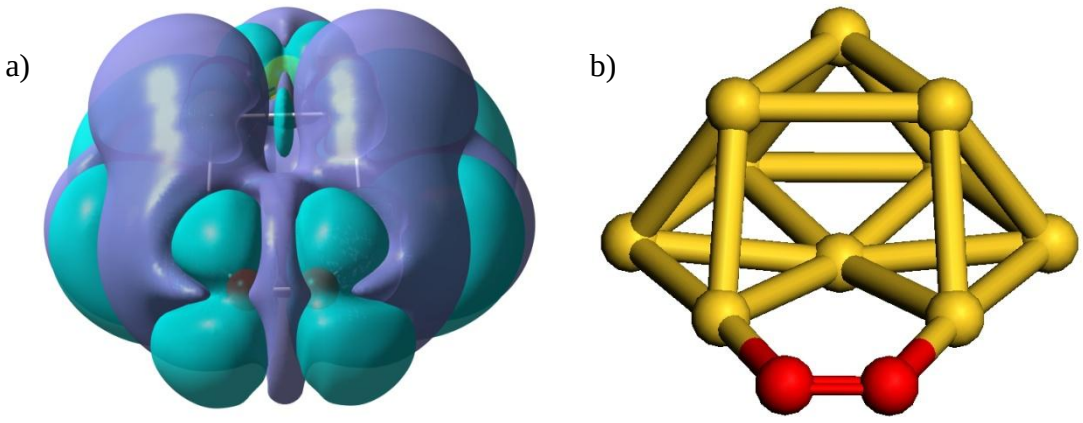

Figure 4.7. O_2 adsorbed on Au_{10} cluster a) spin density with an isosurface value of 4×10^{-5} e $Å^{-3}$, b) diagram to show positions of atoms. Au is yellow and O is red.

H_2O_2

H_2O_2 cleaves at HO – OH when in close proximity to the Au_{10} cluster to create 2 hydroxyls. This would indicate that the cluster has donated an electron to H_2O_2 into the LUMO which has a node in the HO-OH bond resulting in the cleavage of the bond, which is shown in figure 4.8. This has a highly favourable adsorption energy of -237 kJ mol^{-1} with reference to the isolated Au_{10} cluster and H_2O_2, shown in figure 4.9.

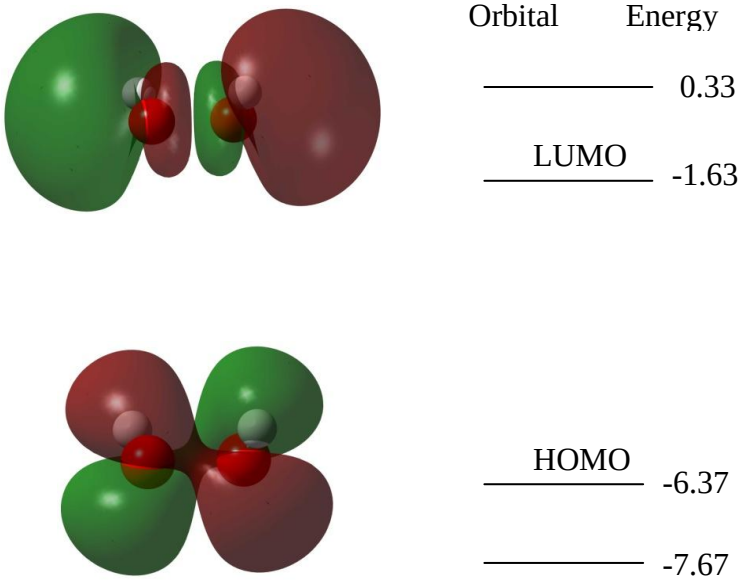

Figure 4.8. The HOMO and LUMO energy levels of H_2O_2 calculated at the B3LYP/6-31G(d,p) level. O is red and H is white.

H_2O_2 dissociation only occurs around the base of the cluster with the (100) face having the most favourable energy, the (111) face having an adsorption energy of -228 kJ mol^{-1} and between the two faces an adsorption energy of -209 kJ mol^{-1}. The charges on the OH groups found by Bader analysis are -0.44e and -0.41e with the Au_{10} cluster having a charge of 0.85e. Over the 3-atom layer (111) surface of the cluster no cleavage occurs and there is low adsorption energy of +6 kJ mol^{-1}. This is comparable to H_2O_2 at 3 Å from the nearest Au atom in the cluster which has an adsorption energy of -16 kJ mol^{-1}, both exhibiting no electron donation. The HO-OH bond can be cleaved on the top but this has a barrier of 46 kJ mol^{-1} and 194 kJ mol^{-1} to form H_2O_2 from two hydroxyls.

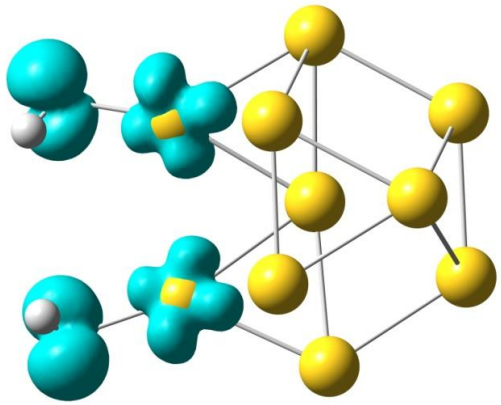

Figure 4.9. The spin density of two hydroxyls bound to Au_{10} cluster with an isosurface value of 4×10^{-4} e $Å^{-3}$, Au is yellow, O is red and H is white.

Additional H_2O_2 can be added to the Au_{10} cluster with up to 2 more molecules cleaving spontaneously around the base with an average adsorption energy per extra H_2O_2 of -226 kJ mol^{-1}. Images of these are shown in figure 4.10. The adsorption energies for additional H_2O_2 are -118 kJ mol^{-1} and -441 kJ mol^{-1}, which indicates the bridging sites are more favourable as these are only present in c). The charges of the hydroxyls vary with the way they are bound to the cluster: -0.31e and -0.47e on terminal hydroxyls and -0.55e, -0.56e, -0.59e and -0.65e for the bridging hydroxyls and 3.14e for the Au_{10} cluster. This shows a single electron is donated for each H_2O_2 which explains why the HO – OH cleavage continues to be spontaneous but as the top site is only available for further binding it would be expected to not continue.

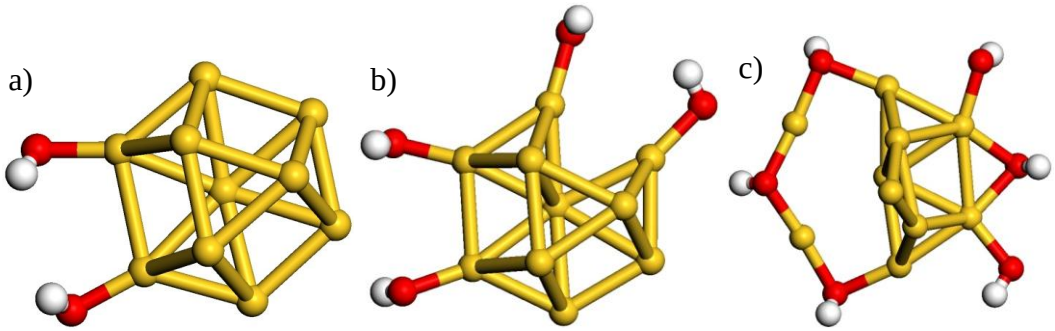

Figure 4.10. Au_{10} cluster with increasing numbers of H_2O_2 molecules adsorbed as hydroxyls a) one H_2O_2 as two hydroxyls, b) two H_2O_2 as four hydroxyls, c) three H_2O_2 as six hydroxyls. Au is yellow, O is red and H is white.

In figure 4.10. the structure shown in part c) has a two linear HO–Au–OH bond angles (176°, 174°) meaning that these Au atoms are oxide in nature, which is further supported by the Bader charges for these Au atoms (0.75e and 0.63e). A further four near linear HO–Au–Au bond angles (173°, 168°, 165° and 163°) are present but the Bader charges are (0.51e, 0.37e, 0.77e and 0.20e) which would indicate these are only partially oxide in nature. No linear Au bond angles are seen with one or two H_2O_2 adsorbed and all the hydroxyls are terminal, compared to the example when 3 H_2O_2 are adsorbed which has both terminal and bridging hydroxyls.

Whereas the production of hydroxyls would be expected to be the major product of exposing H_2O_2 to a Au_{10} cluster, O – H bond cleavage could occur with the transfer of a hydrogen atom to the cluster. This however forms a system which has a very small adsorption energy of -16 kJ mol^{-1} on the top of the Au_{10} cluster (an image of this structure is shown in figure 4.11.) or unfavourable adsorption energies of +11 kJ mol^{-1}, +29 kJ mol^{-1} and +79 kJ mol^{-1}. The barrier for the cleavage of H-OOH is 103 kJ mol^{-1} and has an associated peroxide formation barrier of 169 kJ mol^{-1}.

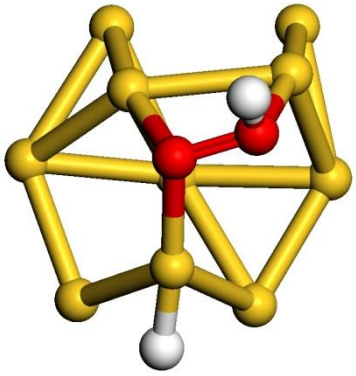

Figure 4.11. Au_{10} cluster with OOH and hydrogen atom adsorbed to the top of the cluster. Au is yellow, O is red and H is white.

The d-band centre shows a shift from the Fermi level for the hydroxyls and OOH of 0.29 eV and 0.54 eV respectively meaning the Au_{10} cluster states when the hydroxyls are adsorbed are closer to the Fermi level.

CH_3OOH

CH_3OOH weakly adsorbs to the (111) faces of the cluster, which is shown in figure 4.12. It has a binding energy of 0 kJ mol^{-1} to the top of the cluster with Au – O distances of 3.05 Å and 3.28 Å, a C – O distance of 1.42 Å and an O – O distance of 1.48 Å. It also has a binding energy of -13 kJ mol^{-1} to the base of the cluster with Au – O distances of 2.76 Å and 2.64 Å, a C – O distance of 1.43 Å and an O – O distance of 1.50 Å. Over the (100) face, the O – O cleaves to form a CH_3O and a hydroxyl with a binding energy of -217 kJ mol^{-1}, which is shown in figure 4.12. It has a Au – OH distance of 2.02 Å, a Au – OCH_3 distance of 2.04 Å and a C – O distance of 1.42 Å.

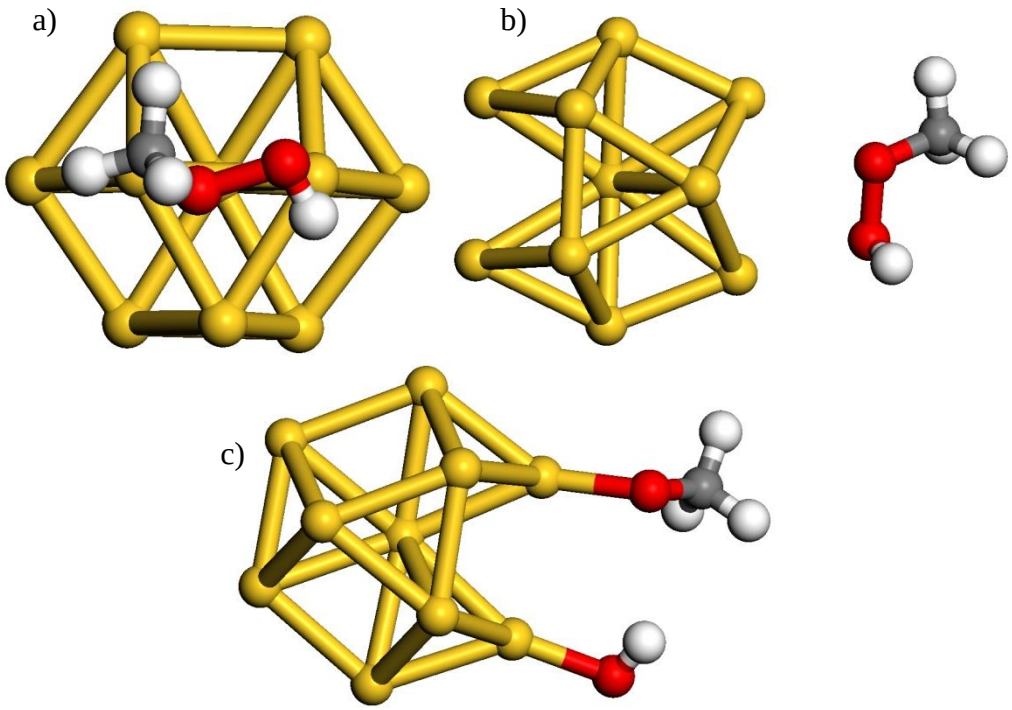

Figure 4.12. Images of CH_3OOH over a Au_{10} cluster a) over top b) CH_3O – OH parallel to (111) face on base of cluster c) CH_3O – OH bond cleaved to form CH_3O and hydroxyl by (100) face on base of cluster. Au is yellow, O is red, C is grey and H is white.

CH_3OOH can be formed from a CH_3 and an OOH with both start and end points shown in figure 4.13. The CH_3, OOH and two hydrogen atoms have a binding energy of 40 kJ mol^{-1}, a Au – C distance of 2.07 Å, a Au – O distance of 2.04 Å, Au – H distances of 1.61 Å, 1.73 Å and 1.75 Å and an O – O distance of 1.48 Å. The CH_3OOH and two hydrogen atoms have a binding energy of -26 kJ mol^{-1}, a Au – O distance of 3.20 Å, Au – H distances of 1.80 Å, 1.76 Å, 1.71 Å and 1.91 Å, a C – O distance of 1.43 Å and an O – O distance of 1.48 Å.

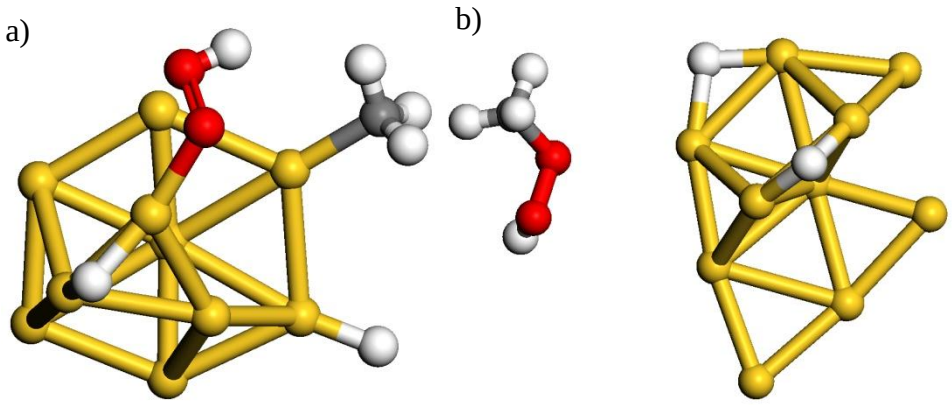

Figure 4.13. Images of a) CH_3OOH and two hydrogen atoms on a Au_{10} cluster and b) CH_3, OOH and two hydrogen atoms on a Au_{10} cluster. Au is yellow, O is red, C is grey and H is white.

CH_3OH

CH_3OH adsorbs to all the sites of the Au_{10} cluster, which are shown in figure 4.14. CH_3OH adsorbs the strongest on the base of cluster over the (100) face with a binding energy of -86 kJ mol^{-1}, a Au – O distance of 2.61 Å and a C – O distance of 1.45 Å. CH_3OH adsorbs on the base over the (111) face with a binding energy of -18 kJ mol^{-1}, a Au – O distance of 2.51 Å and a C – O distance of 1.45 Å. CH_3OH adsorbs on top of the cluster over a (111) face with a binding energy of 3 kJ mol^{-1}, a Au – O distance of 3.33 Å and a C – O distance of 1.43 Å. CH_3OH adsorbs between the (111) and (100) faces with a binding energy of -3 kJ mol^{-1}, a Au – O distance of 3.35 Å and a C – O distance of 1.43 Å.

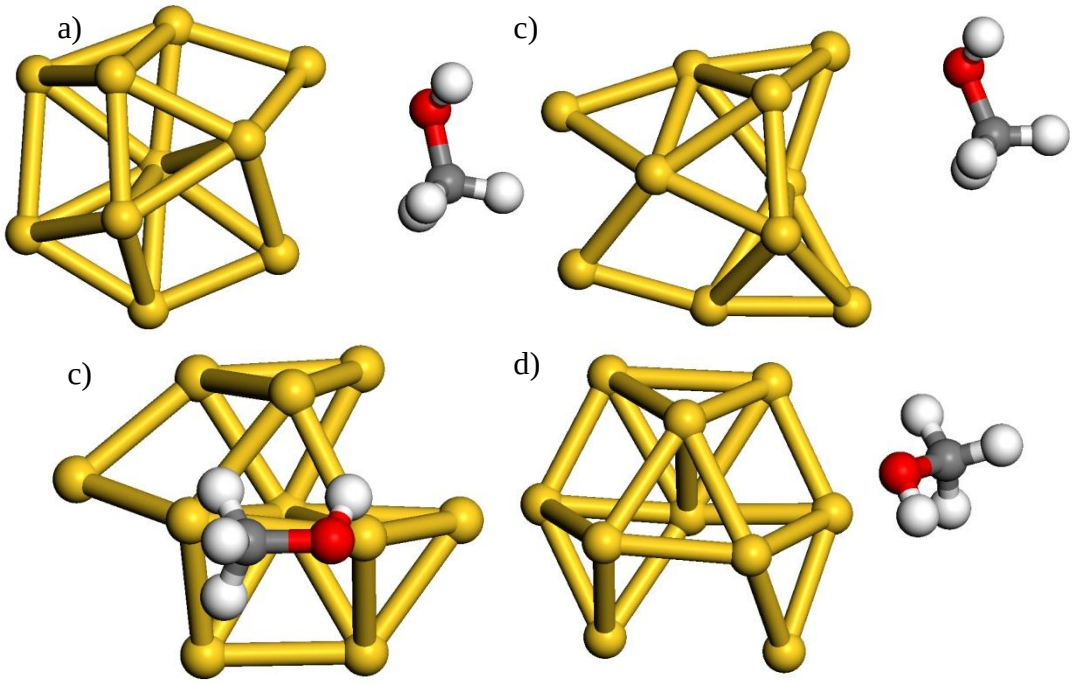

Figure 4.14. Images of CH_3OH adsorbed in several positions on a Au_{10} cluster, a) adsorbed to the base over the (111) face, b) adsorbed to the base over the (100) face, c) adsorbed to the top over the (111) face and d) adsorbed between the (111) face and (100) face. Au is yellow, O is red, C is grey and H is white.

Water would be produced in addition to the CH_3OH, and both of these adsorb to the Au_{10} cluster, which is shown in figure 4.15. It has a binding energy of -45 kJ mol^{-1}, a Au – OH distance of 2.51 Å, a Au – $O(H)CH_3$ distance of 2.66 Å and a C – O distance of 1.45 Å.

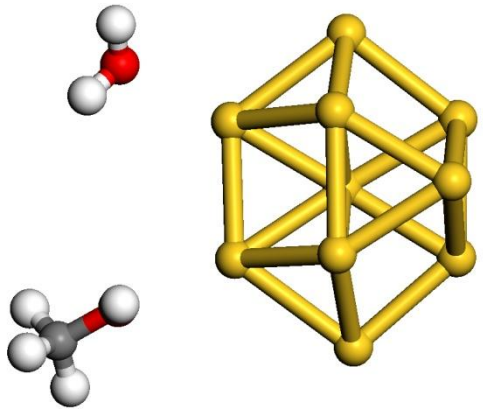

Figure 4.15. An image of CH_3OH and H_2O on a Au_{10} cluster. Au is yellow, O is red, C is grey and H is white.

The water can be broken into a hydroxyl and hydrogen atom on the cluster, two with CH_3OH on the base of cluster favourably co-adsorbing, which are shown in figure 4.16. A CH_3OH and a hydroxyl are adsorbed on the base of the cluster either side of the (100) face and a hydrogen atom on the base over a (111) face with a binding energy of -27 kJ mol^{-1}. It has a Au – OH distance of 2.04 Å, a Au – $O(H)CH_3$ distance of 2.48 Å, Au – H distances of 1.75 Å and 1.79 Å and a C – O distance of 1.45 Å. The second favourable structure is a CH_3OH and a hydroxyl are adsorbed on the base of the cluster either side of the (111) face and a hydrogen atom on the base over a (111) face with a binding energy of -5 kJ mol^{-1}. It has a Au – OH distance of 2.02 Å, a Au – $O(H)CH_3$ distance of 2.61 Å, Au – H distances of 1.69 Å and 1.97 Å and a C – O distance of 1.45 Å. The first unfavourable structure is a CH_3OH and a hydroxyl are adsorbed on the top of the cluster either side of the (111) face and a hydrogen atom on the base over a (111) face with a binding energy of +52 kJ mol^{-1}. It has a Au – OH distance of 2.02 Å, a Au – $O(H)CH_3$ distance of 2.38 Å, Au – H distances of 1.75 Å and 1.79 Å and a C – O distance of 1.46 Å. The second unfavourable structure is a CH_3OH on the top of the cluster on a (111) face, a hydroxyl on the base of the cluster on a (111) face and the hydrogen atom on the base of the cluster on a (111) face. It has a binding energy of +44 kJ mol^{-1}, a Au – OH distance of 2.03 Å, a Au – $O(H)CH_3$ distance of 3.53 Å, Au – H distances of 1.75 Å and 1.88 Å and a C – O distance of 1.43 Å.

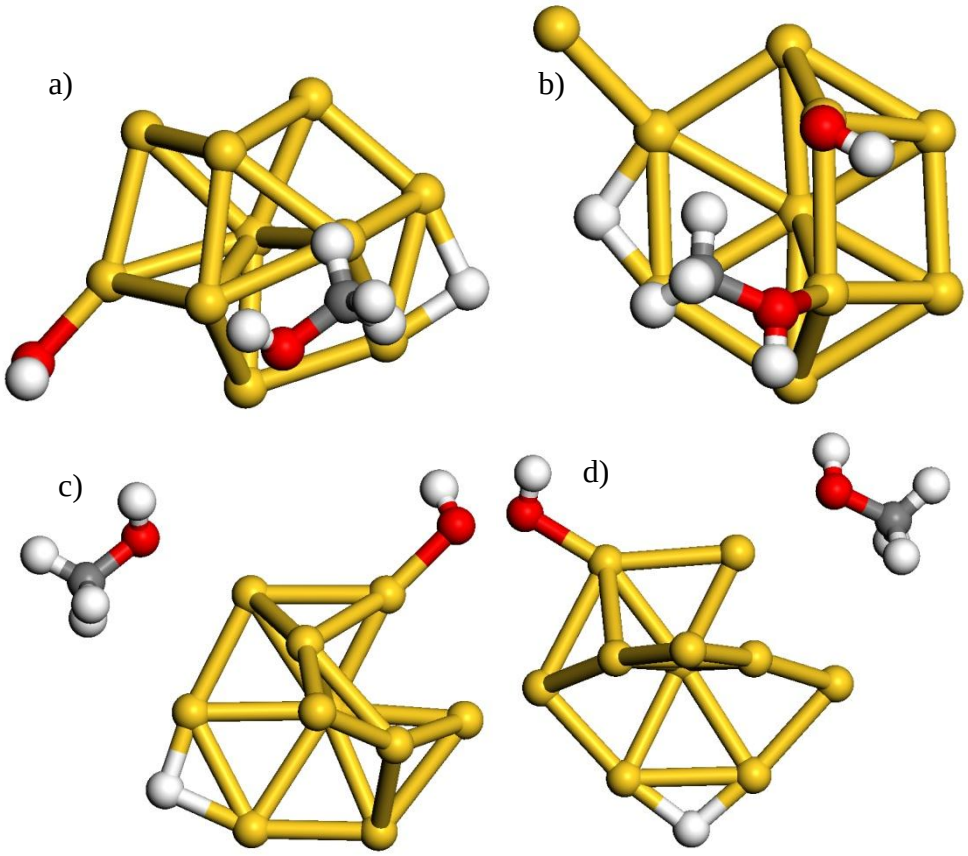

Figure 4.16. Images of CH_3OH, a hydroxyl and a hydrogen atom on a Au_{10} cluster. Au is yellow, O is red, C is grey and H is white.

Mechanisms

From the reactants discussed so far mechanisms can be produced for both the reactions being studied. These would indicate the products and intermediates that should be studied. These mechanisms can be compared to experimental work from the group of G. Hutchings, which will be used to explore parts of the reaction that maybe overlooked without this.

As H_2O_2 can be used in the reaction starting as H_2O_2 or in-situ i.e. from H_2 and O_2, two mechanisms are studied: direct synthesis of H_2O_2 from H_2 and O_2 and CH_4 oxidation to produce CH_3OH via H_2O_2.

Direct synthesis of H_2O_2

There are two possible routes for the formation of H_2O_2. The first route is the H_2 and O_2 adsorbing to the Au_{10} cluster and the H_2 bond breaking to form two hydrogen

atoms on the cluster and the hydrogen atoms transferring onto the adsorbed O_2 to form the H_2O_2. The second route is both the H_2 and O_2 adsorbing and both bonds breaking to have two oxygen atoms and two hydrogen atoms and then reforming as two hydroxyl groups to form H_2O_2.

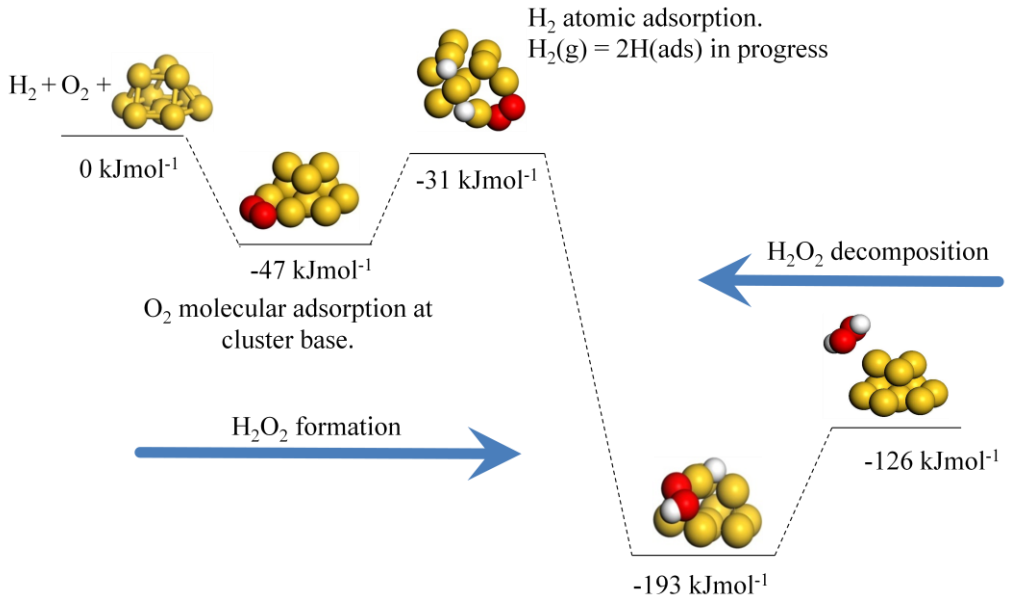

Figure 4.17. Proposed mechanism for H_2O_2 production from H_2 and O_2 by second route

The second route requires an O – O bond breaking step, the barrier for which has been shown to be high in energy on Au_{10}[2,4] at 141 kJ mol^{-1}, which would make that step difficult. The second route also requires the formation of H_2O_2 from two hydroxyl groups. However as H_2O_2 has been shown to cleave spontaneously and form hydroxyl groups and these are highly favourable (between -209 kJ mol^{-1} and -237 kJ mol^{-1}) it is unlikely this process would occur to form H_2O_2.

The first route only requires the H – H bond to break and transfer reactions with the hydrogen atoms. A reaction scheme for this route is shown in figure 4.17.. O_2 adsorbs to the Au_{10} cluster favourably with the O – O bond lengthening to 1.33 Å which indicates a superoxide species and charge transfer from the Au. The hydrogen atoms strongly bind to the Au_{10} cluster with the H – H bond break requiring 54 kJ mol^{-1}. The second hydrogen atom transfer which is a hydrogen atom to OOH is prohibitive at 169 kJ mol^{-1}. This is likely to be the reaction barrier that determines the rate of reaction. As stated previously H_2O_2 cleaves spontaneously to two

hydroxyl groups over the base of a Au_{10} cluster which would mean that H_2O_2 near a free site is likely to cleave. This means a pseudo-equilibrium would exist between hydroxyl groups and H_2O_2. The H_2O_2 breaks down until all the sites have hydroxyl group bound to them. The sites can be cleared by hydrogen atoms transferring to the hydroxyl groups to form water.

CH_4 oxidation

There are several possible routes for the formation of CH_3OH from CH_4: The first is a methyl binding to the Au_{10} cluster the after a hydrogen atom has transferred to the Au_{10} cluster, the scheme for which is shown in figure 4.18. This is followed by the methyl transferring to an OOH species formed from a hydrogen atom transferring from a H_2O_2 forming CH_3OOH. The CH_3OOH is broken down in a similar way to H_2O_2 with the CH_3O – OH cleaving on the base of the cluster on the (100) face to form a methoxy and hydroxyl group. These can have a hydrogen atom transferred to each to produce CH_3OH and H_2O.

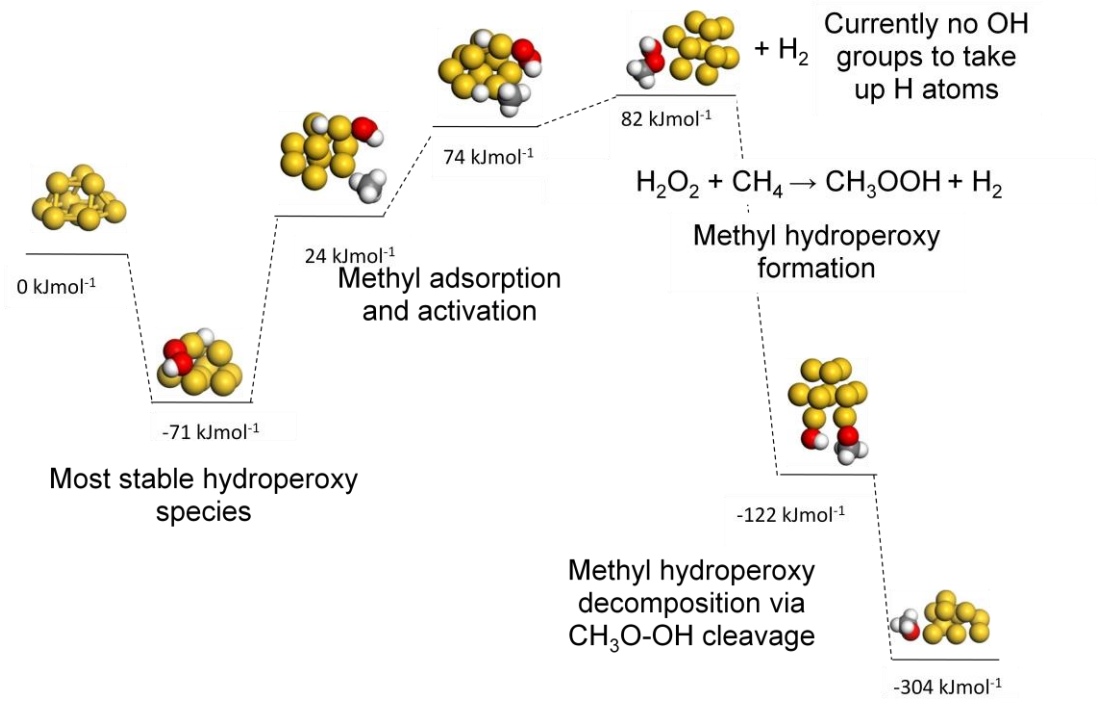

Figure 4.18. Proposed mechanisms for oxidation of methane to methanol

Other possible routes include replacing the OOH with one of the hydroxyl group and the CH_4 directly interacting with the OOH or OH so the methyl never is contact with the cluster. These have been precluded because in the experimental results CH_3OOH

is seen as an intermediate and CH_4 does not react in the presence of the catalysts without H_2O_2.

The first route is likely to be dominated by the hydroxyl group blocking sites. However a reduction of the quantity of H_2O_2 available will be caused by cleavage of the H_2O_2 and the production of more hydroxyl groups.

4.2. TiO_2 (rutile)

Continuing from the Au_{10} cluster model shown in the previous section, the TiO_2 support is modelled. In this section the rutile structure of TiO_2 is investigated as it is the most stable structure. A (110) surface is cut and a three layer slab produced which is shown in figure 4.19. The surface has 4 different atom co-ordinations, 2 oxygen and 2 titanium, which are labelled in figure 4.19. The oxygen atoms are in 2 co-ordinate bridging site and 3 co-ordinate in the surface, and the titanium atoms are 5 and 6 co-ordinate.

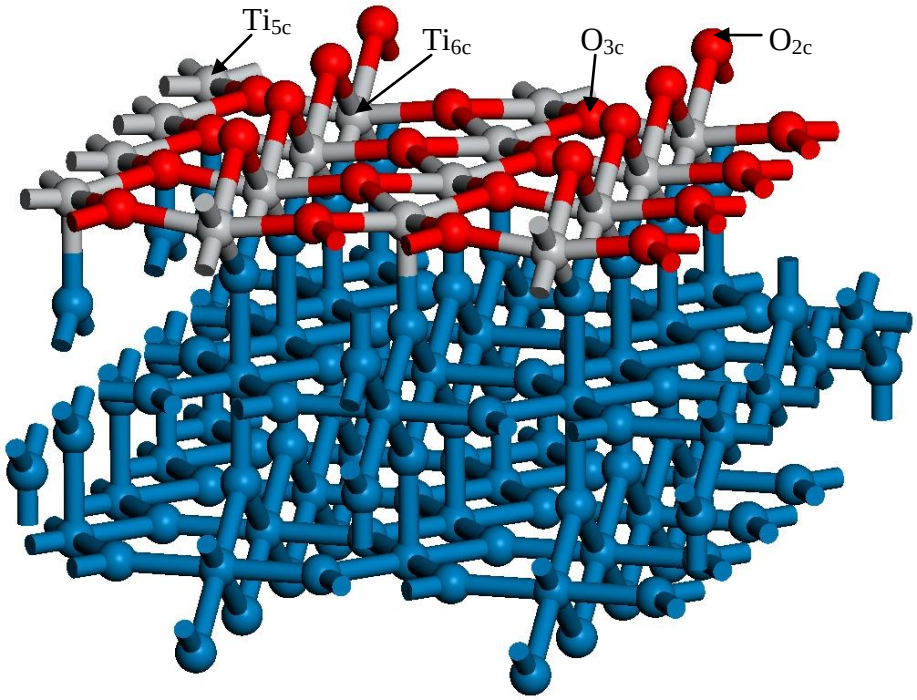

Figure 4.19. Rutile structure TiO_2 (110) surface with atom co-ordinations.

The bulk structure has a optimised cell lengths of (4.72 Å × 4.72 Å × 3.04 Å), which is a 7.5% increase in the cell volume from the experimental structure.

Calculations are performed in a c(3×2) cell (9.01 Å × 13.19 Å × 24.16 Å) and c(4×2) cell (12.01 Å × 13.19 Å × 24.16 Å), and all surfaces have a 15 Å vacuum gap. Distances between Ti – O atoms vary with atom co-ordination. The $Ti_{5c} – O_{3c}$ distance is 1.96 Å, $Ti_{6c} – O_{3c}$ distance is 2.08 Å, $Ti_{6c} – O_{2c}$ distance is 1.86 Å, $Ti_{6c} – O_{bulk}$ distance is 2.10 Å and $Ti_{5c} – O_{bulk}$ distance is 1.87 Å. This is the expected bond distance as the lower co-ordinate Ti and O atoms have the shorter atomic distances.

The average Bader charge of the atom types shows that the 2 co-ordinate oxygen atoms are less negatively charged than the 3 co-ordinate oxygen atoms with the bulk oxygen atoms having a similar charge (-0.85e, -0.97e and -0.98e). The titanium atoms show very little difference between the different co-ordinations and these are within the error in calculating the average. The difference between the surface and bulk titanium has a small variation with the surface found to be less positive (1.91e and 1.97e).

The surface energy is calculated by subtracting the energy of bulk corrected to the same number of atoms from the energy of the slab and dividing by twice the surface area (because two surfaces are cut as it is periodic in the c-direction with a vacuum gap). The surface energy is calculated for the TiO_2 with different numbers of layers, and this has been plotted against the surface energy, as shown in figure 4.20. Multiple layers are required to make the centre of the slab have more characteristics of the bulk material. The slabs modelled have odd numbers of layers due the symmetry of the slab and to avoid large oscillations in the surface energy.

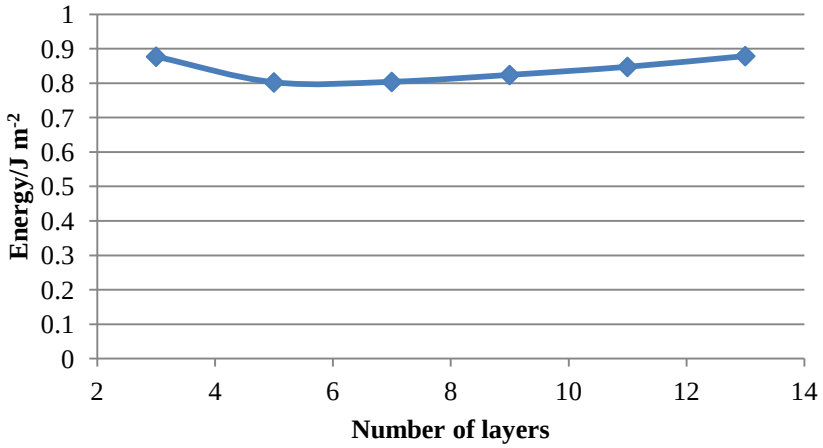

Figure 4.20. Plot of surface energy against number of layer in a TiO_2 slab.

The variation of the surface energy between the different numbers of layers is 8.7%. The surface energy approaches convergence with a large number of layers but no convergence has been reached at present. Using a large number of layers generates a system too large to be modelled in a reasonable length of time. For calculations of adsorption energies, errors due to the thickness of the slab are likely to cancel out.

A 3 layer slab was selected for use in subsequent calculations because the variation of the surface energy with increasing thickness is low, and the calculation can run in a shorter time period. The surface energy of the 3 layer (110) slab is 0.88 J m^{-2}. This is similar to the value quoted by Vanderbilt *et al.*[5] of 0.89 J m^{-2} using Vanderbilt ultrasoft pseudopotentials and plane wave basis set with 340 eV cutoff and local-density approximation.

H_2O

As the experimental work is performed in aqueous conditions, the interactions of one molecule, two molecules and a monolayer of H_2O will be investigated. A single H_2O molecule has a binding energy of -123 kJ mol^{-1} with a $Ti_{5c} – OH_2$ distance of 2.30 Å, which is shown in figure 4.21.a). A hydrogen atom can be transferred to the surface to a bridging O_{2c} site forming a hydroxyl group over a Ti_{5c} site, which is shown in figure 4.21.b). The hydroxyl group and the hydrogen atom has a binding energy of -49 kJ mol^{-1} with a $Ti_{5c} – OH$ distance of 1.82 Å and an $O_{2c} – H$ distance of 0.97 Å. This indicates that the water molecule is favoured on the surface but both structures are strongly binding.

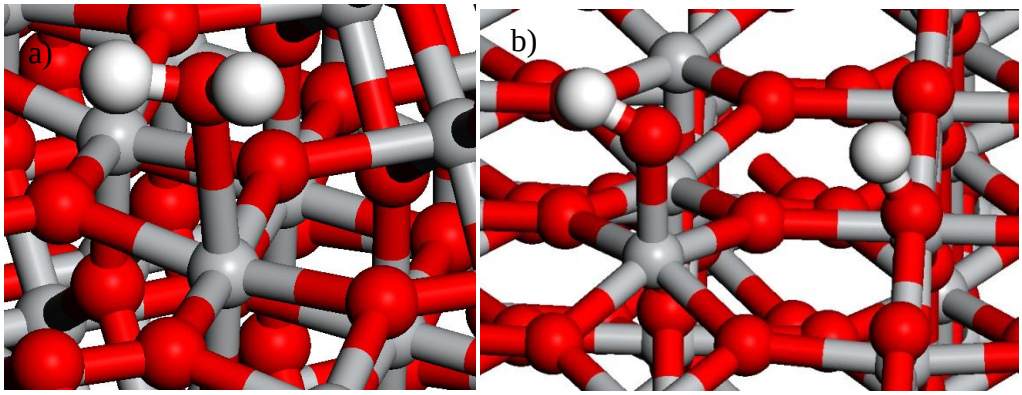

Figure 4.21. Image of a) Water on TiO_2 (110) and b) OH and H on TiO_2 (110)

A second H_2O can be added on an adjacent Ti_{5c}, which is shown in figure 4.22.a) This has a binding energy per H_2O molecule of -138 kJ mol^{-1} with Ti_{5c} – O distances of 2.25 Å and 2.40 Å. One hydrogen atom can transfer from each water molecule producing two hydroxyl groups and two hydrogen atoms on the surface O_{2c}. These can have different hydrogen bonding patterns, which are shown in figure 4.22.b) and c). b) has a binding energy of -78 kJ mol^{-1} per water molecule and c) has a binding energy of -100 kJ mol^{-1} with c) having O - H distance between two of the hydroxyl group of 1.95 Å. The effect of the hydrogen bonding is in line with the work of Perron *et al.*[6]

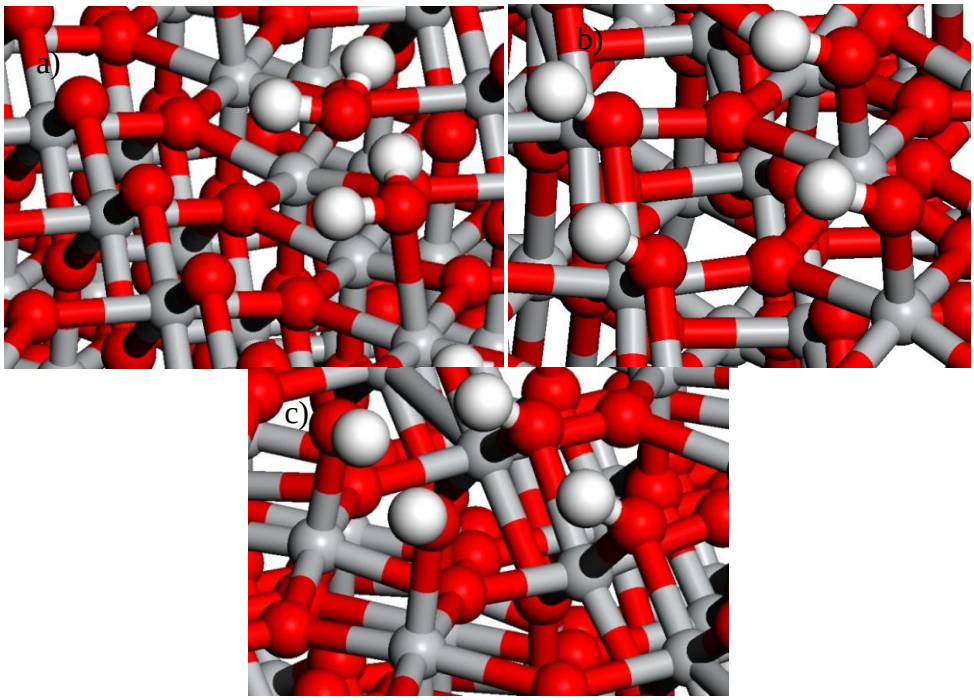

Figure 4.22. Image of a) Two water molecules on TiO_2 (110) and b) and c) Two OH and Two H on TiO_2 (110)

Hydroxyl groups can be placed on all the Ti_{5c} sites and hydrogen atoms on all the O_{2c} sites to a full monolayer coverage. This has a binding energy per water molecule of -50 kJ mol^{-1}. A molecular dynamics simulation was used to view the stability over time. The Born-Oppenheimer molecular dynamics (MD) with the mircocanonical (NVE) over a simulation time of 300 fs with a 1 fs step was preformed, with the result of this run shown in figure 4.23. The MD had an initial temperature of 500 K but this reduces to 270 K after 50 fs and remains at 268 ± 15 K for the rest of the simulation. This shows at 75 fs a transfer starts to occur with a hydrogen atom on an O_{2c} to produce water. This indicates the hydrogen atoms can move in the tens of femtoseconds time scale and exchange would be rapid.

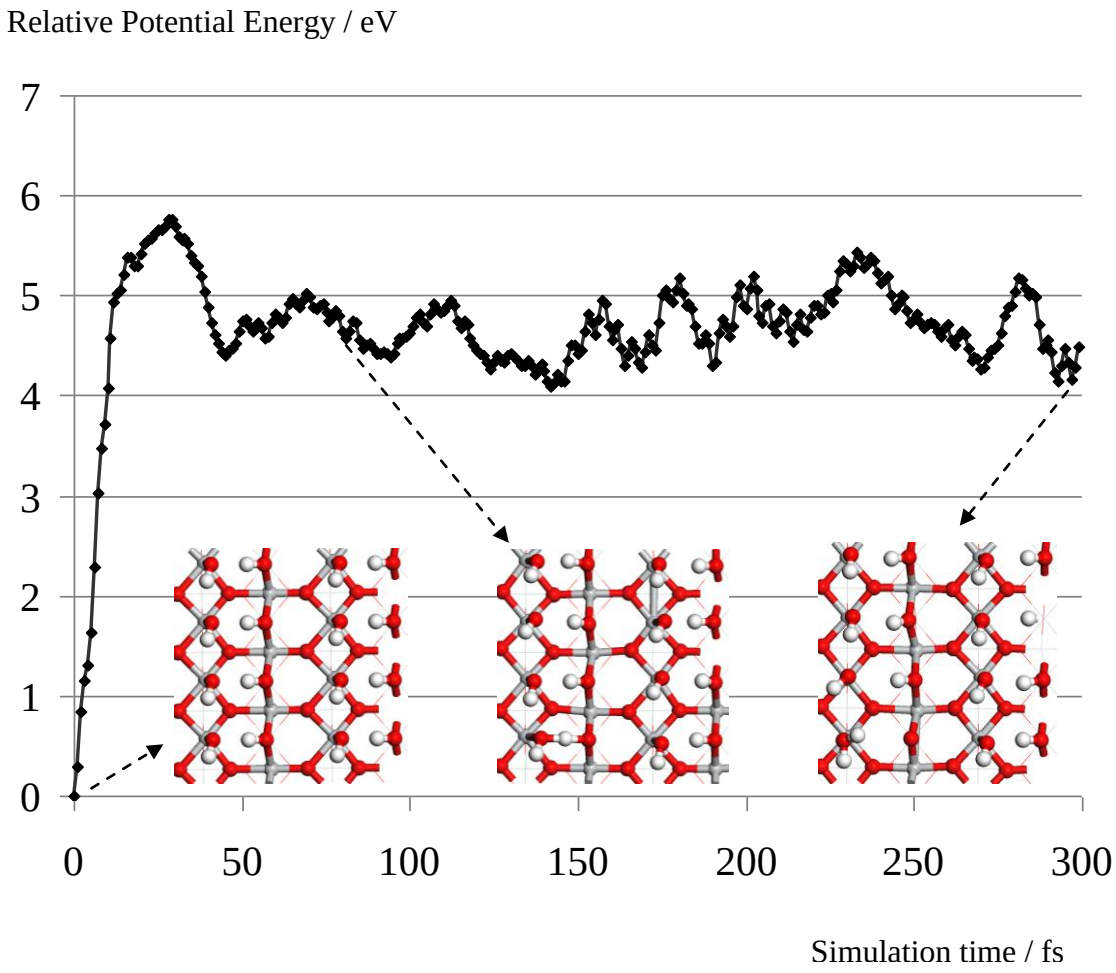

Figure 4.23. The relative potential energy as a function of time for molecular dynamics (MD) simulations of the fully hydroxylated surface of TiO_2(110). The inset structures are snapshots at 0, 75 and 300 fs as indicated by the arrows. Atom colours follow: Ti, grey; O, red and H, white.

Water is shown to be more favoured than the hydroxyl groups but the TiO_2 isoelectric point is at pH 6 and work by Bond *et al.*[7] has shown that hydroxylation may be higher than thermodynamics or experiment under vacuum would suggest.

H_2O_2

H_2O_2 can replace a water molecule in the hydroxylated TiO_2 because the energy to remove a water molecule is +44 kJ mol^{-1} and H_2O_2 has a binding energy of -68

kJ mol^{-1}. This mean replacement of water with H_2O_2 is the favourable process, and an image of H_2O_2 on hydroxylated TiO_2 (110) is shown in figure 4.24.a)

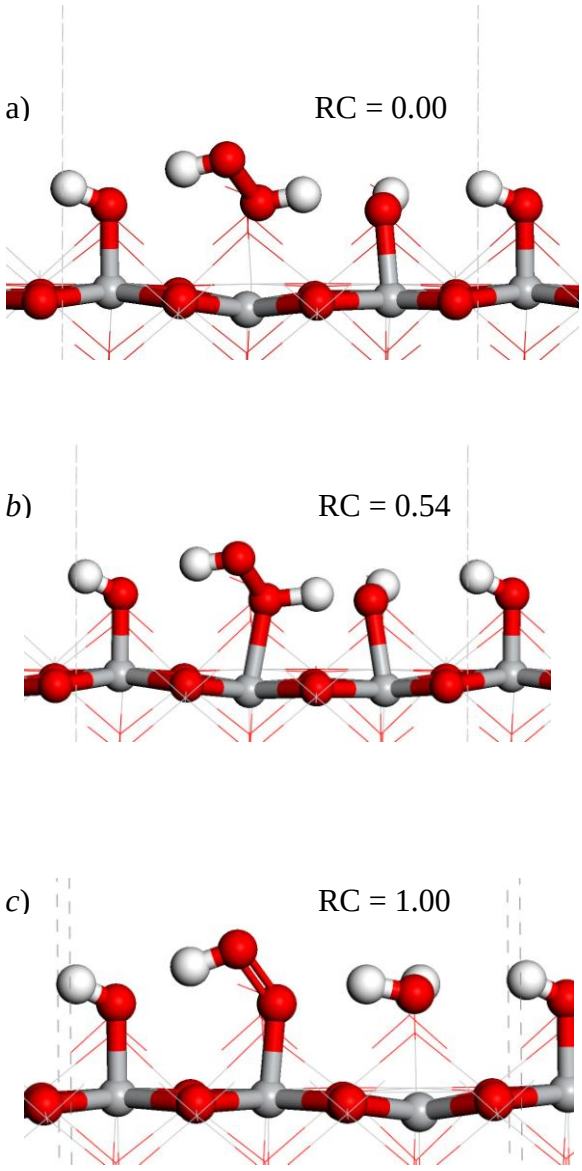

Figure 4.24. Structures shown a) – c) are at the reaction co-ordinate (RC) values indicated. Atom colours follow: Ti, grey; O, red and H, white.

The H_2O_2 is used for the start point of a barrier with the end point OOH and water, which is shown in figure 4.24.c). This has a binding energy of -87 kJ mol^{-1}. The transfer of the hydrogen atom has a barrier of 9 kJ mol^{-1} to break the HOO – H bond with the reverse barrier of 28 kJ mol^{-1}, which is shown in figure 4.25.a).

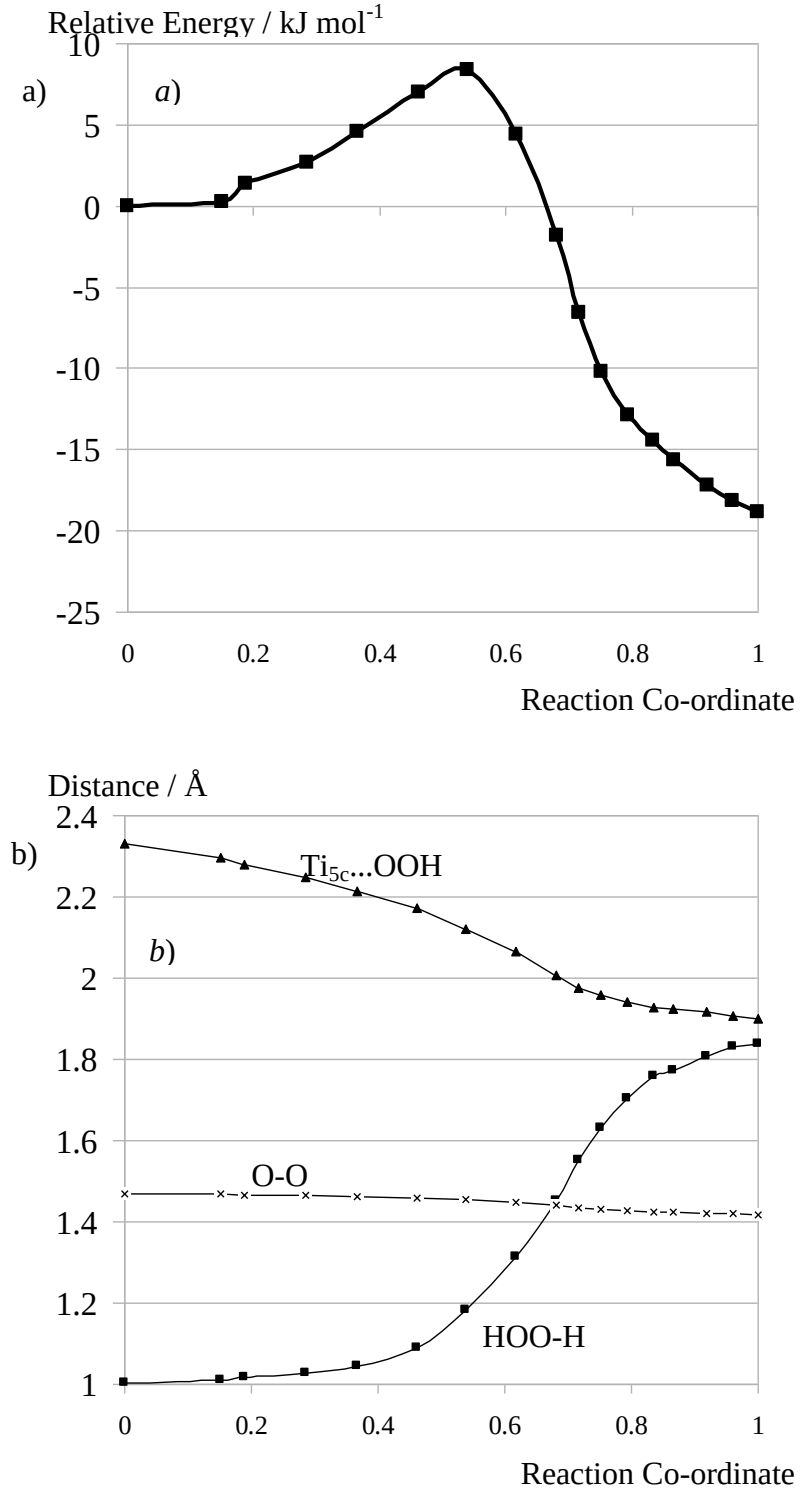

Figure 4.25. A barrier for the deprotonation of H_2O_2 over a Ti_{5c} site on the hydroxylated surface of TiO_2(110). (*a*) Relative energy versus reaction coordinate (RC), (*b*) atom–atom distances versus RC.

Figure 4.25.b) shows the Ti – OOH distance decreasing steadily with the HOO – H distance starting to increase at 0.58 along the reaction co-ordinate (RC), which corresponds with the high point on the energy barrier and is shown in figure 4.24.b).

4.3. Au_{10} supported on TiO_2

A Au_{10} cluster adsorbs to TiO_2 over the O_{2c} atoms in the ridge of oxygen atoms, which is shown in figure 4.26. The Au_{10} cluster has a binding energy of -286 kJ mol^{-1} and Au – O distances of 2.16 Å, 2.17 Å and 2.25 Å.

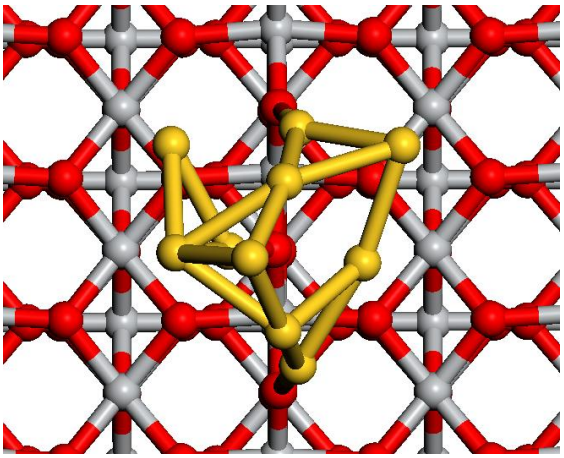

Figure 4.26. An image of a Au_{10} cluster over a TiO_2 (110) surface.

A Au_{10} cluster adsorbs to a partially hydroxylated TiO_2 (110) surface binding over a gap in the hydroxylation of the surface, which is shown in figure 4.27. The Au_{10} cluster has a binding energy of -244 kJ mol^{-1}, Au – O_b distances of 2.22 Å and 2.31 Å and Au – OH distances of 2.22 Å, 2.25 Å and 2.26 Å.

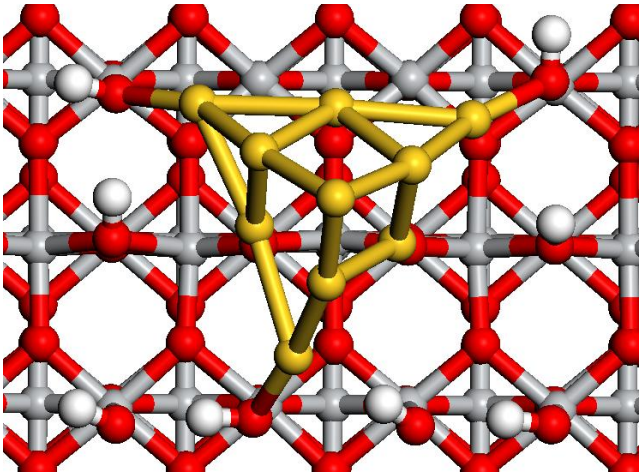

Figure 4.27. An image of a Au_{10} cluster over a hydroxylated TiO_2 (110) surface.

CH_4

CH_4 only adsorbs favourably over the top the Au_{10} cluster supported by the TiO_2 (110) surface, which is shown in figure 4.28. CH_4 has a binding energy of -50 kJ mol^{-1} to the Au_{10} cluster and supporting TiO_2 surface. The CH_4 has C – Au distance of 4.18 Å but the Au – O distances between the TiO_2 and the Au_{10} cluster are 2.08 Å, 2.08 Å and 2.09 Å, which is reduced from the distance stated for the Au_{10} cluster supported by TiO_2. When CH_4 is removed from the final structure, the Au_{10} cluster has a binding energy of -334 kJ mol^{-1} to the TiO_2 support when the system is fixed to allow no structural changes, which gives a -48 kJ mol^{-1} difference between this and the optimised structure. This would indicate that the arrangement of the Au_{10} cluster has the largest effect on the energy of the system. The CH_4 will have less reliable energies due to the lack of dispersion in the DFT calculation. CH_4 in a different position with respect to the cluster in this case to one side of the cluster, adsorbs unfavourably to the cluster, which is shown in figure 4.28. The CH_4 has a binding energy of +57 kJ mol^{-1} and a C – Au distance of 3.29 Å.

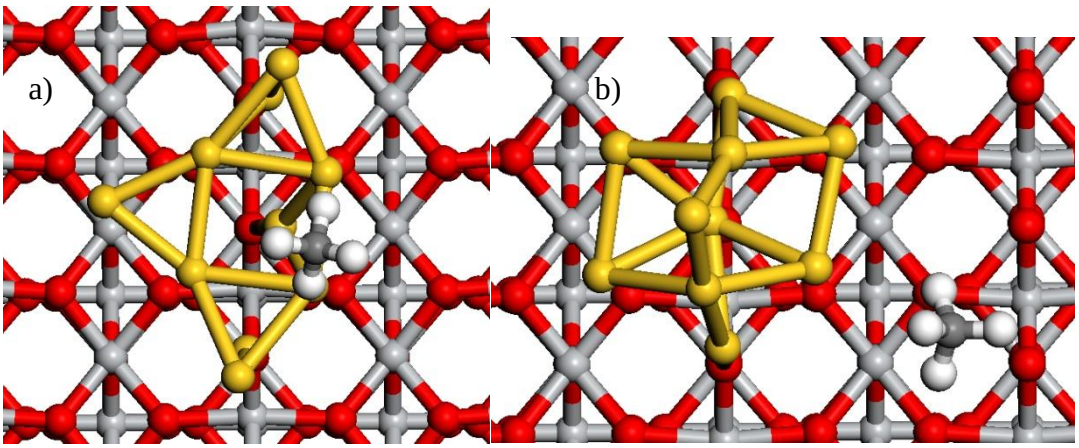

Figure 4.28. Images of CH_4 over Au_{10} supported on TiO_2 (110).

The C – H bond can be cleaved to form a methyl and a hydrogen atom on the cluster, and two example of this are shown in figure 4.29. The first case of a methyl and a hydrogen atom have a binding energy of +126 kJ mol^{-1}, a C – Au distance of 2.09 Å and Au – H distances of 1.75 Å and 1.81 Å. The second case of a methyl and a hydrogen atom have a binding energy of +155 kJ mol^{-1}, a C – Au distance of 2.07 Å and a Au – H distance of 1.60 Å.

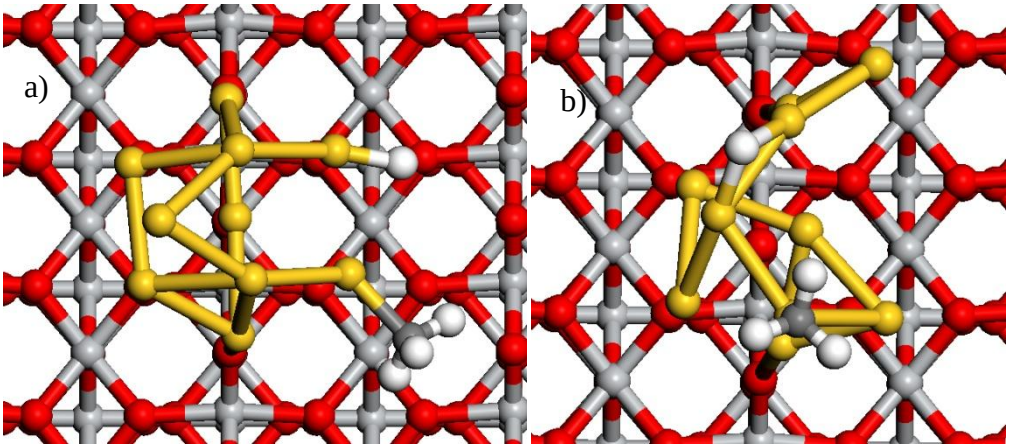

Figure 4.29. Images of CH_3 and a hydrogen atom over Au_{10} supported on TiO_2 (110).

O_2

O_2 adsorbs to TiO_2 (110) surface supporting a Au_{10} cluster in two ways; bridging between two Ti atoms in the surface and over atop Ti atom in the surface, which are shown in figure 4.30. O_2 in the bridging position has a binding energy of -98 kJ mol^{-1}, Ti – O distances of 1.93 Å and 2.01 Å and an O – O distance of 1.41 Å. The O_2 in the atop position has a binding energy of -73 kJ mol^{-1}, Ti – O distances of 1.88 Å and 1.97 Å, a Au – O distance of 2.25 Å and an O – O distance of 1.44 Å.

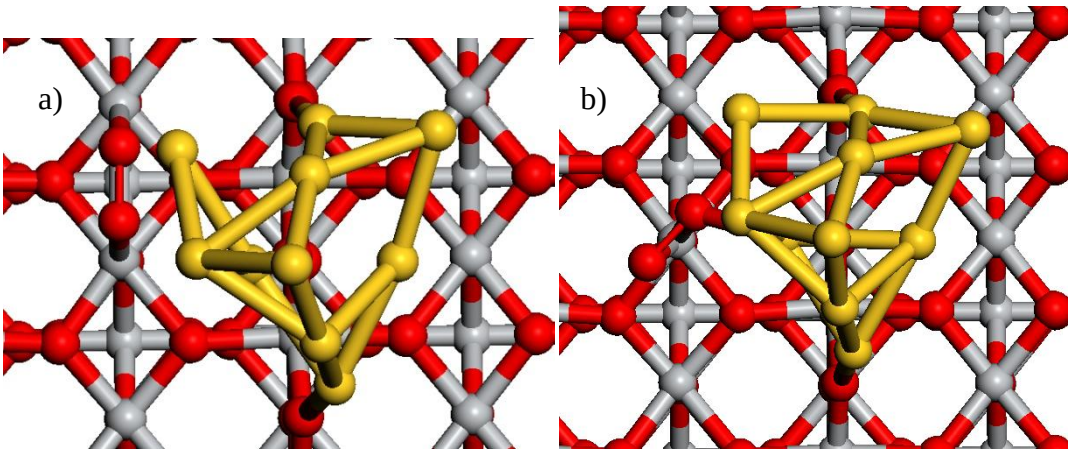

Figure 4.30. Images of O_2 over TiO_2 (110) and Au_{10} cluster.

H_2

H_2 interacts with the Au_{10} cluster and TiO_2 (110) surface in a various positions around the cluster, images of which are shown in figure 4.31. and binding energies and atomic distances are shown in table 4.2.

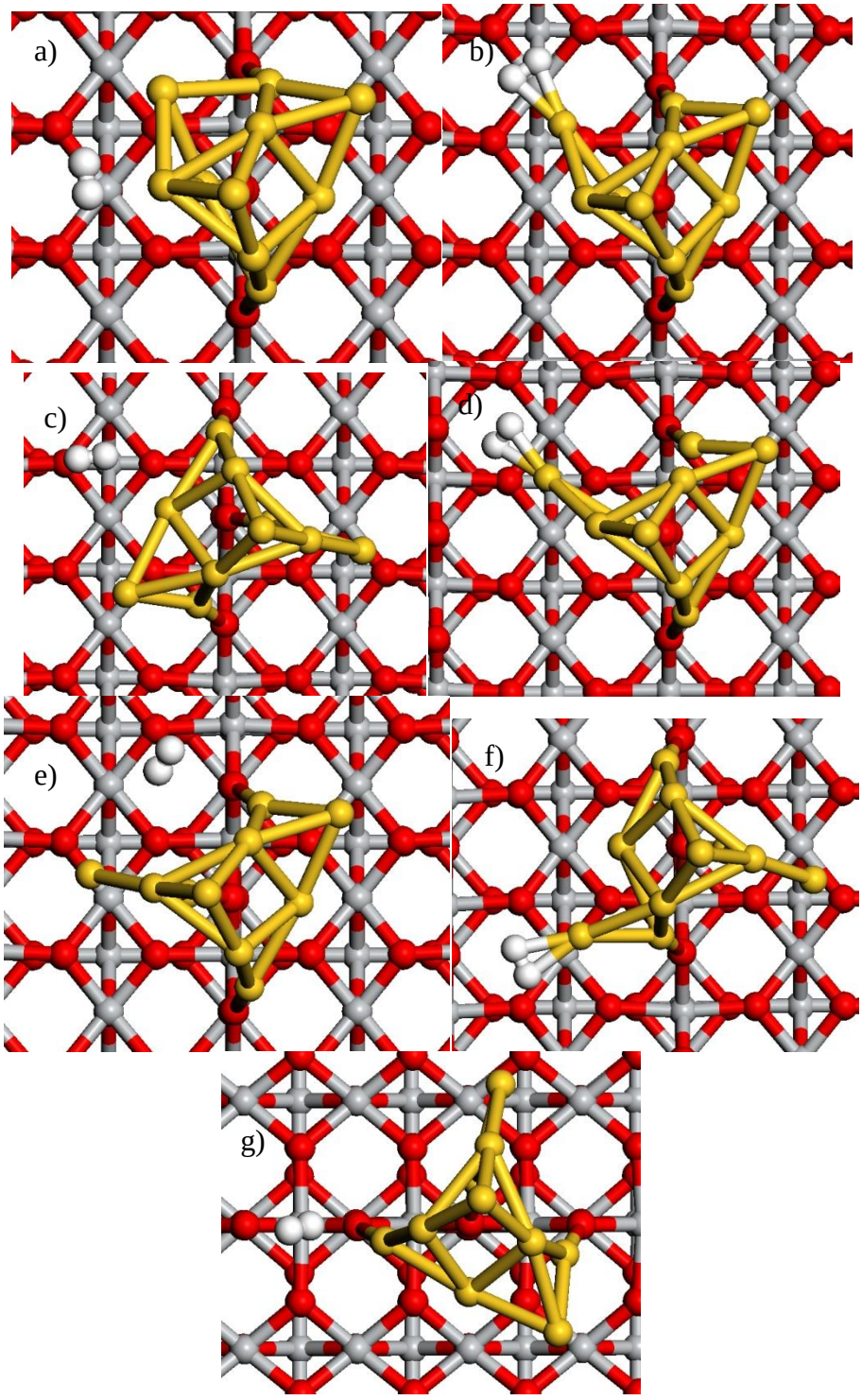

Figure 4.31. Images of H_2 interacting with a Au_{10} cluster and a TiO_2 (110) surface.

Image	Binding energy / kJ mol^{-1}	Au – H_a distance / Å	Au – H_b distance / Å	H – H distance / Å
a	+36	2.78	3.20	0.75
b	-5	1.84	1.84	0.83
c	-22	1.86	1.81	0.83
d	+15	3.12	3.20	0.75
e	+5	2.37	2.94	0.76
f	-21	1.86	1.85	0.82
g	+13	3.56	2.85	0.75

Table 4.2. A table of the binding energies and atomic distances for H_2 interacting with a Au_{10} cluster and a TiO_2 (110) surface with the images corresponding to Figure 4.31.

H_2 can also be broken into two hydrogen atoms on the Au_{10} cluster, which is shown in figure 4.32. The two hydrogen atoms have a binding energy of -2 kJ mol^{-1} and Au – H distances of 1.58 Å, 1.71 Å and 1.79 Å.

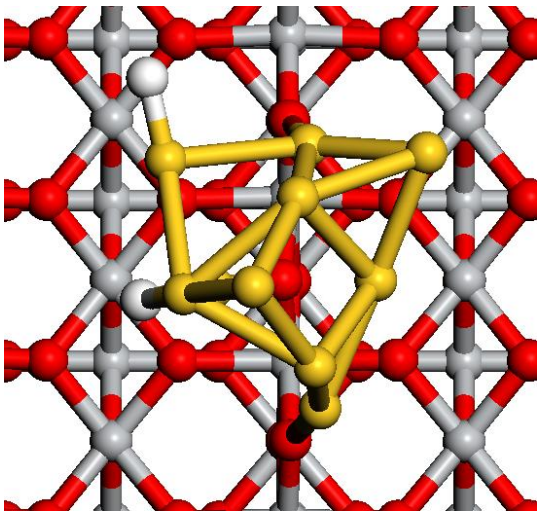

Figure 4.32. An image of two hydrogen atom interacting with a Au_{10} cluster and a TiO_2 (110) surface.

H_2O_2

H_2O_2 adsorbs to a TiO_2 (110) surface with a Au_{10} cluster present, which is shown in figure 4.33. H_2O_2 has a binding energy of +3 kJ mol^{-1}, Ti – O distances of 2.40 Å and 2.78 Å and an O – O distance of 1.47 Å. The binding energy for these systems will have errors due to the large energy difference between the Au_{10} cluster in different arrangements.

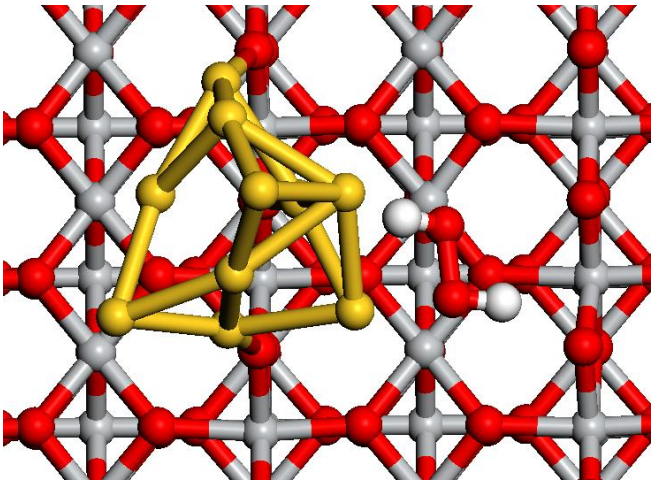

Figure 4.33. An image of H_2O_2 over TiO_2 (110) supporting a Au_{10} cluster.

H_2O_2 adsorbing to the Au_{10} cluster can result in the HO – OH bond getting cleaved to form two hydroxyls, which are shown in figure 4.34. In the first two cases these hydroxyls are bound to the Au_{10} cluster. The first has the hydroxyl at the top of the cluster. The hydroxyls have a binding energy of -78 kJ mol^{-1} and Au – OH distances of 2.00 Å and 2.02 Å. The second has the hydroxyls at the side of the cluster, and the hydroxyls have a binding energy of -106 kJ mol^{-1} and Au – OH distances of 1.99 Å and 2.02 Å. The hydroxyls can get transferred to the TiO_2 (110) surface, One can form a bridging site between the cluster and the surface. The hydroxyls have a binding energy of -154 kJ mol^{-1}, a Au – OH_t distance of 2.02 Å, a Au – OH_b distance of 2.24 Å and a Ti – OH_b distance of 1.96 Å. The hydroxyl can be transferred to the surface in a different arrangement, which forms a bridging Ti – OH. The hydroxyls have a binding energy of -221 kJ mol^{-1}, a Au – OH_t distance of 2.01 Å, a Au – OH_b distance of 2.26 Å and a Ti – OH_b distance of 1.97 Å. The second hydroxyl can be fully transferred to the surface leaving a Ti – OH and a bridging Au – O(H) – Ti, which is shown in figure 4.34. The hydroxyls have a binding energy of -295 kJ

mol^{-1}, a Ti – OH distance of 1.88 Å, a Au – OH distance of 2.18 Å and a Ti – OH_b distance of 1.99 Å.

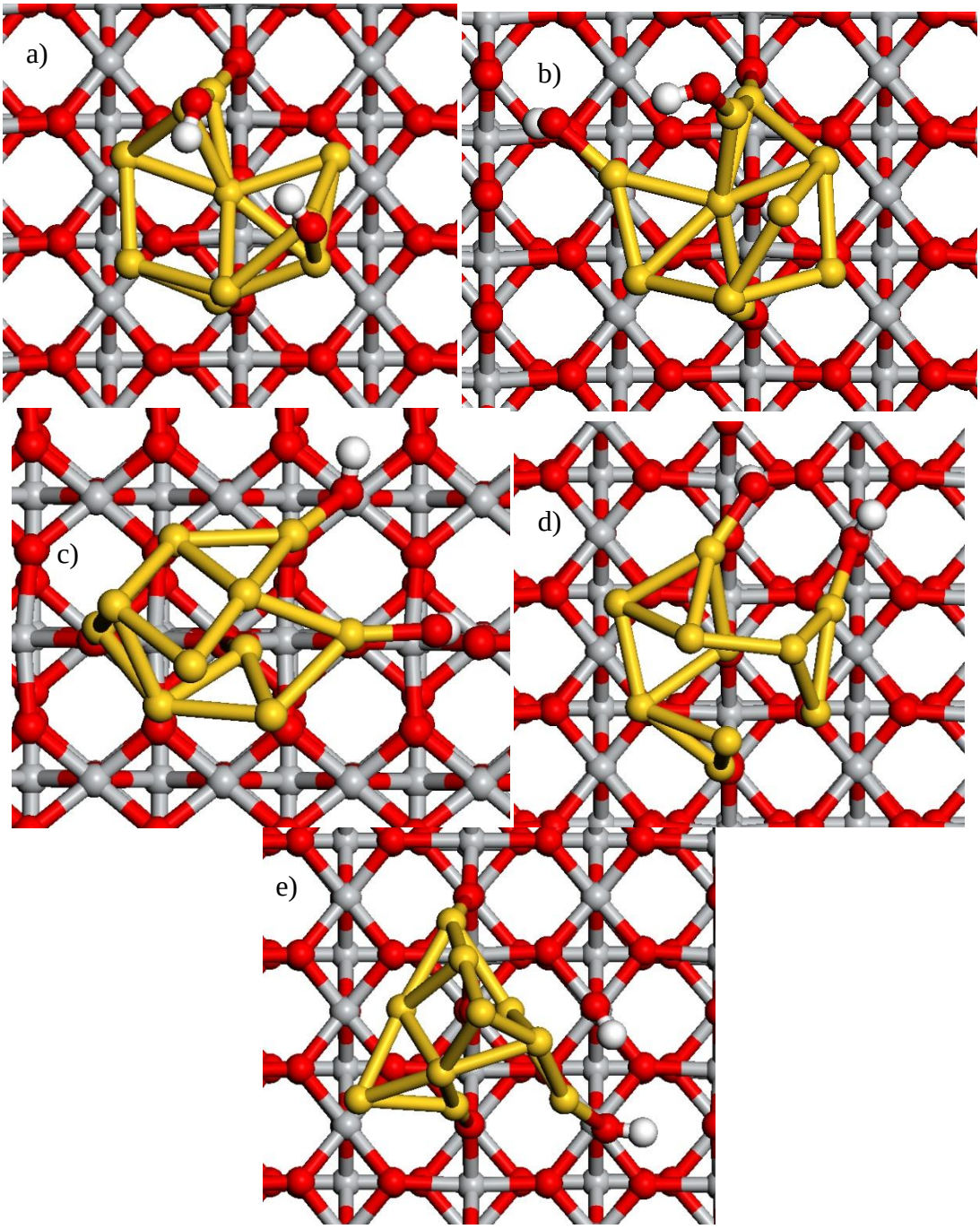

Figure 4.34. Image of H_2O_2 as hydroxyls on the Au_{10} and TiO_2 (110) surface.

H_2O_2 can have a H – OOH bond cleaved to form a OOH and a hydrogen atom. Various arrangements of this are shown in figure 4.35. The first of these have the OOH and the hydrogen atom on the Au_{10} cluster. The only favourable adsorption to the Au_{10} cluster is OOH and hydrogen atom over the top of cluster, which has a

binding energy of -4 kJ mol^{-1} with a Au – OOH distance of 2.06 Å, an O – O distance of 1.51 Å and Au – H distances of 1.71 Å and 1.72 Å. The next three arrangements have unfavourable adsorption energies with OOH and a hydrogen atom bound around the sides of the cluster. The first has a binding energy of 46 kJ mol^{-1} with a Au – OOH distance of 2.05 Å, an O – O distance of 1.50 Å and Au – H distances of 1.72 Å and 1.76 Å. The second has a binding energy of +52 kJ mol^{-1} with a Au – OOH distance of 2.05 Å, an O – O distance of 1.50 Å and Au – H distances of 1.71 Å and 1.78 Å. The third has a binding energy of +99 kJ mol^{-1} with a Au – OOH distance of 2.09 Å, an O – O distance of 1.49 Å and Au – H distances of 1.72 Å and 1.89 Å.

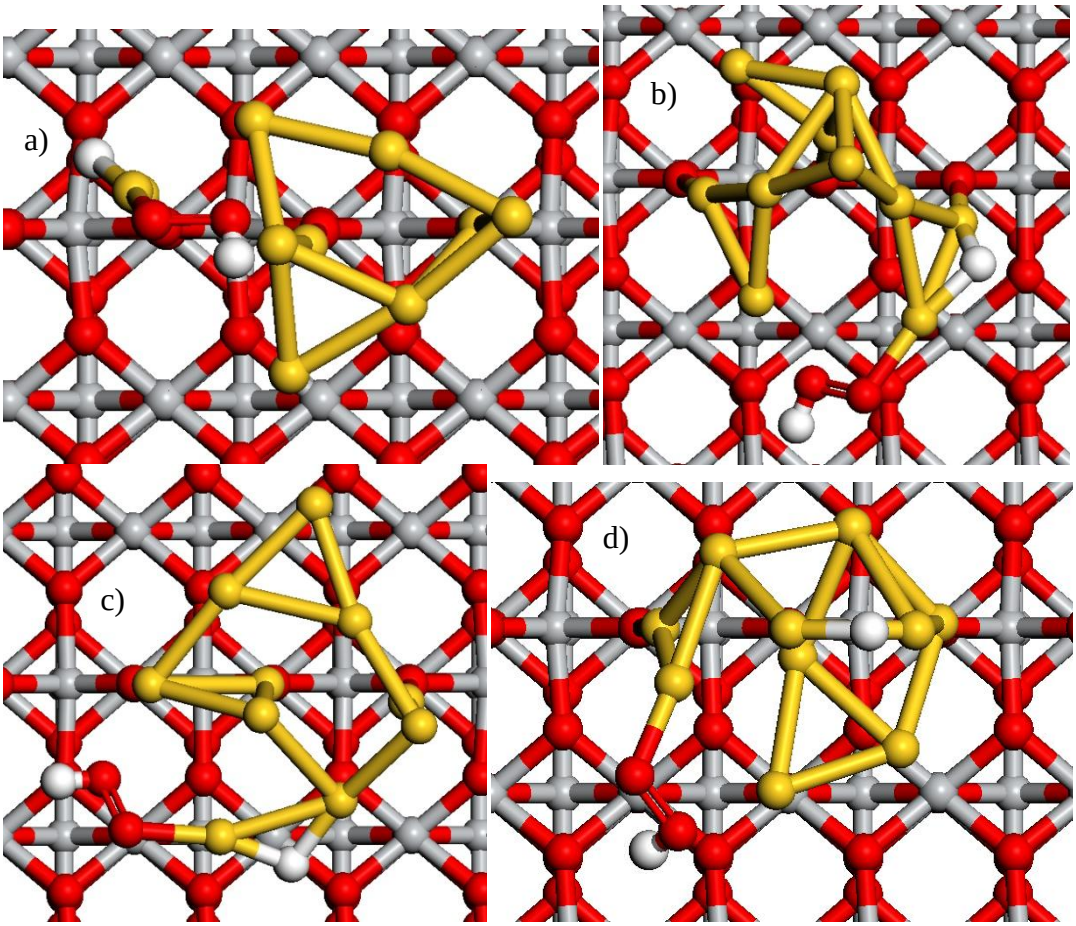

Figure 4.35. Image of H_2O_2 as OOH and a hydrogen atom on the Au_{10} and TiO_2 (110) surface.

The OOH can be transferred to the TiO_2 (110) surface and bound over the Ti_{5c} site, which are shown in figure 4.36. With the hydrogen atom still on the Au_{10} cluster two arrangements are obtained. The first gives a binding energy of +83 kJ mol^{-1} with a Ti

– OOH distance of 1.97 Å, a Ti – O(H)O distance of 2.31 Å, an O – O distance of 1.45 Å and a Au – H distance of 1.60 Å. The second gives a binding energy of 118 kJ mol^{-1} with a Ti – OOH distance of 1.90 Å, an O – O distance of 1.46 Å and a Au – H distance of 1.60 Å. Finally the hydrogen atom can be transferred to the TiO_2 (110) surface to one of the bridging two co-ordinate oxygen atoms in the surface, which is also shown in figure 4.36. The OOH and hydrogen atom have a binding energy of -65 kJ mol^{-1}, a Ti – OOH distance of 1.95 Å, an O – O distance of 1.45 Å and an O – H distance for the hydrogen atom on the surface of 0.98 Å.

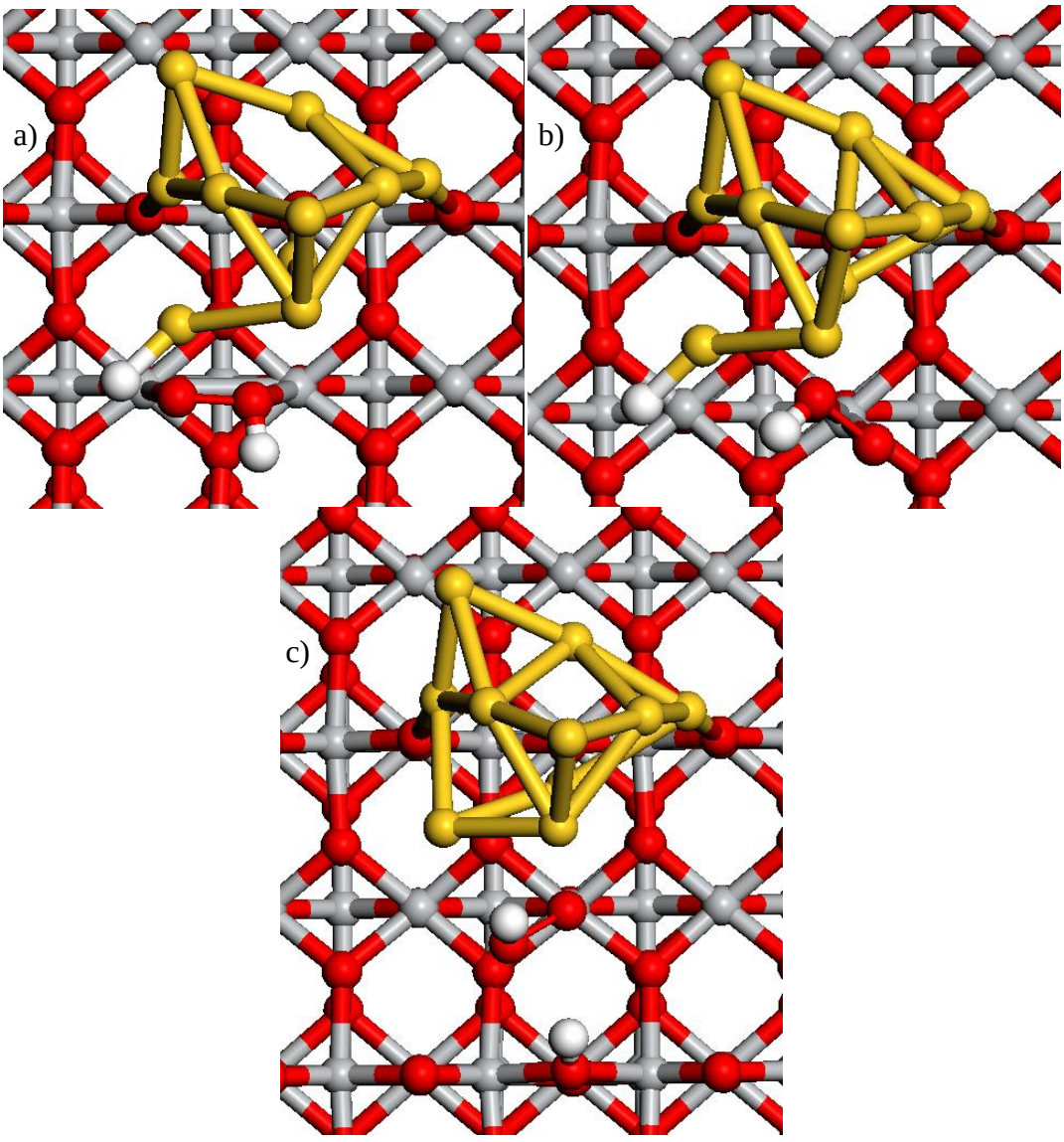

Figure 4.36. Image of H_2O_2 as OOH and a hydrogen atom on the Au_{10} and TiO_2 (110) surface.

H_2O_2 can also be adsorbed to the Au_{10} cluster supported by a hydroxylated TiO_2 (110). H_2O_2 adsorbs over the TiO_2 (110) next to the Au_{10} cluster, which is shown in figure 4.36. H_2O_2 has a binding energy of -6 kJ mol^{-1}, a Au – O distance of 2.50 Å, an O – O distance of 1.47 Å and a hydrogen bonding distance of 1.83 Å between one of hydrogen atoms on the H_2O_2 and a bridging OH in the surface. The HO – OH bond can be cleaved to form two hydroxyls over Ti atoms in the surface, which is shown in figure 4.36. The hydroxyls have a binding energy of -564 kJ mol^{-1}, Ti – OH distances of 1.87 Å and 1.91 Å and a Au – OH distance of 2.27 Å. The H – OOH bond can be cleaved to form OOH over a Ti atom and a hydrogen atom on one of the surface hydroxyls to form water, which is shown in figure 4.36. The OOH and the surface hydrogen atom has a binding energy of -11 kJ mol^{-1}, Au – O distances of 2.44 Å and 2.79 Å, a Ti – OOH distance of 2.01 Å, an O – O distance of 1.46 Å and an O – H distance of 0.97 Å in the water molecule.

CH_3OH

CH_3OH adsorbs to the TiO_2 (110) supported Au_{10} cluster in four different positions, which are shown in figure 4.37. In the first of these position the CH_3OH unfavourably adsorbs to the side of the Au_{10} cluster with a binding energy of 10 kJ mol^{-1}, a Au – O distance of 2.42 Å and a C – O distance of 1.45 Å. Three other positions adsorb favourably. The first CH_3OH adsorbs to the side of the cluster with a hydrogen bonding distance. CH_3OH has a binding energy of -6 kJ mol^{-1}, a Au – C distance of 2.28 Å, a C – O distance of 1.45 Å and a hydrogen bonding O – H distance of 1.78 Å between the CH_3OH and a bridging O_{2c} atom in the ridge in the (110) surface. The second case has a CH_3OH on the top of the cluster with a binding energy of -20 kJ mol^{-1}, a Au – C distance of 2.38 Å and a C – O distance of 1.46 Å. In the last case a CH_3OH adsorbs to the side of the cluster with a hydrogen bonding distance. CH_3OH has a binding energy of -60 kJ mol^{-1}, a Au – C distance of 2.24 Å, a C – O distance of 1.46 Å and a hydrogen bonding O – H distance of 1.97 Å between the CH_3OH and a bridging O_{2c} atom in the ridge in the (110) surface.

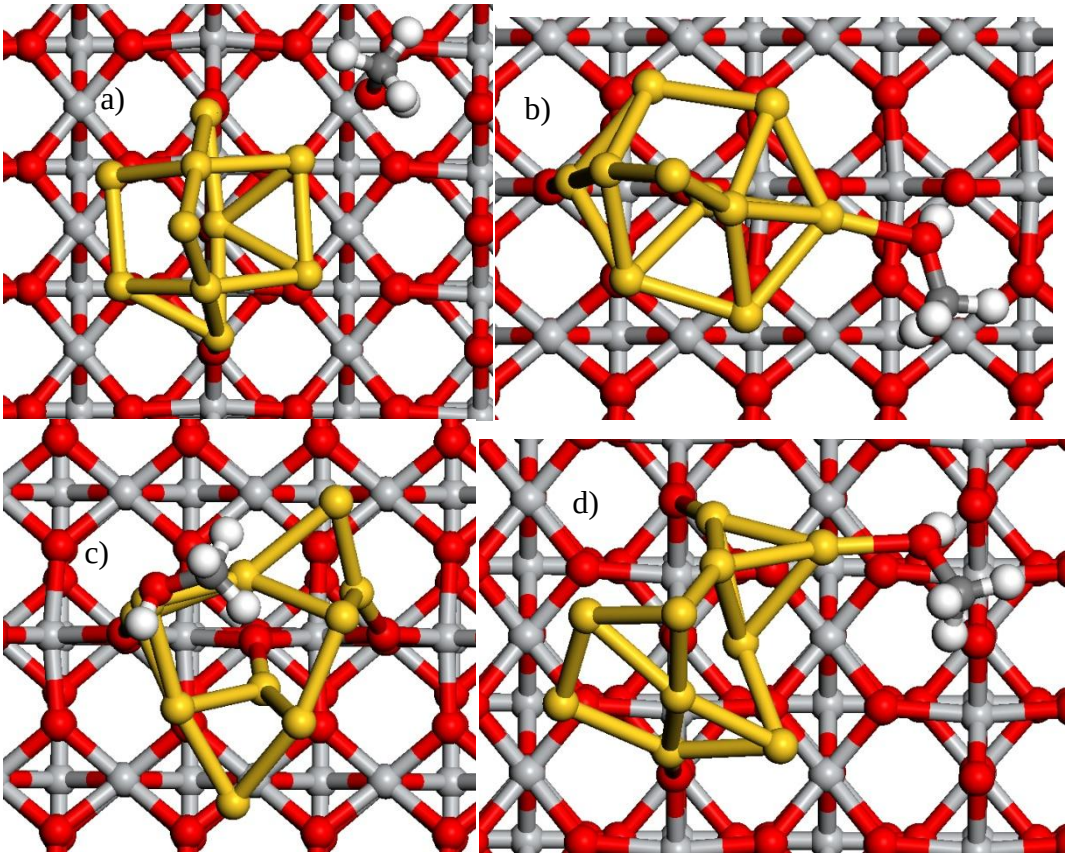

Figure 4.37. Images of CH_3OH on Au_{10} supported on TiO_2 (110) surface.

4.3. TiO_2, a new model

TiO_2 surfaces

Rutile (110)

This structure is the same as the structure in section 4.2. which is cut from the TiO_2 rutile structure in the (110) plane optimised using the U parameters discussed in chapter 3 with a value of $U_d = 8$ and $U_p = 8$ on the Ti d band and the O p band. The surface has 4 different atom co-ordinations, 2 oxygen and 2 titanium, these are labelled in figure 4.38. The oxygen atoms are in 2 co-ordinate bridging site and 3 co-ordinate in the surface, the titanium atoms are 5 and 6 co-ordinate.

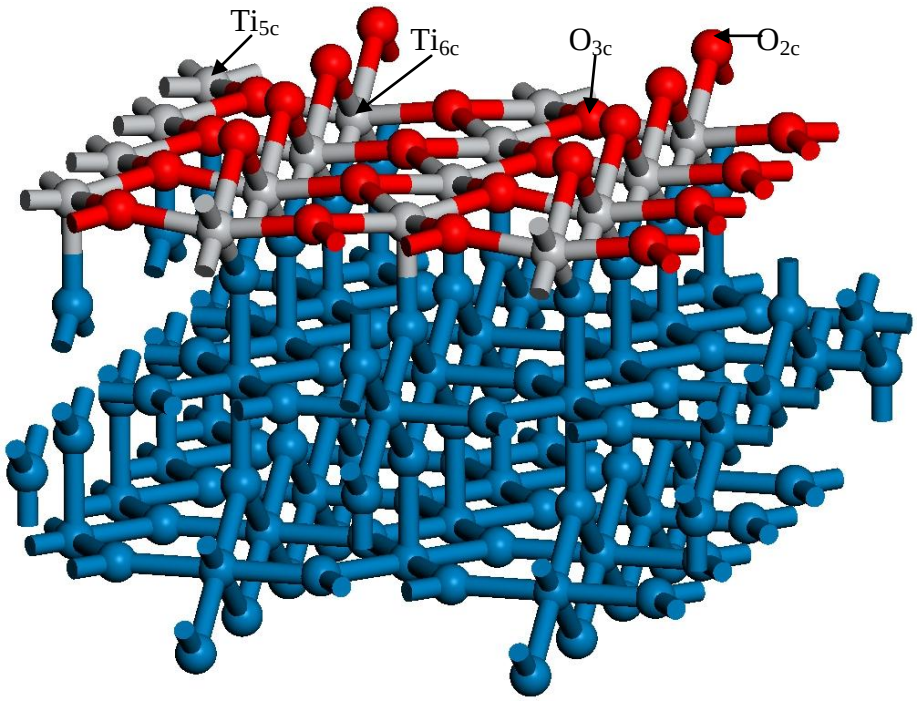

Figure 4.38. Rutile structure TiO_2 (110) surface with atom co-ordinations.

Calculations are performed in a c(4×2) cell (12.24 Å × 13.44 Å × 29.33 Å), and all surfaces have a 20 Å vacuum gap. Distances between Ti – O atoms vary with atom co-ordination and less so with the same co-ordination so the values shown are averages of like co-ordination distance. The $Ti_{5c} – O_{3c}$ distance is 2.09 Å, $Ti_{6c} – O_{3c}$ distance is 1.98 Å, $Ti_{6c} – O_{2c}$ distance is 2.08 Å, $Ti_{6c} – O_{bulk}$ distance is 2.00 Å and $Ti_{5c} – O_{bulk}$ distance is 2.10 Å.

Anatase (101)

TiO_2 has a second low energy structure with the anatase structure, which has two low energy stoichiometric surfaces. The first of these is cut along the (101) plane. The surface has 4 different atom co-ordinations, 2 oxygen and 2 titanium, which are labelled in figure 4.39. The oxygen atoms are in 2 co-ordinate bridging site and 3 co-ordinate in the surface with the 3 co-ordination oxygen atoms having two chemically different positions, the titanium atoms are 5 and 6 co-ordinate.

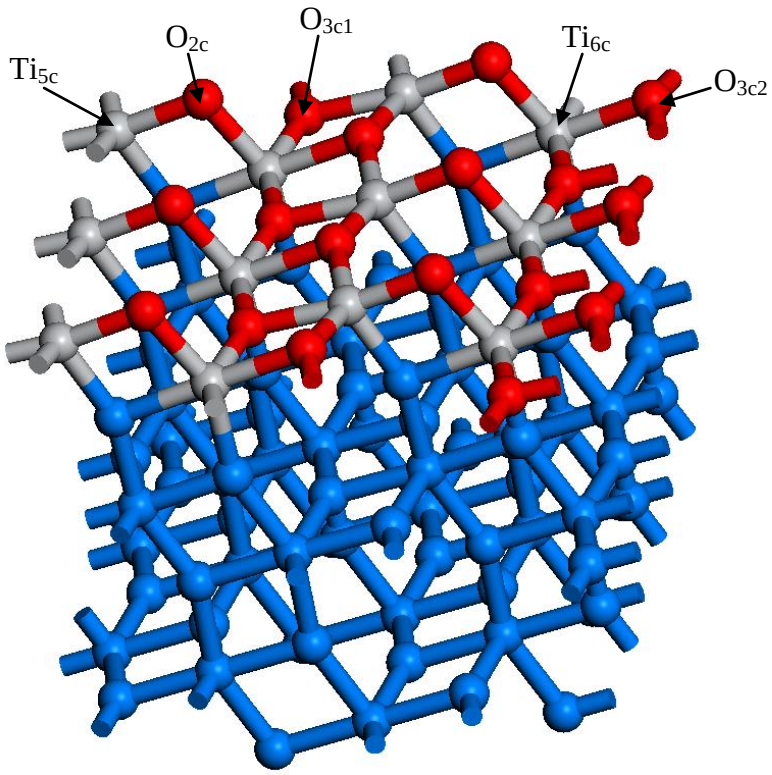

Figure 4.39. Anatase structure TiO_2 (101) surface with atom co-ordinations.

Calculations are performed in a c(1×3) cell (10.65 Å × 11.82 Å × 24.74 Å), and all surfaces have a 15 Å vacuum gap. Distances between Ti – O atoms vary with atom co-ordination. The $Ti_{5c} – O_{3c1}$ distance is 2.05 Å, $Ti_{5c} – O_{3c2}$ distance is 2.04 Å, $Ti_{6c} – O_{3c1}$ distance is 2.02 Å, $Ti_{6c} – O_{3c2}$ distance is 2.08 Å, $Ti_{6c} – O_{2c}$ distance is 1.96 Å, $Ti_{6c} – O_{bulk}$ distance is 2.10 Å and 2.07 Å and $Ti_{5c} – O_{bulk}$ distance is 1.93 Å.

Anatase (001)

The second surface can be cut along the (001) plane. The surface has 3 different atom co-ordinations, 2 oxygen and 1 titanium, which are labelled in figure 4.40. The Oxygen atoms are in 2 co-ordinate bridging site and 3 co-ordinate in the surface, the Titanium atoms are 5 co-ordinate.

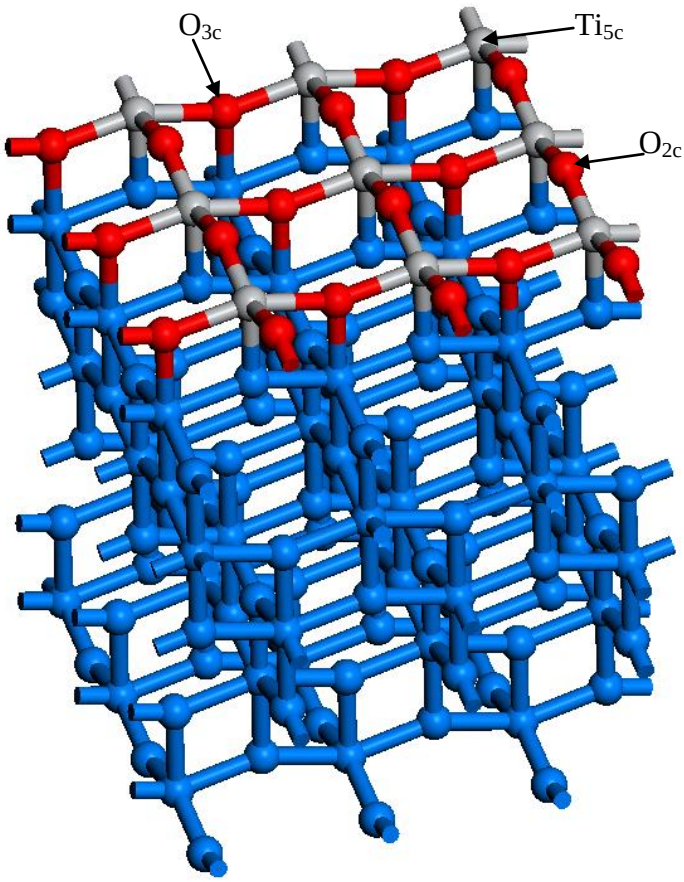

Figure 4.40. Anatase structure TiO_2 (001) surface with atom co-ordinations.

Calculations are performed in a c(3×3) cell (11.82 Å × 11.82 Å × 28.24 Å), and all surfaces have a 15 Å vacuum gap. Distances between Ti – O atoms varies with atom co-ordination. The $Ti_{5c} – O_{3c}$ distance is 2.01 Å, $Ti_{5c} – O_{2c}$ distance is 2.02 Å, $O_{3c} – Ti_{bulk}$ distance is 2.03 Å and $Ti_{5c} – O_{bulk}$ distance is 2.00 Å.

Surface Oxygen Vacancy

Each of the surfaces are cut from the rutile (110) and anatase ((101) and (001)) structures. In all of these slabs, one of the lowest co-ordination oxygen atoms is removed to create the vacancy. In all of these this is a 2 co-ordination oxygen atom.

Rutile (110)

The rutile (110) surface has one of the bridging 2 co-ordinate oxygen atoms removed, which is shown in figure 4.41. With the oxygen atoms removed, the 6 co-ordinate titanium atoms adjacent to the vacancy become 5 co-ordinate. The titanium

atoms on either side move into surface, the Ti – O_{3c} distance reduces to 1.94 Å and the Ti – O_{2c} distance increases to 2.17 Å.

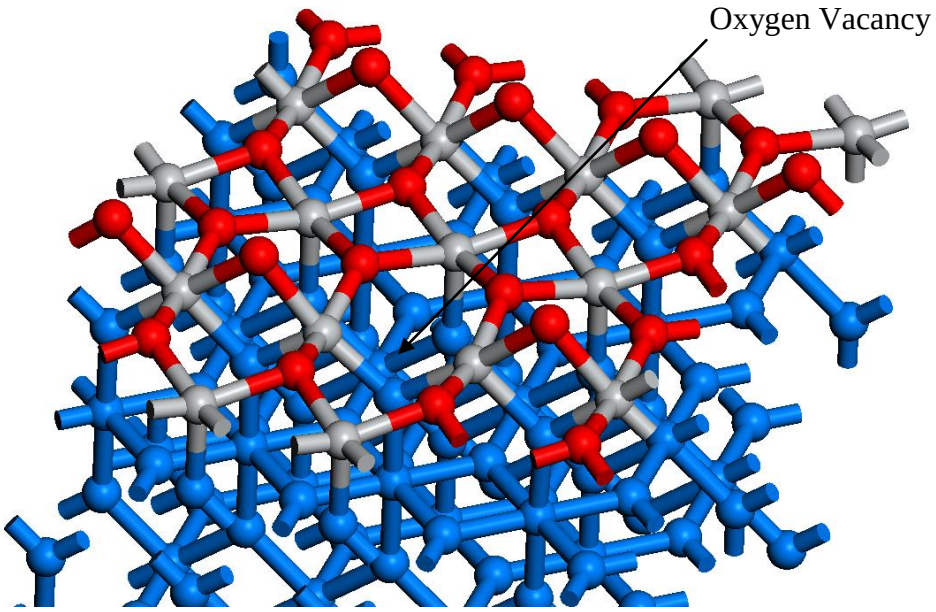

Figure 4.41. An image of a TiO_2 rutile (110) surface with an oxygen vacancy.

Anatase (101)

The anatase (101) surface has one of the bridging 2 co-ordinate oxygen atoms removed, which is shown in figure 4.42. With the oxygen removed, the 6 co-ordinate titanium atom adjacent to the vacancy become a 5 co-ordinate titanium atom and the 5 co-ordinate titanium atom adjacent to vacancy become a 4 co-ordinate titanium atom. The titanium atoms on either side move into surface, the Ti_{4c} – O_{3c1} distance reduces to 2.03 Å, the Ti_{4c} – O_{3c2} distance is 2.04 Å, the Ti_{5c} – O_{3c1} is 2.03 Å and the Ti_{5c} – O_{3c2} is 2.12 Å.

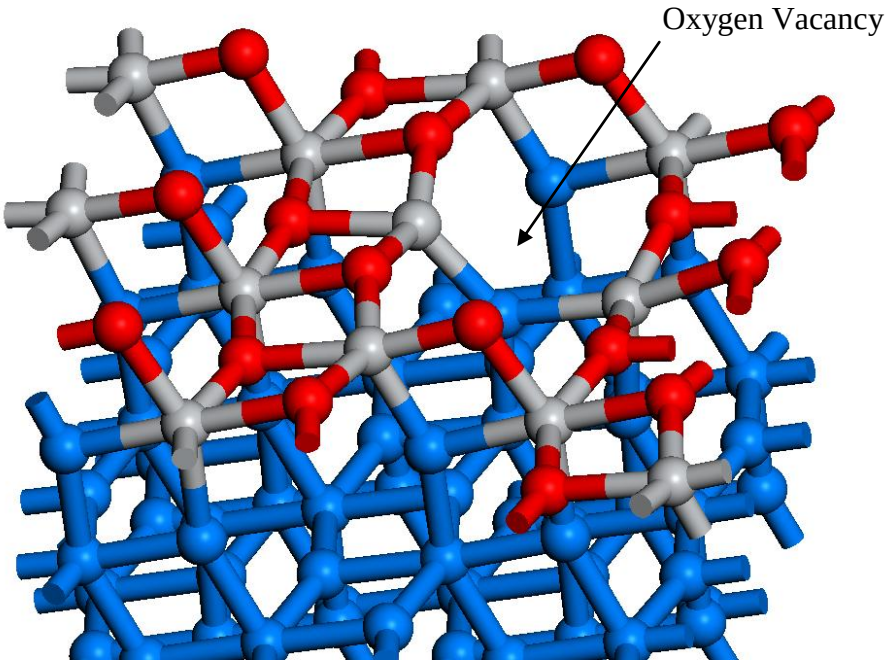

Figure 4.42. An image of TiO_2 anatase (101) surface with an oxygen vacancy.

The charges of the atoms around the vacancy show a decreased positive charge on the two adjacent titanium atoms, with charges of 1.84 e and 1.80 e compared to 2.10 e and 2.08 e without the vacancy.

Anatase (001)

The anatase (001) surface has one of the bridging 2 co-ordinate oxygen atoms removed, which is shown in figure 4.43. With the oxygen atoms removed, the 5 co-ordinate titanium atoms adjacent to the vacancy become 4 co-ordinate. The titanium atoms on either side move into surface, the Ti – O_{3c} distance is 2.04 Å and the Ti – O_{2c} distance is 1.96 Å.

The charges on the Titanium atoms adjacent to the vacancy decrease from 2.07 e to 1.81 e, when the vacancy is formed.

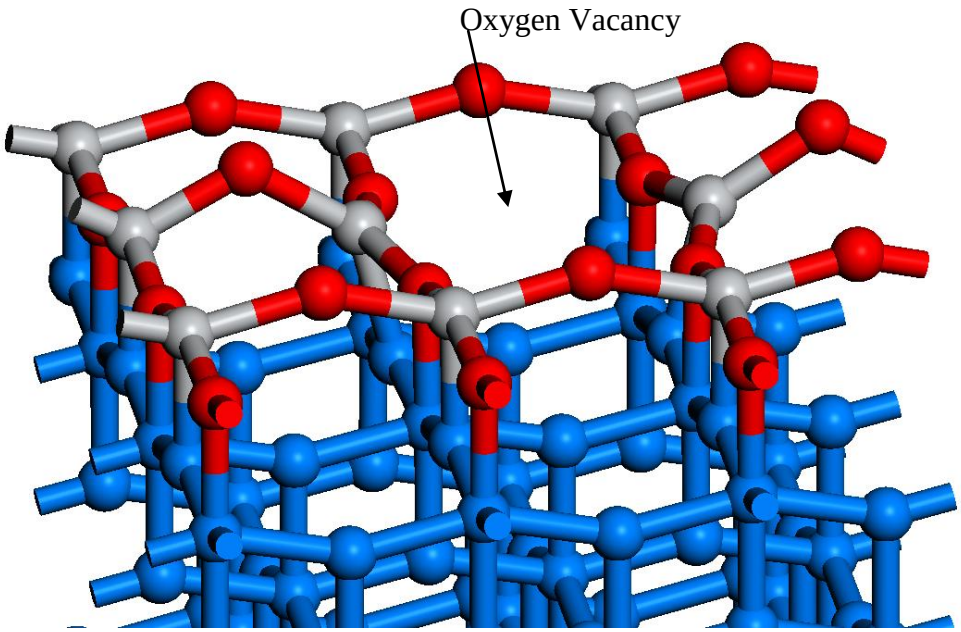

Figure 4.43. An image of TiO_2 anatase (001) surface with an oxygen vacancy.

CH_4

CH_4 adsorbs weakly to the TiO_2 rutile (110) surface with a binding energy of -6 kJ mol^{-1} and a Ti – C distance of 2.98 Å, which is shown in figure 4.44.a) A hydrogen atom can be transferred to the surface cleaving the C – H bond forming a methyl over a Ti atom and the hydrogen on a bridging oxygen atom, which is shown in figure 4.45.b) It has a binding energy of +22 kJ mol^{-1} with a Ti – C distance of 2.15 Å and an O – H distance of 0.97 Å.

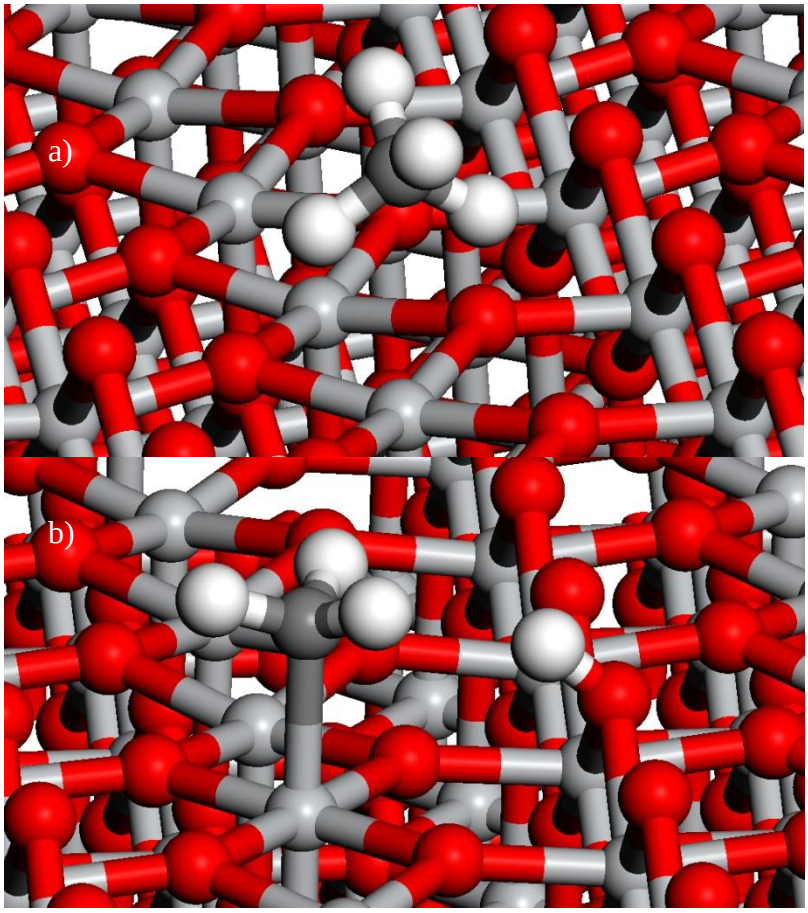

Figure 4.44. Images of a) methane and b) methyl and a hydrogen atom on a TiO_2 rutile (110) surface.

CH_4 adsorbs to a TiO_2 anatase (101) surface with a binding energy of -10 kJ mol^{-1} with a C – H distance of 3.07 Å, which is shown in figure 4.45.a) A hydrogen atom can be transferred on a 2 co-ordinate oxygen in the surface cleaving a C – H bond to form a methyl over a Ti atom in the surface and a hydrogen atom on the surface, which is shown in figure 4.45.b) It has a binding energy of -12 kJ mol^{-1}, a Ti – C distance of 2.09 Å and an O – H distance of 0.96 Å.

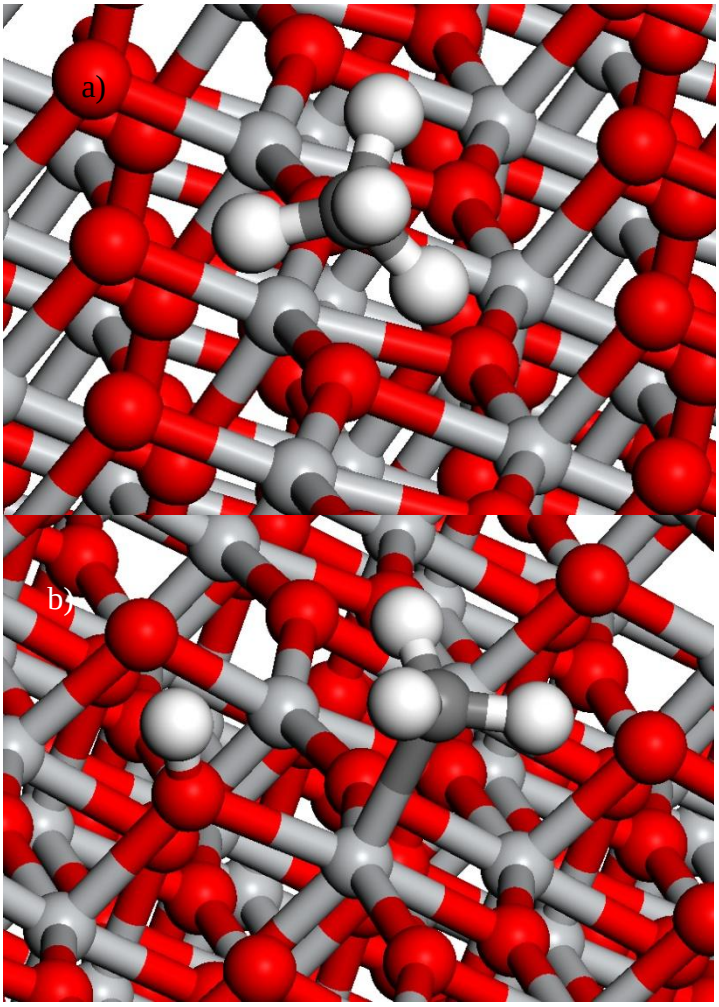

Figure 4.45. Images of a) methane and b) methyl and a hydrogen atom on a TiO_2 anatase (101) surface.

CH_4 shows no interaction with TiO_2 anatase (001) surface having a binding energy of 0 kJ mol^{-1} with a Ti – C distance of 2.90 Å, which is shown in figure 4.46.a) A hydrogen atom can be transferred to the surface to a two co-ordinate oxygen atom and form a methyl over a Ti atom in the surface and a hydrogen atom on a surface oxygen atom, which is shown in figure 4.46.b) It has a binding energy of -36 kJ mol^{-1}, a Ti – C distance of 2.16 Å and an O – H distance of 0.96 Å.

The barrier for transfer of a hydrogen atom from the methane to the surface cleaving the C – H bond is 21 kJ mol^{-1} with the reverse 60 kJ mol^{-1}, which is shown in figure 4.47.

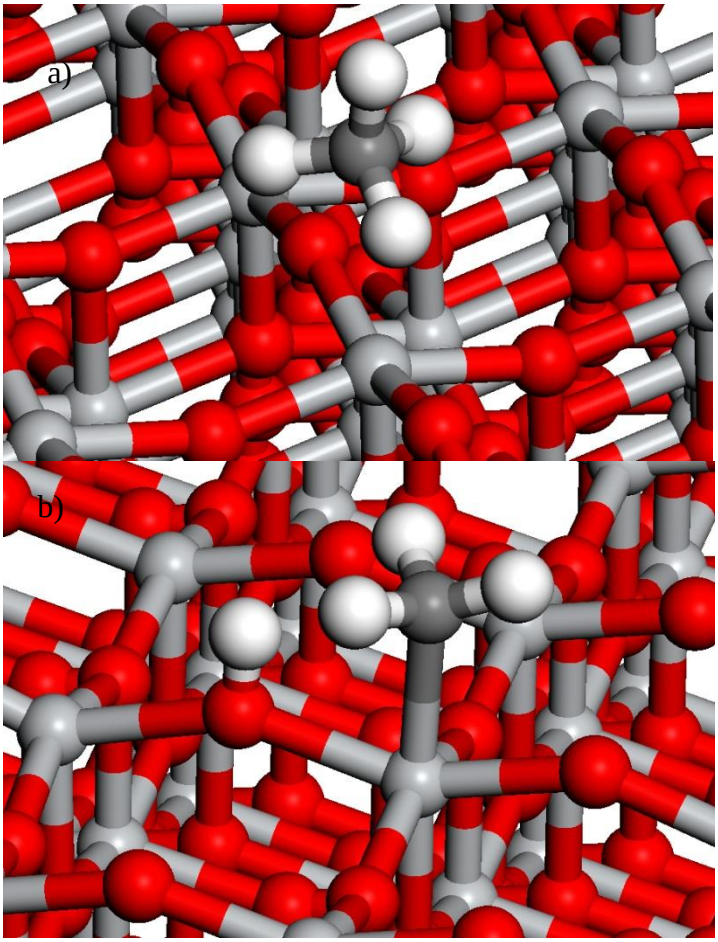

Figure 4.46. Images of a) methane and b) methyl and a hydrogen atom on a TiO_2 anatase (001) surface.

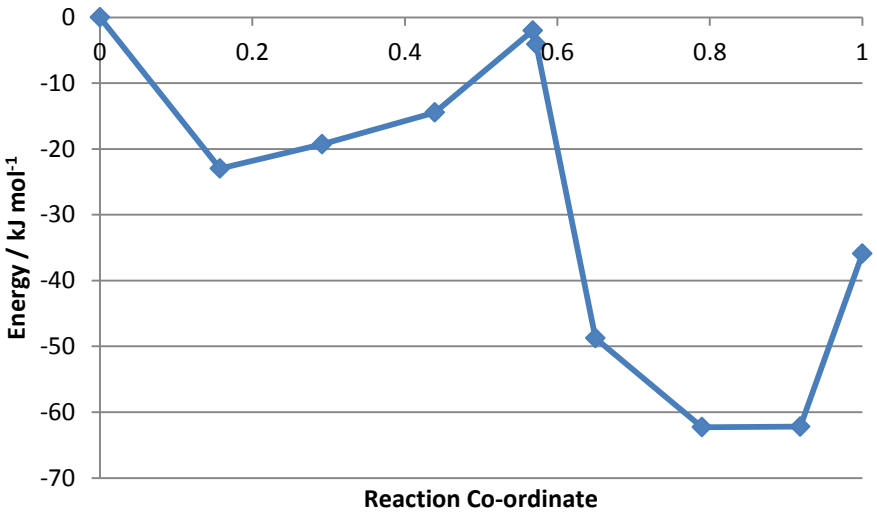

Figure 4.47. Plot of the barrier for hydrogen transfer and C – H bond cleavage over TiO_2 anatase (001).

CH_4 adsorbs weakly to TiO_2 anatase (001) over an oxygen vacancy with a binding energy of -6 kJ mol^{-1} and a Ti – C distance of 2.95 Å, which is shown in figure 4.48.a) A hydrogen atom can be transferred to the surface to a two co-ordinate oxygen atom and form a methyl over a Ti atom in the surface and a hydrogen atom on a surface oxygen atom, which is shown in figure 4.48.b) It has a binding energy of +49 kJ mol^{-1}, a Ti – C distance of 2.22 Å and an O – H distance of 0.96 Å.

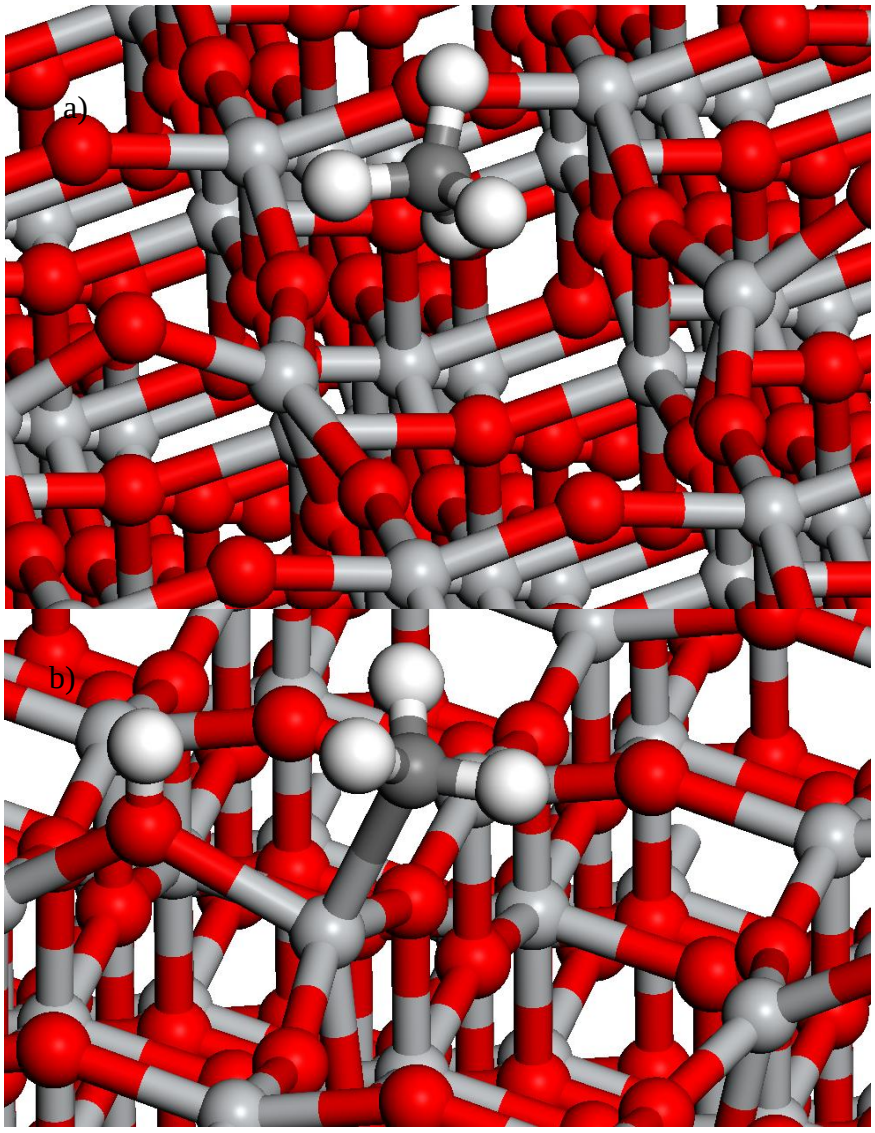

Figure 4.48. Images of a) methane and b) methyl and a hydrogen atom on a TiO_2 anatase (001) surface with an oxygen vacancy.

O_2

O_2 can interact with the oxygen vacancy in the TiO_2 rutile (110), placing the O_2 along the *a* lattice parameter producing the O_2 molecule bridging the gap between the

two Ti atoms on either side of the vacancy, which is shown in figure 4.49. It has a binding energy of +16 kJ mol^{-1}, Ti – O distances of 2.13 Å and 2.14 Å, an O – O distance of 1.33 Å and Ti – Ti distance of 3.17 Å across the vacancy which is compared to 3.20 Å without the oxygen present. In the direction of the *b* and *c* parameters one of the oxygen atoms in the O_2 molecule replaces the missing oxygen atom from the vacancy, which is shown in figure 4.4.X. In the *b* direction the binding energy is -24 kJ mol^{-1} with two Ti – O distances of 2.11 Å, an O – O distance of 1.37 Å and a Ti – Ti distance of 3.10 Å. In the *c* direction the binding energy is -21 kJ mol^{-1} with Ti – O distances of 2.09 Å and 2.10 Å, an O – O distance of 1.36 Å and a Ti – Ti distance of 3.11 Å.

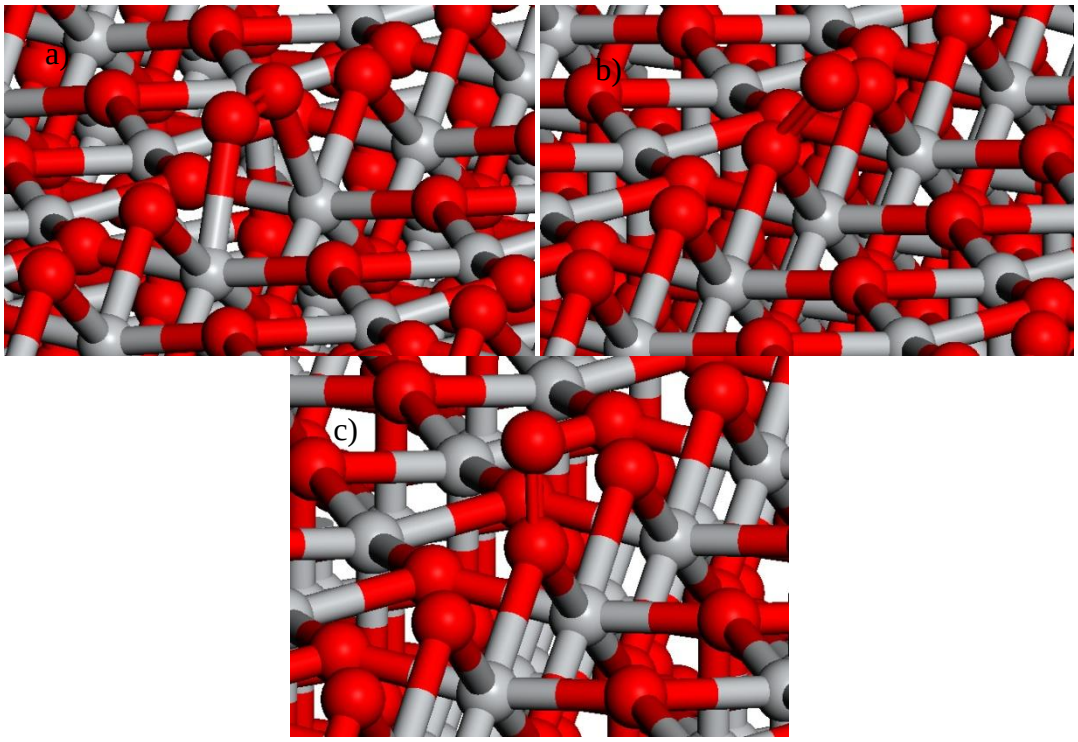

Figure 4.49. O_2 adsorbed on TiO_2 rutile (110) in 3 different orientations.

The same can be done with the TiO_2 anatase (101) surface with an oxygen vacancy, placing O_2 along the *a* lattice direction producing an O_2 molecule bridging the gap between the two Ti atoms on either side of the vacancy, which is shown in figure 4.50.a). It has a binding energy of -13 kJ mol^{-1}, Ti – O distances of 2.06 Å and 2.26 Å, an O – O distance of 1.35 Å and Ti – Ti distance of 3.32 Å across the vacancy which is compared to 3.48 Å without the oxygen present. In the *b* direction the O_2 adsorbs to a single Ti atom with longer distances to the second Ti atom, which is shown in figure 4.50.b) In the *b* direction the binding energy is +37 kJ mol^{-1} with Ti

– O distances of 2.16 Å and 2.21 Å to one Ti atom and 2.47 Å and 2.51 Å to the other Ti atom, an O – O distance of 1.39 Å and a Ti – Ti distance of 3.23 Å. In the direction of the *c* parameters one of the oxygen atoms in the O_2 molecule replaces the missing oxygen atom from the vacancy, which is shown in figure 4.50.c) In the *c* direction the binding energy is -57 kJ mol^{-1} with Ti – O distances of 2.11 Å and 2.15 Å, an O – O distance of 1.37 Å and a Ti – Ti distance of 3.30 Å.

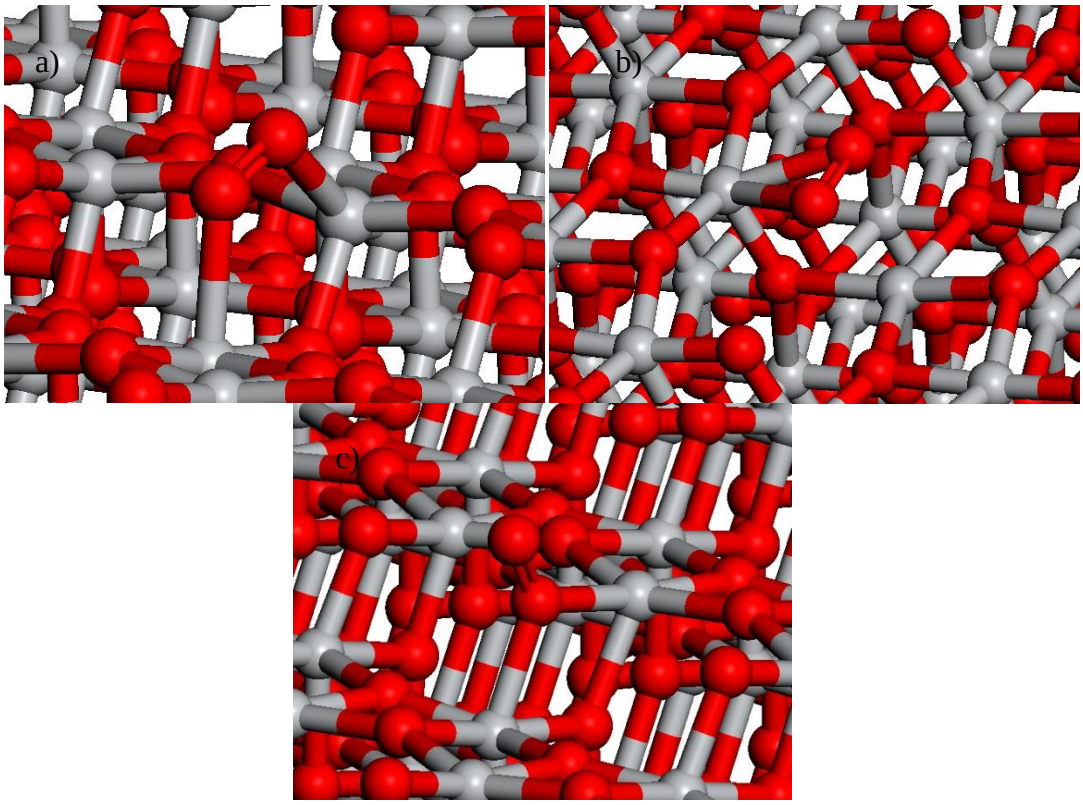

Figure 4.50. O_2 adsorbed on TiO_2 anatase (101) in 3 different orientations.

The TiO_2 anatase (001) surface with a surface oxygen vacancy interacts differently with O_2 compared to the other TiO_2 surfaces with vacancy. Placing O_2 along the *a* lattice direction has an O_2 molecule over the vacancy, which is shown in figure 4.51.a) It has a binding energy of -1 kJ mol^{-1}, Ti – O distances of 2.61 Å and 2.82 Å, an O – O distance of 1.23 Å and Ti – Ti distance of 5.18 Å across the vacancy which is compared to 5.14 Å without the oxygen present. In the *b* and *c* directions the O_2 molecule sits over the vacancy, which is shown in figure 4.51.b) and c) In the *b* direction it has a binding energy of -2 kJ mol^{-1}, Ti – O distances of 2.77 Å and 3.10 Å, an O – O distance of 1.23 Å and a Ti – Ti distance of 5.14 Å. In the *c* direction it

has a binding energy of -89 kJ mol^{-1}, two Ti – O distances of 2.86 Å, an O – O distance of 1.23 Å and Ti – Ti distance of 5.23 Å.

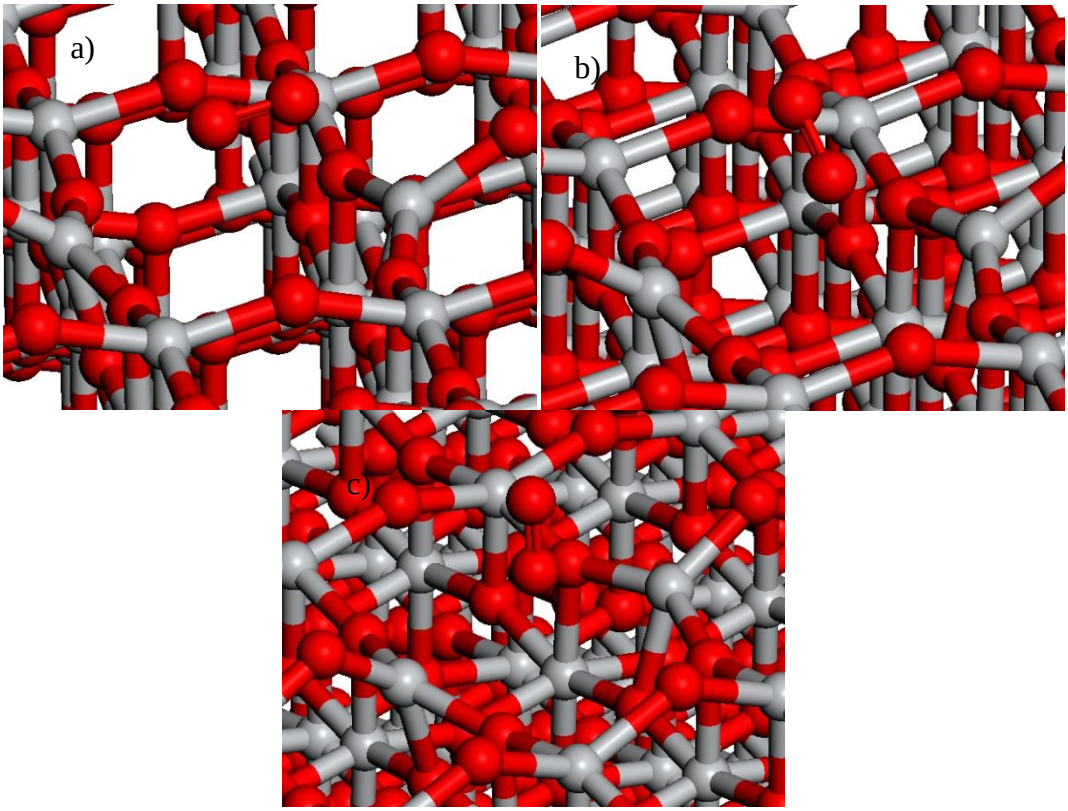

Figure 4.51. O_2 adsorbed on TiO_2 anatase (001) in 3 different orientations

H_2O_2

H_2O_2 adsorbs to a TiO_2 anatase (101) surface with a binding energy of -68 kJ mol^{-1}, which is shown in figure 4.52.a) It has a Ti – O distance of 2.29 Å and an O – O distance of 1.48 Å. A hydrogen atom can be transferred from the H_2O_2 to the surface to the 2 co-ordinate oxygen cleaving the O – H bond with the OOH over a Ti atom, which is shown in figure 4.52.b) It has a binding energy of -134 kJ mol^{-1}, a Ti – O distance of 2.38 Å, an O – O distance of 1.37 Å and an O – H distance of 0.96 Å to the transferred hydrogen atom.

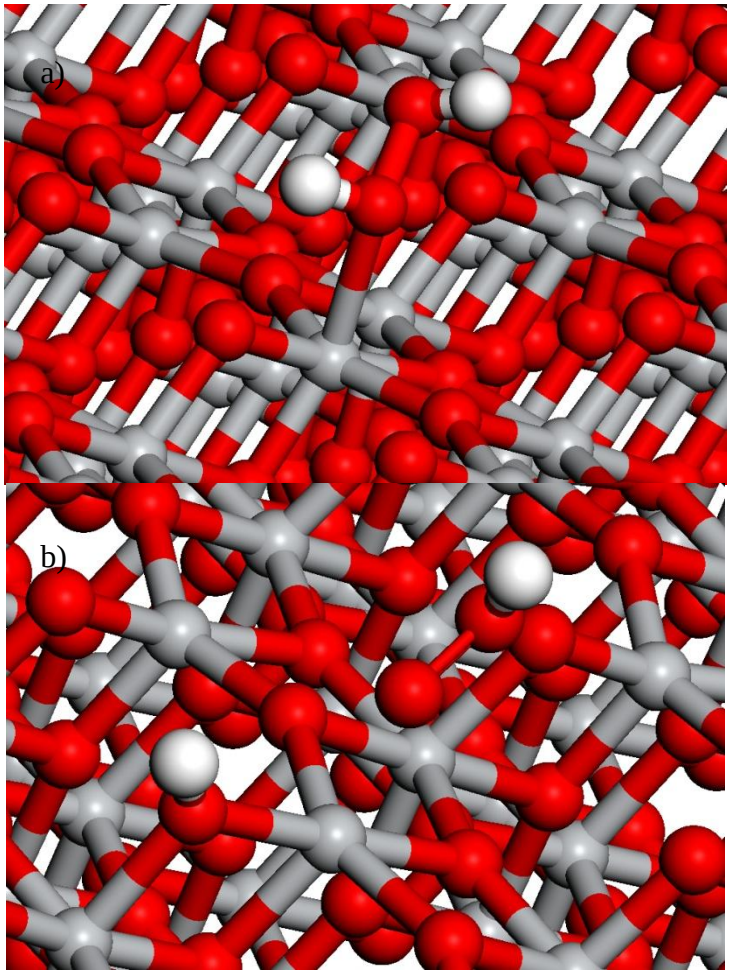

Figure 4.52. Images of a) H_2O_2 and b) OOH and a hydrogen atom on a TiO_2 anatase (101) surface.

H_2O_2 adsorbs to a TiO_2 anatase (001) surface, binding at a Ti atom to an O atom in the H_2O_2, which is shown in figure 4.53. It has a binding energy of -58 kJ mol^{-1}, Ti – O distance of 2.19 Å and an O – O distance of 1.47 Å. H_2O_2 can also adsorb via two oxygen atoms, which is shown in figure 4.53.a) and b). It has a binding energy of -76 kJ mol^{-1}, two Ti – O distances of 2.55 Å, an O – O distance of 1.49 Å and a hydrogen bonding distance between one hydrogen atom on the H_2O_2 and a surface oxygen atom of 1.71 Å. A hydrogen atom can be transferred from the H_2O_2 to the surface cleaving the O – H bond producing an OOH and a surface hydrogen atom, which is shown in figure 4.53.c) It has a binding energy of -156 kJ mol^{-1}, a Ti – O distance of 2.02 Å, an O – O distance of 1.47 Å and an O – H distance of 0.97 Å from a surface oxygen atom to the transferred hydrogen atom. The HO – OH bond in H_2O_2 can be cleaved over the surface to form two hydroxyl groups over two Ti

atoms, which is shown in figure 4.53.d) It has a binding energy of -274 kJ mol^{-1} and has Ti – O distances of 1.92 Å and 1.94 Å.

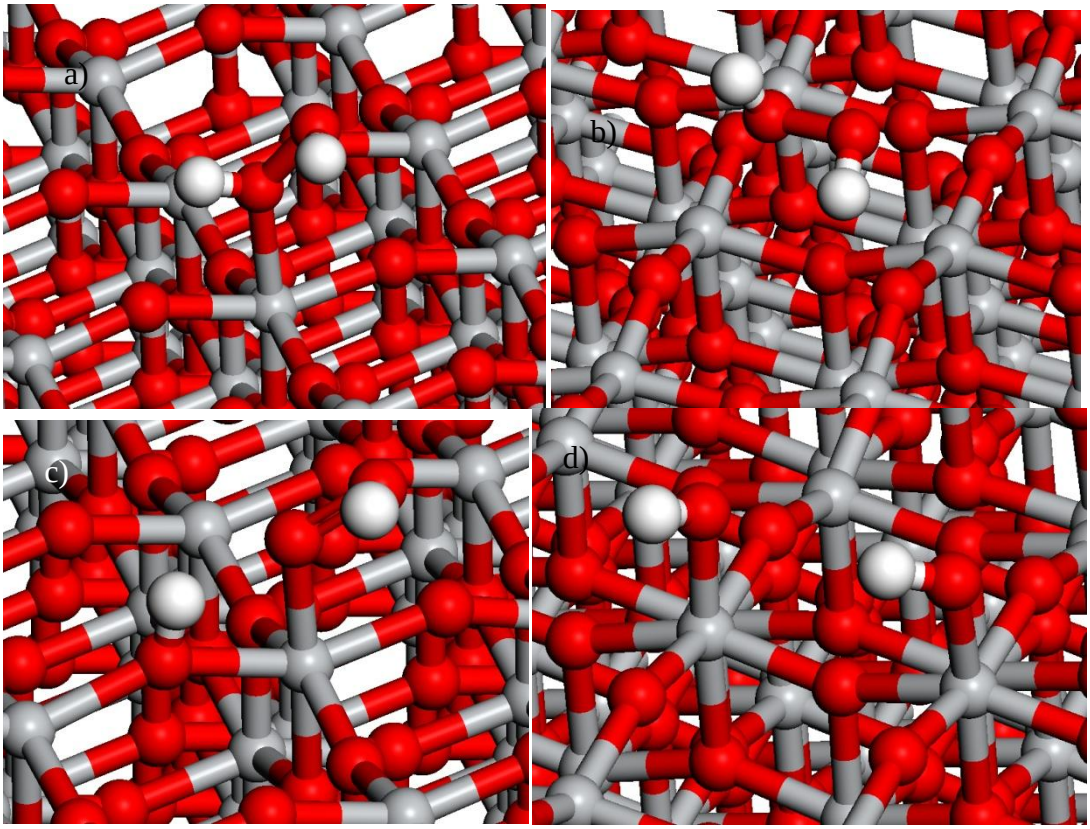

Figure 4.53. Images of H_2O_2, OOH and 2OH over a TiO_2 anatase (001) surface.

The barrier for the transfer of a hydrogen atom from H_2O_2 to the surface is 7 kJ mol^{-1} with the reverse 96 kJ mol^{-1}, which is shown in figure 4.54. The barrier for the HO – OH bond cleavage is 12 kJ mol^{-1} with the reverse 210 kJ mol^{-1}, which is shown in figure 4.55.

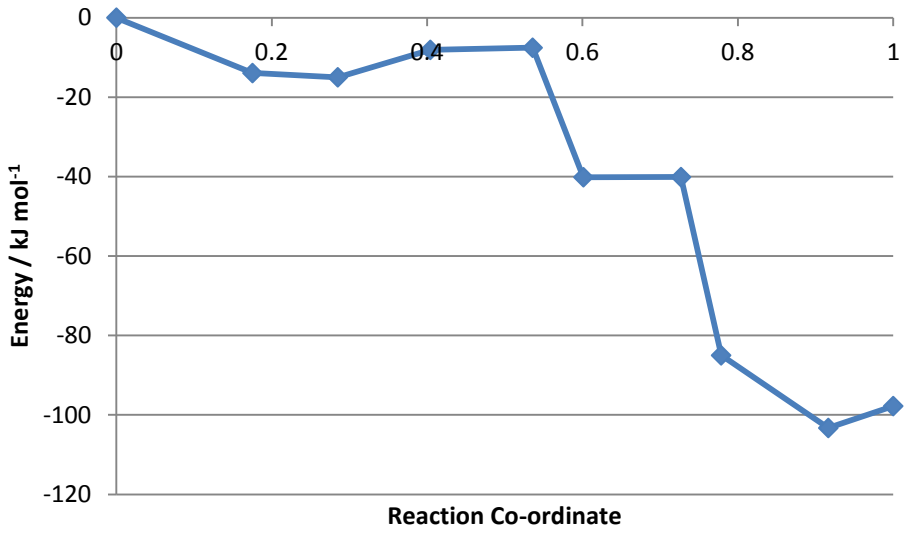

Figure 4.54. A plot of the barrier for the dissociation of H – OOH bond to form a OOH and surface hydrogen from H_2O_2.

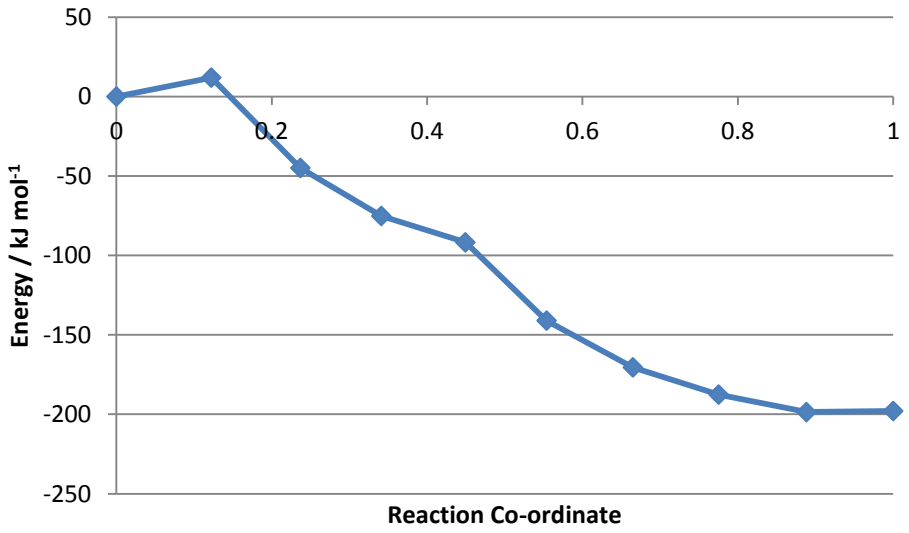

Figure 4.55. A plot of the barrier for the dissociation of HO –OH bond to form two hydroxyls from H_2O_2.

H_2O_2 adsorbs to a TiO_2 anatase (001) surface with an oxygen vacancy. The H_2O_2 adsorbs over the oxygen vacancy, and two examples of this are shown in figure 4.56.a) and b) H_2O_2 bound across the vacancy has a binding energy of -24 kJ mol^{-1}, Ti – O distances of 2.36 Å and 2.98 Å, an O – O distance of 1.49 Å and Ti – Ti distance across the vacancy of 5.06 Å, which is compared to 5.14 Å for the oxygen vacancy with no adsorbate. The second example of H_2O_2 adsorbed over an oxygen

vacancy on a TiO_2 anatase (001) surface has a binding energy of -101 kJ mol^{-1}, Ti – O distances of 2.49 Å and 2.90 Å, an O – O distance of 1.49 Å, a Ti – Ti distance of 4.95 Å and a hydrogen bonding O – H distance of 1.84 Å between the an oxygen atom in the surface adjacent to the vacancy and one of the hydrogen atoms in H_2O_2. H_2O_2 can have the H – OOH bond cleaved to form a surface hydrogen atom bound to a surface oxygen atom and OOH bound to Ti atom, which is shown in figure 4.56.c) The OOH and surface hydrogen atom has a binding energy of -145 kJ mol^{-1}, a Ti – OOH distance of 2.11 Å, a Ti – O(H)O distance of 2.27 Å, an O – O distance of 1.53 Å, an O – H distance of 0.96 Å to the surface hydrogen atom and a Ti – Ti distance of 4.40 Å. The O – O bond in H_2O_2 can be cleaved to produce two hydroxyls bound to Ti atoms either side of the oxygen vacancy, which is shown in figure 4.56.d) The hydroxyls have a binding energy of -204 kJ mol^{-1}, Ti – O distances of 1.86 Å and 1.94 Å, a Ti – Ti distance of 4.67 Å and a hydrogen bonding O – H distance of 1.70 Å between an oxygen atom on one hydroxyl to a hydrogen atom on the other.

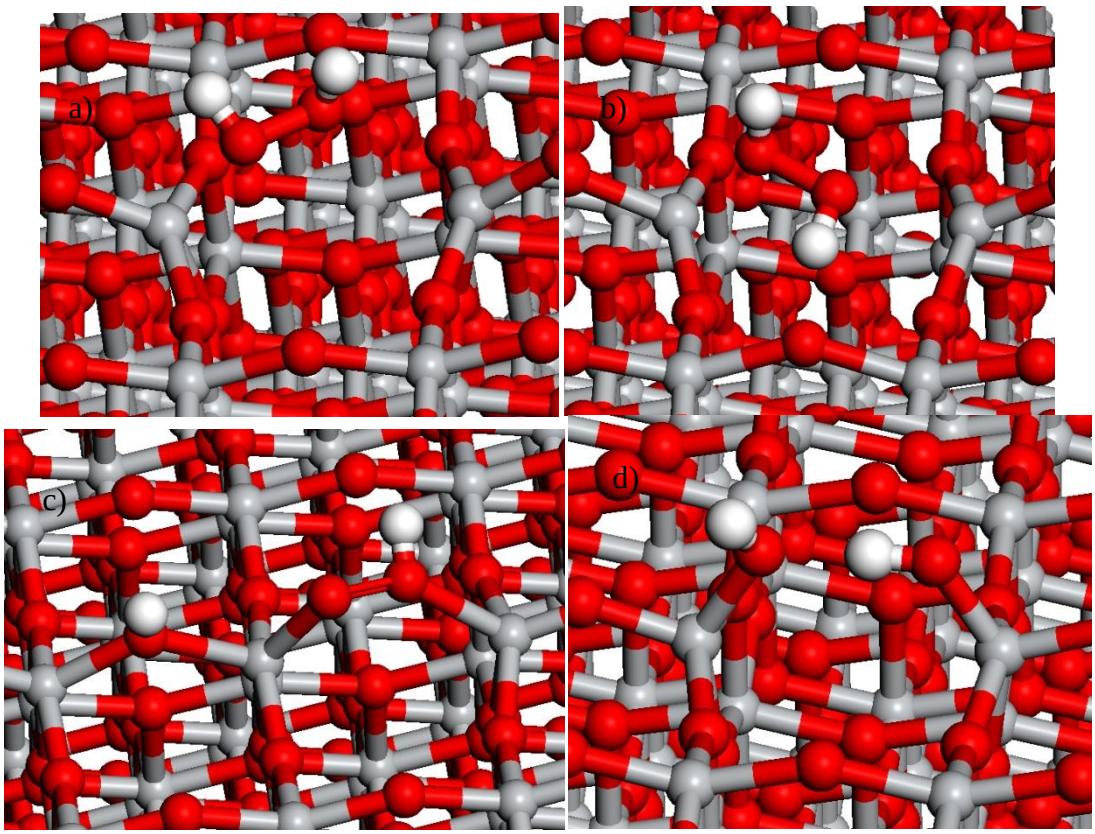

Figure 4.56. Image of H_2O_2 over TiO_2 anatase (001) surface with an oxygen vacancy a) H_2O_2 b) H_2O_2 with hydrogen bond c) OOH and hydrogen atom d) two hydroxyls.

CH_3OOH

CH_3OOH adsorbs unfavourably to a TiO_2 anatase (001) surface with the O – O bond running parallel to the surface, which is shown in figure 4.57.a) This structure has a binding energy of 40 kJ mol^{-1} with respect to an isolated CH_3OOH molecule and clean TiO_2 anatase (001) surface. CH_3OOH has Ti – O distances of 2.55 Å and 2.56 Å to the surface, a C – O distance of 1.42 Å and an O – O distance of 1.48 Å. CH_3OOH is adsorbed over the surface with two surface hydrogen atoms so it can be compared to H_2O_2 and CH_4 , which is shown in figure 4.57.b) This allows CH_3OOH to be compared to H_2O_2 and CH_4 and relate it to the reaction to produce it. This has a binding energy of -426 kJ mol^{-1} with respect to H_2O_2, CH_4 and the clean surface but this cannot be compared to the single CH_3OOH on the surface as it has a different baseline. The CH_3OOH has a Ti – O distance of 2.39 Å to the surface, a C – O distance of 1.42 Å and an O – O distance of 1.49 Å. The surface hydrogen atoms have O – H distances of 0.96 Å and 0.95 Å.

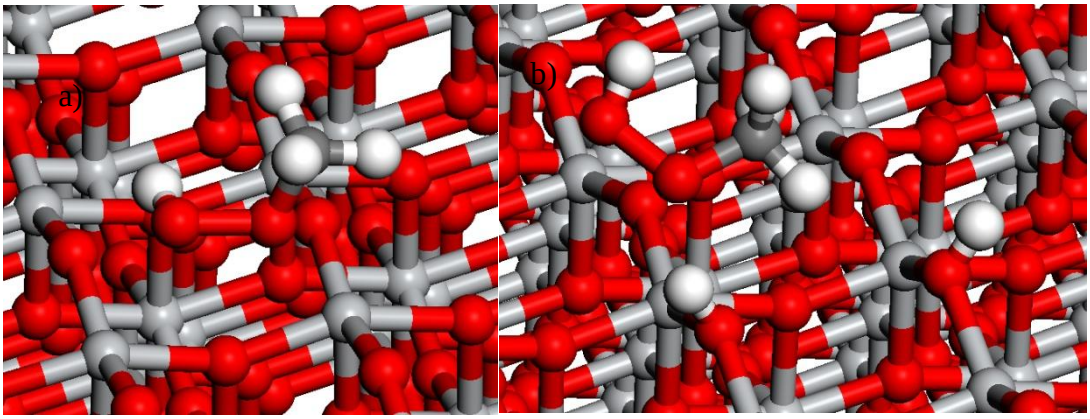

Figure 4.57. Images of CH_3OOH over TiO_2 anatase (001) surface a) CH_3OOH b) CH_3OOH and two surface hydrogen atoms.

CH_3OOH can be formed from CH_3 and OOH adsorbed on TiO_2 anatase (001) surface which are bound to Ti atoms in the surface, which is shown in figure 4.58.a) The CH_3, OOH and two surface hydrogen atoms have a binding energy of -217 kJ mol^{-1} with respect to CH_3OOH and a clean surface, a Ti – C distance of 2.17 Å, a Ti – O distance of 2.03 Å, an O – O distance of 1.48 Å and two O – H distances to the O atoms in the surface of 0.96 Å and 0.97 Å. The CH_3OOH can be cleaved by the O – O bond in the same way as the HO – OH in H_2O_2 to form a CH_3O and a hydroxyl, which is shown in figure 4.58.b) The CH_3O and the hydroxyl have a binding energy

of -157 kJ mol^{-1} with respect to CH_4, H_2O_2 and a clean surface, a Ti – OCH_3 distance of 1.91 Å, a Ti – OH distance of 1.90 Å and a C – O distance of 1.38 Å.

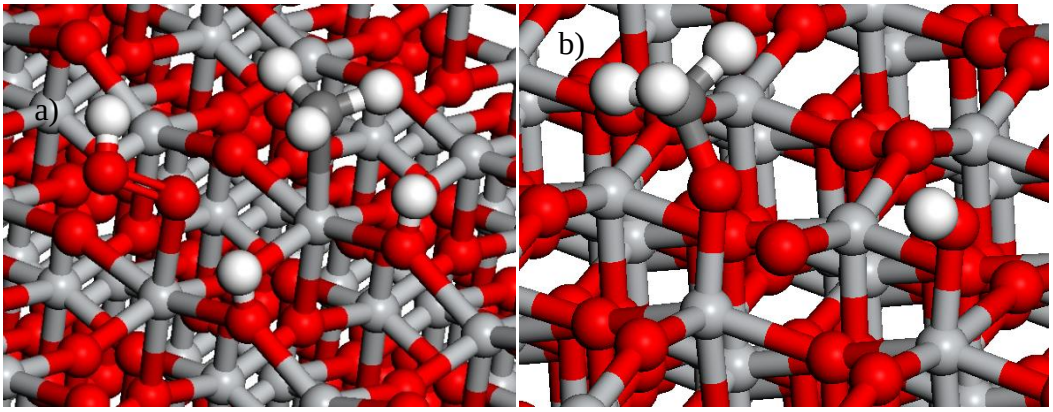

Figure 4.58. Images of CH_3OOH over TiO_2 anatase (001) surface with CH_3OOH a) CH_3, OOH and two surface hydrogen atoms and b) CH_3O and OH.

The barrier for the formation of CH_3OOH from CH_3 and OOH is 175 kJ mol^{-1} with the reverse 385 kJ mol^{-1}, which is shown in figure 4.59.

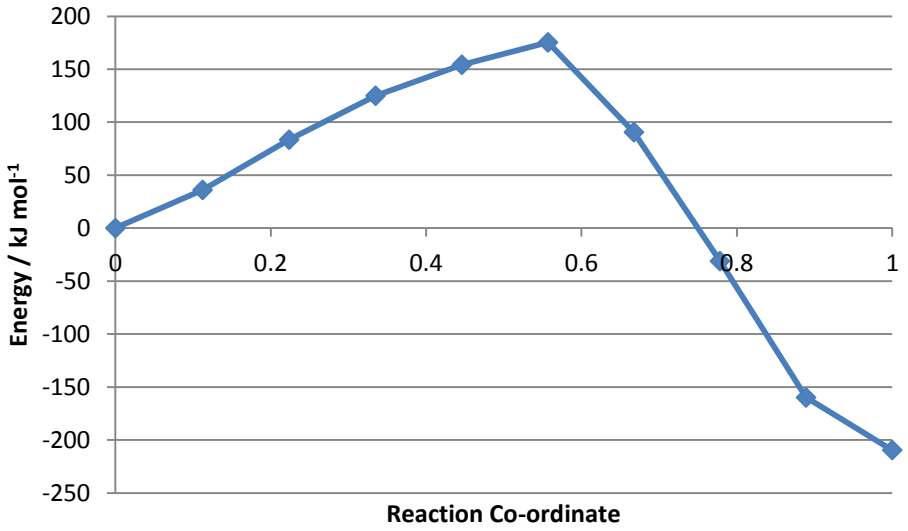

Figure 4.59. A plot of the barrier for the formation of CH_3OOH from CH_3 and OOH.

The barrier for the dissociation of the CH_3O – OH in CH_3OOH is negligible due to two minima existing for CH_3OOH and CH_3O and OH and no maximum being found in the barrier. The difference between CH_3OOH and the lowest point on the barrier, CH_3O and a hydroxyl is 213 kJ mol^{-1}, which is shown in figure 4.60.

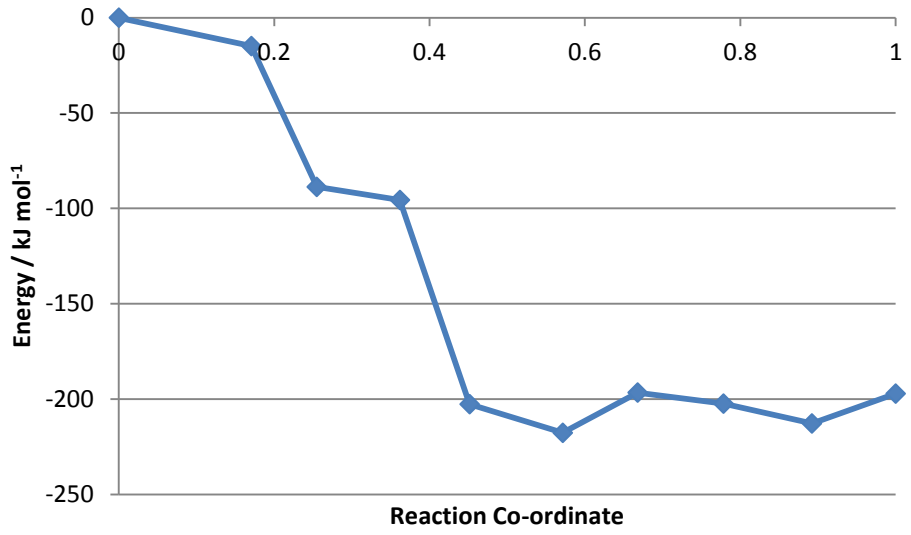

Figure 4.60. A plot of the barrier for the dissociation of CH_3OOH to CH_3O and OH.

CH_3OH

CH_3OH adsorbs to TiO_2 anatase (001) surface to a Ti atom in the surface, which is shown in figure 4.61.a) It has a binding energy of -33 kJ mol^{-1}, a Ti – O distance of 2.18 Å and a C – O distance of 1.42 Å. The CH_3OH can be formed from a CH_3O and a surface hydrogen atom with the CH_3O over a Ti atom and the surface hydrogen atom is bound to an oxygen atom in the surface, which is shown in figure 4.61.b) It has a binding energy of -120 kJ mol^{-1}, a Ti – O distance of 1.96 Å, a C – O distance of 1.40 Å and an O – H distance of 0.98 Å.

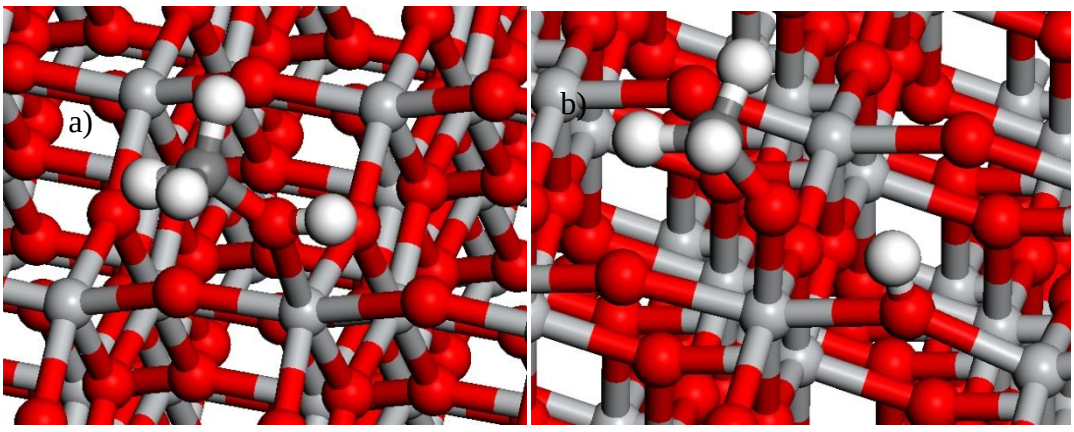

Figure 4.61. Images of CH_3OH and CH_3O and a surface hydrogen atom over TiO_2 anatase (001) surface.

The barrier for dissociation of the CH_3O – H bond to form CH_3O and a surface hydrogen atom is 2 kJ mol^{-1} with the reverse barrier of 69 kJ mol^{-1}, which is shown in figure 4.62. This shows that the CH_3OH is likely to remain as CH_3O and a H atom, which is supported by the binding energies.

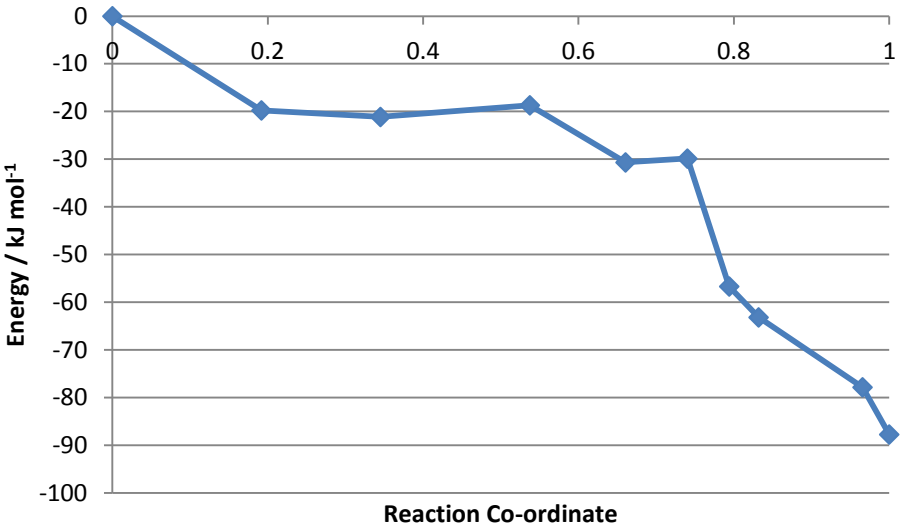

Figure 4.62. A plot of the barrier of the dissociation of CH_3OH to form CH_3O and a surface hydrogen atom.

H_2O

Water is adsorbed to a TiO_2 anatase (001) surface over a Ti atom in the surface, which is shown in figure 4.63.a) It has a binding energy of -44 kJ mol^{-1} and a Ti – O distance of 2.16 Å. A hydrogen atom can be transferred from the water to the surface to form a hydroxyl and a surface hydrogen atom, which is shown in figure 4.63.b) It has a binding energy of -110 kJ mol^{-1}, a Ti – O distance of 1.96 Å and an O – H distance of 0.97 Å.

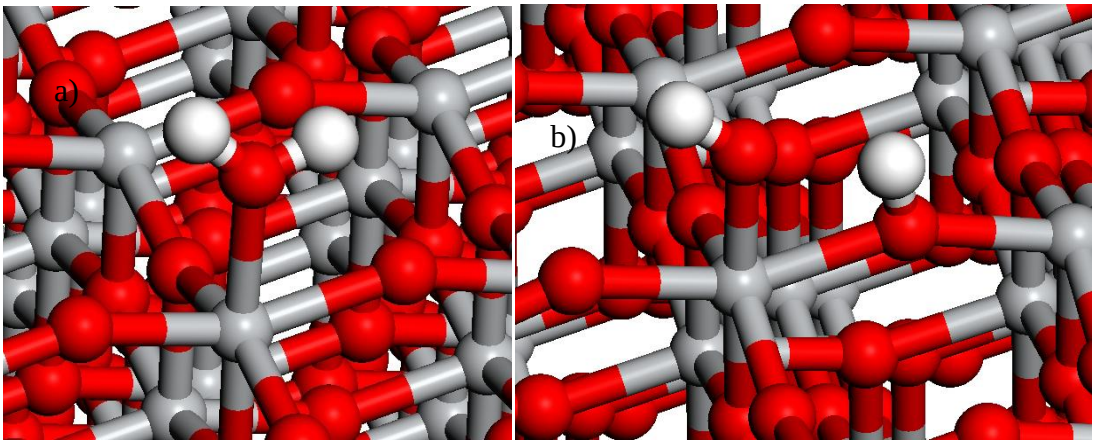

Figure 4.63. Images of water and hydroxyl and a surface hydrogen atom over a TiO_2 anatase (001) surface.

The barrier to the dissociation of the HO – H bond to form a hydroxyl and a surface hydrogen atom is 15 kJ mol^{-1} with the reverse barrier of 82 kJ mol^{-1}, which is shown in figure 4.64.

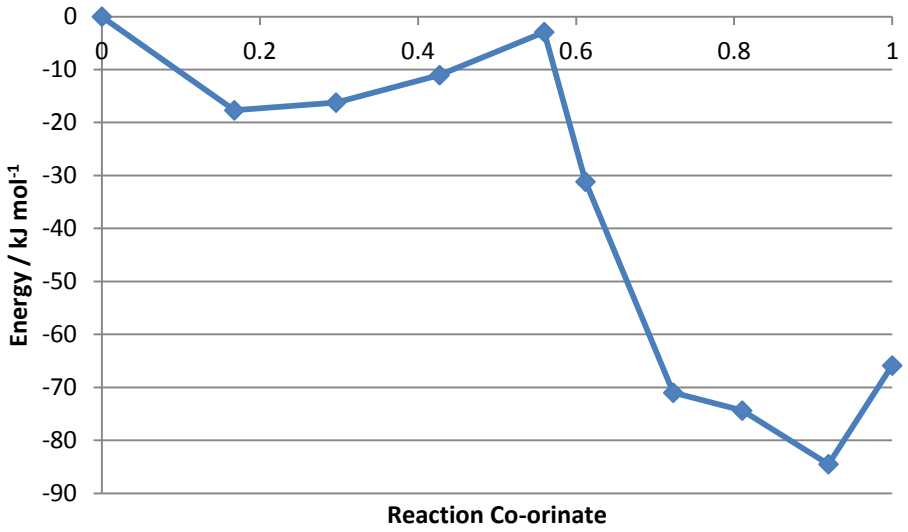

Figure 4.64. A plot of the barrier of the dissociation of water to a hydroxyl group and a hydrogen atom.

Au_{10}

Au_{10} adsorbs to TiO_2 rutile (110) surface between two ridges of oxygen atoms, which is shown in figure 4.65.a) It has a binding energy of -262 kJ mol^{-1}, Au – O distances of 2.09 Å, 2.11 Å, 2.19 Å and 2.26 Å, a Au – Ti distance of 3.17 Å and a

Bader charge on the Au_{10} cluster of 2.29 e. This is a similar to the result for the binding energy to the one found without the U value used on the oxygen atoms but it shows better wetting of the surface. Au_{10} adsorbs over an oxygen vacancy in a TiO_2 rutile (110) surface, again between the two ridges of bridging oxygen atoms, which is shown in figure 4.65.b). It has a binding energy of -223 kJ mol^{-1}, Au – O distances of 2.12 Å, 2.18 Å, 2.18 Å, 2.22 Å, 2.57 Å and 2.75 Å, a Au – Ti distance of 2.98 Å and a Bader charge of 2.13 e on the Au_{10} cluster.

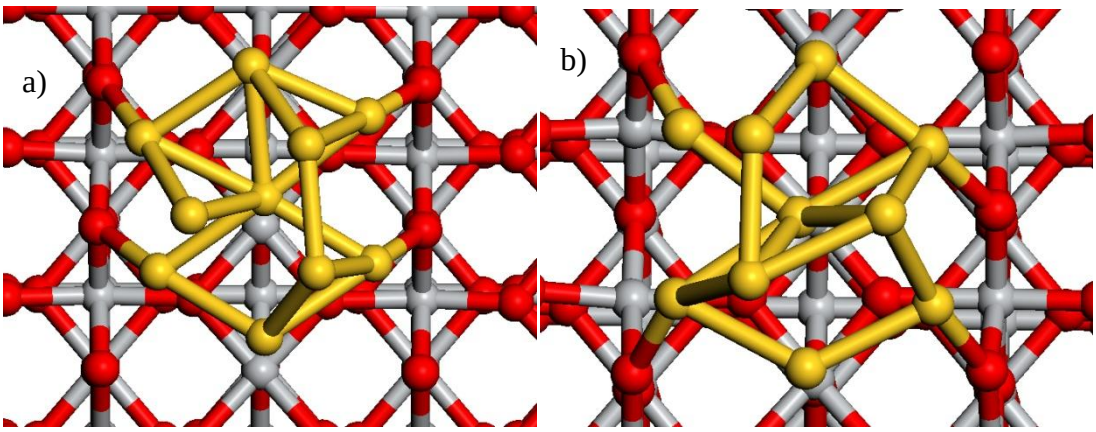

Figure 4.65. Images of a Au_{10} cluster over a TiO_2 rutile (110) with and with an oxygen vacancy

Au_{10} adsorbs to a TiO_2 anatase (101) surface over one of the steps, which is shown in figure 4.66.a) It has a binding energy of -255 kJ mol^{-1}, Au – O distances of 2.17 Å, 2.19 Å, 2.26 Å, 2.51 Å, 2.56 Å, 2.83 Å and 3.15 Å and a Bader charge of 2.08 e on the Au_{10} cluster. Au_{10} adsorbs into an oxygen vacancy on a TiO_2 anatase (101) with an oxygen vacancy, which is shown in figure 4.66.b) It has a binding energy of -503 kJ mol^{-1}, Au – O distances of 2.08 Å, 2.09 Å, 2.13 Å and 2.13 Å, Ti – Au distances of 2.84 Å and 2.86 Å and a Bader charge of 1.90 e on the Au_{10} cluster.

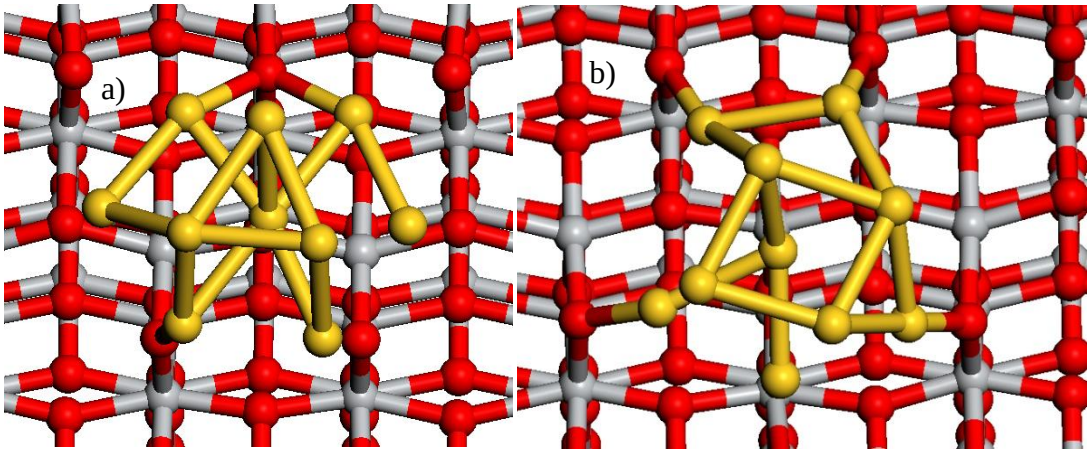

Figure 4.66. Image of a Au_{10} cluster over a TiO_2 anatase (101) with and without a vacancy.

Au_{10} adsorbs to a TiO_2 anatase (001) surface, which is shown in figure 4.67.a) It has a binding energy of -611 kJ mol^{-1}, Au – O distances of 2.09 Å, 2.12 Å, 2.14 Å, 2.17 Å, 2.23 Å, 2.95 Å and 2.95 Å, a Ti – Au distance of 2.93 Å and a Bader charge of 1.88 e. Au_{10} adsorbs over an oxygen vacancy on a TiO_2 anatase (001) with an oxygen vacancy, which is shown in figure 4.67.b) It has a binding energy of -416 kJ mol^{-1}, Au – O distances of 2.10 Å, 2.15 Å and 2.16 Å, Ti – Au distances of 2.86 Å and 3.04 Å and a Bader charge of 1.26 e on the Au_{10} cluster.

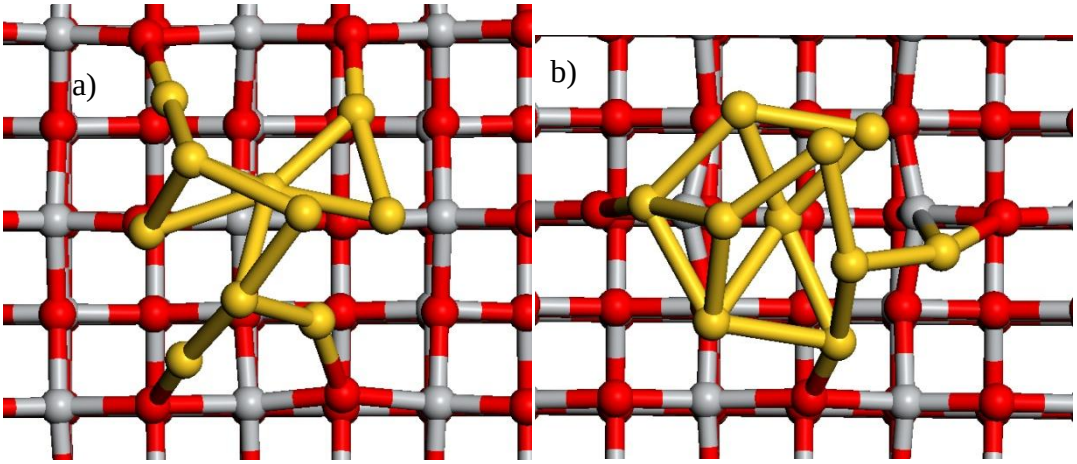

Figure 4.67. Image of a Au_{10} cluster over a TiO_2 anatase (001) with and without a vacancy.

Pd_{10}

Pd_{10} adsorbs to TiO_2 rutile (110) surface in much the same way as the previously mentioned Au_{10} cluster between the ridges of bridging oxygen atom, which is shown

in figure 4.68.a) It has a binding energy of -914 kJ mol^{-1}, Pd – O distances of 2.07 Å, 2.11 Å, 2.13 Å, 2.16 Å, 2.17 Å, 2.30 Å, 2.62 Å and 2.73 Å, Ti_{6c} – Pd distances of 2.89 Å, 2.93 Å, 3.03 Å and 3.17 Å, Ti_{5c} – Pd distances of 2.68 Å, 2.79 Å and 2.89 Å and a Bader charge of 2.47 e on the Pd_{10} cluster. The Pd_{10} cluster also adsorbs over TiO_2 rutile (110) surface with an oxygen vacancy staying in the same place as the TiO_2 rutile (110) without the oxygen vacancy, which is shown in figure 4.68.b) It has a binding energy of -679 kJ mol^{-1}, Pd – O distances of 2.09 Å, 2.14 Å, 2.14 Å, 2.19 Å, 2.53 Å and 2.57 Å, Ti_{6c} – Pd distances of 2.93 Å and 3.01 Å, Ti_{5cv} – Pd distances of 2.87 Å and 2.95 Å, Ti_{5c} – Pd distances of 2.66 Å, 2.75 Å and 2.76 Å and a Bader charge of 1.77 e on the Pd_{10} cluster.

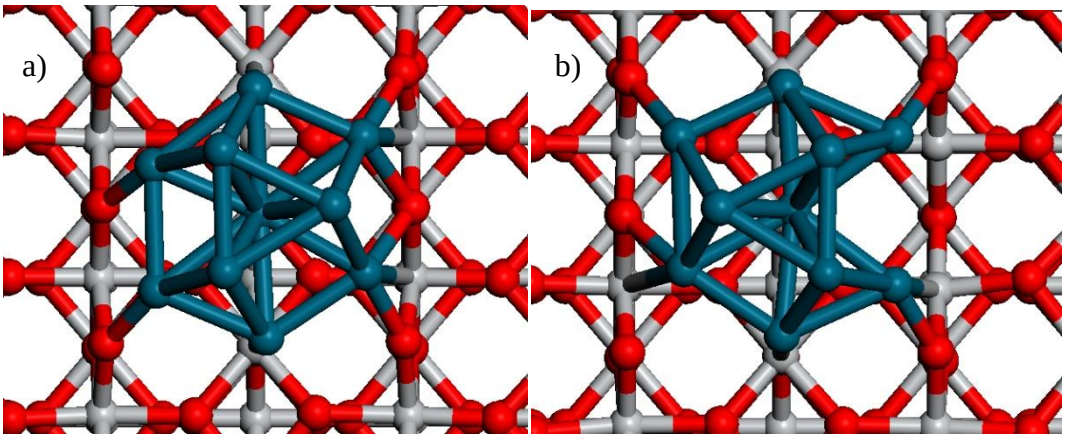

Figure 4.68. Images of Pd_{10} on TiO_2 rutile (110) surface with and without an oxygen vacancy.

Pd_{10} adsorbs to TiO_2 anatase (101) surface over a step in the surface, with is shown in figure 4.69.a) It has a binding energy of -780 kJ mol^{-1}, Pd – O distances of 1.99 Å, 2.14 Å, 2.15 Å, 2.21 Å, 2.24 Å, 2.27 Å and 2.33 Å, a Ti – Pd distance of 2.63 Å and a Bader charge of 2.09 e on the Pd_{10} cluster. The Pd_{10} cluster adsorbs into the oxygen vacancy of the TiO_2 anatase (101) surface, which is shown in figure 4.69.b) It has a binding energy of -818 kJ mol^{-1}, Pd – O distances of 2.07 Å, 2.11 Å, 2.20 Å, 2.22 Å, 2.28 Å, 2.42 Å and 2.54 Å, Ti – Pd distances of 2.57 Å, 2.83 Å, 2.95 Å and 3.00 Å and a Bader charge of 1.67 e on the Pd_{10} cluster.

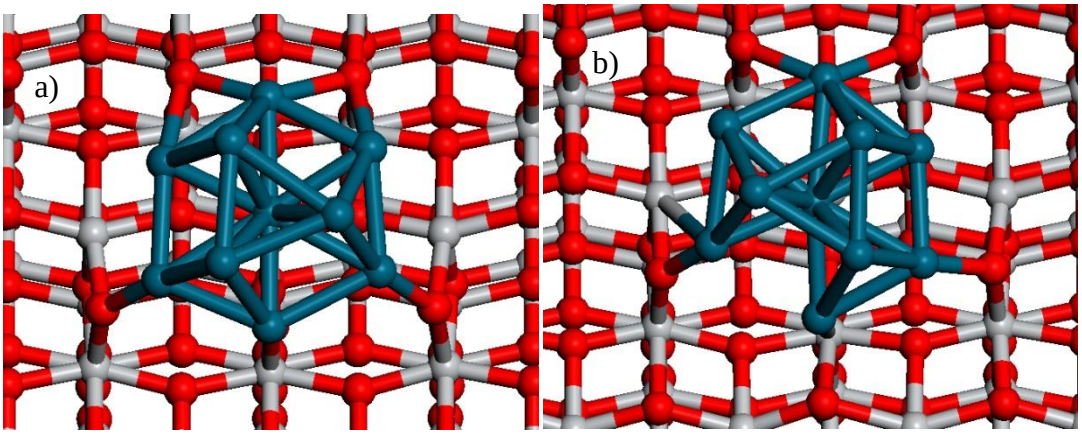

Figure 4.69. Images of Pd_{10} on TiO_2 anatase (101) surface with and without an oxygen vacancy.

Pd_{10} adsorbs to a TiO_2 anatase (001) surface over a 3 co-ordinate oxygen atom, which is shown in figure 4.70.a) It has a binding energy of -961 kJ mol^{-1}, three Pd – O_{2c} distances of 2.04 Å and one of 2.05 Å, Pd – O_{3c} distances of 2.74 Å and 2.91 Å, Ti – Pd distances of 2.86 Å, 2.94 Å, 2.97 Å, 2.99 Å, 3.01 Å, 3.04 Å, 3.09 Å, 3.13 Å, 3.23 Å and 3.34 Å and a Bader charge of 1.69 e on the Pd_{10} cluster. The Pd_{10} cluster adsorbs over an oxygen vacancy on a TiO_2 anatase (001) surface with an oxygen vacancy, with is shown in figure 4.70.b) It has a binding energy of -839 kJ mol^{-1}, Pd – O distances of 2.03 Å, 2.08 Å, 2.14 Å, 2.36 Å and 2.44 Å, Ti – Pd distances of 2.66 Å, 2.67 Å, 2.79 Å, 2.86 Å, 2.91 Å, 2.97 Å and 3.00 Å and a Bader charge of 1.26 e on the Pd_{10} cluster.

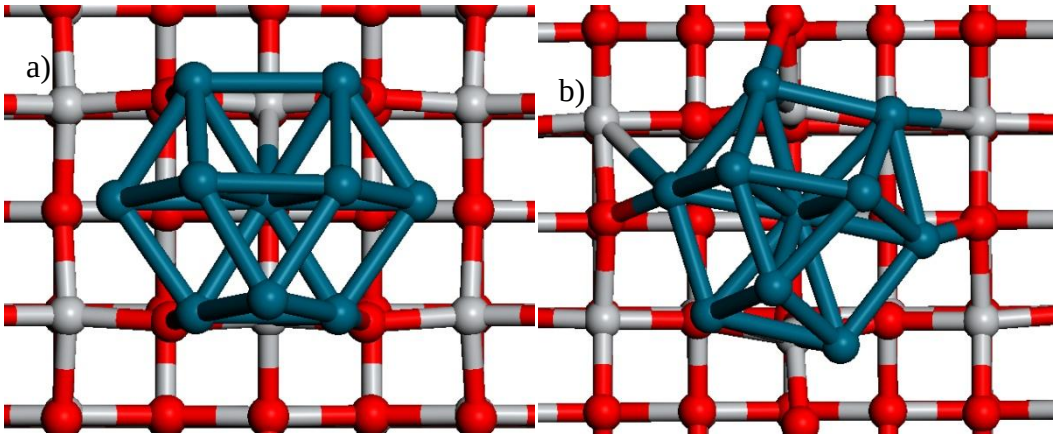

Figure 4.70. Images of Pd_{10} on TiO_2 anatase (001) surface with and without an oxygen vacancy.

Conclusions

The initial mechanism obtained on an isolated Au_{10} cluster shows a path involving the breaking of a H_3C – H and HOO – H bonds and the formation of a H_3C – OOH bond. The breaking of the H_3CO – OH bond is shown to be a fast process as it can be broken spontaneously on the base of the (100) face of the Au_{10} cluster. CH_4 and H_2 show no interaction with the cluster but this could be due to the lack of the dispersive force in DFT. H_2O_2 will spontaneously cleave the HO – OH bond on either face on the base of the cluster. This will result in a number of hydroxyl groups around the cluster, which gives the cluster a charge increasing with number of hydroxyl groups, with six hydroxyl groups giving a charge of 3.14e. The Bader charges show the Au_{10} with the hydroxyl groups is partially oxide, in nature which could result in different reaction pathways for the cluster. On the Au_{10} cluster the breaking of the H – OOH bond is a slow process with a barrier of 170 kJ mol^{-1}. This evidence shows that on an isolated Au_{10} this reaction is unlikely to produce any products but the mechanism can be tested as a start point on the supported Au_{10} cluster to observe how the support alters the interactions of the cluster.

H_2O_2 and H_2O both show low energy O – H bond breaking; H_2O_2 with a barrier of H – OOH bond breaking at 9 kJ mol^{-1} and transfer of hydrogen atom during MD run in the short time period for H_2O indicating a rapid process.

A Au_{10} cluster will adsorb onto a rutile TiO_2 (110) surface but is only adsorbed along one ridge of O_{2c} and is repelled from the Ti_{5c} site during geometry optimisation which disagrees with experimental results that show the Au clusters wetting the surface of the TiO_2. When the surface has been hydroxylated, the Au_{10} cluster does wet the surface and reforms from the bilayer to form a trilayer cluster with only (111) faces.

The HO – OH bond breaks H_2O_2 spontaneously in the presence of the supported $Au_{10,}$ which again would lead to a number of hydroxyl groups on the Au_{10} cluster. These hydroxyl groups can also be transferred to the TiO_2 surface on a Ti_{5c} site, leading to a hydroxylation of the surface near the cluster. This occurs on both the clean and partially hydroxylated surfaces.

Changing the U value of the Ti and O in the support, alter how the Au_{10} cluster binds to the rutile TiO_2 (110) with wetting of the surface now observed. This result shows much better agreement with experiment results. The barrier obtained for H_3C – H bond breaking on anatase (001) is 21 kJ mol^{-1}, which can be compared to the same barrier on the Au cluster, which is 92 kJ mol^{-1}. This shows the C – H cleavage on TiO_2 is a low barrier for this process. The H – OOH bond breaking in H_2O_2 on anatase (001) is 7 kJ mol^{-1}, which is similar to the hydroxylated rutile surface, which would indicate the change of U value has no effect on the interactions of H_2O_2. The interactions of the water molecule further support this. The addition of a vacancy decreases the binding energy for both Pd_{10} and Au_{10} on the anatase (001) and rutile (110) surface but increases the binding energy on the anatase (101) surface. This is most likely due to the space created by the vacancy being the right size for the Au_{10} and Pd_{10} clusters as these are a similar size.

References

1. A. A. Herzing, C. J. Kiely, A. F. Carley, P. Landon, and G. J. Hutchings, *Science*, 2008, **321**, 1331–1335.

2. A. F. Carley, D. J. Morgan, N. Song, M. W. Roberts, S. H. Taylor, J. K. Bartley, D. J. Willock, K. L. Howard, and G. J. Hutchings, *Physical chemistry chemical physics : PCCP*, 2011, **13**, 2528–38.

3. L. Xiao, B. Tollberg, X. Hu, and L. Wang, *The Journal of chemical physics*, 2006, **124**, 114309.

4. K. L. Howard and D. J. Willock, *Faraday Discussions*, 2011, **152**, 135.

5. M. Ramamoorthy, R. D. King-Smith, and D. Vanderbilt, *Phys. Rev. B*, 1994, **49**, 7709–7715.

6. H. Perron, C. Domain, J. Roques, R. Drot, E. Simoni, and H. Catalette, *Theoretical Chemistry Accounts: Theory, Computation, and Modeling (Theoretica Chimica Acta)*, 2007, **117**, 565–574.

7. F. Moreau and G. C. Bond, *Catalysis Today*, 2007, **122**, 260–265.

5. CH_4 oxidation to CH_3OOH and CH_3OH on AuPd nano-particles

The direct synthesis of H_2O_2 and the oxidation of methane can be studied on extended surfaces to model the effect of larger clusters. In this chapter the adsorption and dissociation of the reactants (CH_4, H_2, O_2, H_2O_2) on extended surfaces (Au(111), Pd(111) and PdO(101)) will be discussed, together with catalytic reaction mechanisms and how these can be related to a larger cluster.

These surfaces have been studied to produce a better picture of a large cluster. AuPd catalysts which are active for the direct synthesis of H_2O_2 have been found to have a wide range of sizes[1] from 4 – 10 nm, These would contain in the order of 1000 atoms which cannot be modelled in the same way as the Au_{10} cluster used in the previous section. These clusters are large enough to be modelled as extended surfaces and can have different slabs modelling different sections of the surface, which can give an insight into how the different materials may affect the mechanism. All unless otherwise stated are coloured Au in yellow, Pd in blue, C in grey, O in red and H in white.

5.1. Au(111) surface

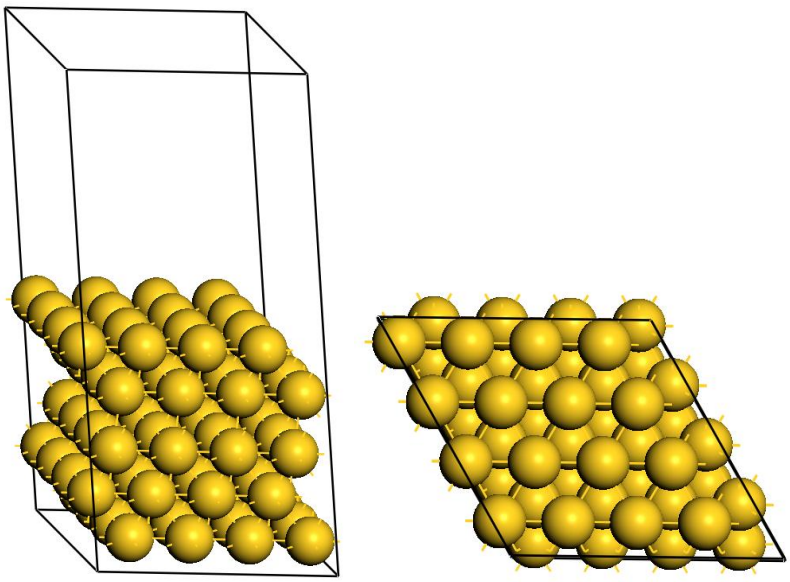

Figure 5.1. Au(111) slab in unit cell.

The Au(111) surface is cut from the fcc bulk structure of Au. It has a Au – Au distance of 2.95 Å in the layers and a distance of 2.97 Å between the layers. The surface has four different sites; atop, bridging, hcp hollow and fcc hollow. It has a 15 Å vacuum gap and a 11.81 Å × 11.81 Å × 24.65 Å unit cell with the lower two layer fixed, shown in figure 5.1.

CH_4

CH_4 weakly interacts with a Au(111) surface, which is shown in figure 5.2.a) It has a binding energy of +4 kJ mol^{-1} and has a Au – C distance of 3.26 Å over the atop site of a Au atom. A hydrogen atom can be transferred to the surface from the methane, which is also shown in figure 5.2.b) It has a binding energy for the system of 140 kJ mol^{-1}, a Au – C distance of 2.13 Å and Au – H distances of 1.82 Å and 1.81 Å. It also has a charge of -0.47e on the methyl and a charge of -1.51e on the surface hydrogen atom.

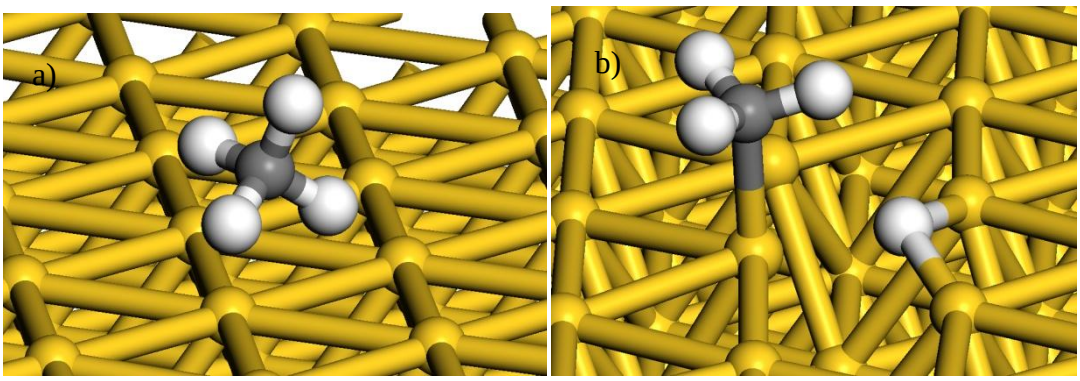

Figure 5.2. Images of a) methane over a Au(111) surface and b) methyl and a surface hydrogen atom on a Au(111) surface.

The barrier for transfer of a hydrogen atom from the methane to the Au(111) surface is 200 kJ mol^{-1} with the reverse 36 kJ mol^{-1}, which is shown in figure 5.3. The change in C – H bond distance shows a rapid change in the distance at the peak of the barrier with respect to energy.

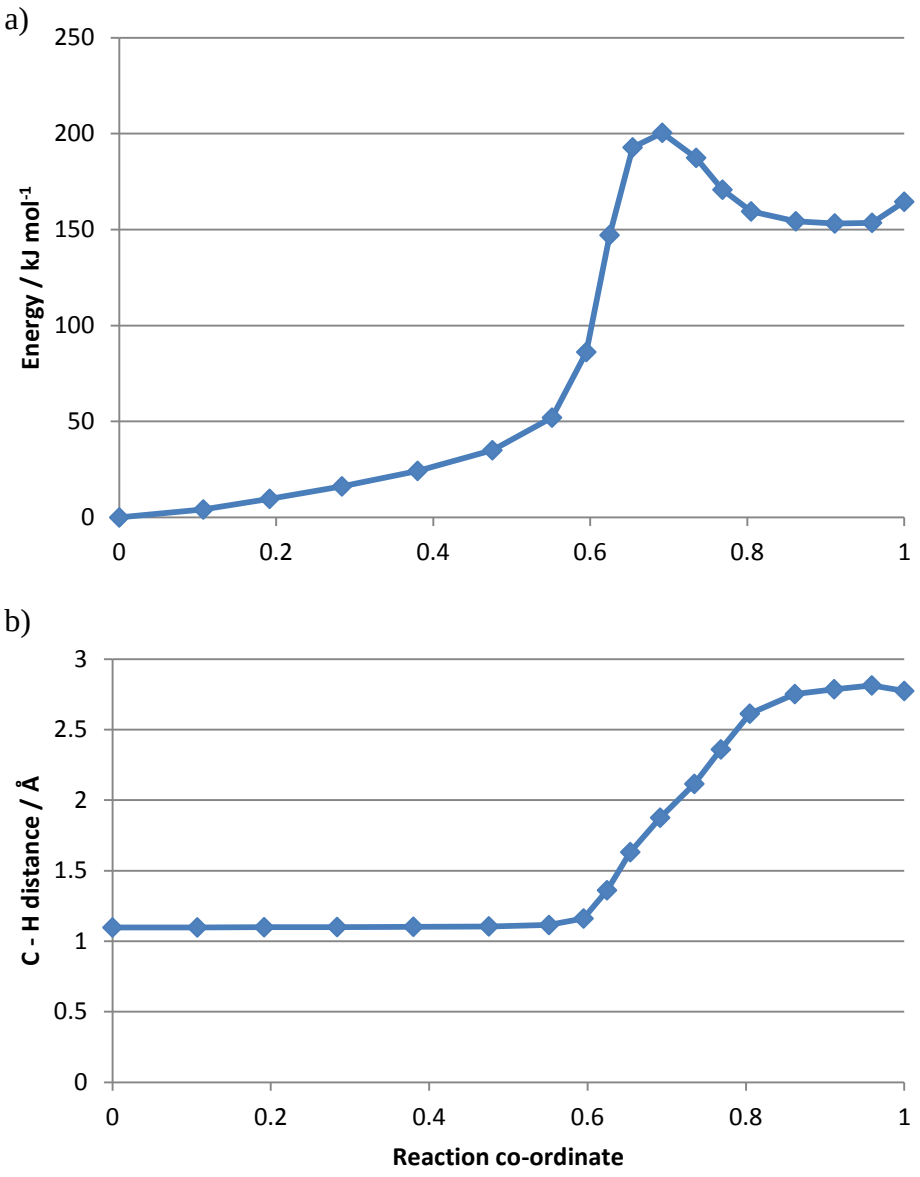

Figure 5.3. A plot of the barrier for the dissociation of methane and the transfer of a hydrogen atom to the surface, both energy and C – H distance against reaction co-ordinate.

H_2O_2

H_2O_2 adsorbs in two ways to a Au(111) surface. One weakly adsorbs with one oxygen nearer the surface, which has a binding energy of -7 kJ mol^{-1} and is shown in figure 5.4.a) It has a Au – O distance of 3.07 Å and a charge of -0.22e on the H_2O_2. The other spontaneously cleaves the HO – OH bond two produce to hydroxyls on the Au(111) with one in a terminal arrangement and one bridging between two Au atoms, which is shown in figure 5.4.b) It has binding energy of -87 kJ mol^{-1} for the

system and charges on the hydroxyls of -0.79e and -0.75e. It also has a Au – O distance of 2.09 Å for the terminal hydroxyl and distances of 2.24 Å and 2.26 Å for the bridging hydroxyl. A hydrogen atom atom can be transferred from H_2O_2 to the Au(111) surface to form an OOH and a surface hydrogen, which is shown in figure 5.4.c) It has a binding energy of 120 kJ mol^{-1} and charges of -0.64e on the OOH and -1.42e on the surface hydrogen. It also has a Au – O distance of 2.25 Å, a Au – H distances of 1.84 Å, 1.95 Å and 1.92 Å and an O – O distance of 1.44 Å.

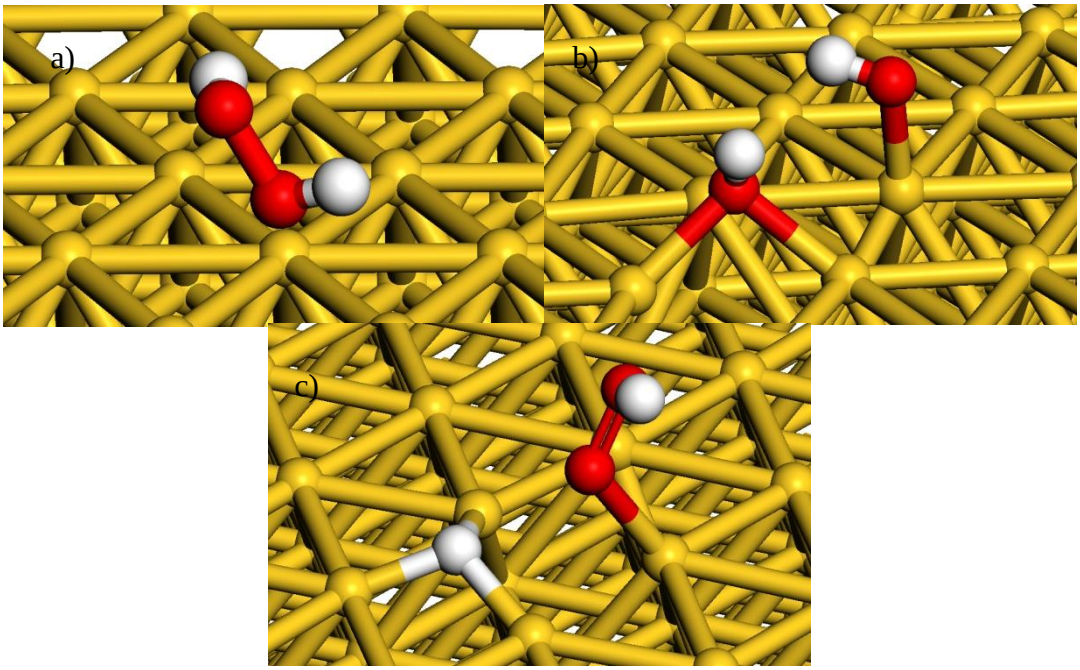

Figure 5.4. An image of H_2O_2 bound to Au(111) surface, two hydroxyls bound to Au(111) surface and OOH and a surface hydrogen over Au(111) surface.

The barrier for dissociation and transfer of the hydrogen atom to the Au(111) surface from H_2O_2 to form OOH will be at least 126 kJ mol^{-1}, which would be a large barrier. As hydroxyls would be produced in abundance, these could be involved in the hydrogen transfer from H_2O_2 to produce a water molecule. An image of this is shown in figure 5.5.a) This system has a binding energy of -38 kJ mol^{-1} with Au – O distances of 2.61 Å to H_2O_2, 2.09 Å to a terminal hydroxyl and 2.42 Å and 2.31 Å to a bridging hydroxyl. The H_2O_2 has an O – O distance of 1.47 Å with a charge of -0.46e. The hydroxyls have charges of -0.74e and -0.53e. A suspected hydrogen bond exists between the H_2O_2 and the terminal hydroxyl, the hydrogen on the H_2O_2 with an O – H distance of 1.63 Å. The hydrogen bonding hydrogen atom can be

transferred to the hydroxyl it is hydrogen bonding to, which produces a water molecule, OOH and leaves a hydroxyl. This is shown in figure 5.5.b) This has a binding energy of -58 kJ mol^{-1}, a Au – OOH distance of 2.23 Å, a Au – OH distance of 2.08 Å, a Au – OH_2 distance of 2.87 Å with charges of -0.46 e on the OOH, -0.73 e on the OH and -0.36 e on the H_2O. There is a further hydrogen bond between the water and the OOH with an O – H distance of 1.71 Å.

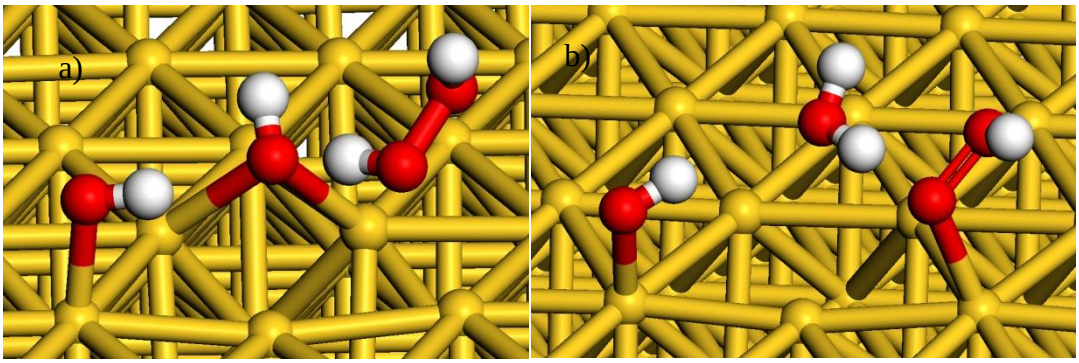

Figure 5.5. An image of two hydroxyls and H_2O_2 over a Au(111) surface and a hydroxyl, water and OOH over a Au(111) surface.

The barrier for the transfer of a hydrogen atom between H_2O_2 and a hydroxyl to form water and an OOH is 7 kJ mol^{-1} with the reverse 22 kJ mol^{-1} which is shown in figure 5.6.

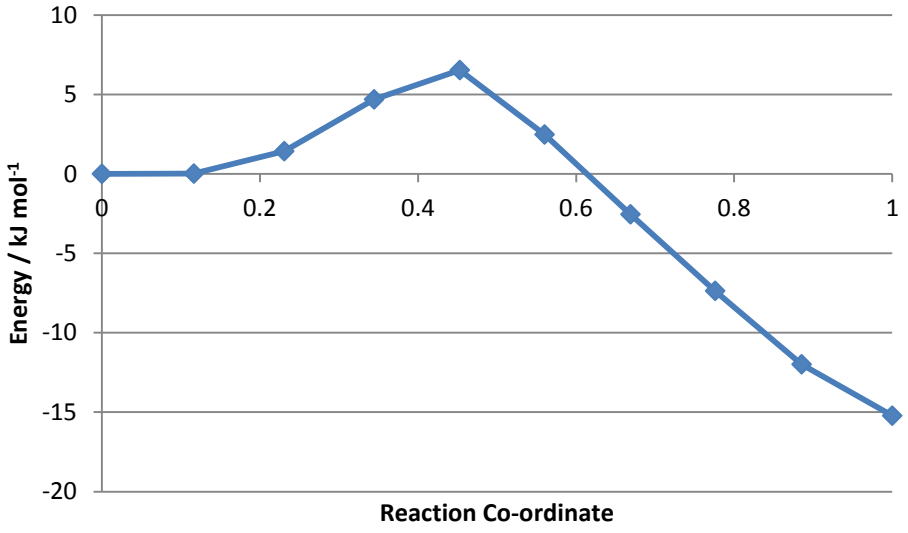

Figure 5.6. A plot of the barrier for the energy for the transfer of a hydrogen atom between H_2O_2 and a hydroxyl to form water and an OOH.

O_2

O_2 weakly interacts with a Au(111) surface, which is shown in figure 5.7. It has a binding energy of +9 kJ mol^{-1}, Au – O distances of 2.70 Å and 2.72 Å and an O – O distance of 1.25 Å. The O – O bond length indicates it is neutral oxygen molecule.

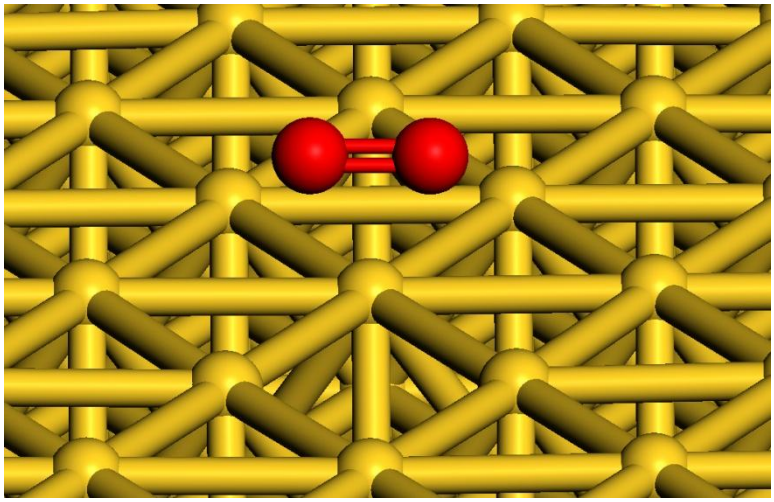

Figure 5.7. An image of O_2 over a Au(111) surface.

CH_3OOH

CH_3OOH weakly adsorbs to a Au(111) surface with a binding energy of -2 kJ mol^{-1}. CH_3OOH binds though a surface Au atom with a Au – O distance of 3.15 Å, a C – O distance of 1.42 Å and an O – O distance of 1.48 Å. Unlike the HO – OH bond, no cleavage occurs in the presence of the Au(111) surface. To model the formation of CH_3OOH involves two water molecules as hydrogen atoms give high energy when over the Au(111) surface. CH_3OOH can be produced from CH_3 and OOH making a C – O bond, which is shown in figure 5.8.a) The CH_3, OOH and two water molecules bind to the Au(111) surface with a binding energy of -210 kJ mol^{-1}. It has a Au – CH_3 distance of 2.12 Å, a Au – OOH distance of 2.22 Å, Au – OH_2 distances of 2.63 Å and 2.69 Å, an O – O distance of 1.45 Å and hydrogen bond distances HOH – OOH and HOH – OH_2 of 1.59 Å and 1.85 Å. It also has charges of -0.52 e on the CH_3, -0.45 e on the OOH and -0.28 e and -0.29 e on the water molecules. CH_3OOH can be bound to the Au(111) surface with two water molecules which has a binding energy of -331 kJ mol^{-1} and is shown in figure 5.8.b) CH_3OOH has a charge of -0.12 e and the water molecules have charges of -0.26 e and -0.30 e. The Au – O distance to the CH_3OOH is 3.12 Å with a C – O distance of 1.43 Å and an O

– O distance of 1.47 Å. The Au – OH_2 distances are 2.61 Å and 3.13 Å with hydrogen bond distances $(CH_3)(OH)O$ – OH_2 and HOH – OH_2 of 1.81 Å and 1.76 Å.

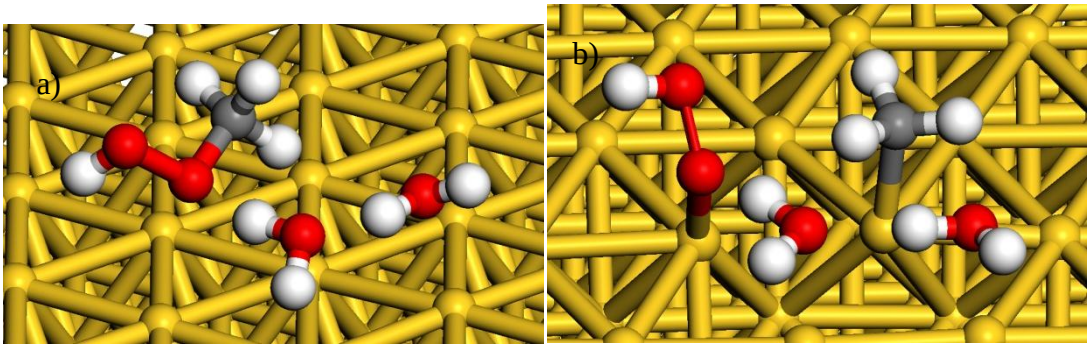

Figure 5.8. Images of CH_3OOH and $2H_2O$ over Au(111) surface and CH_3, OOH and $2H_2O$ over Au(111).

The barrier to form CH_3OOH from CH_3 and OOH is 129 kJ mol^{-1} with the reverse 249 kJ mol^{-1}, which is shown in figure 5.9.

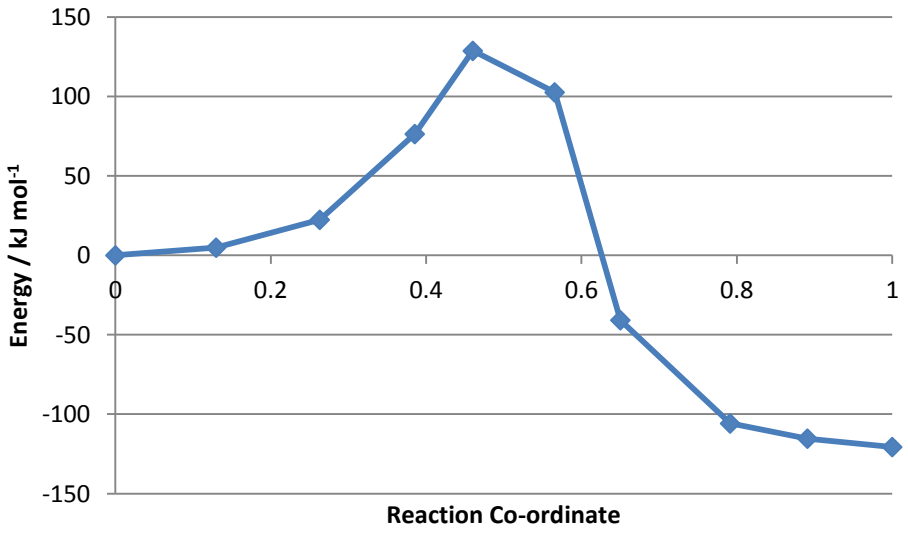

Figure 5.9. A plot of the barrier to the formation of CH_3OOH from CH_3 and OOH over a Au(111) surface.

5.2. Pd(111) surface

The Pd(111) surface is cut from the fcc bulk structure of Pd. It has a Pd – Pd distance of 2.80 Å in the layers and a distance of 2.79 Å between the layers. The surface has four different sites; atop, bridging, hcp hollow and fcc hollow. It has a 15 Å vacuum gap and a 10.21 Å × 10.21 Å × 24.15 Å unit cell with the lower two layers fixed, shown in figure 5.10.

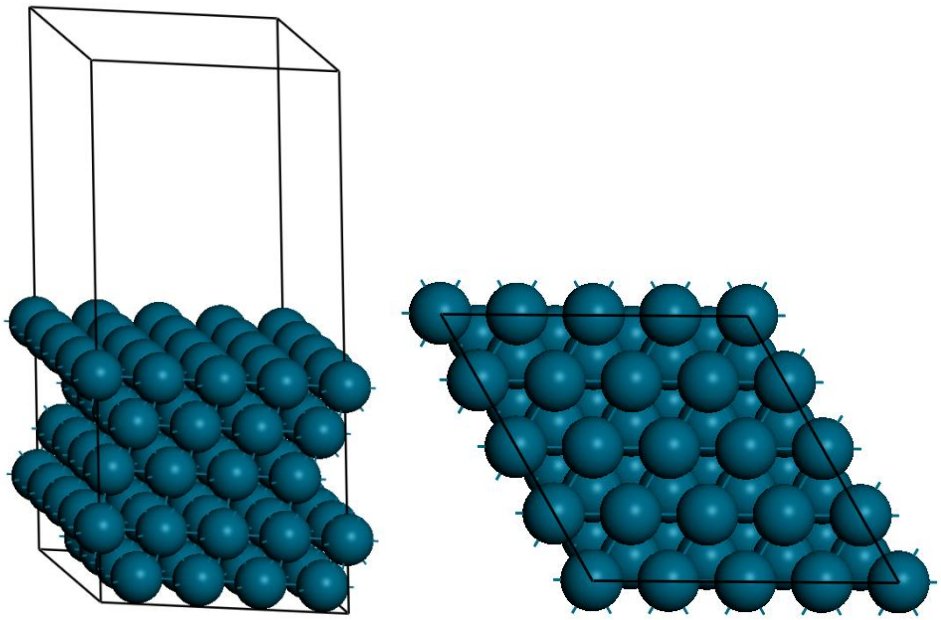

Figure 5.10. A Pd(111) slab in unit cell.

CH_4

CH_4 interacts weakly with the Pd(111) surface with a binding energy of +2 kJ mol^{-1} and has a Pd – C distance of 2.96 Å. An image of this is shown in Figure 5.11.a) C – H bond cleavage can occur to produce a methyl and a hydrogen atom on the surface. An image of this is shown in figure 5.11.b) The methyl adsorbs to a Pd atop site with a Pd – C distance of 2.06 Å and has a Bader charge of -0.44e on the methyl. The hydrogen atom adsorbs to a fcc hollow site with Pd – H distances of 1.75 Å, 1.77 Å and 1.85 Å. It has a charge of -1.33e on the hydrogen atom and a binding energy of 33 kJ mol^{-1}, which indicates it is a hydride but the unfavourable binding energy for the system means it is unlikely to form on the surface.

The barrier for the transfer of the hydrogen atom to the surface from methane is 76 kJ mol^{-1} and the reverse is 45 kJ mol^{-1}, which is shown in figure 5.12.

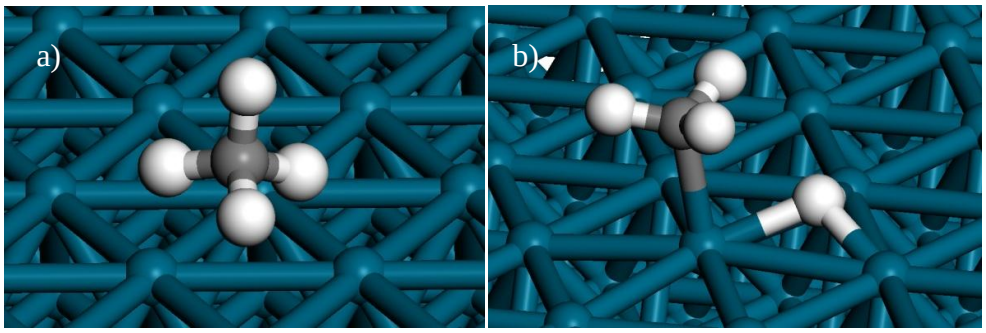

Figure 5.11. Methane over Pd(111) and methyl and hydrogen atom bound to Pd(111).

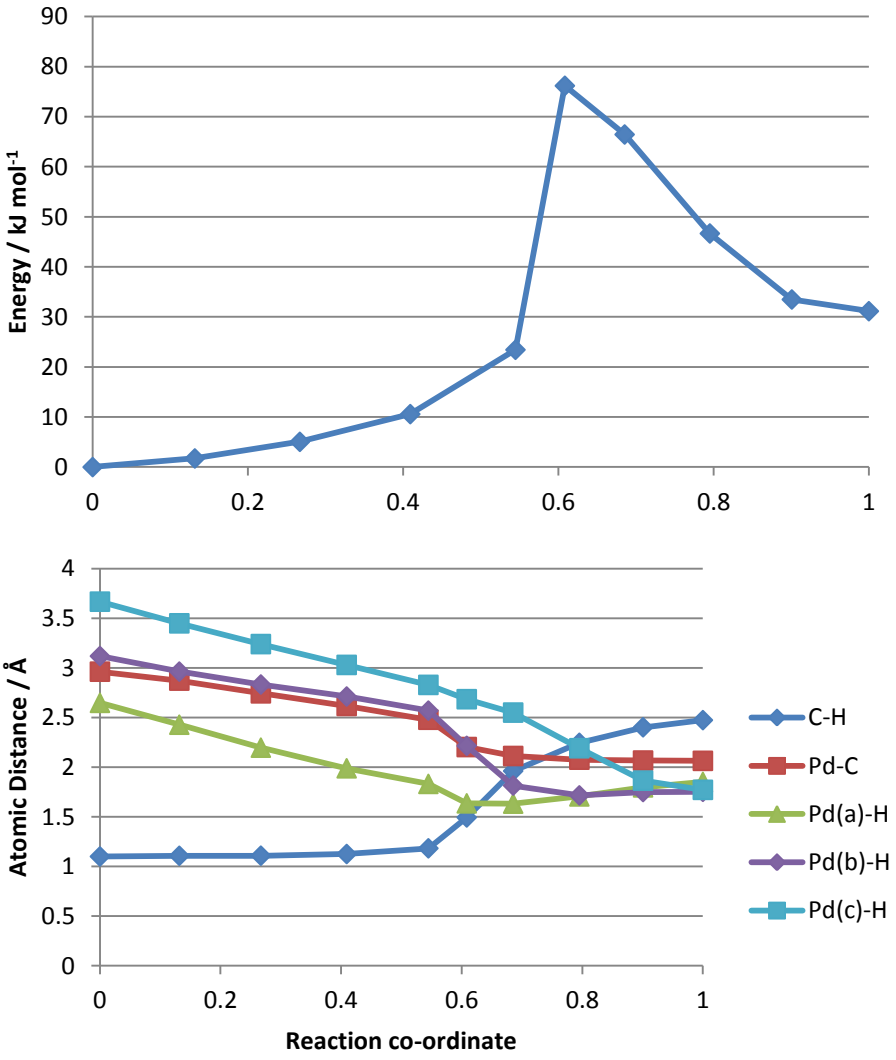

Figure 5.12. The plot of the barrier for hydrogen atom transfer onto Pd(111) surface from methane

H_2O_2

H_2O_2 adsorbs to two positions with one remaining intact and the second cleavaging spontaneously, and these are shown in figure 5.13.a) and b) The H_2O_2 that remains as the molecule is over a fcc hollow at distances from the nearest Pd atoms of 2.78 Å, 2.80 Å and 2.74 Å. It also has an O – O distance of 1.50 Å with only the one oxygen near the surface and a binding energy of -10 kJ mol^{-1}. The H_2O_2 that cleaves the HO – OH bond forms two hydroxyls which bind terminally to a Pd atop site or a bridging site between the two Pd atoms and has a binding energy of -157 kJ mol^{-1}. The terminal hydroxyl has a Pd – O distance of 2.04 Å and a Bader charge of -0.68e on the hydroxyl. The bridging hydroxyl has a Pd – O distances of 2.15 Å and 2.11 Å and a charge of -0.74e on the hydroxyl. A hydrogen atom can be transferred to the surface giving an OOH and a surface hydrogen atom, which is also shown in figure 5.13.c) It has a binding energy of 12 kJ mol^{-1} and charges of -0.59e on the OOH and -1.32e on the surface hydrogen atom. It also has a Pd – O distance of 2.06 Å, an O – O distance of 1.45 Å and Pd – H distances of 1.83 Å, 1.86 Å and 1.72 Å.

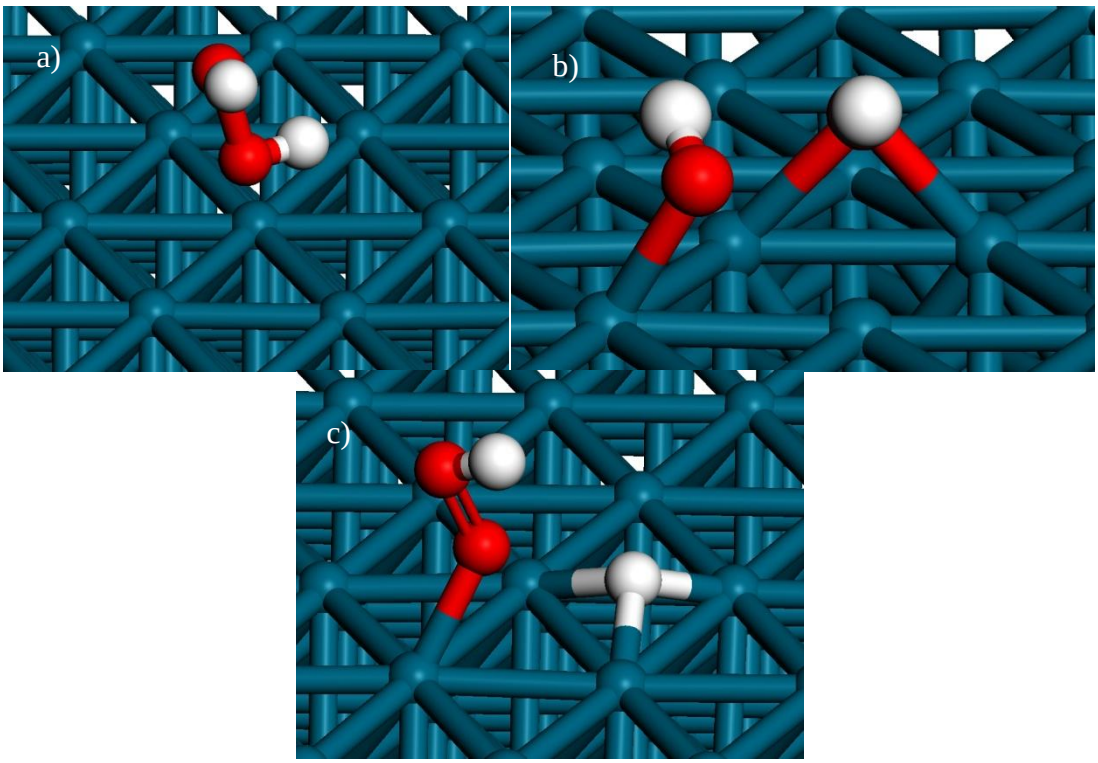

Figure 5.13. Images on H_2O_2 on Pd(111) surface, hydroxyls on Pd(111) surface and OOH and a surface hydrogen on Pd(111) surface.

The H_2O_2 can have a hydrogen transferred to the Pd(111) surface, and the barrier is 83 kJ mol^{-1} and the reverse 60 kJ mol^{-1}. This is shown in figure 5.14.

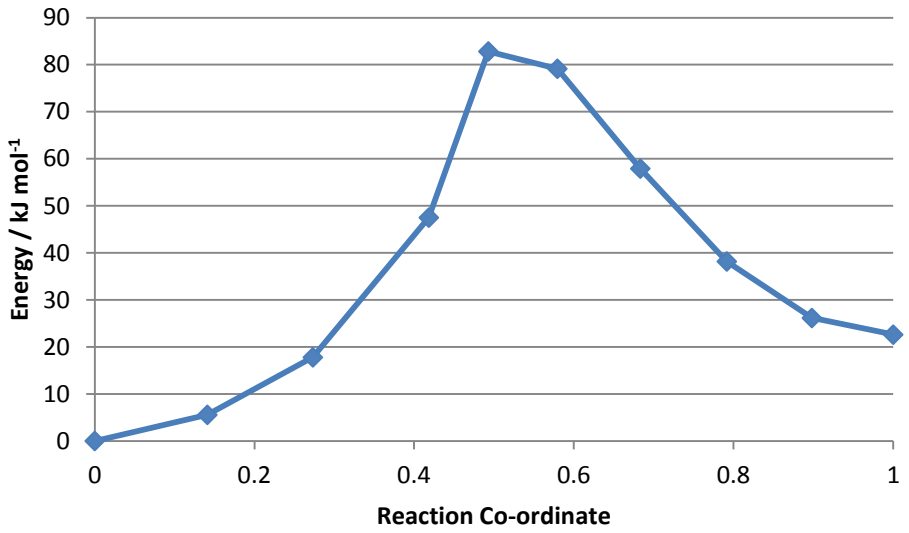

Figure 5.14. Plot of the barrier of hydrogen transfer from H_2O_2 to the Pd(111) surface.

The surface hydroxyls produced by the cleavage of the HO – OH bond can be used to affect the hydrogen transfer by producing water as an alternative product and change the pathway. The H_2O_2 is unaffected by the additional presence of the hydroxyls, having only a small interaction with the surface with Pd – O distances of 2.71 Å, 3.00 Å and 2.68 Å. An image of this is shown in figure 5.15.a) The hydroxyls are again in terminal and bridging sites with Pd – O distances of 2.07 Å for the terminal hydroxyl and 2.12 Å and 2.15 Å for the bridging hydroxyl groups. These have a binding energy of -77 kJ mol^{-1}. The hydrogen can be transferred to one of the hydroxyls and produce water. An image of this is shown in figure 5.15.b) The Pd – OH_2 distance is 2.35 Å, the Pd – OOH distance is 2.13 Å and Pd – OH distances are 2.14 Å and 2.17 Å as it is a bridging position between to Pd atoms. The binding energy for this system is -107 kJ mol^{-1} with charges of -0.33e on the H_2O, -0.73e on the OH and -0.58e on the OOH. This would indicate that the surface hydroxyls can act as leaving group for the transferring hydrogen.

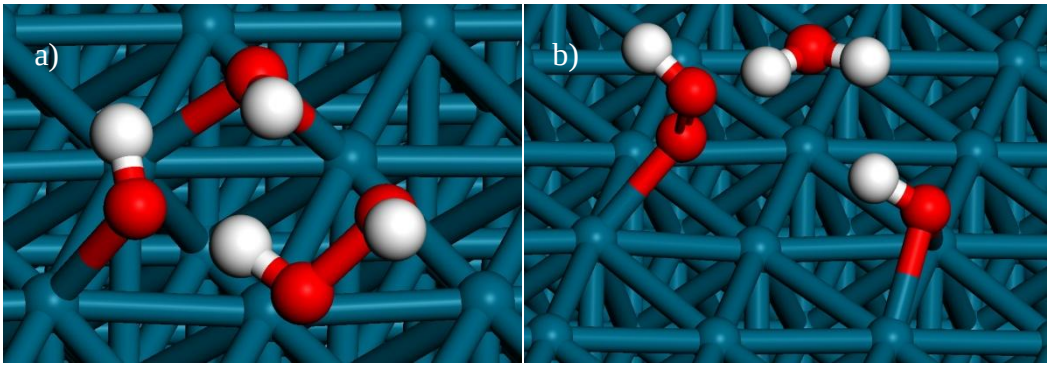

Figure 5.15. Two hydroxyls and H_2O_2 bound to a Pd(111) surface and OOH, OH and H_2O bound to a Pd(111) surface.

The barrier to transfer of the hydrogen atom from H_2O_2 to one of the hydroxyls to form water is 3 kJ mol^{-1} with the reverse 32 kJ mol^{-1}, which is shown in figure 5.16. This shows that the hydrogen atom transferring to the hydroxyl is far more favourable than transferring to the Pd(111) surface.

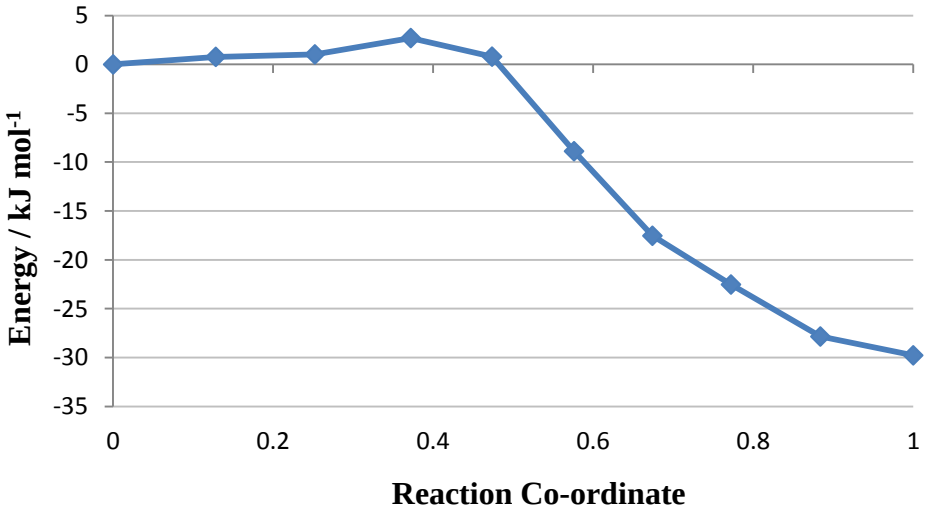

Figure 5.16. A plot of the barrier of the transfer of a hydrogen atom from H_2O_2 to a hydroxyl to form water.

O_2

O_2 binds to the Pd(111) surface with a binding energy of -75 kJ mol^{-1}, which is shown in figure 5.17.a) It has two Pd – O distances of 2.04 Å, an O – O distance of 1.33 Å and a charge on the O_2 of -0.80e. The charge and O – O bond distance indicate a superoxy, which is further supported by the spin density shown in figure

5.17.b) showing four lobes rather than the two rings in the oxygen molecule triplet state.

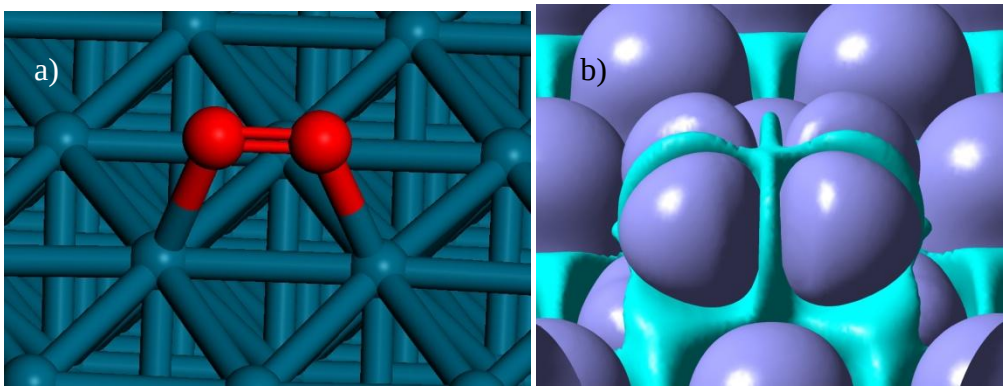

Figure 5.17. An image of O_2 bound to Pd(111) surface and spin density of the same system with an isovalue of 4×10^{-5} eÅ^{-3}.

H_2

H_2 unfavourably interacts with a Pd(111) surface with a binding energy of 31 kJ mol^{-1} with a Pd – H distance of 5.40 Å, which shown in figure 5.18.a) Dissociation of the H_2 results in two surface hydrogen atoms over two hollow sites with a binding energy of +77 kJ mol^{-1}, which is shown in figure 5.18.b) It has Pd – H distances of 1.80 Å, 1.80 Å, 1.82 Å, 1.82 Å, 1.80 Å and 1.80 Å and charges of -1.34 e and -1.33 e.

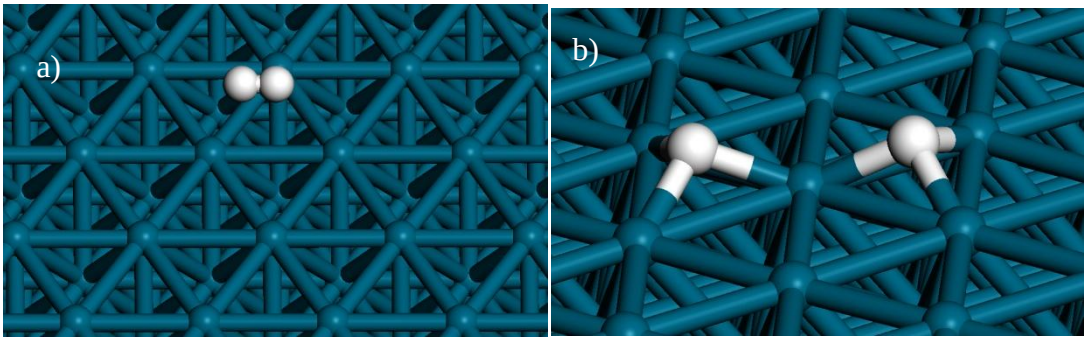

Figure 5.18. Images of H_2 over a Pd(111) surface and two hydrogen atom on a Pd(111) surface.

The barrier for the dissociation of H_2 over Pd(111) to produce two hydrogen atoms on the surface is 6 kJ mol^{-1} with the reverse 79 kJ mol^{-1}, which is shown in figure

5.19. This would indicate that the dissociation of the H_2 would produce surface hydrogen atoms as these are more favoured.

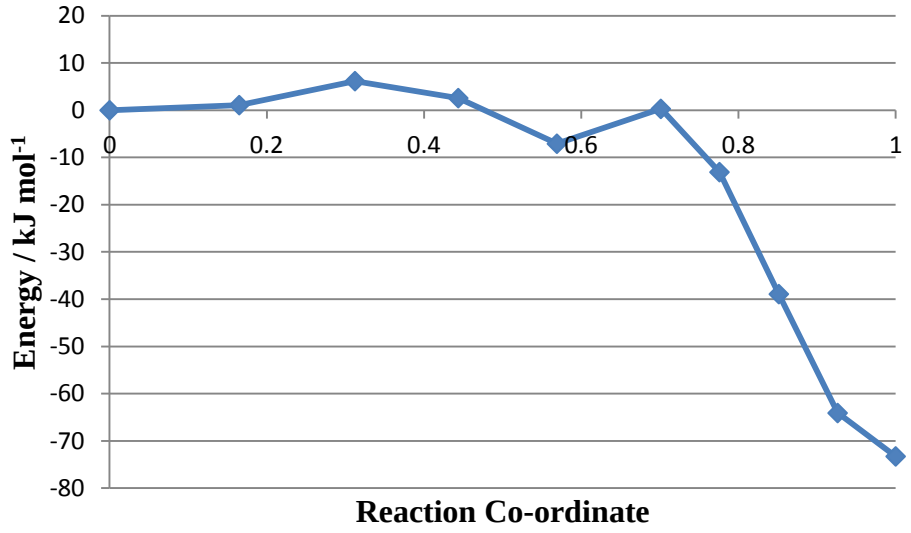

Figure 5.19. A plot of the barrier for the dissociation of H_2 over Pd(111) to form two surface hydrogen atoms.

H atom transfer to O_2

A surface hydrogen can be transferred to an O_2 bound to the surface to form OOH. The barrier to the transfer of the hydrogen atom to the oxygen molecule on the Pd(111) surface is 89 kJ mol^{-1} with the reverse 98 kJ mol^{-1}, which is shown in figure 5.20. This would mean the hydrogen would transfer between the surface and the oxygen molecule with a similar difficulty.

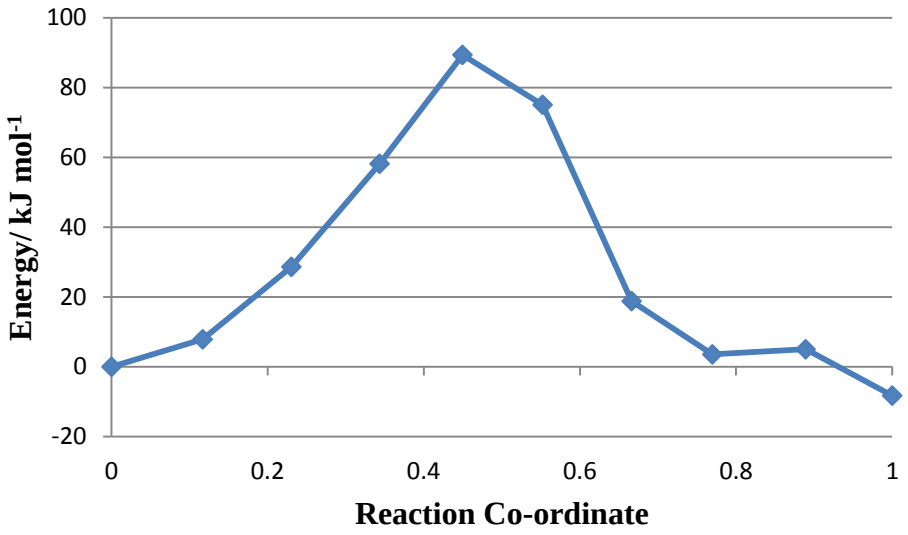

Figure 5.20. A plot of the barrier for the transfer of a hydrogen atom from a Pd(111) surface to an O_2.

CH_3OOH

CH_3OOH can be formed from a surface CH_3 and surface OOH. An image of these is shown in figure 5.21. The CH_3 and OOH system has a binding energy of +12 kJ mol^{-1} to the Pd(111) surface. It has a Pd – C distance of 2.05 Å, a Pd – O distance of 2.03 Å and an O – O distance of 1.44 Å. It also has charges on the CH_3 of -0.48e and on the OOH of -0.61e. The CH_3OOH has a binding energy of -28 kJ mol^{-1} with a Bader charge of -0.35e on the CH_3OOH. It has a Pd – O distance of 2.55 Å, a C – O distance of 1.43 Å and an O – O of 1.48 Å.

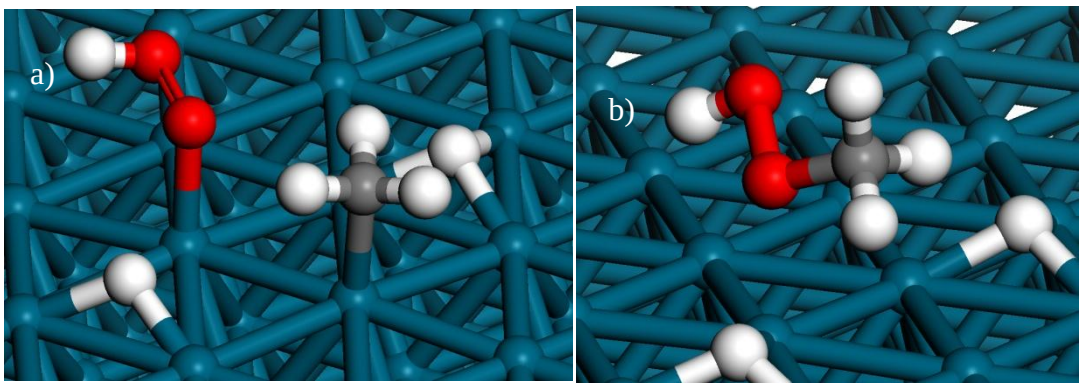

Figure 5.21. An image of methyl and OOH bound to Pd(111) surface and CH_3OOH bound to Pd(111) surface.

The barrier to form CH_3OOH on a Pd(111) surface is 173 kJ mol^{-1} with the reverse 213 kJ mol^{-1}. This is shown in figure 5.22. The barrier is large and therefore unlikely to be viable.

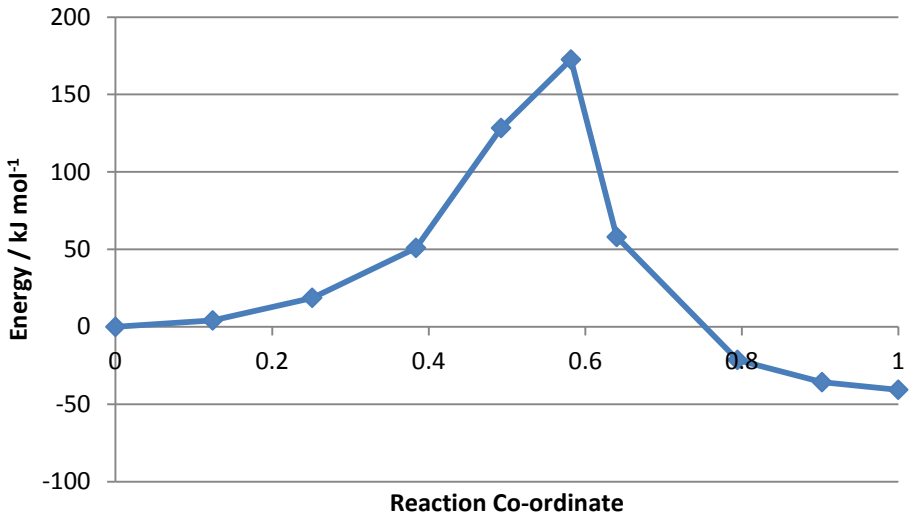

Figure 5.22. Plot of the barrier to form CH_3OOH from CH_3 and OOH on Pd(111) surface.

CH_3OOH has a similar interaction to H_2O_2 with the Pd(111) surface as it spontaneously cleaves the O – O bond when over a bridging site between two Pd atoms, which is shown in figure 5.23. This forms a CH_3O and a hydroxyl on the surface with Pd – OCH_3 distances of 2.24 Å and 2.10 Å and a Pd – OH distance of 1.98 Å. It has a binding energy of -115 kJ mol^{-1} but the large difference is likely due to hydrogen atoms not being present in this example.

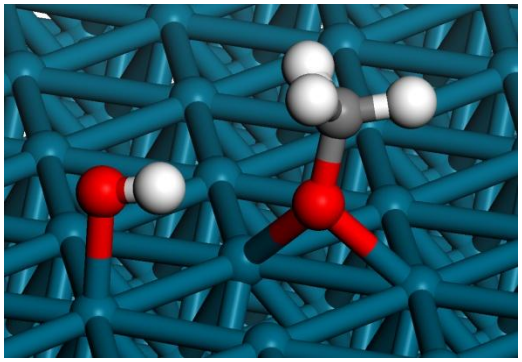

Figure 5.23. An image of a hydroxyl and CH_3O bound to Pd(111) produced from CH_3OOH.

CH_3OH

CH_3OH can be formed from CH_3O and a surface hydrogen atom by the hydrogen atom transferring to the CH_3O. CH_3OH absorbs to the Pd(111) to atop site over a Pd atom with a binding energy of -19 kJ mol^{-1}, which is shown in figure 5.24.a) It has a Pd – O distance of 2.39 Å and a charge of -0.24e on the CH_3OH. CH_3O and a surface hydrogen atom unfavourably interact with the Pd(111) with a binding energy of +56 kJ mol^{-1}, which is shown in figure 5.24.b) It has a Pd – O distance of 2.04 Å and Pd – H distances of 1.70 Å and 1.73 Å bridging between two Pd atoms. It also has charges of -0.67e on the CH_3O and -1.18e of the surface hydrogen atom.

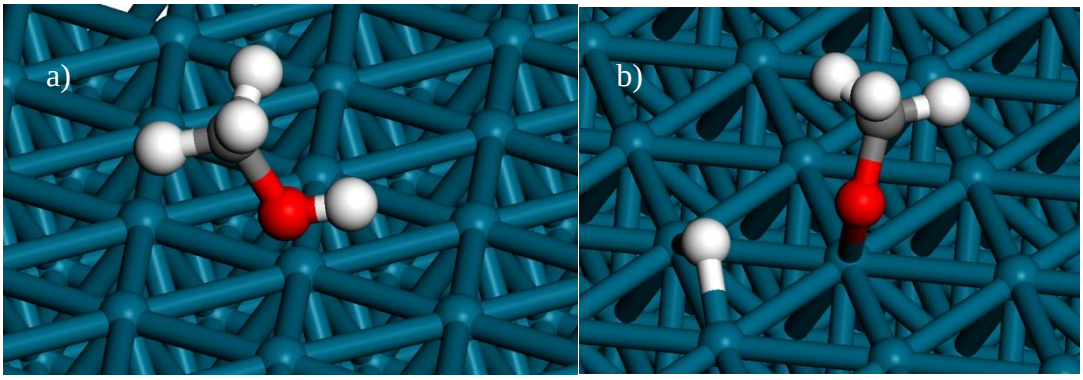

Figure 5.24. Images of CH_3OH bound to a Pd(111) surface and CH_3O and a surface hydrogen atom bound to a Pd(111) surface.

The barrier to form CH_3OH with a hydrogen atom transferred from the surface to CH_3O is 83 kJ mol^{-1} with the reverse 159 kJ mol^{-1}, which is shown in figure 5.25.

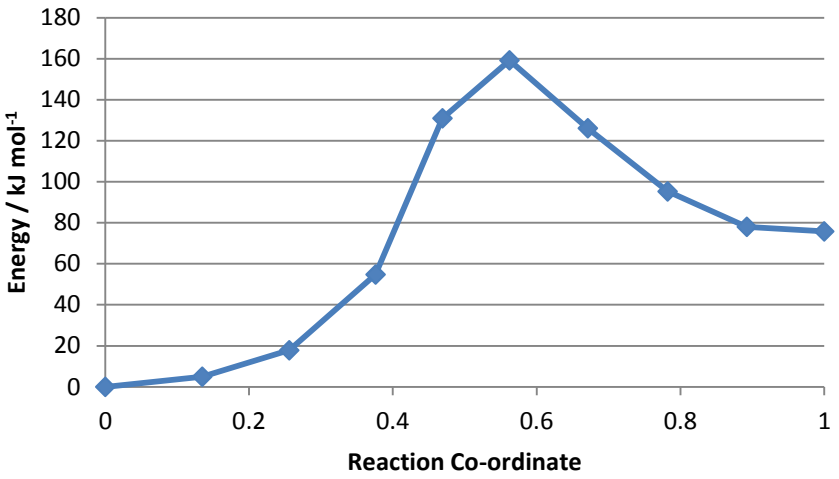

Figure 5.25. A plot of the barrier for the hydrogen transfer to produce CH_3OH from a surface hydrogen atom and CH_3O.

H_2O

Water unfavourably interacts with a Pd(111) surface with a binding energy of +25 kJ mol^{-1}, which is shown in figure 5.26.a) It has a Pd – O distance of 2.42 Å and a charge of -0.23e on the water. A hydrogen atom can be transferred from the water to the Pd(111) surface to form a surface hydrogen atom and a hydroxyl, which is shown in figure 5.26.b) This system unfavourably binds to a Pd(111) surface with a binding energy of +115 kJ mol^{-1}. It has a Pd – O distance of 2.00 Å and Pd – H distances of 1.74 Å and 1.73 Å. It also has charges of -0.58e on the hydroxyl and -1.32e on the hydrogen atom on the surface.

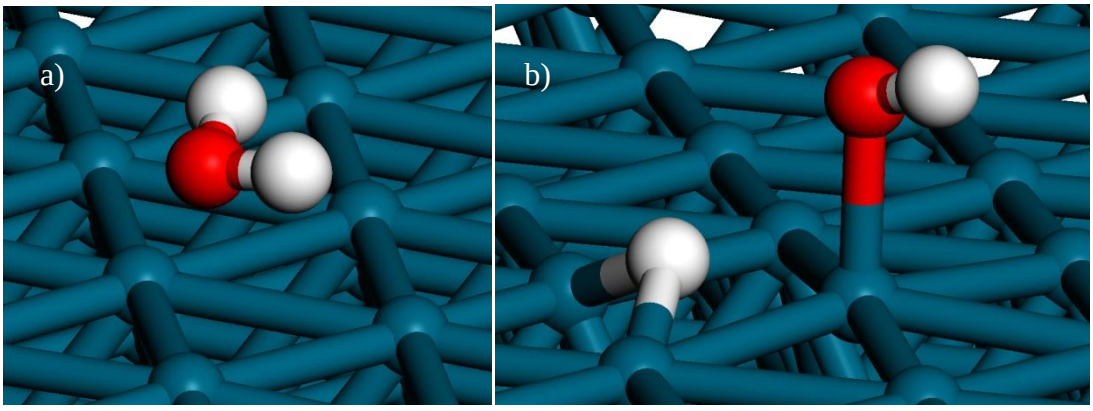

Figure 5.26. Images of water on a Pd(111) surface and a hydroxyl and a surface hydrogen atom on a Pd(111).

The barrier to transfer of the hydrogen from the water to the Pd(111) surface is 137 kJ mol^{-1} with the reverse 46 kJ mol^{-1}, which is shown in figure 5.27.

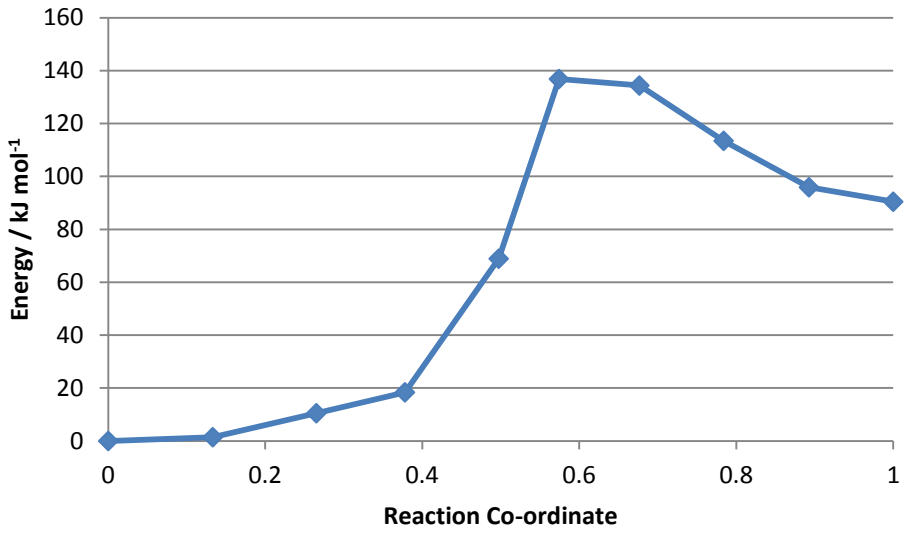

Figure 5.27. A plot of the barrier for the hydrogen transfer from water to a Pd(111) surface.

5.3. PdO (101) surface

The (101) surface of PdO is cut from the PdO bulk structure and it is the only stoichiometric surface with no dipole. The surface of PdO is shown in figure 5.3.1. The surface has 3 co-ordinate and 4 co-ordinate Pd and O atoms. The unit cell has dimensions of 12.66 Å × 9.21 Å × 29.40 Å for a c(2 × 3) unit cell with a vacuum gap of 20 Å and a 4 layer slab, which is shown in figure 5.28. It has a surface energy of 0.83 J m^{-2} for both 3 × 3 × 1 and 5 × 5 × 1 k-points and c(2 × 3) and c(2 × 4) unit cells. The 4 layer slab was chosen because it matches with the thickness of PdO found in work by Weaver et al[2–4].

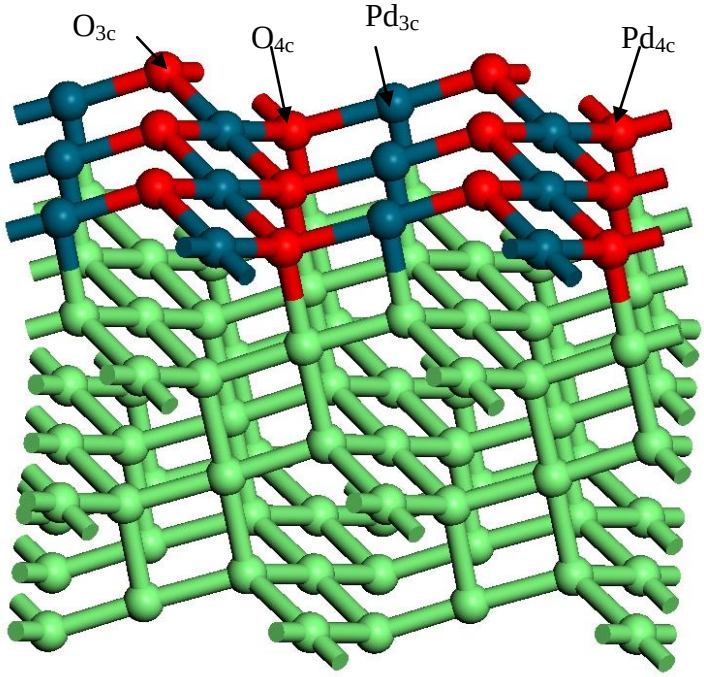

Figure 5.28. PdO (101) surface, showing the different co-ordination of the atoms. Pd atoms are blue, O atoms are red and bulk atoms of both O and Pd are green.

CH_4

CH_4 only adsorbs to the surface weakly with a binding energy of -11 kJ mol^{-1} with respect to an isolated CH_4 and the clean surface. As with all methane adsorption the value is likely to be unreliable due to the lack of dispersion in the DFT calculation. The Bader charges shows a small interaction with the CH_4 having a charge of -0.18e

and the surface having a charge of 0.18e. A weak interaction is further supported by the C – Pd distance being 2.97 Å, where the Pd is the nearest surface Pd.

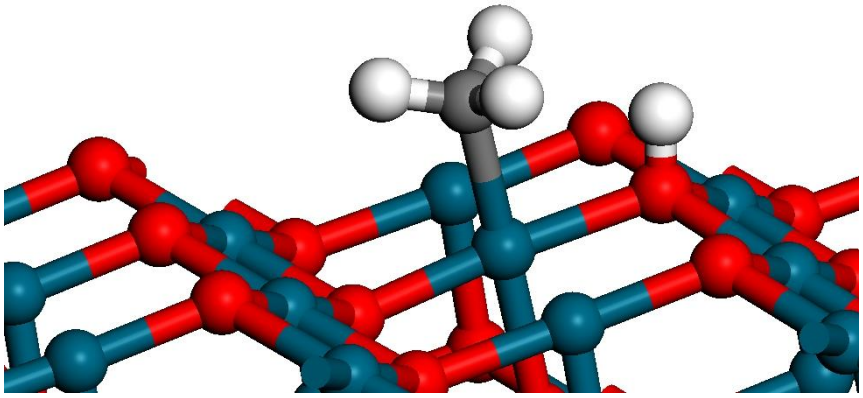

Figure 5.29. CH_3 and H atom bound to PdO surface. Pd atoms are blue, O atoms are red, C atoms are white and H atoms are white.

C – H bond dissociation can produce CH_3 and H atom on the surface, and an image of this is shown in Figure 5.29. The CH_3 is square planar arrangement with the Pd with O as the neighbouring atoms including the CH_3. The hydrogen atom is in a tetrahedral arrangement with the O with Pd atoms neighbouring including a hydrogen atom. It has a binding energy of -73 kJ mol^{-1} with respect to an isolated CH_4 and the clean surface. CH_3 has a Bader charge of -0.43 e and the H atom has a charge of -0.48e. The O atom that binds to the H atom has a charge of -0.21 e, which is compared -1.09 e as an average for the other O atom in the same co-ordination. The surface has a charge of 0.91 e which mostly is from the change in the charge of the O bound to the lone H atom. The Pd – C distance is 2.03 Å, which would indicate a bond between the Pd and C atoms. The O – H distance is 0.97 Å

The C – H dissociation barrier is 57 kJ mol^{-1} as shown in Figure 5.30.a) The barrier is a transfer of a hydrogen atom between the carbon atom and the surface. The reverse of this barrier is 120 kJ mol^{-1}, which would indicate the transfer of the hydrogen to the surface would be the more favourable process. The distances shown in figure 5.30.b) show that a O – H bond formed as a C – H bond breaks, the C – Pd bond forms to counteract the charge on the surface. The high point of the barrier has a single imaginary bond stretch at 1535 cm^{-1}, the motion of which is consistent with the transfer of the hydrogen atom but an additional bend occurs at 91 cm^{-1} so it

would be a likely transition state shown in figure 5.31. and clearly shows a hydrogen transfer reaction.

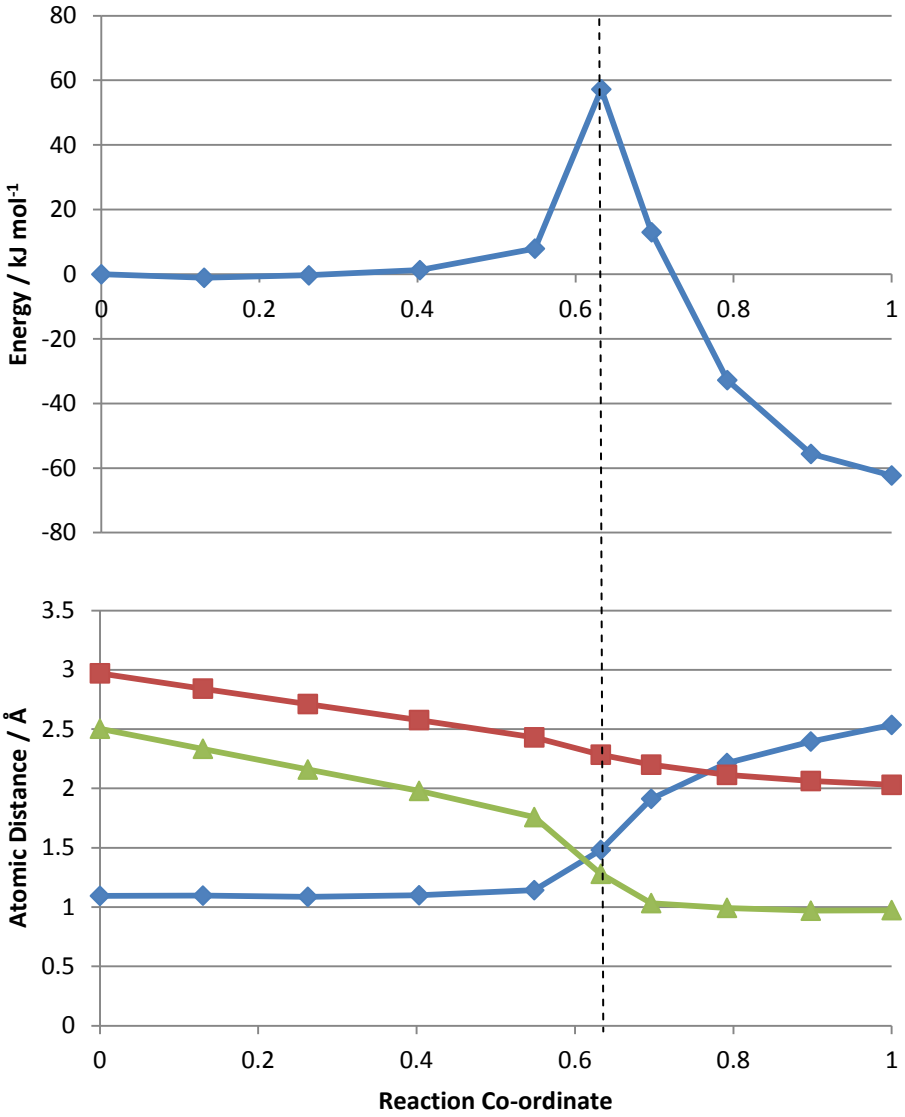

Figure 5.30. Reaction barrier of C – H bond cleavage in methane over PdO (101) surface. Plot of reaction energy against reaction co-ordinate in top plot. Plot of atomic distances, (green line is O – H distance, red line is Pd – C distance and blue line is C – H distance) against reaction co-ordinate.

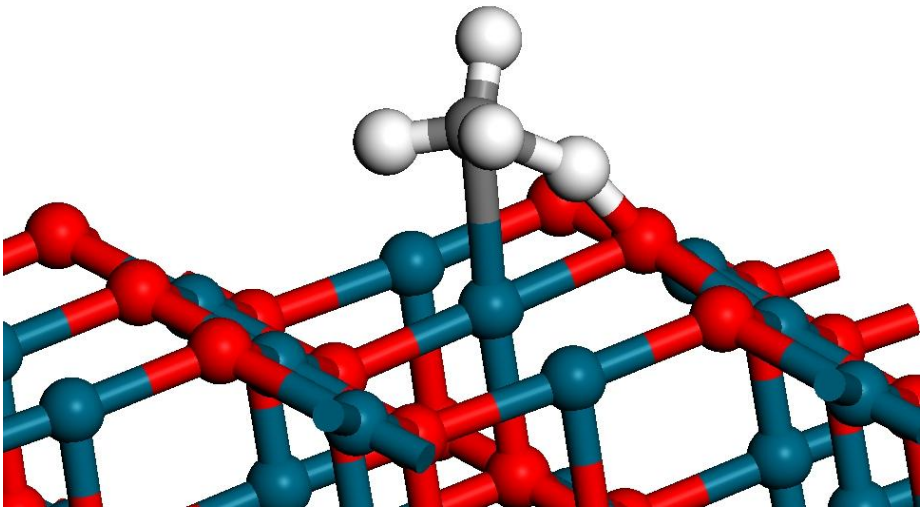

Figure 5.31. Transition state structure located for C – H cleavage over PdO. Pd atoms are blue, O atoms are red, C atoms are white and H atoms are white.

H_2O_2

H_2O_2 binds over the three co-ordinate Pd atom site, either over a single site or bridging between the two Pd sites, and images of these are shown in Figure 5.32. The single co-ordinated H_2O_2 has a binding energy of -104 kJ mol^{-1} with respect to an isolated H_2O_2 and the clean surface. The shortest Pd – O distance is 2.10 Å and an O – O distance of 1.47 Å. In addition the singly co-ordinated H_2O_2 has a Bader charge of -0.28e, which indicates a charge transfer between the surface and one of the oxygen atoms in the H_2O_2. The bridging H_2O_2 has a binding energy of -118 kJ mol^{-1} and Pd – O distances of 2.27 Å and 2.20 Å, a O – O distance of 1.50 Å and the H_2O_2 molecule has a charge of -0.31e. This indicates a weaker interaction with each O atom but a stronger interaction with the whole molecule as 0.3 of an electron is involved in both interactions.

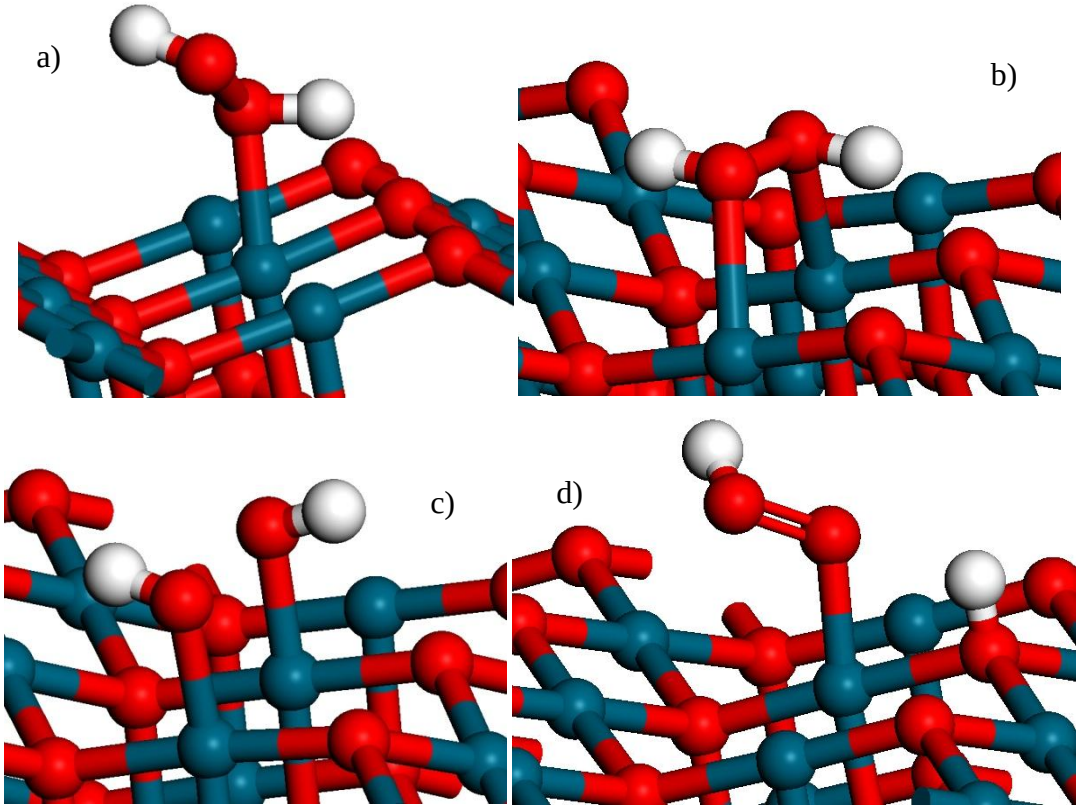

Figure 5.32. Images of H_2O_2 and direct products bound to PdO(101) surface a) H_2O_2 bound to single Pd site, b) H_2O_2 bound to two Pd sites, c) two hydroxyls bound to Pd sites and d) OOH and H atom bound to Pd and O site. Pd atoms are blue, O atoms are red and H atoms are white.

Unlike the Pd(111) and Au(111) surfaces, H_2O_2 does not spontaneously cleave over the PdO(101) surface meaning both HO – OH bond cleavage and HOO – H bond cleavage will have barriers that can be ascertained by a NEB approach. Both images of these end points are shown in Figure 5.32.c) and d) The 2 hydroxyls bind to the 3 co-ordinate Pd atom site with Pd – O distances of 1.96 Å and 1.94 Å and a binding energy of -144 kJ mol^{-1}. The Bader charges of the hydroxyls are -0.48e and -0.52e, which would indicate these are strongly bound to the surface as there is a charge transfer between the hydroxyl and surface. The barrier shown in figure 5.33. to form the hydroxyls is 6 kJ mol^{-1} with the reverse to form H_2O_2 from the hydroxyls is 35 kJ mol^{-1}.

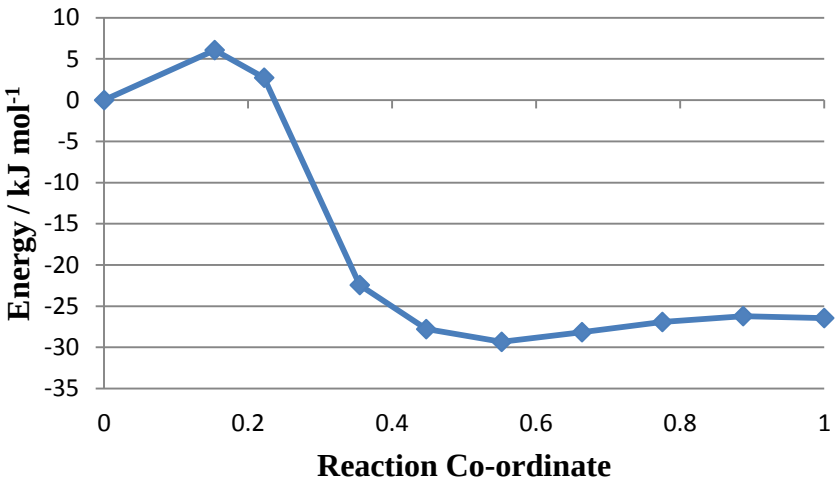

Figure 5.33. HO – OH bond cleavage to form two hydroxyls bound to PdO(101) surface.

In the dissociated state the OOH binds to the 3 co-ordinate Pd atom site and the hydrogen atom is bound to the 3 co-ordinate oxygen atom site. The Pd – O distance is 1.99 Å, the O – H distance is 0.98 Å and the O – O distance is 1.44 Å. The binding energy is -142 kJ mol^{-1} and has charges of -0.49e on the OOH and -0.47e on the H atom. All of this would indicate that the OOH and H atom bind strongly to the surface due to the charge transfer indicated by the Bader charges. The barrier for the transfer of the H atom to the surface shown in figure 5.34. is 5 kJ mol^{-1} and the reverse is 43 kJ mol^{-1}.

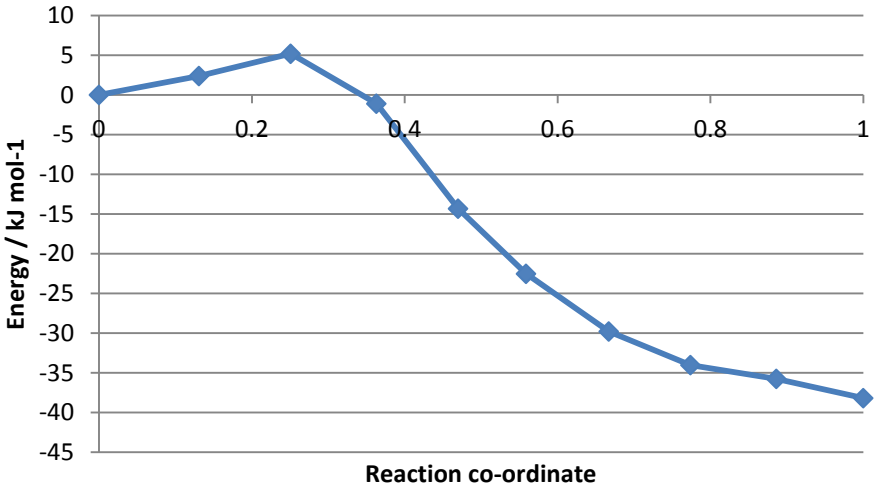

Figure 5.34. HOO – H bond cleavage to form OOH and H atom bound to PdO(101) surface.

O_2

O_2 will adsorb to both a single three co-ordinate Pd atom and a pair of three co-ordinate Pd atoms, these are shown in figure 5.35. The O_2 molecule bound to the single Pd has a O – O bond length of 1.26 Å and a Pd – O distance of 2.11 Å. The O_2 molecule has a Bader charge of -0.30e with the O atom bound to the Pd atom in the surface with a charge of -0.22e. The O_2 bound to the pair of Pd has a O – O bond length of 1.31 Å and two Pd – O distances of 2.10 Å. The O_2 molecule has a charge of -0.53e with charges of -0.32e and -0.21e on the O atoms. The spin distributions for the two binding positions shown in figure 5.36. have both oxygen atoms with the spin in the same direction making both triplet states. Both spin densities are showing the expected density for a triplet state oxygen. The charges along with the O – O bond length would indicate a superoxy species in the bridging O_2.

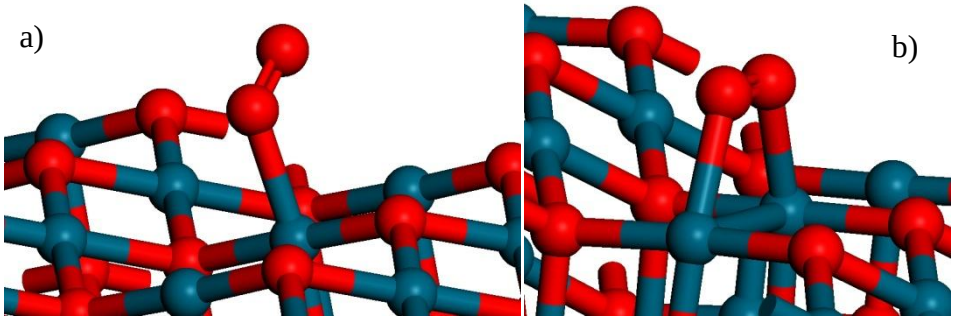

Figure 5.35. Images of O_2 bound to PdO surface a) single oxygen atom bound b) both oxygen atoms bound. Pd atoms are blue and O atoms are red.

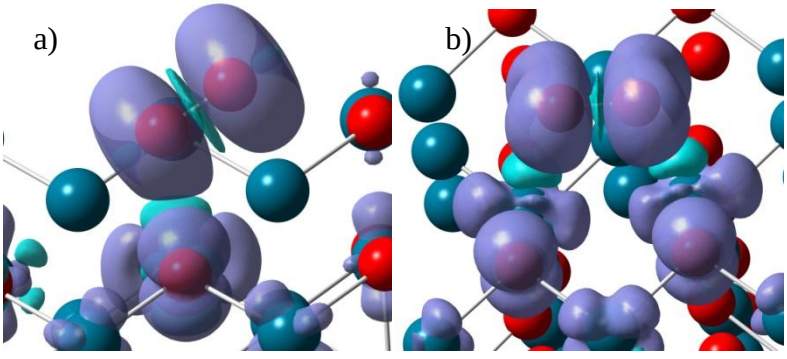

Figure 5.36. Spin densities of O_2 in top and bridging sites a) O_2 over top site b) bridging site O_2 both with an isovalue of 4×10^{-4} eÅ^{-3}. Pd atoms are blue and O atoms are red.

H_2

A H_2 molecule adsorbs unfavourably to the PdO(101) surface with a binding energy of 25 kJ mol^{-1} with an O – H distance of 2.70 Å. Cleavage of the H – H bond forms two surface hydrogen atoms bound to the three co-ordinate Pd atom site with a binding energy of +132 kJ mol^{-1} or bound to the three co-ordinate O atom site with a binding energy of -220 kJ mol^{-1}, which are shown in figure 5.37. This would indicate that the H atom bound to the O site is far more favourable and therefore the other case can be ignored. The H atoms bound to the Pd atoms have Pd – H distances of 1.53 Å and a Bader charge on the H atoms of -0.74e, which would indicate these are hydride in nature. The H atoms bound to O sites have an O – H distance of 0.97 Å with a charge on the H atoms of -0.48e.

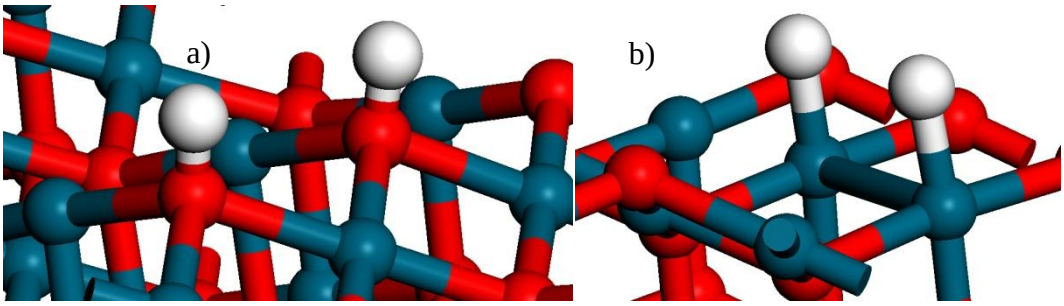

Figure 5.37. Two Hydrogen atoms bound to b) Pd and a) O in PdO(101) surface. Pd atoms are blue, O atoms are red and H atoms are white.

The barrier to cleave the H – H in H_2 to form two surface hydrogen atoms on the three co-ordinate oxygen atoms in the surface is 100 kJ mol^{-1} with the reverse 349 kJ mol^{-1}. The plot of this barrier is shown in figure 5.38. The barrier to cleave the H – H bond is high but the reverse barrier can be considered very unlikely.

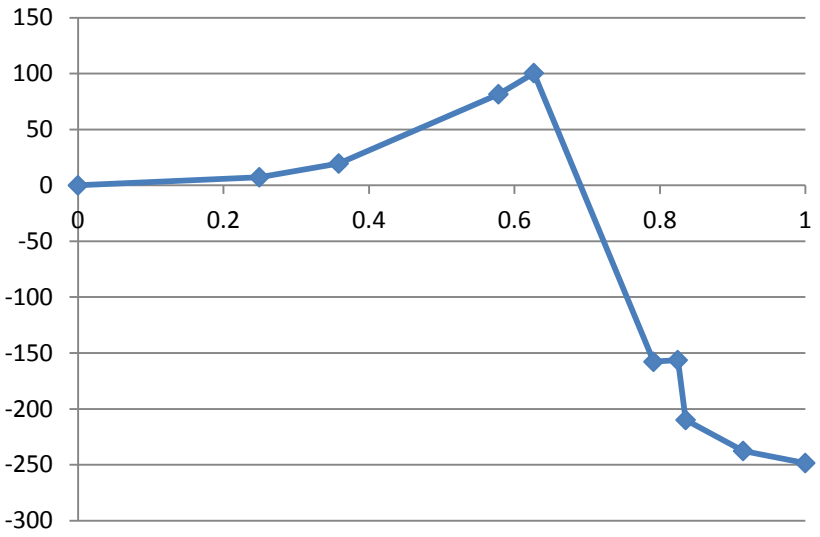

Figure 5.38. Plot of barrier of H – H bond cleavage in H_2 on PdO(101) surface.

H atom transfer to O_2

A surface hydrogen atom can be transferred to O_2 bound to the surface to form OOH. The barrier to the transfer of the hydrogen atom to the oxygen molecule on the PdO(101) surface is 65 kJ mol^{-1} with the reverse 52 kJ mol^{-1}, which is shown in figure 5.39. This would mean the hydrogen would transfer between the surface and the oxygen molecule favouring the hydrogen atom on the surface but as there is only a 13 kJ mol^{-1} difference between the hydrogen atom on the surface and the hydrogen atom on the O_2 molecule it would be reasonable to expect a population at the end point, and therefore at a high enough temperature an equilibrium could be established.

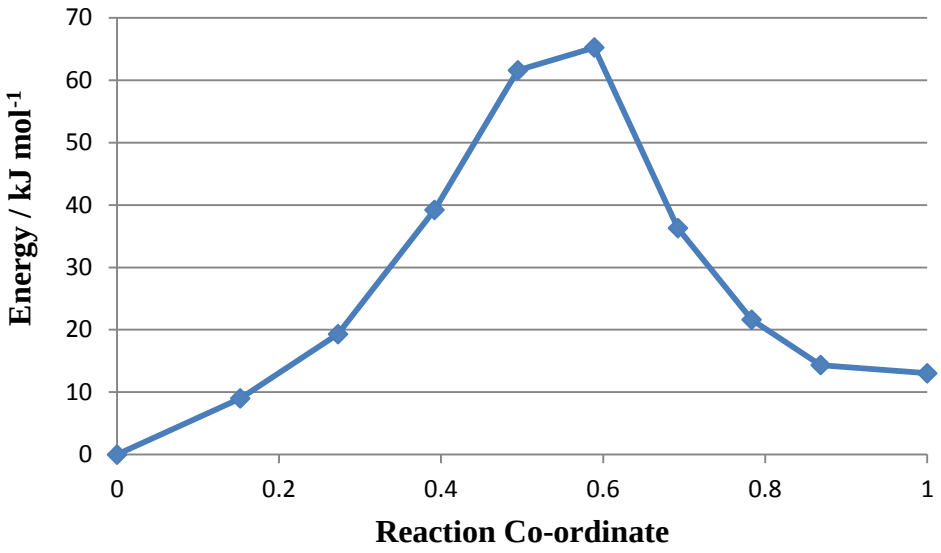

Figure 5.39. Plot of hydrogen atom transfer between surface and oxygen molecule on PdO(101).

CH_3OOH

CH_3OOH is studied as an intermediate of the reaction. It is produced from CH_3 and OOH as with Au(111) and Pd(111). The CH_3 and OOH are bound on adjacent 3 co-ordinate Pd atom sites with a C – Pd distance of 2.03 Å, a Pd – O distance of 1.99 Å and an O – O distance of 1.43 Å. An image of this is shown the figure 5.40.a) The binding energy for the CH_3, OOH and two H atoms is -181 kJ mol^{-1}. The Bader changes are -0.43e for CH_3 and -0.50e for OOH. These are unchanged from both CH_3 and OOH alone on the surface. CH_3OOH is bound to the 3 co-ordinate Pd atom site with the Pd – O distance of 2.19 Å, an O – O distance of 1.46 Å and a C – O distance of 1.44 Å. An image of this is shown in figure 5.40.b) The binding energy for the CH_3OOH and two H atoms is -200 kJ mol^{-1}. The charge on CH_3OOH is -0.47e showing it is bound to the surface and the C – O and O – O distances indicate that bonds exist between them.

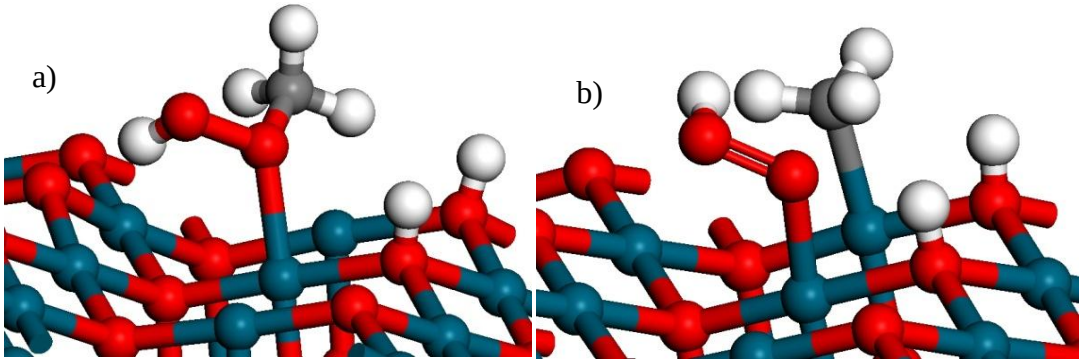

Figure 5.40. CH_3OOH on PdO(101) surface as a) CH_3OOH and b) CH_3 and OOH. Pd atoms are blue, O atoms are red, C atoms are white and H atoms are white.

The barrier to produce CH_3OOH from CH_3 and OOH shown in figure 5.41.a) is 166 kJ mol^{-1} with the reverse, 185 kJ mol^{-1}. These are both considered to be large barriers and would have a slow reaction. The high point of the barrier is shown in figure 5.41.b) The high point shows a planar CH_3 which has a charge of -0.15e, which would indicate that the CH_3 has become more radical in nature.

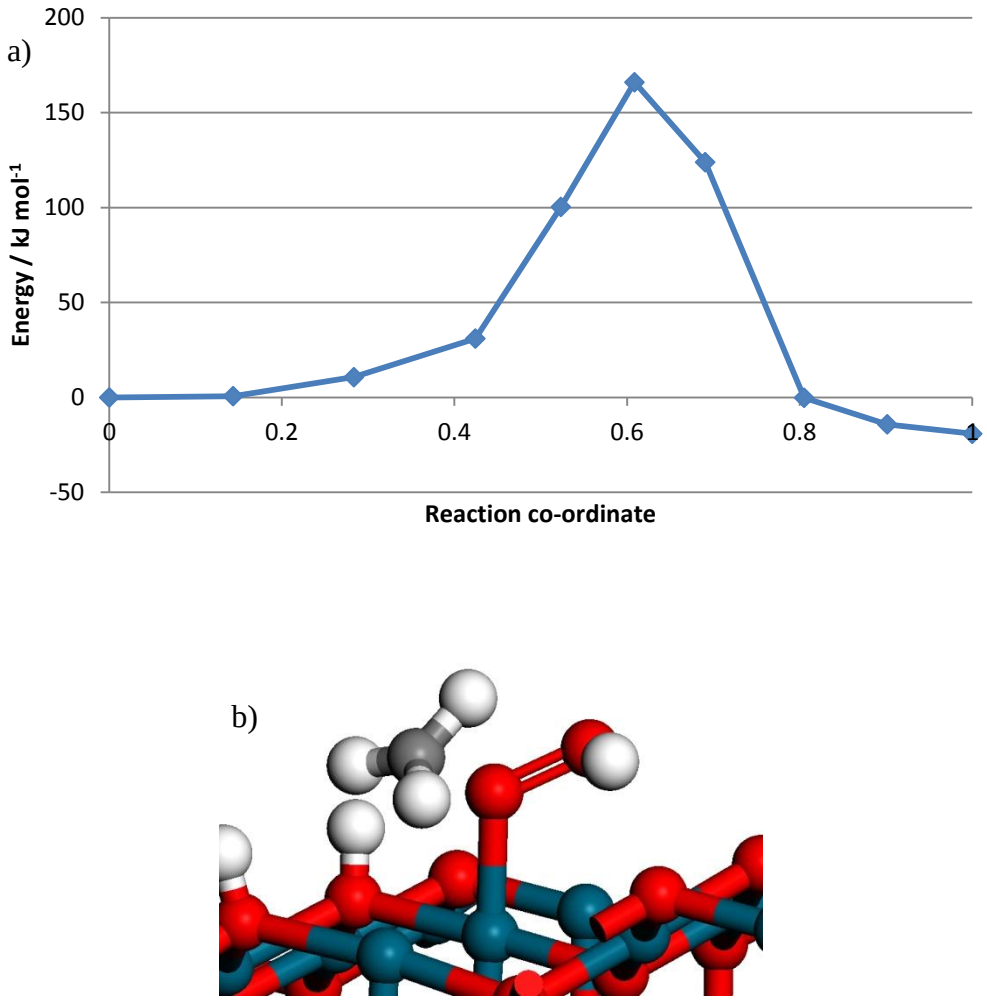

Figure 5.41. Barrier of C – O bond formation to form CH_3OOH and high point of the barrier. Pd atoms are blue, O atoms are red, C atoms are white and H atoms are white.

Once the CH_3OOH has been formed it can decompose on the surface in the same way H_2O_2 has been previously been shown to. O – O bond cleavage will leave a methoxy and hydroxyl on the surface, which are shown in figure 5.42.

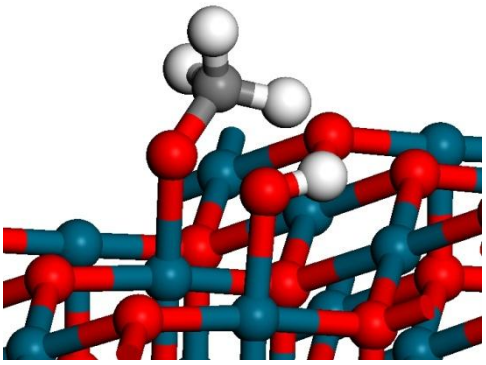

Figure 5.42. Methoxy and hydroxyl bound to PdO(101) surface. Pd atoms are blue, O atoms are red, C atoms are white and H atoms are white.

The methoxy has a Pd – O distance of 2.01 Å, a C – O distance of 1.40 Å and a charge of -0.36e. The hydroxyl has a Pd – O distance of 1.98 Å and a charge of -0.51e. The binding energy for the methoxy and hydroxyl is -108 kJ mol^{-1}, which can be compared to CH_3OOH bound to the surface at -75 kJ mol^{-1}. The barrier to break the O – O bond is 12 kJ mol^{-1} with the reverse 45 kJ mol^{-1} which is shown in figure 5.43.

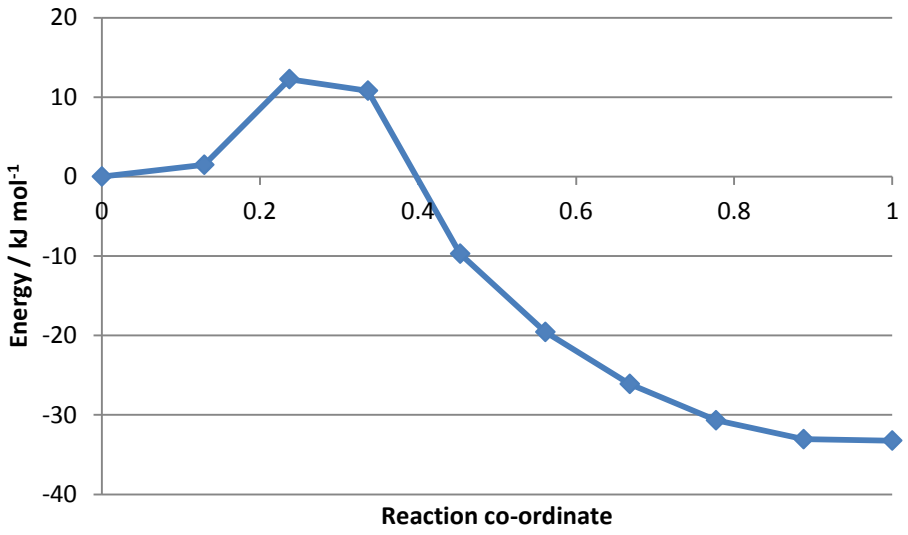

Figure 5.43. Plot of the barrier for the cleavage of O – O bond in CH_3OOH on PdO(101) surface.

CH_3OH

CH_3OH can be produced from the methoxy and a hydrogen atom on the surface of PdO(101). The surface hydrogen would be present from the earlier steps of the

reaction from the hydrogen transfer off H_2O_2 or CH_4. The methoxy would be produced from the O – O bond cleavage of CH_3OOH. An image of the hydrogen atom and methoxy on the surface is shown in figure 5.44.a)

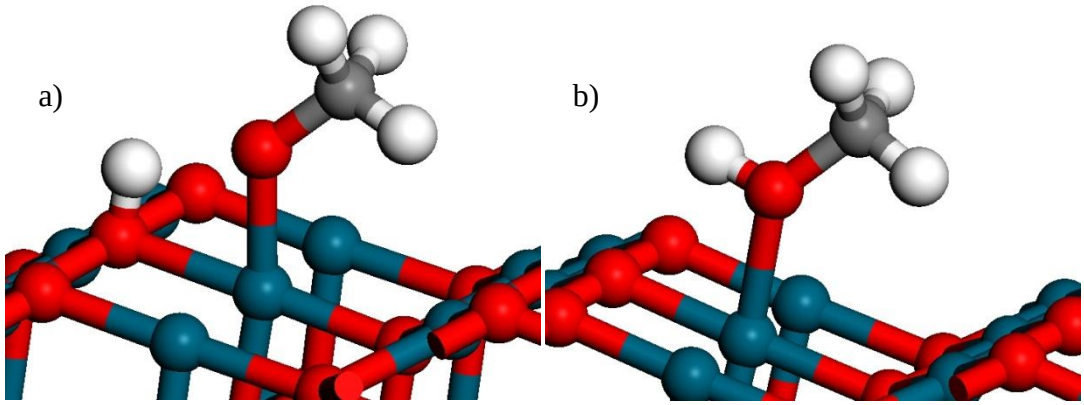

Figure 5.44. Images of methoxy and a hydrogen atom on PdO(101) and methanol on PdO(101). Pd atoms are blue, O atoms are red, C atoms are white and H atoms are white.

The methoxy is bound to the 3 co-ordinate Pd atom site. It has Pd – O distance of 2.00 Å and a C – O distance of 1.41 Å. The hydrogen atom is bound to the 3 co-ordinate O atom site and has a O – H distance of 0.99 Å. The binding energy for methoxy and a H atom is -111 kJ mol^{-1}. The Bader charge for the methoxy is -0.54e and the H atom is -0.48e.

Methanol is bound to a 3 co-ordinate Pd atom site, which is shown in figure 5.44.b) It has Pd – O distance of 2.12 Å, a C – O distance of 1.44 Å and a binding energy of -98 kJ mol^{-1}. The charge of the methanol is -0.15e.

The barrier to form CH_3OH from CH_3O and H is 27 kJ mol^{-1} with the reverse 40 kJ mol^{-1}. This is shown the figure 5.45. This would indicate a low energy transfer between the two points.

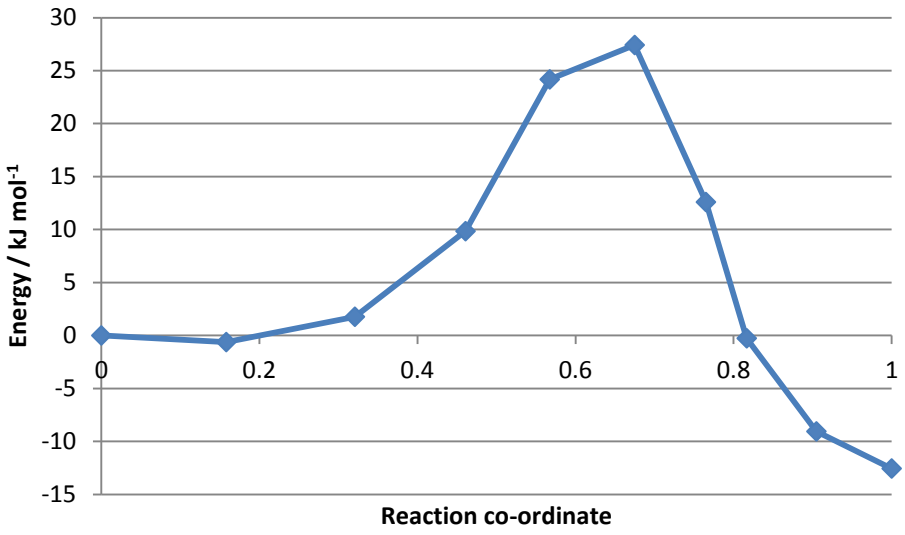

Figure 5.45. Plot of barrier of hydrogen transfer between CH_3OH and PdO(101) surface and form a methoxy.

H_2O

Water is both the final product and the solvent of the reaction. It can be produced from a hydroxyl and a hydrogen on the PdO(101) surface. Water is bound to the 3 co-ordinate Pd atom site, an image of which is shown in figure 5.46, and has a binding energy to the surface of -49 kJ mol^{-1}. It has a Pd – O distance of 2.14 Å with a charge on the water of -0.25e.

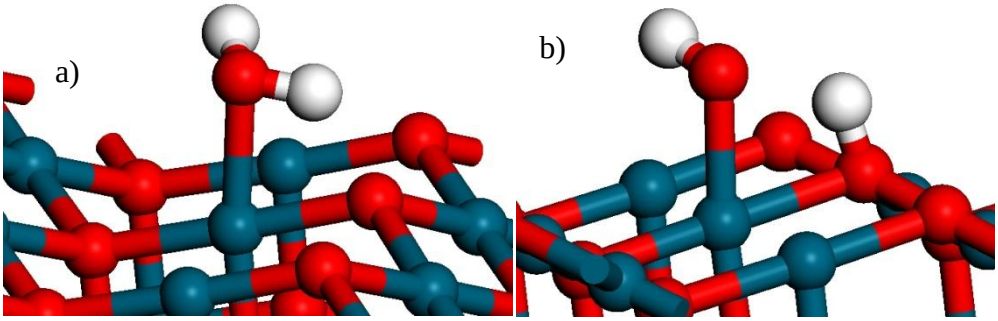

Figure 5.46. Image of water bound to the PdO(101) surface, and a hydroxyl and hydrogen atom bound to the surface. Pd atoms are blue, O atoms are red and H atoms are white.

The hydroxyl is bound to the 3 co-ordinate Pd atom site and the hydrogen atom is bound to the 3 co-ordinate O atom site. The binding energy is -53 kJ mol^{-1}. It has a charge of -0.49e on the hydroxyl and -0.51e on the surface hydrogen atom. It has a Pd – O distance of 2.00 Å and an O – H distance of 1.00 Å.

The barrier between water and the hydroxyl and surface hydrogen is 10 kJ mol^{-1} and the reverse 15 kJ mol^{-1} with the hydrogen atom transferring between the water and the surface, which is shown in figure 5.47.

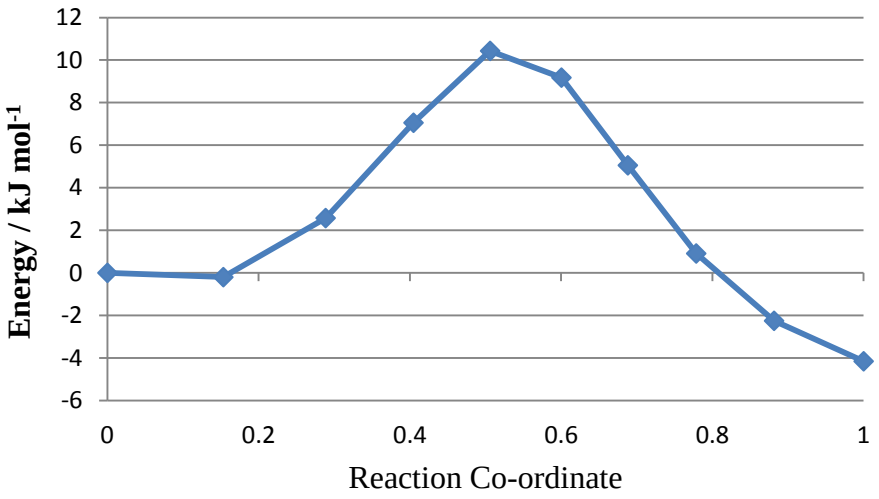

Figure 5.47. A plot of the barrier for the transfer of a hydrogen atom from a water molecule to produce a surface hydrogen atom and a hydroxyl.

Mechanisms

The mechanism for this process involves six steps, which are shown in a catalytic cycle in figure 5.48. The six are as follows: 1. CH_4 adsorption and C – H bond breaking, 2. H_2O_2 adsorption and O – H bond breaking, 3. C – O bond formation from CH_3 and OOH, 4. CH_3O – OH bond cleavage. 5. O – H bond formation on both OH and CH_3O and 6. desorption of CH_3OH and H_2O to obtain starting catalyst.

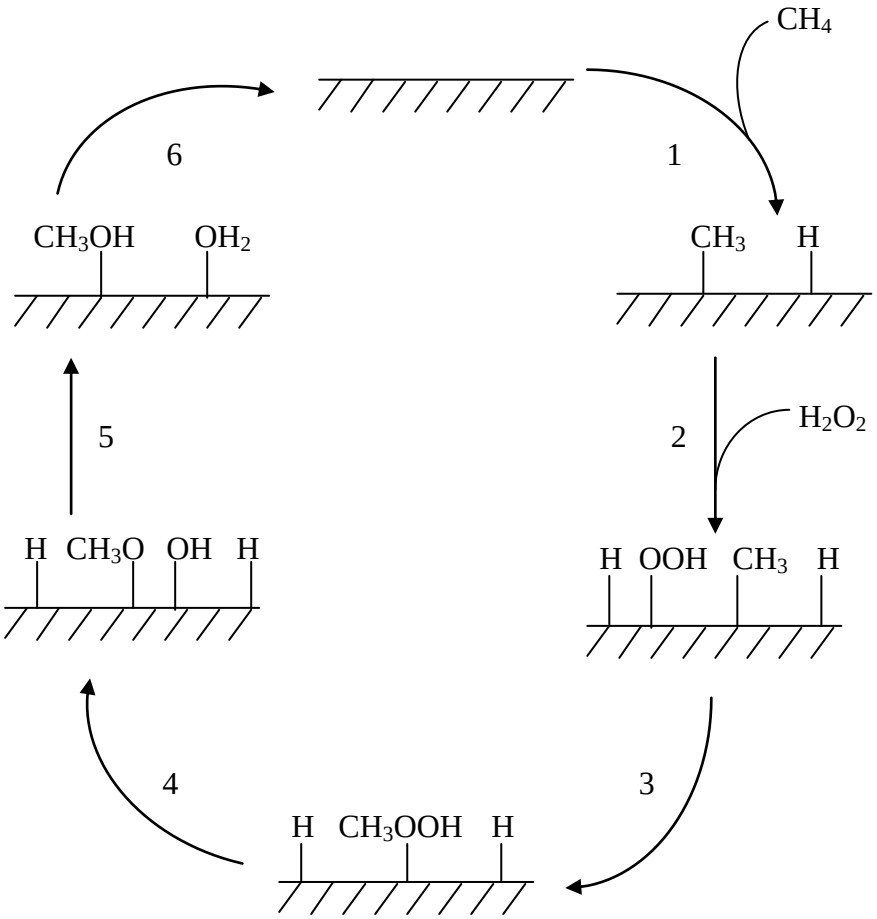

Figure 5.48. Proposed catalytic cycle for the oxidation of methane to produce CH_3OH.

If the mechanism was looked at on just one of the surfaces, the Au(111) would have C – H bond breaking in methane as a rate determining step at 200 kJ mol^{-1} but the H_3C – OOH bond formation has the lowest barrier at 129 kJ mol^{-1}. If it is assumed that the CH_3, OOH, CH_3O, OH and hydrogen atoms can move over the surface, then each part of the mechanism can happen in different places on the cluster. Step 1, 2 and 5 all involve the transfer of a hydrogen atom to and from a surface. In this case the PdO(101) has the lowest barriers, in some cases by as much as an order of magnitude. In the case of H_2O_2 the oxide does not have the spontaneous cleavage of the HO – OH bond but the barrier for this process is relatively lower than the H – OOH bond breaking due to the start position of the barrier being 14 kJ mol^{-1} lower. Steps 3 and 4 have the best results on the Au(111) surface but step 4 would occur spontaneously on both Au(111) and Pd(111). Using these results together explain

why Au/Pd supported TiO_2 catalysts are more active than Pd or Au supported TiO_2. This is because both components of the catalyst are required for the best catalyst but the individual components can still produce a product at a lower rate.

The mechanism for H_2O_2 production involves an O_2 adsorbing to one of the surfaces. H_2 has to be adsorbed in addition to this. As discussed in Chapter 4, there are two available paths, one with both O_2 and H_2 breaking into atom and the other with just the H_2. On Au(111), O_2 requires a high energy to cleave[5] of 183 kJ mol^{-1} but H_2 requires far less so just H_2 cleaving[6] at 28 kJ mol^{-1} is far more likely rather than both. On Pd(111), H_2 cleaves easily but this is not the case on PdO(101) which has a barrier for cleavage of 100 kJ mol^{-1}. The transfer of hydrogen atoms to O_2 is the easiest on PdO(101) so hydrogen cleavage may occur on the Au or Pd surface and the hydrogen atom transfer could happen on the PdO surface.

Conclusions

Combining the results from the three surfaces produce more paths, that may have not been available with just the one surface available. Both Au(111) and Pd(111) spontaneously cleave the HO – OH in H_2O_2 on the bridging site on the surface. On PdO(101) a barrier of 6 kJ mol^{-1} exists for HO – OH cleavage but the blocking of the sites with hydroxyl groups will allow the transfer of a hydrogen atom to form OOH to occur due the restricted space due to the likely build up of hydroxyl groups as two adjacent sites are required for this process. The hydroxyl groups should have a large effect on the mechanism due to the excess that would be produced on these surface and any further studies would have to take account of these.

Large barriers exist for C – H bond breaking with the Au and Pd metal surfaces (200 kJ mol^{-1} and 76 kJ mol^{-1}) but on the PdO(101) the barrier is 57 kJ mol^{-1}. With the C – O bond formation the order of the barrier energy is reversed compared to C – H bond breaking, meaning all the parts are important as the Pd is required to produce the PdO.

References

1. J. K. Edwards, E. Ntainjua, A. F. Carley, A. a Herzing, C. J. Kiely, and G. J. Hutchings, *Angewandte Chemie (International ed. in English)*, 2009, **48**, 8512–5.

2. H. H. Kan and J. F. Weaver, *Surface Science*, 2008, **602**, L53–L57.

3. J. F. Weaver, C. Hakanoglu, J. M. Hawkins, and A. Asthagiri, *The Journal of chemical physics*, 2010, **132**, 024709.

4. J. F. Weaver, J. a. Hinojosa Jr., C. Hakanoglu, A. Antony, J. M. Hawkins, and A. Asthagiri, *Catalysis Today*, 2010, **160**, 213–227.

5. J. L. C. Fajín, M. N. D. S. Cordeiro, and J. R. B. Gomes, *Chemical communications (Cambridge, England)*, 2011, **47**, 8403–5.

6. A. Corma, M. Boronat, S. González, and F. Illas, *Chemical Communications*, 2007, 3371.

6. CH_4 oxidation to CH_3OOH on Fe/ZSM-5

CH_4 oxidation is investigated in zeolites, initially starting with a model catalyst using the CHA (Chabazite) structure with framework Si replaced with Ti, Fe and Al and the interaction of CH_4 and H_2O_2 are studied. An extra-framework Fe_2O_2 from work by Goddard *et al*[1]. is used as the initial active species. The interactions of the active species with CH_4, H_2O_2, CH_3OOH and CH_3OH are investigated. The structure is modified with the addition of water and the transfer of hydrogen atoms between water and the bridging oxygen atoms to produce a new active species. Using the results from the model structure and new active site, the larger MFI structure is employed as a new model. The interactions of the new active species with CH_4, H_2O_2 and CH_3OOH are investigated. A mechanism will be produced for CH_4 oxidation to produce CH_3OOH.

6.1. CHA structure model

CHA structure

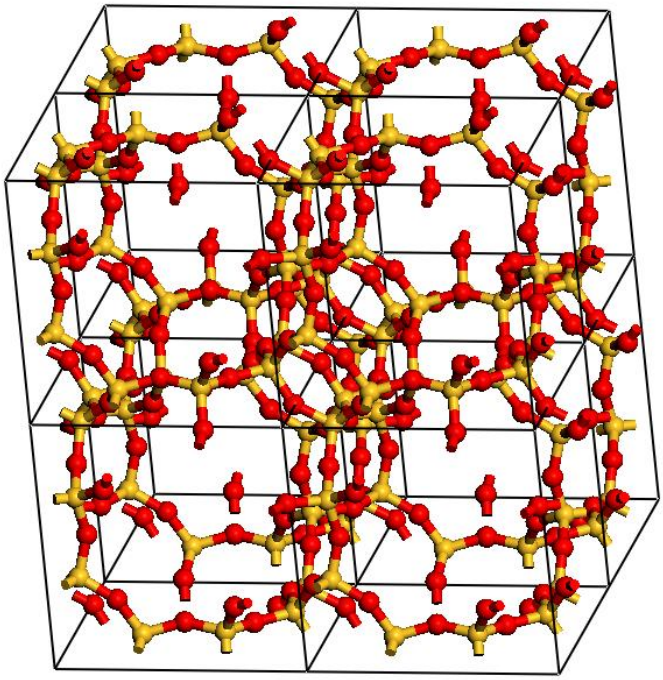

Figure 6.1. An image of 8 CHA unit cells. Si in yellow and O in red.

The chabazite (CHA) structure has unit cell of 9.42 Å × 9.42 Å × 9.42 Å, which was optimised to the minimum energy expansion factor. The CHA structure consists of four co-ordinated Si atoms and two co-ordinate O atoms and has Si – O distances of 1.63 Å, which is shown in figure 6.1. A DFT+U approach using the PBE functional is used with the Ti atoms having a U value[2–4] of 4.2 eV applied and the Fe atoms has a U value[5] of 4.0 eV applied.

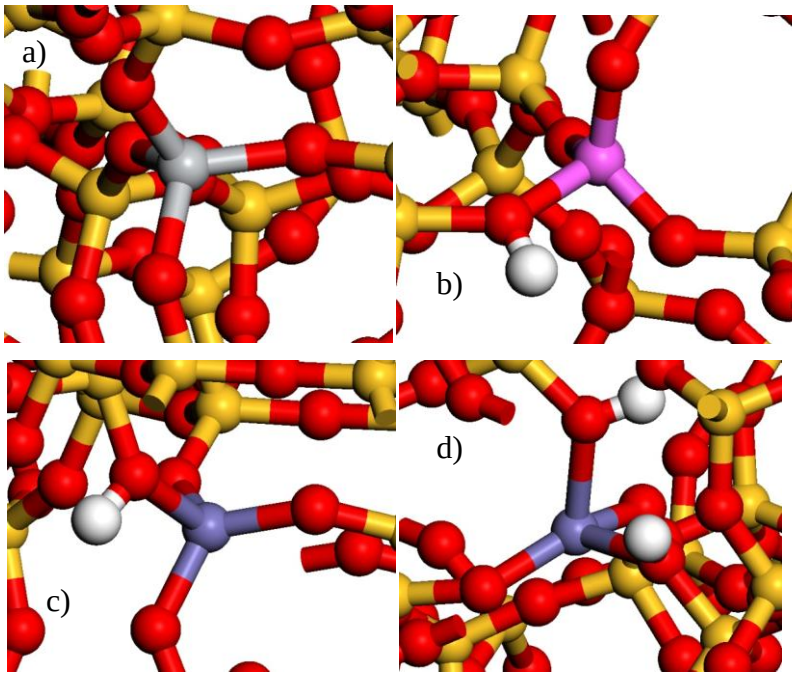

Figure 6.2. Images of a) Ti, b) Al and c) Fe(3+) d) Fe(2+) replacing Si in CHA structure. Si in yellow, O in red, Al in pink, Fe in blue, Ti in light grey and H in white.

The Si atoms can be replaced by a number of metal atoms to alter how the zeolite interacts with molecules. In this study Al, Fe and Ti are investigated, which are shown in figure 6.2. Ti is a 4+ ion so can directly replace a Si atom, with Ti – O distances of 1.81 Å. Al is a 3+ ion and also replaces a Si atom but requires a H atom to balance the charges, with an Al – OH distance of 1.87 Å, an average Al – O distance of 1.70 Å and a Si – OH distance of 1.70 Å. Fe can be a 3+ and a 2+ ion, the 3+ requiring the H atom to balance the charges and the 2+ requiring two H atoms to balance the charges. The Fe 3+ ion has a Fe – OH distance of 2.02 Å, an average Fe – O distance of 1.82 Å and a Si – OH distance of 1.67 Å. The Fe 2+ ion has a Fe – OH distance of 2.15 Å, Fe – O distances of 1.85 Å and 1.87 Å and two Si – OH

distances of 1.66 Å. In all cases the Si – O distances fall in between 1.60 Å and 1.63 Å.

Additional Si atoms can be replaced to have two of different atoms, which has been investigated with two Al 3+ and two Fe 3+ having at least one Si atom between them to obey Lowensteins′ rule, and these are shown in figure 6.3. The additional 3+ ion replaces a Si atom in the same way as the first 3+ ion. The Al atom produces Al – OH distances of 2.85 Å and 2.86 Å, an average Al – O distance of 1.72 Å and a Si – OH distance of 1.70 Å. The Fe 3+ ion has a Fe – OH distance of 2.01 Å, an average Fe – O distance of 1.82 Å and a Si – OH distance of 1.67 Å.

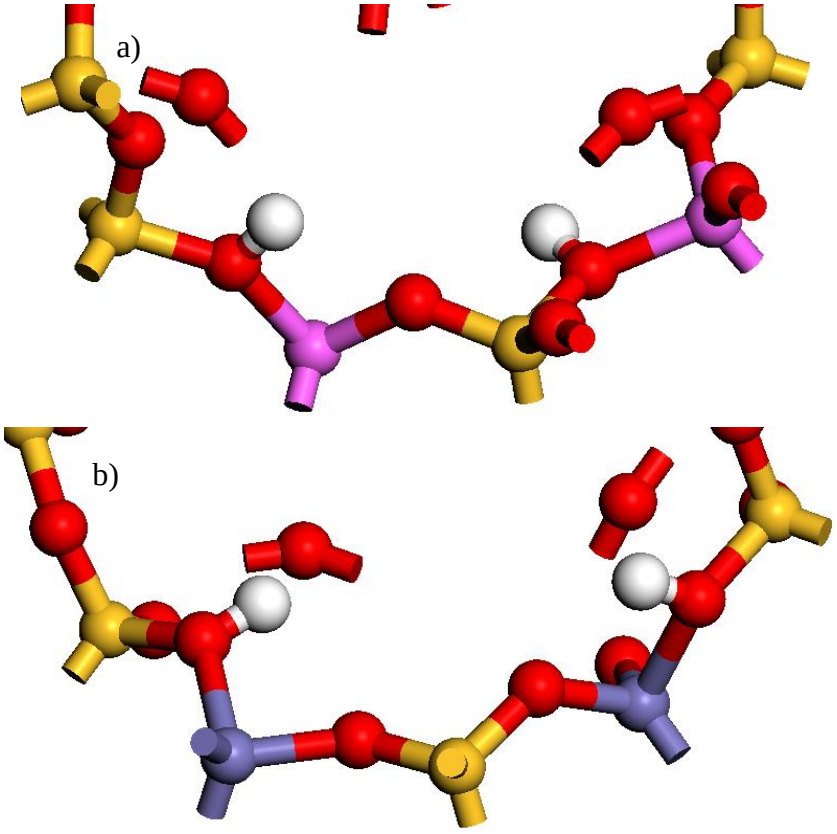

Figure 6.3. Images of a) two Al and b) two Fe replacing Si in CHA structure. Si in yellow, O in red, Al in pink, Fe in blue and H in white.

CH_4

CH_4 interacts weakly with Al – CHA (CHA structure with Al replacing one Si atom) sitting in a channel near the Al atom, which is shown in figure 6.1.X. CH_4 has a binding energy of -4 kJ mol^{-1} and an Al – C distance of 4.15 Å. The C – H bond can be cleaved to form a CH_3 over an O atom and a hydrogen atom over a Si atom,

which is shown in figure 6.4. The hydrogen atom will not adsorb to an O atom as it forms CH_4 under geometry optimisation with the CH_3. The CH_3 and H atom have a binding energy of +282 kJ mol^{-1}, a C – O distance of 1.47 Å and a Si – H distance of 1.65 Å.

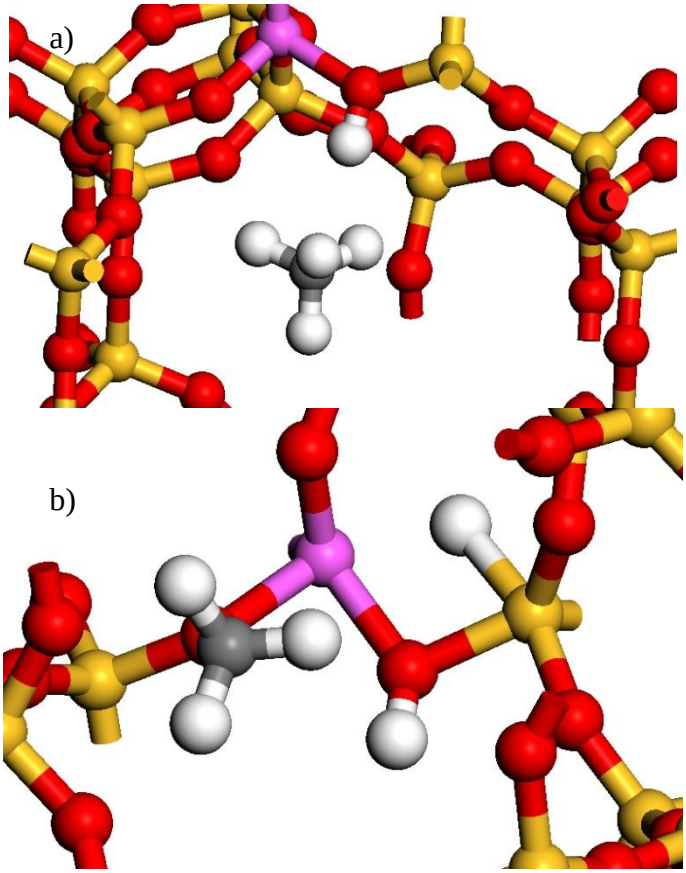

Figure 6.4. Images of a) CH_4 and b) CH_3 and H in the Al-CHA structure. Si in yellow, O in red, Al in pink, C in grey and H in white.

H_2O_2

H_2O_2 adsorbs to CHA in a channel, which is shown in figure 6.5. H_2O_2 has a binding energy of -18 kJ mol^{-1}, a Si – O distance to the nearest Si of 3.45 Å, an O – O distance of 3.15 Å between an O atom in the CHA and an O atom in the H_2O_2 and an O – O distance of 1.47 Å in the H_2O_2.

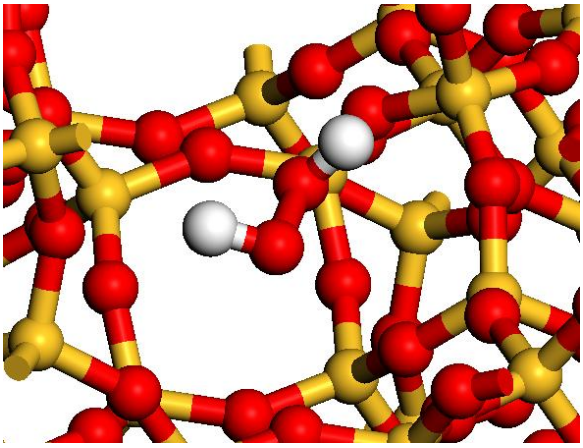

Figure 6.5. Image of H_2O_2 in the CHA structure. Si in yellow, O in red and H in white.

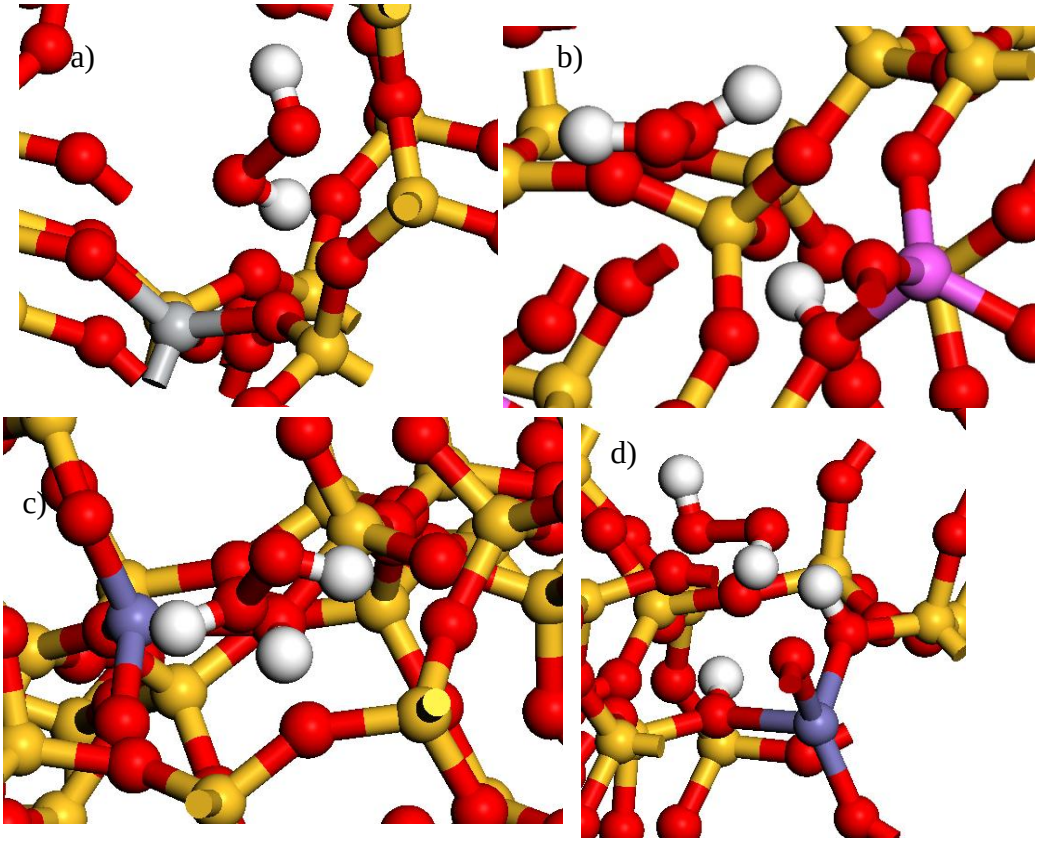

Figure 6.6. Image of H_2O_2 in the a) Ti, b) Al, c) Fe(3+) and d) Fe(2+) CHA structure. Si in yellow, O in red, Al in pink, Fe in blue, Ti in light grey and H in white.

H_2O_2 adsorbs to CHA with a Si replaced with Al, Fe and Ti over the metal centre. A table of energies and atomic distances are shown in table 6.1. and images of these are shown in figure 6.6.

Metal Centre (M)	Binding Energy / kJ mol^{-1}	M – O distance / Å	O – O distance / Å
Al	-18	3.64	1.47
Fe(2+)	-77	3.51	1.47
Fe(3+)	-22	3.31	1.47
Ti	-14	2.57	1.46

Table 6.1. A table of binding energies and atomic distances of H_2O_2 interacting with CHA with metal centre.

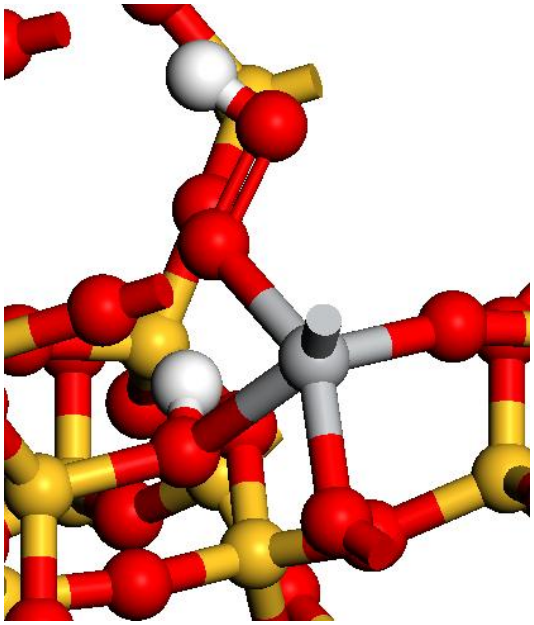

Figure 6.7. Image of OOH and H in the Ti-CHA structure. Si in yellow, O in red, Ti in light grey and H in white.

H_2O_2 can have a hydrogen atom transferred from the H_2O_2 to an O atom bound to the metal centre with an OOH bound to the metal centre. With all metal centres (Al, Si, Fe), the OOH and hydrogen atom reform H_2O_2, apart from the Ti centre, which remains as an OOH. The binding energy and atomic distances for OOH and a hydrogen atom are shown in table 6.2. with image of the Ti centre shown in figure 6.7. The strong binding energies can be attributed to the hydrogen bonding network formed by the hydrogen atoms on the oxygen adjacent to the metal centre with the Fe(2+) showing two and three hydrogen bonding distances respectively in order of

the examples, Fe(3+) shows one and two respectively and Al and Si showing no hydrogen bonding distances.

Metal Centre (M)	Binding Energy / kJ mol^{-1}	M – O distance / Å	O – O distance / Å	O – H distance / Å
Si	-15	3.11	1.47	2.77
Al	-25	3.55	1.47	2.28
Fe(2+)	-82	3.49	1.47	1.58
Fe(3+)	-52	3.45	1.48	1.92
Ti	+44	1.96	1.46	0.99

Table 6.2. A table of binding energies and atomic distances of H_2O_2 interacting with CHA with metal centre.

CHA – Fe_2O_2

Fe can be placed into the CHA structure outside the framework, becoming an extra-framework species. Work by Goddard et al.[1] has placed $[Fe_2O_2]^{2+}$ into the extra-framework position of the MFI structure binding to 2 Al centres without hydrogen atoms giving a single negative charge on each Al atom. The CHA structure has the same position but both Al and Fe can be used to give the CHA the counter charge to the $[Fe_2O_2]^{2+}$. O atoms can be framework (O_f) and extra-framework (O_{ef}) and Fe can be used also in both the framework and extra-framework (Fe_f and Fe_{ef}). Images of these structures are shown in figure 6.8. The $[Fe_2O_2]^{2+}$ structure bound to CHA with Al has a Fe – Fe distance of 2.43 Å, an average Fe – O_{ef} distance of 1.82 Å, an average Fe – O_f distance of 2.08 Å an average Al – O_f distance of 1.80 Å to the oxygen atoms that are bound to the $[Fe_2O_2]^{2+}$ dimer with the other Al – O distance the same as would be expected without the dimer present and an average Fe – Al distance of 2.81 Å. The $[Fe_2O_2]^{2+}$ structure bound to CHA with Fe has a Fe_{ef} – Fe_{ef} distance of 2.61 Å, an average Fe_{ef} – O_{ef} distance of 1.86 Å, an average Fe – O_f distance of 2.04 Å an average Fe_f – O_f distance of 1.94 Å to the oxygen atoms that are bound to the $[Fe_2O_2]^{2+}$ dimer with the other Fe_f – O_f distance the same as would be expected without the dimer present and an average Fe_f – Fe_{ef} distance of 2.87 Å.

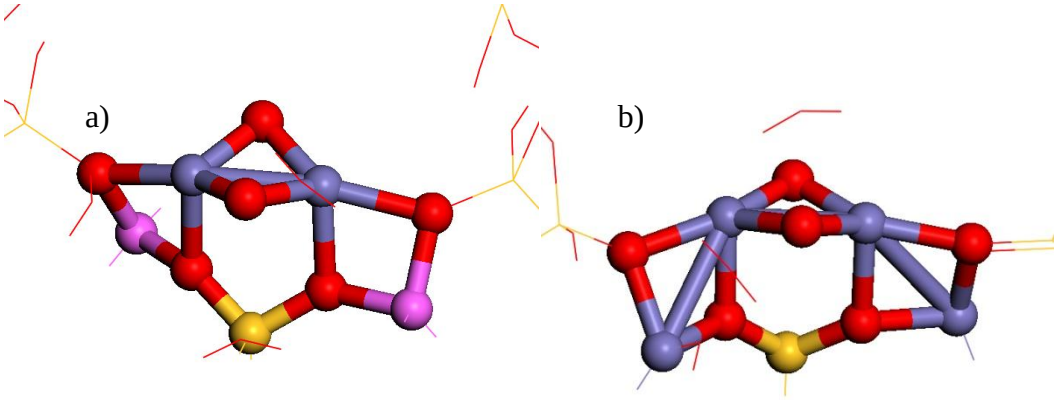

Figure 6.8. Image of Fe_2O_2 extra-framework species with a) Al and b) Fe acting as the framework counter ion. Si in yellow, O in red, Al in pink and Fe in blue.

H_2O_2

H_2O_2 adsorbs over the extra-framework Fe, which is shown in figure 6.9.a). H_2O_2 has a binding energy of -94 kJ mol^{-1}, a Fe – O distance of 2.17 Å and an O – O distance of 1.47 Å. A hydrogen atom can be transferred from the H_2O_2 to one of the extra-framework oxygen atoms resulting in an OOH and the hydrogen atom bound to the extra-framework oxygen atom, which is shown in figure 6.9.b) The OOH and hydrogen atom have a binding energy of -157 kJ mol^{-1}, a Fe – O distance of 1.93 Å, an O – H distance of 0.98 Å and an O – O distance of 1.38 Å. The addition of the OOH and hydrogen atom or H_2O_2 has no effect of the formal charge of 3+ on each of the Fe ions as H_2O_2 is neutral and the OOH is -1 and the hydrogen atom is +1 but both are required to keep the unit cell neutral.

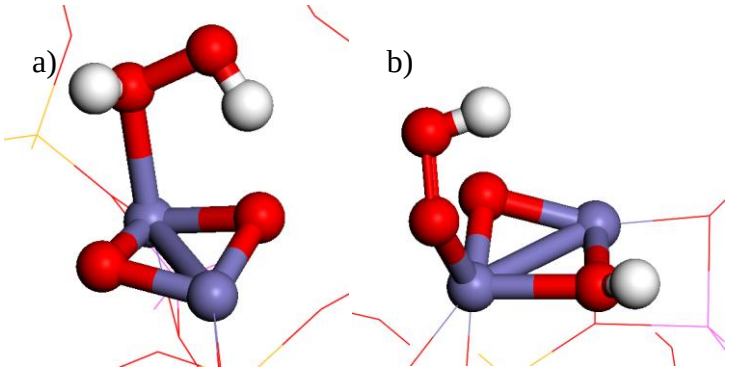

Figure 6.9. Images of a) H_2O_2 and b) OOH and H on extra-framework Fe_2O_2. Si in yellow, O in red, Al in pink, Fe in blue and H in white.

The barrier for the transfer of a hydrogen atom from H_2O_2 to form OOH and a hydrogen atom on the Fe_2O_2 dimer is 39 kJ mol^{-1} with the reverse 102 kJ mol^{-1}, which is shown in figure 6.10.

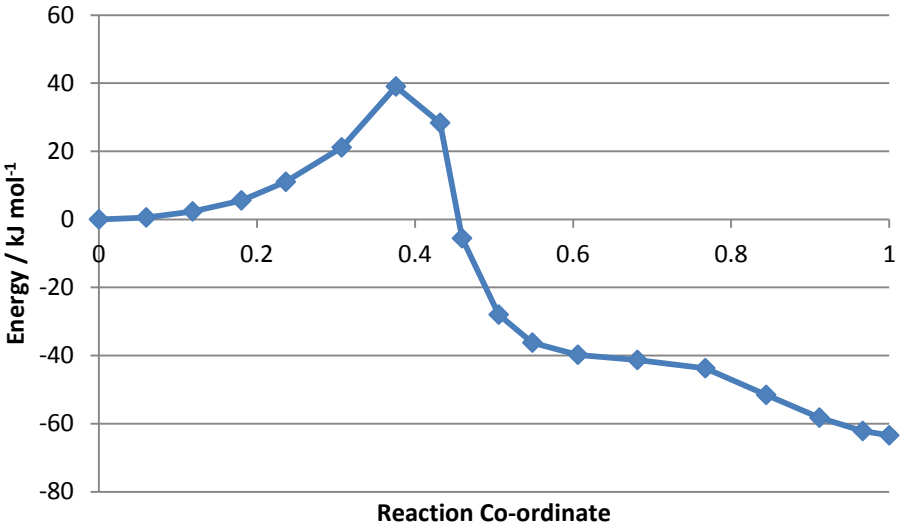

Figure 6.10. A plot of the barrier for hydrogen transfer from H_2O_2 on extra-framework Fe_2O_2.

An additional OOH and hydrogen atom can interact with the Fe_2O_2, which is shown in figure 6.11. The OOH and hydrogen atom have a binding energy of -279 kJ mol^{-1} relative to the Fe_2O_2-CHA and two H_2O_2 and -122 kJ mol^{-1} compared to one H_2O_2.

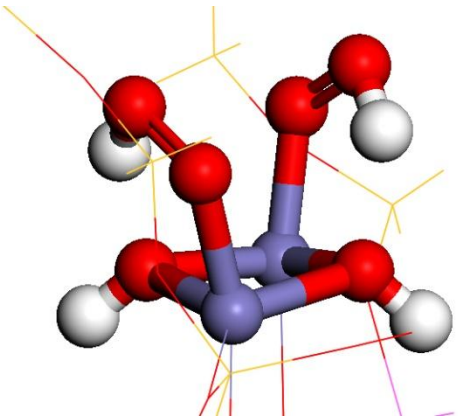

Figure 6.11. An image of two OOH and two H on extra-framework Fe_2O_2. Si in yellow, O in red, Al in pink, Fe in blue and H in white.

A H_2O_2 can be rearranged on the Fe_2O_2 dimer into several forms, which are shown in figure 6.12. Energies and important atomic distances are shown in table 6.3.

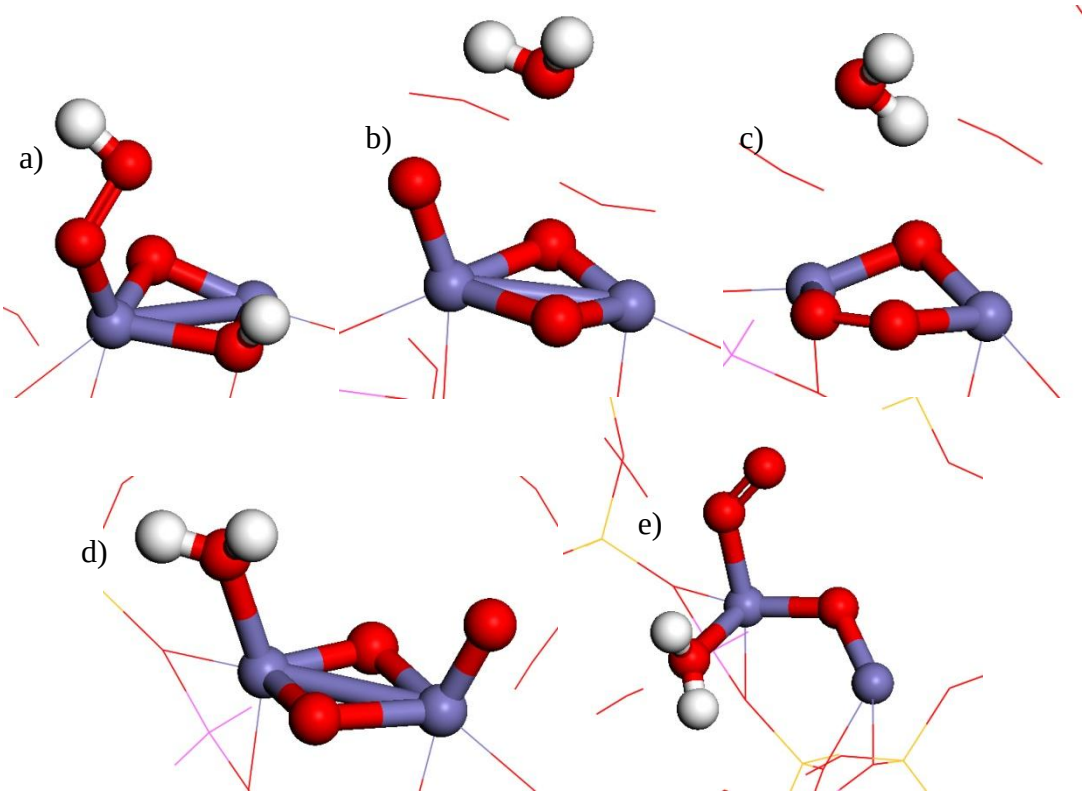

Figure 6.12. Images of H_2O_2 rearranged in several different configurations on extra-framework Fe_2O_2. Si in yellow, O in red, Al in pink, Fe in blue and H in white.

Structure	**Energy / kJ mol^{-1}**	**Fe – Fe distance / Å**	**Fe – O$_{ef}$ distance / Å**	**Fe - O$_{ads}$ distance / Å**	**O – O distance / Å**
a	-123	2.74	1.92	1.87	1.43
b	+4	2.74	1.85	1.77	n/a
c	-120	2.95	1.82	1.98	1.33
d	-110	2.77	1.85	1.63	n/a
e	-172	3.13	1.81	1.94	1.27

Table 6.3. Energies and important atomic distances for the structures shown in figure 6.12.

With both H_2O_2 and OOH bound to the Fe_2O_2 dimer no change in the formal charge of the Fe occurs as only hydrogen transfer reactions have happened but when Fe = O

bonds are formed the Fe atom bound to this oxygen atom gains a 5+ formal charge or a 4+ formal charge if the charge is delocalised between both Fe atoms with the other Fe atoms having a 3+ or 4+ formal charge respectively seen as in figure 6.12.b) and d). O_2 can be produced from the rearrangement of H_2O_2. In figure 6.12.e) water and O_2 are produced but only one of the extra-framework oxygen atom remains so both Fe atoms have a formal charge of 2+. O_2 can also be incorporated into the Fe_2O_2 replacing one of the oxygen atoms, which gives the Fe atoms a 2+ formal charge, which is shown in figure 6.12.c)

CH_4

CH_4 has no interaction with the $[Fe_2O_2]^{2+}$ dimer or the CHA and sits in the channel, which is shown in figure 6.13.a). CH_4 has a binding energy of -4 kJ mol^{-1} and a C – O distance of 3.33 Å between the CH_4 and the extra-framework oxygen atom. A hydrogen atom can be transferred to the dimer from the CH_4 to form CH_3 and the hydrogen atom on the dimer, which is shown in figure 6.13.b). The CH_3 and hydrogen atom have a binding energy of 65 kJ mol^{-1}, a C – O distance of 3.29 Å between the CH_3 and an extra-framework oxygen atom and an O – H distance of 0.97 Å. The CH_3 is planar so therefore radical and not charged.

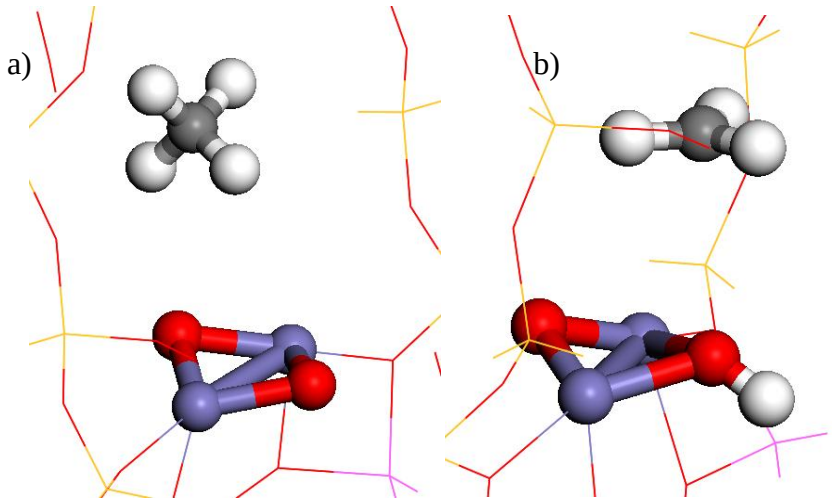

Figure 6.13. Images of a) CH_4 and b) CH_3 and H on extra-framework Fe_2O_2. Si in yellow, O in red, Al in pink, Fe in blue, C in grey and H in white.

CH_4 can be placed in the structure with OOH and a hydrogen atom as seen when the H – OOH bond is cleaved with H_2O_2. CH_4 has no interaction with the $[Fe_2O.OH.OOH]^{2+}$, which is shown in figure 6.14.a). The CH_4 has a binding energy

of -1 kJ mol^{-1} and a C – Fe distance of 2.84 Å. Stronger bonding interactions can be observed but these can attributed to the hydrogen bonding interaction between the OOH and an extra-framework oxygen atom in the Fe_2O_2 dimer, that distance changing from 2.15 Å in the -1 kJ mol^{-1} binding energy case to 1.77 Å with a binding energy of -42 kJ mol^{-1} and 1.82 Å with a binding energy of -55 kJ mol^{-1}. In both these cases the CH_4 is over 3 Å away from the nearest neighbour in the $[Fe_2O_2OH.OOH]^{2+}$ system.

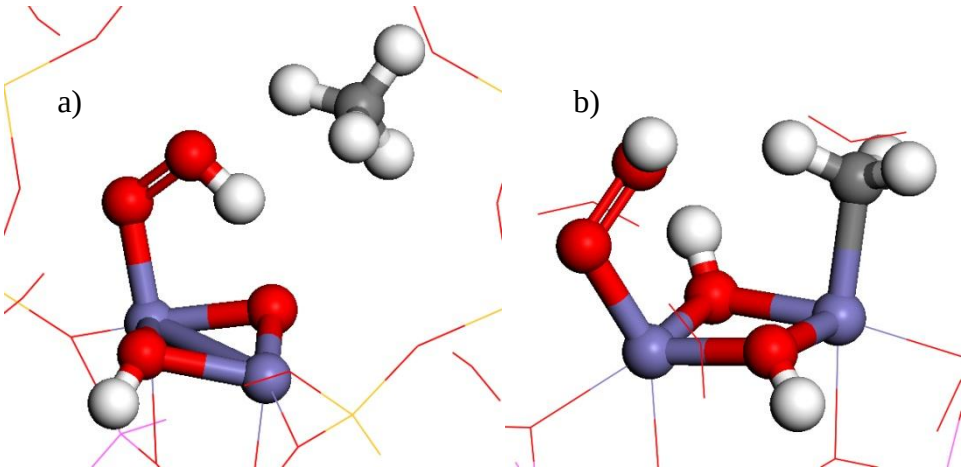

Figure 6.14. Images of a) CH_4 and b) CH_3 and H on extra-framework Fe_2O_2 with OOH and H. Si in yellow, O in red, Al in pink, Fe in blue, C in grey and H in white.

A hydrogen atom can be transferred from the CH_4 to the Fe_2O_2 dimer with CH_3 moving to the other open Fe site, which is shown in figure 6.14.b). The CH_3 and hydrogen atom have a binding energy of -57 kJ mol^{-1}, a Fe – C distance of 2.03 Å, Fe – O distance of 1.88 Å, a FeO – OH distance of 1.44 Å and an O – H distance of 0.97 Å between the transferred hydrogen atom and a extra-framework oxygen atom in the Fe_2O_2 dimer.

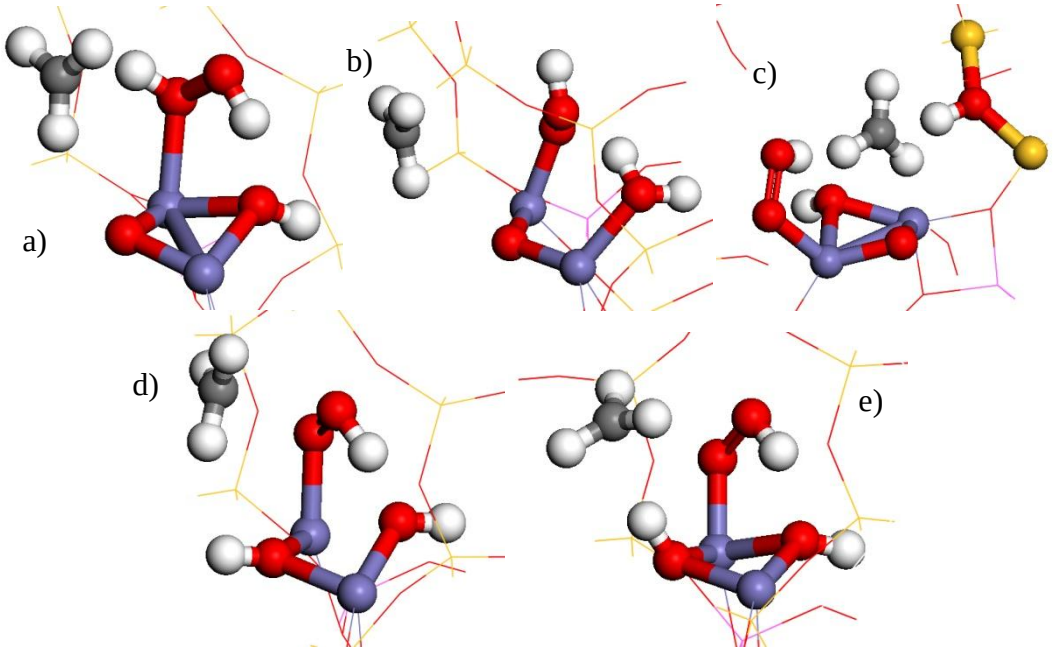

Figure 6.15. Images of planar CH_3 with the hydrogen atom in several different positions on extra-framework Fe_2O_2 and on the framework. Si in yellow, O in red, Al in pink, Fe in blue, C in grey and H in white.

Structure	**Energy / kJ mol^{-1}**	**Fe – Fe distance / Å**	**Fe – O_{ef} distance / Å**	**Fe - OOH distance / Å**	**O – O distance / Å**
a	112	2.73	1.96	2.16	1.47
b	59	3.06	1.99	2.02	1.37
c	283	2.66	1.96	1.87	1.44
d	85	3.04	1.80	1.88	1.45
e	45	2.96	2.02	1.90	1.40

Table 6.4. Energies and important atomic distances for the structures shown in figure 6.12.

The CH_3 can become planar. Table 6.4. shows the energies and important atomic distances for the hydrogen atom transferred to different position with images of these shown in figure 6.15. The hydrogen atom can be transferred to the following locations; a) to the OOH to reform H_2O_2, b) to the extra-framework oxygen atom on Fe_2O_2 dimer, c) to a framework oxygen atom, d) to the extra-framework oxygen atom on Fe_2O_2 dimer with a hydrogen atom present from the H_2O_2 and e) same as b) but the hydrogen atom on the extra-framework is pointing towards the methyl. The

planar CH_3 can be shown to be a radical species by use of the spin density as this shows unpaired electrons, which is shown in figure 6.16. The spin density for the CH_3 shows two lobes of electron distribution perpendicular to the plane of the CH_3 which would indicate the unpaired electron is in the $2p_z$ orbital assuming the $2p_x$ and $2p_y$ orbitals are in the plane.

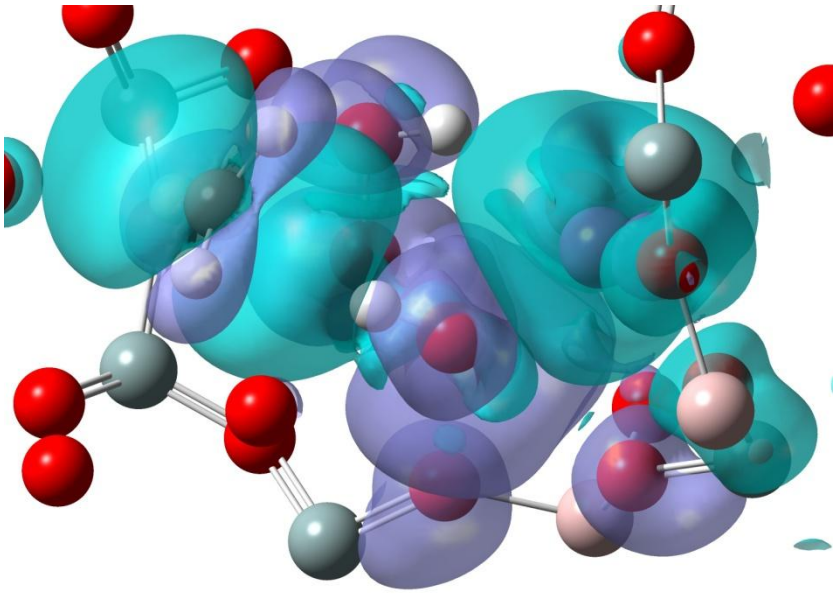

Figure 6.16. Spin density of figure 6.15e) with an isosurface value of 4×10^{-4} e $Å^{-3}$. Si in blue/grey, O in red, Al in light pink, Fe in blue, C in grey and H in white.

The CH_3 can also adsorb to the directly to the OOH species to the oxygen atom bound to the Fe in Fe_2O_2 dimer forming CH_3OOH, which is shown in figure 6.17. The CH_3 and hydrogen atom have a binding energy of -181 kJ mol^{-1}, a C – O distance of 1.43 Å, an O – H distance of 0.97 Å, a Fe – O distance of 2.16 Å and an O – O distance of 1.47 Å. These form CH_3OOH, which explains the more favourable binding energy.

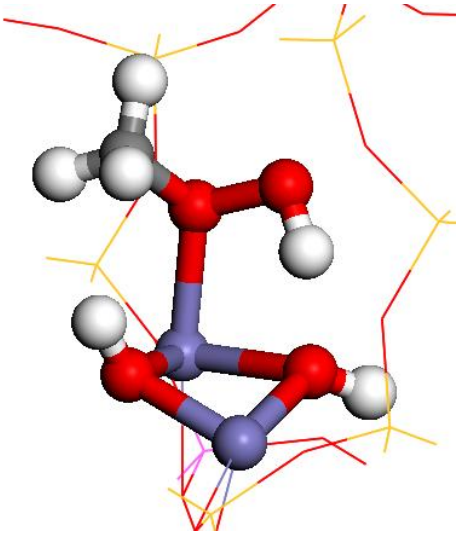

Figure 6.17. CH_3OOH on extra-framework Fe_2O_2. Si in yellow, O in red, Al in pink, Fe in blue, C in grey and H in white.

A barrier can be produced between CH_4 and CH_3OOH but it goes through the radical methyls as they are energy minima, therefore the barrier is complex and misses key reaction steps. To bypass this problem two barriers can be run, one from CH_4 to the radical CH_3 and the second from the radical CH_3 to CH_3OOH. The barrier for the transfer of hydrogen from CH_4 to form a planar CH_3 and a hydrogen atom on the Fe_2O_2 dimer is 84 kJ mol^{-1} with the reverse 37 kJ mol^{-1}, which is shown in figure 6.18.

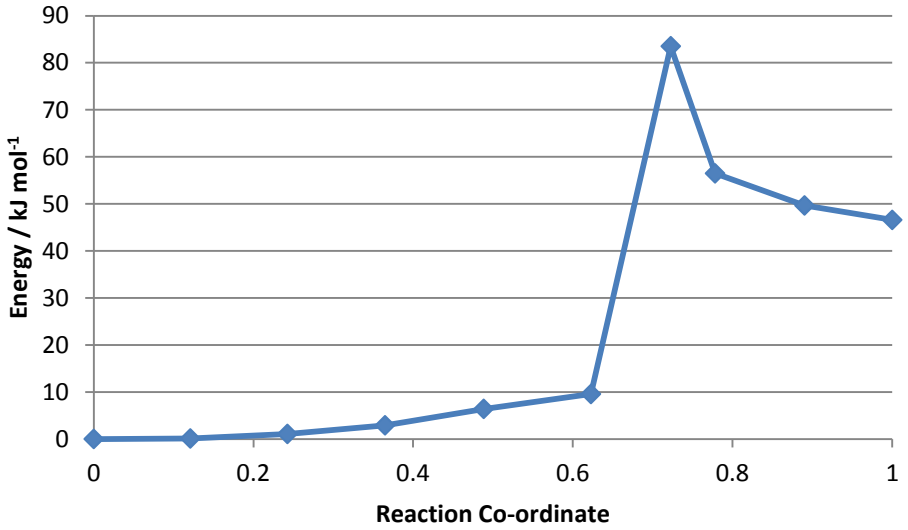

Figure 6.18. Plot of the barrier for C – H bond cleavage in CH_4 on extra-framework Fe_2O_2 to form CH_3 radical.

The barrier for the translation of CH_3 to form CH_3OOH on the Fe_2O_2 dimer is 36 kJ mol^{-1} with the reverse 266 kJ mol^{-1}, which is shown in figure 6.19.

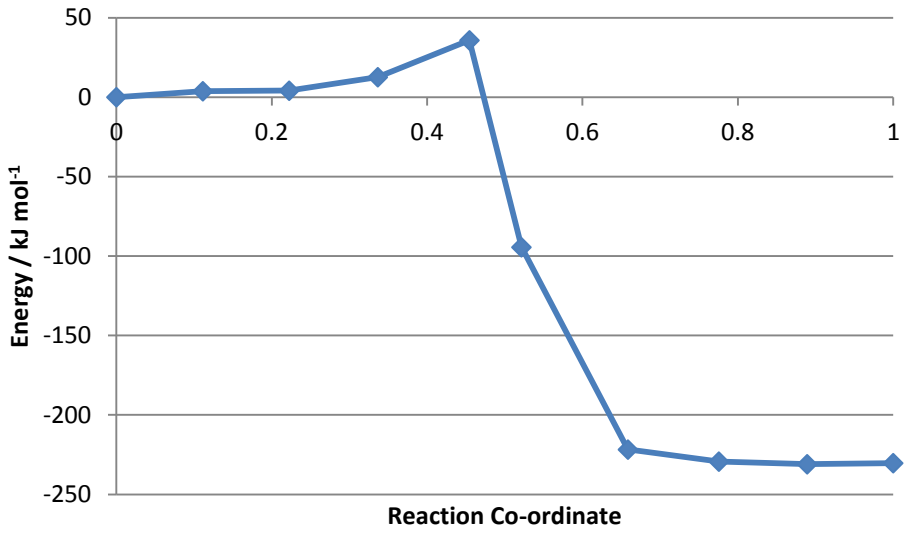

Figure 6.19. Plot of the barrier for formation of a C – O in CH_3OOH form the CH_3 radical.

CH_3OOH

CH_3OOH adsorbs to the Fe_2O_2 extra-framework species but as it is produced from CH_4 and H_2O_2, as shown in the previous section. Two hydrogen atoms remain on the Fe_2O_2 extra-framework species as well, which is shown in figure 6.17. To remove CH_3OOH, a $Fe_2(OH)_2.4H_2O$ extra-framework species which would have the Fe as 2+ ion. The CH_3OOH has a binding energy of -71 kJ mol^{-1} replacing a water, a Fe – O distance of 2.15 Å, a C – O distance of 1.43 Å and an O – O distance of 1.48 Å.

CH_3OH

CH_3OH can formed directly from CH_4 interacting with an extra-framework oxygen atom in Fe_2O_2. This forms CH_3OH by removing one of the extra-framework oxygen atoms, breaking Fe_2O_2 and making Fe_2O, which is shown in figure 6.20. Both the Fe centres in Fe_2O have a formal charge of 2+ due to the loss of the oxygen atom from Fe_2O_2. CH_3OH has a binding energy of -71 kJ mol^{-1} to the Fe_2O extra-framework species and a formation energy of -154 kJ mol^{-1} to form CH_4 and the Fe_2O_2 extra-

framework species. CH_3OH has a Fe – O distance of 2.14 Å and a C – O distance of 1.45 Å.

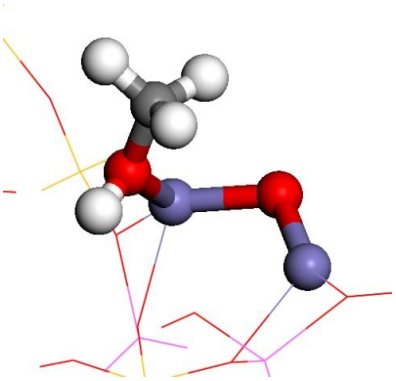

Figure 6.20. CH_3OH on extra-framework Fe_2O_2 formed from CH_4. Si in yellow, O in red, Al in pink, Fe in blue, C in grey and H in white.

CH_3OH can also be formed from the decomposition of CH_3OOH on $Fe_2(OH)_2$ leaving CH_3OH on $Fe_2(OH)_2O$. The extra oxygen atom is bound to a Fe centre and forms a Fe ═ O distance, which is shown in figure 6.21. CH_3OH has a formation energy of -243 kJ mol^{-1} from CH_4 and extra-framework $Fe_2O.OH.OOH$, -373 kJ mol^{-1} with respect to CH_4, H_2O_2 and extra-framework Fe_2O_2 and -111 kJ mol^{-1} with respect to CH_3OOH and extra-framework $Fe_2(OH)_4$. CH_3OH has a Fe – O distance of 2.09 Å, a Fe ═ O distance of 1.64 Å and a C – O distance of 1.49 Å.

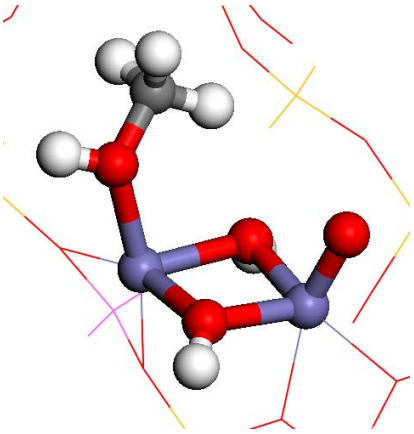

Figure 6.21. CH_3OH on extra-framework Fe_2O_2 formed from the decomposition of CH_3OOH. Si in yellow, O in red, Al in pink, Fe in blue, C in grey and H in white.

H_2O

H_2O can be used to modify the structure of Fe_2O_2. With increasing numbers of water molecules the Fe – Fe distance increases until both Fe centres are octahedral with respect to oxygen ligands. The binding energy and important atomic distances are shown in table 6.5. and images of these are shown in figure 6.22. When more water molecules are added a hydrogen bonding network is formed. Additional sites are used for binding to the Fe_2O_2 dimer with the fourth site not used due to size constraints.

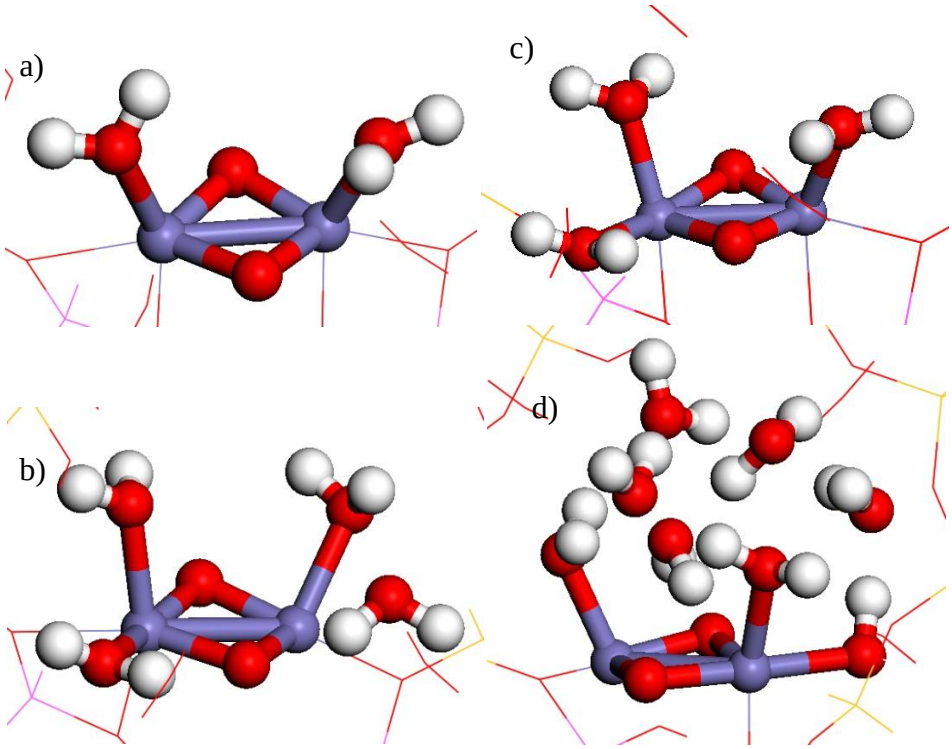

Figure 6.22. Images of increasing number of water molecule a) 2, b) 3, c) 4, and d) 8 on extra-framework Fe_2O_2. Si in yellow, O in red, Al in pink, Fe in blue and H in white.

Hydrogen atoms can be transferred from the water molecules to the extra-framework oxygen atoms. This produces two hydroxyl groups and two water molecules on the Fe centre and two hydroxyls groups bridging between the Fe centres, which is shown in figure 6.23. This has a Fe – Fe distance of 3.18 Å, an average Fe – O_{ef} distance of 2.02 Å, an average Fe - OH distance of 1.82 Å and a Fe – OH_2 distance of 2.15 Å. This has a binding energy of -127 kJ mol^{-1}.

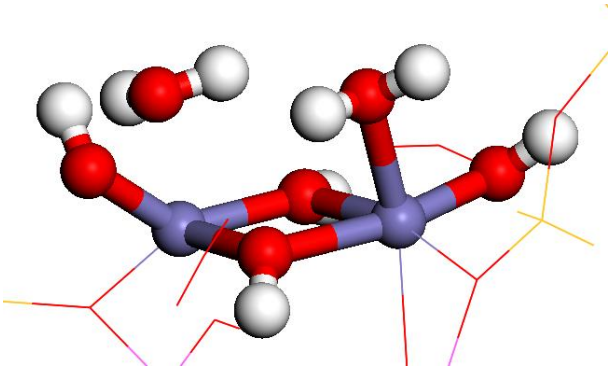

Figure 6.23. An image of two H_2O and two OH on Fe_2O_2. Si in yellow, O in red, Al in pink, Fe in blue and H in white.

Number of water molecules	**Energy / kJ mol^{-1}**	**Fe – Fe distance / Å**	**Fe – O_{ef} distance / Å**	**Fe – OH_2 distance / Å**
2	-99	2.55	1.84	2.10
3	-108	2.61	1.87	2.15
4	-93	2.65	1.87	2.17
8	-140	2.61	1.86	2.10

Table 6.5. Energies and important atomic distances for the structures shown in figure 6.22. and figure 6.23.

The atomic distances can be altered by changing the spin of the electrons on each Fe. The Fe centres are 3+ ions and 5 d orbital electrons with all 5 electrons with parallel spin. Both Fe centres interact and can have parallel spin or anti-parallel spin between the two centres. The parallel spin has a longer Fe – Fe distance, shown in table 6.6. but the average Fe – O is similar, also shown in table 6.6.

Spin	**Energy / kJ mol^{-1}**	**Fe – Fe distance / Å**	**Fe – O_{ef} distance / Å**	**Fe – OH_2 distance / Å**
Parallel	-92	2.71	1.88	2.16
Anti-parallel	-97	2.66	1.87	2.17

Table 6.6. Comparison of energies and important atomic distances for parallel and anti-parallel spin states.

Fe can replace Al in the framework which can change the bond lengths using the same method as stated earlier in this section but the altering of the spin state of Fe centre has a greater effect as there are four and not two Fe centres. The binding energy and important atomic distances are shown in table 6.7. and an image of this is shown in figure 6.24.a). The spins are arranged as a starting point but remain in the same direction after the calculation as all anti-parallel (UDUD), all parallel (UUUU) and the extra-framework Fe parallel and the framework Fe anti-parallel, all with 4 water molecules around the Fe_2O_2

Spin State	**Energy / kJ mol^{-1}**	**Fe – Fe distance / Å**	**Fe – O_{ef} distance / Å**	**Fe – OH_2 distance / Å**
UUUU	-104	2.74	1.90	2.17
UDDU	-106	2.74	1.89	2.20
UDUD	-108	2.70	1.88	2.18

Table 6.7. Comparison of energies and important atomic distances for parallel and anti-parallel spin states.

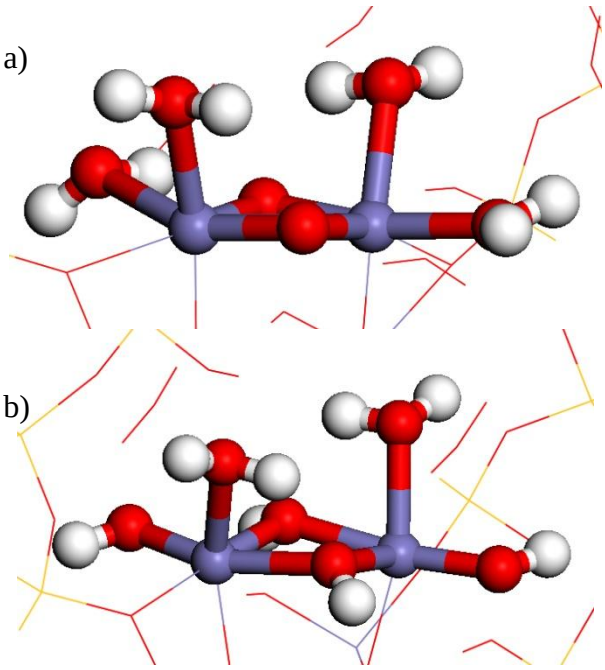

Figure 6.24. Images of a)four water and b) two H_2O and two OH on Fe_2O_2. Si in yellow, O in red, Al in pink, Fe in blue and H in white.

When the addition of water is combined with transferring hydrogen atoms from two of the water molecules to the extra-framework oxygen atom, which is shown in figure 6.24.b) The Fe – Fe in the extra-framework has a distance of 3.19 Å with a binding energy of -155 kJ mol^{-1}.

6.2. MFI structure model

MFI structure

The MFI (Mordenite framework inverted) structure has a unit cell of 20.35 Å × 20.23 Å × 13.60 Å with the lattice parameters minimised to the lowest energy with 1 k-point and with the PBE functional. MFI consists of four co-ordinate Si atoms and two co-ordinate oxygen atoms arranged in a cage structure with linear and sinusoidal channels running through it. The MFI structure has an average Si – O distance of 1.62 Å, and an image of the MFI structure is shown in figure 6.25.

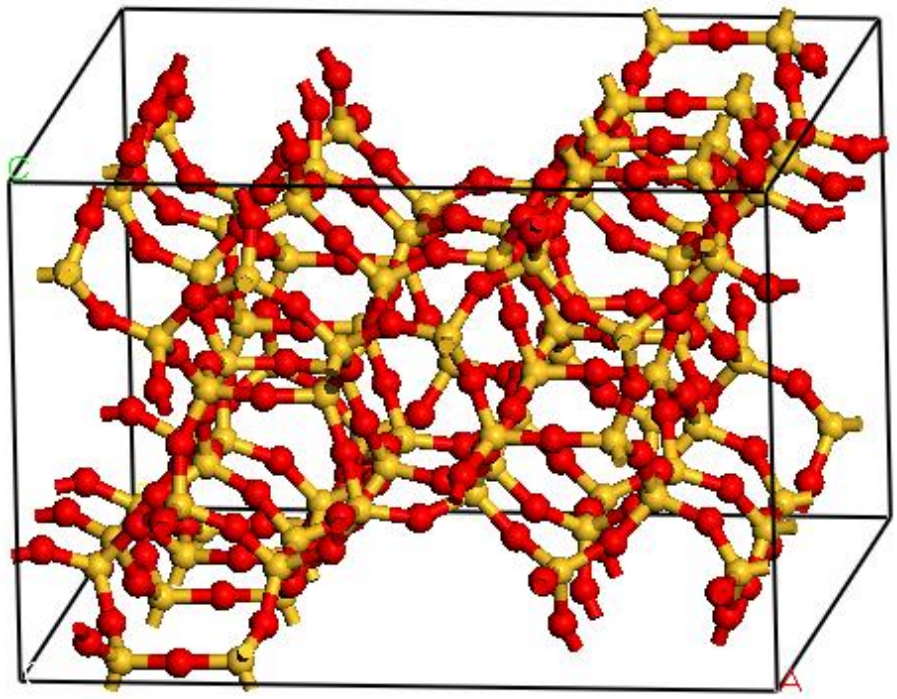

Figure 6.25. An image the MFI unit cell. Si in yellow and O in red.

As with the CHA structure, Si atoms can be replaced with other metal atoms. In this work Fe and Al have been investigated with both having 3+ ions. Two Si atoms are replaced with Al or Fe and two hydrogen atoms placed on adjacent oxygen atoms to the metal atoms in the framework, which is shown in figure 6.26. The Al-MFI structure has an average Si – OH distance of 1.71 Å, an average Al – O distance of 1.72 Å and an average Al – OH distance of 1.87 Å. The Fe-MFI structure has an average Si – OH distance of 1.68 Å, an average Fe – O distance of 1.82 Å and an average Fe – OH distance of 2.01 Å.

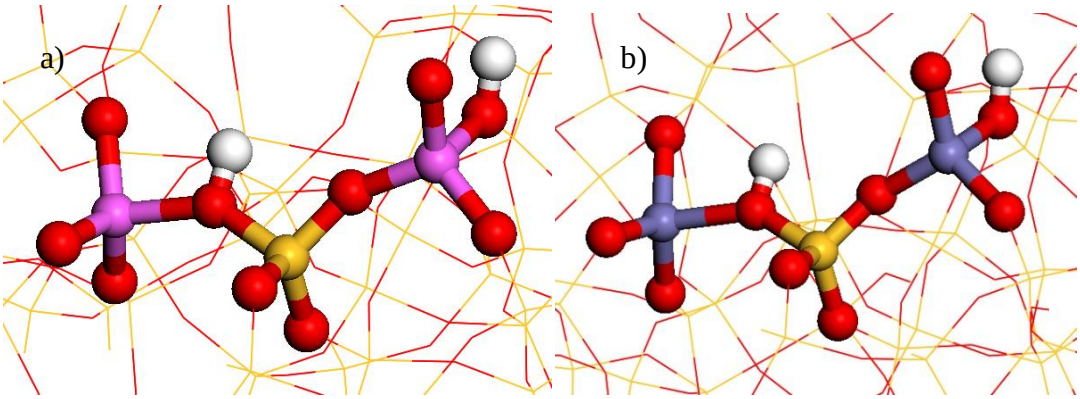

Figure 6.26. Images of a) two Al and b) two Fe replacing framework Si. Si in yellow, O in red, Al in pink, Fe in blue and H in white.

MFI-Fe_2O_2

A $[Fe_2O_2]^{2+}$ structure can be added to the Al-MFI framework in replacement of the two hydrogen atoms as an extra-framework species. As with the CHA structure the removal of the hydrogen atoms produces a 2- charge on the framework which allows a charge compensation between the framework and the Fe_2O_2 extra-framework species, which is shown in figure 6.27. The Fe_2O_2 extra-framework species when bound to the Al-MFI framework has a Fe – Fe distance of 2.46 Å, an average Fe – O_{ef} distance of 1.83 Å, an average Fe – O_f distance of 2.04 Å, an average Al – O_fFe distance of 1.81 Å and an average Al – Fe distance of 2.83 Å. The Fe_2O_2 has the Fe centres with opposite magnetisation to the other centre (4.06 and -4.03). The Al centres can be replaced with Fe to make a Fe-MFI structure as previously described. The Fe_2O_2 structure can bind in the same way to the Fe-MFI as it does the Al-MFI, which is shown in figure 6.27. The Fe_2O_2 extra-framework species when bound to the Fe-MFI framework has a Fe_{ef} – Fe_{ef} distance of 2.45 Å, an average Fe_{ef} – O_{ef}

distance of 1.83 Å, an average $Fe_{ef} - O_f$ distance of 2.01 Å, an average $Fe_f - O_fFe_{ef}$ distance of 1.94 Å and an average $Fe_f - Fe_{ef}$ distance of 2.88 Å.

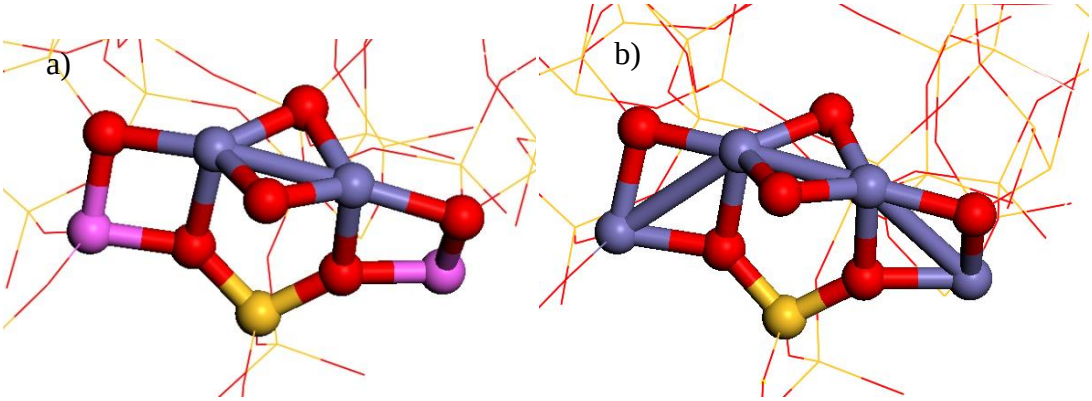

Figure 6.27. Images Fe_2O_2 on a) two Al and b) two Fe. Si in yellow, O in red, Al in pink, Fe in blue and H in white.

As with the CHA structure, the atomic distances for the extra-framework species do not match the experimental EXAFS[6] data from the associated experimental work with work by Battiston *et al*[7,8]. but unlike the CHA structure this cannot be attributed to it being a different structure as the ZSM-5 used has a MFI structure so should match closely if it is the correct extra-framework species. The structure is needed to be modified to match more closely with the EXAFS data and therefore the experimental structure.

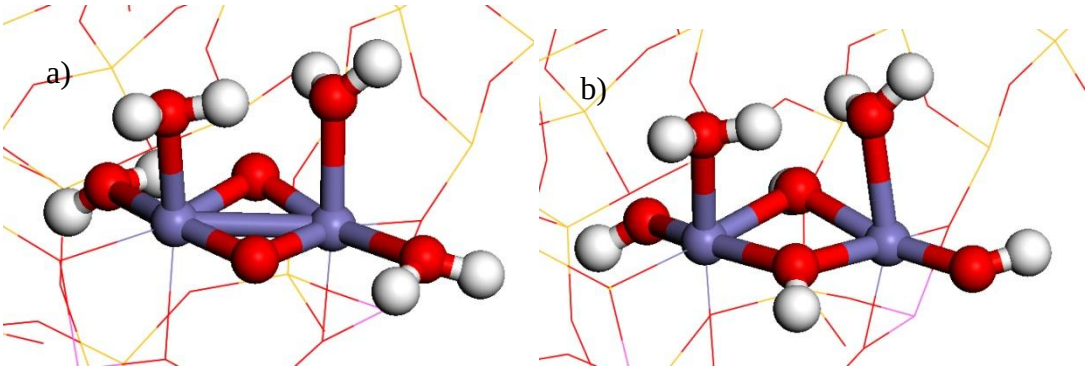

Figure 6.28. Images of a) four water and b) two water and two hydroxyl groups on Fe_2O_2 on Al-MFI. Si in yellow, O in red, Al in pink, Fe in blue and H in white.

Water is added to increase the oxygen atom co-ordination to both Fe centres. Four molecules give the Fe centres the required co-ordination of six, which is shown in

figure 6.28. The four water molecules have a binding energy of -42 kJ mol^{-1}. With the water molecules the Fe_2O_2 extra-framework species has a Fe – Fe distance of 2.58 Å, which is shorter than found experimentally in the EXAFS results at 2.97 Å. The water molecules and the extra-framework Fe_2O_2 have an average Fe – OH_2 distance of 2.18 Å, an average Fe – O_{ef} distance of 1.86 Å and an average Fe – O_f distance of 2.18 Å, which gives an average Fe – O distance of 2.08 Å which is longer than found with the EXAFS results at 2.02 Å but is still close enough to be within error that would be expected.

Two of the water molecules can have a hydrogen atom transferred to the extra-framework oxygen atoms to produce two hydroxyl groups and add a hydrogen atom to each extra-framework oxygen atoms, which is shown in figure 6.28. The water molecules with the hydrogen atoms transferred have a binding energy of -103 kJ mol^{-1}. The system with water molecules with the hydrogen atoms transferred to the Fe_2O_2 extra-framework species has a Fe – Fe distance of 3.08 Å, which is longer than found experimentally in the EXAFS results at 2.97 Å but is still close enough to be within error that would be expected. The water molecules with the hydrogen atoms transferred and the extra-framework Fe_2O_2 have an average Fe – OH_2 distance of 2.19 Å, an average Fe – OH distance of 1.81 Å, an average Fe – O_{ef} distance of 2.02 Å and an average Fe – O_f distance of 2.18 Å, which gives an average Fe – O distance of 2.07 Å which is longer than found with the EXAFS results at 2.02 Å but is still close enough to be within error that would be expected.

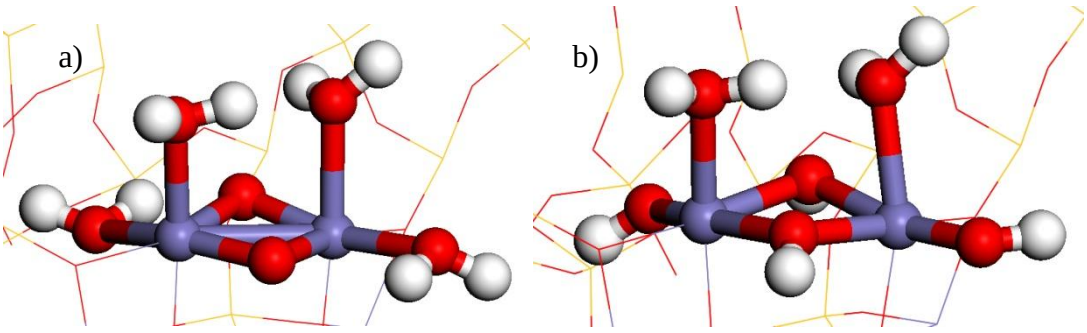

Figure 6.29. Images of a) four water and b) two water and two hydroxyl groups on Fe_2O_2 on Fe-MFI. Si in yellow, O in red, Fe in blue and H in white.

The Fe-MFI with extra-framework Fe_2O_2 can have four water molecules added to it to increase the oxygen atom co-ordination to six, which is shown in figure 6.29. The

four water molecules have a binding energy of -11 kJ mol^{-1} and an average Fe – OH_2 distance of 2.20 Å. The addition of the water molecule increases the Fe_{ef} – Fe_{ef} distance to 2.59 Å and gives an average Fe_{ef} – O_{ef} distance of 1.87 Å and an average Fe_{ef} – O_f distance of 2.14 Å. With the water molecules this gives an average Fe – O distance of 2.07 Å which is the same as with Al added to the framework and can be treated in the same way. The water molecule increases the Fe_{ef} – Fe_f distance to an average of 2.97 Å which gives an average Fe – Fe distance of 2.84 Å. This is shorter than the EXAFS result but could be considered within error, but the low binding energy for the water molecules makes it an unlikely active site.

Two of the water molecules can have a hydrogen atom transferred to the extra-framework oxygen atoms, which is shown in figure 6.29. The water molecules in this form have a binding energy of -90 kJ mol^{-1}. The addition of hydroxyl groups and water molecules alters distances to Fe centres. The Fe_2O_2 extra-framework species has a Fe_{ef} – Fe_{ef} distance of 3.10 Å and an average Fe_{ef} – Fe_f distance of 3.02 Å, which gives an average Fe – Fe distance of 3.05 Å. This is longer than found experimentally in the EXAFS results at 2.97 Å but is still close enough to be within error that would be expected. The addition of the hydroxyl groups and the water molecule also effect the Fe – O distances. The Fe_2O_2 species has an average Fe_{ef} – OH_2 distance of 2.20 Å, an average Fe_{ef} – OH distance of 1.81 Å, an average Fe_{ef} – O_{ef} distance of 2.04 Å and an average Fe_{ef} – O_f distance of 2.15 Å. This give an Fe_{ef} – O distance of 2.06 Å, which is longer than found with the EXAFS results at 2.02 Å but is still close enough to be within error that would be expected.

The $Fe_2(OH)_4.2H_2O$ in the Al-MFI structure was chosen as the active site for further study as it has the higher binding energy for the hydroxyl groups and water molecules and is one the closest matches for the EXAFS results. The same extra-framework species in the Fe-MFI shows only a 13 kJ mol^{-1} less binding energy and has an equally close match to the EXAFS results but the experimental study being performed by the Hutchings group[6] had ZSM-5 producing the best result and as this is an Al containing MFI structure the Al-MFI was chosen.

H_2O_2

H_2O_2 adsorbs to the extra-framework $Fe_2(OH)_4.2H_2O$ by replacing one of the water molecules. The H_2O_2 binds via an oxygen atom to a Fe atom. The binding energies and important atomic distances are shown in table 6.8. and images of these are shown in figure 6.30. The energy differences most likely come from the differences in hydrogen bonding.

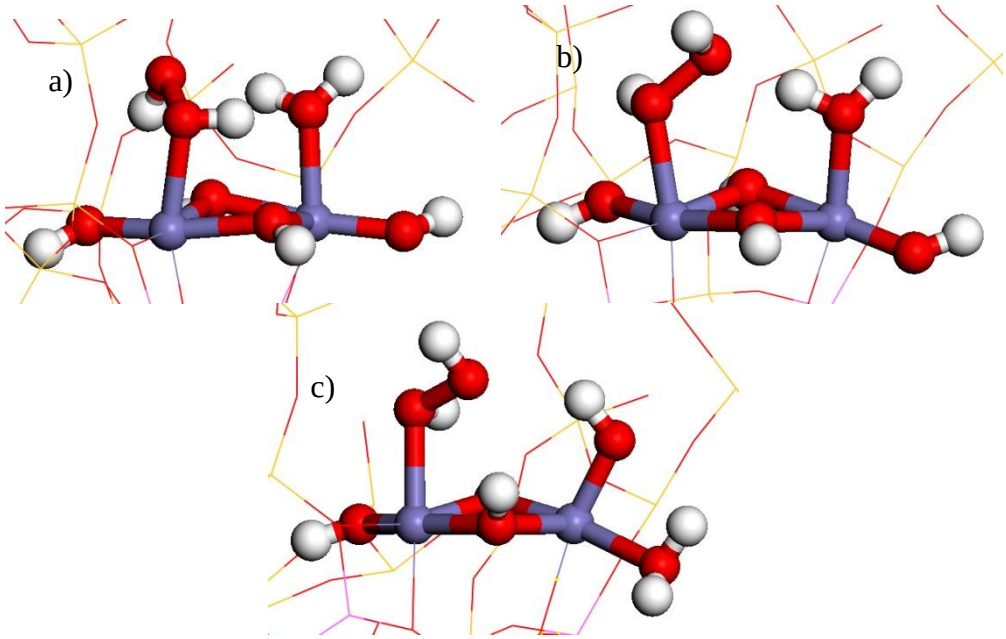

Figure 6.30. Images of H_2O_2 replacing a water molecule on $Fe_2(OH)_4.2H_2O$ in three different positions. Si in yellow, O in red, Al in pink, Fe in blue and H in white.

Structure	**Energy / kJ mol^{-1}**	**Fe – Fe distance / Å**	**Fe – O_{ef} distance / Å**	**Fe – OH distance / Å**	**Fe – OH_2 distance / Å**	**Fe – OOH distance / Å**	**O – O distance / Å**
a	-172	3.09	2.03	1.82	2.17	2.22	1.46
b	-176	3.09	2.00	1.83	2.07	2.22	1.46
c	-168	3.06	2.01	1.83	2.17	2.21	1.45

Table 6.8. Energies and important atomic distances for the structures shown in figure 6.30.

Hydrogen atoms can be transferred around this system to produce several forms, which are shown in figure 6.31. and energies and atomic distances are shown in table 6.9. These primarily produce OOH species on one of the Fe centres with only examples c), d) and g) not having an OOH. A 3+ Fe centre is maintained by having a water molecule on the same Fe centre as the OOH, which is produced by the transfer of a hydrogen atom from H_2O_2 to the hydroxyl group on the same Fe centre, which is seen in a), b) and e). The other way an OOH is seen is with a hydroxyl group on the same Fe centre.

Structure	**Energy / kJ mol^{-1}**	**Fe – Fe distance / Å**	**Fe – O_{ef} distance / Å**	**Fe – OH distance / Å**
a	-221	3.08	1.99	1.81
b	-209	3.02	1.98	1.83
c	17	3.04	1.96	1.83
d	-72	2.95	1.94	n/a
e	-206	2.98	1.99	1.83
f	-87	3.09	1.99	1.82
g	-178	3.05	1.99	1.82
h	-121	2.95	2.00	1.83

Structure	**Fe – OH_2 distance / Å**	**Fe – OOH distance / Å**	**Fe = O distance / Å**	**O – O distance / Å**
a	2.11	1.91	n/a	1.44
b	2.15	1.89	n/a	1.43
c	2.02	n/a	1.63	n/a
d	2.09	n/a	1.64	n/a
e	2.15	1.90	n/a	1.44
f	n/a	n/a	n/a	n/a
g	2.10	1.90	n/a	1.46

h	2.06	1.94	n/a	1.37

Table 6.9. Energies and important atomic distances for the structures shown in figure 6.31.

This form of OOH species is formed by the transfer of a hydrogen atom between two Fe centres from H_2O_2 to a hydroxyl group on the other Fe centre, which is shown in g) and h). This produces a formal charge of 4+ on one Fe centre and a formal charge of 2+ on the other Fe centre. A Fe centre with two hydroxyl groups can be produced by the transfer of a hydrogen atom from a water molecule to the H_2O_2 cleaving the HO – OH bond and making a water molecule. Both Fe centres have a 4+ formal charges and are shown in c) and f). A Fe ═ O can be produced when two hydroxyl group are present on the same Fe centre from the transfer of a hydrogen atom from a hydroxyl group to the other hydroxyl group. This causes no change in charge as it all occurs on one Fe centre. Fe ═ O occur in c) and d). Energies are for the binding of H_2O_2 and the removal of a water molecule.

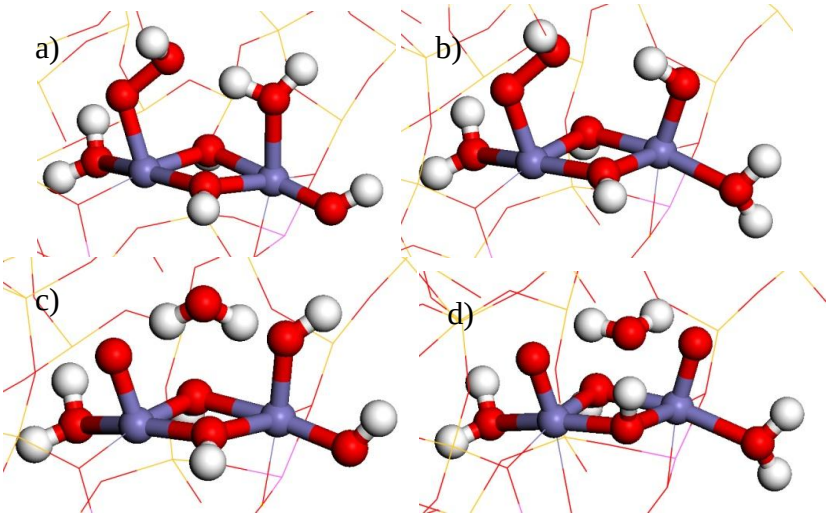

e)

f)

g)

h)

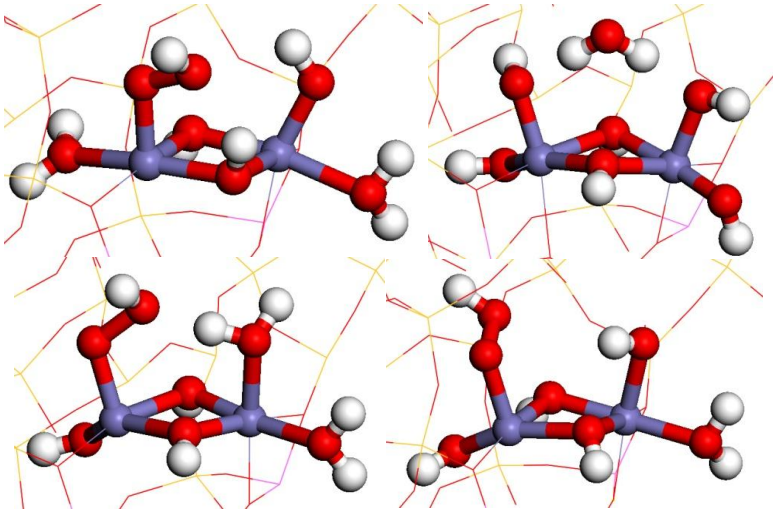

Figure 6.31. Images of OOH and H replacing water on $Fe_2(OH)_4.2H_2O$ in three different positions. Si in yellow, O in red, Al in pink, Fe in blue and H in white.

The strongest adsorption are shown with the OOH species with a hydroxyl group on the other Fe centre which reduces when the hydroxyl group is transferred to the same Fe centre but the energy still remains favourable. The loss of a water molecule from the system gives an unfavourable binding energy which is reduced further with the formation of each Fe ═ O. The magnetisation of each Fe centre shows little change until a Fe ═ O is formed meaning that the charge is shared equally between the Fe centres suggesting delocalisation of the electrons in the Fe_2O_2 with the Fe ═ O preventing this and a Fe centre with two hydroxyl groups to a lesser extent.

The barrier for the transfer of a hydrogen atom from H_2O_2 to a hydroxyl group on the same Fe centre is 21 kJ mol^{-1} with the reverse 61 kJ mol^{-1}, which is shown in figure 6.32.

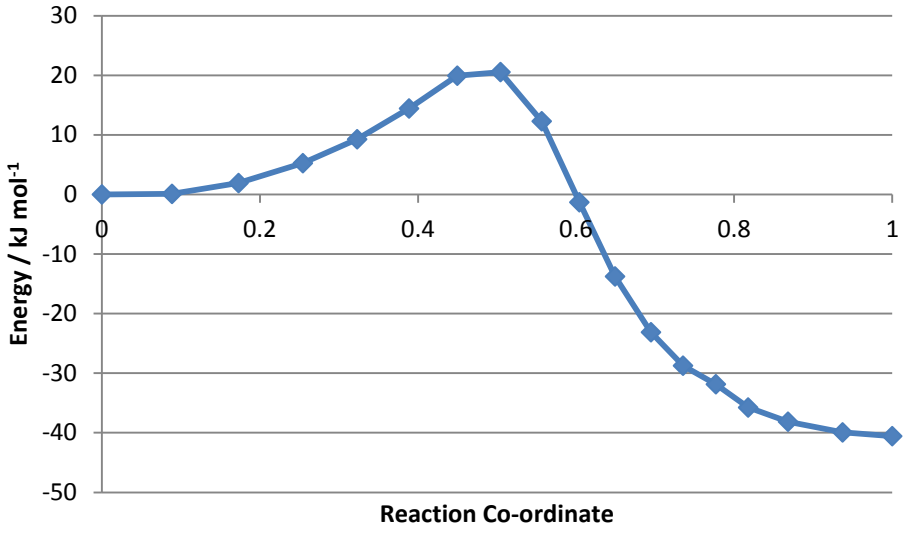

Figure 6.32. Plot of the barrier transfer of a hydrogen atom from H_2O_2 to a hydroxyl group on Fe_2O_2.

A second H_2O_2 can replace a second water molecule to give a $Fe_2(OH)_4.2H_2O_2$, which is shown in figure 6.33.a) The H_2O_2 has a binding energy of -57 kJ mol^{-1} to replace a water molecule in the extra-framework $Fe_2(OH)_4.H_2O_2.H_2O$ and a binding energy of -109 kJ mol^{-1} to replace two water molecules with H_2O_2 on the extra-framework $Fe_2(OH)_4.2H_2O$. The H_2O_2 has Fe – O distances of 2.14 Å and 2.24 Å, two HO – OH distances of 1.46 Å and the extra-framework Fe_2O_2 has a Fe – Fe distance of 3.07 Å.

Two hydrogen atoms can be transferred to hydroxyl groups on the Fe centres, one hydrogen atom to each creating a water molecule and an OOH, which is shown in figure 6.33.b). The OOH has a binding energy of -169 kJ mol^{-1}, Fe – OOH distances of 1.87 Å and 1.90 Å, O – O distances of 1.42 Å and 1.43 Å in the OOH species and a Fe – Fe distance of 3.00 Å.

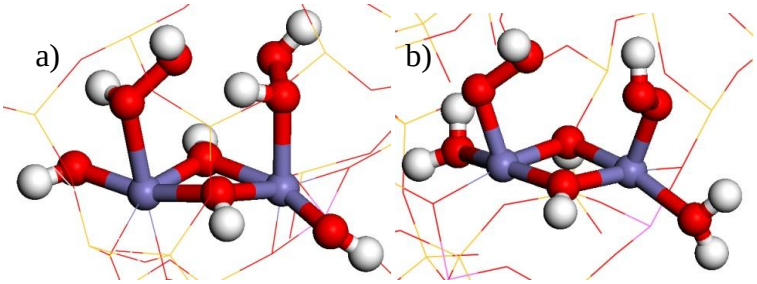

Figure 6.33. Images of a) two H_2O_2 and b) two OOH and two H on $Fe(OH)_4$ replacing two water molecules. Si in yellow, O in red, Al in pink, Fe in blue and H in white.

The two H_2O_2 can also have a hydrogen atom transferred between them resulting in two hydroxyl groups on one Fe centre and a hydroxyl group and an OOH on the other Fe centre and the loss of a water molecule, which is shown in figure 6.34.a) This system has a binding energy of -88 kJ mol^{-1} without the water molecule and -109 kJ mol^{-1} with the water molecule. The improved binding with the water molecule can be attributed to hydrogen bonding. The OOH formed has a Fe – OOH distance of 2.01 Å and an O – O distance of 1.36 Å.

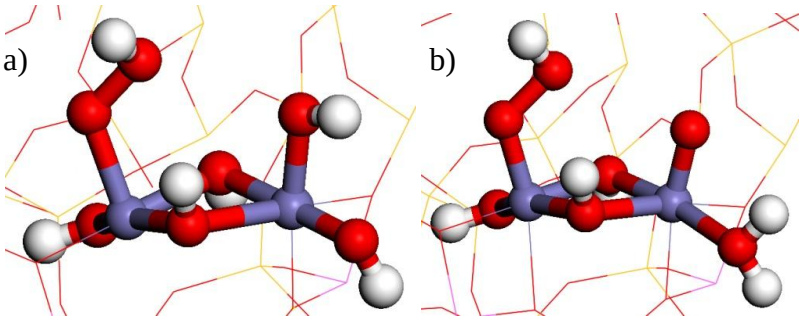

Figure 6.34. Images of a) $Fe_2(OH)_5$.OOH and b) $Fe_2(OH)_3$.OOH.O.H_2O. Si in yellow, O in red, Al in pink, Fe in blue and H in white.

Once the $Fe_2(OH)_5$.OOH has formed a hydrogen atom can be transferred from a hydroxyl group to another hydroxyl group to produce a water molecule and Fe ═ O species on one of the Fe centres, which is shown in figure 6.34.b). This has a binding energy of -28 kJ mol^{-1}. The OOH species has a Fe – OOH distance of 1.78 Å and an O – O distance of 1.40 Å. The Fe_2O_2 species has a Fe – Fe distance of 2.98 Å and a Fe ═ O distance of 1.63 Å. As the binding is negative it is highly likely that this structure exists as it is still more favourable than water binding to the $Fe_2(OH)_4$.

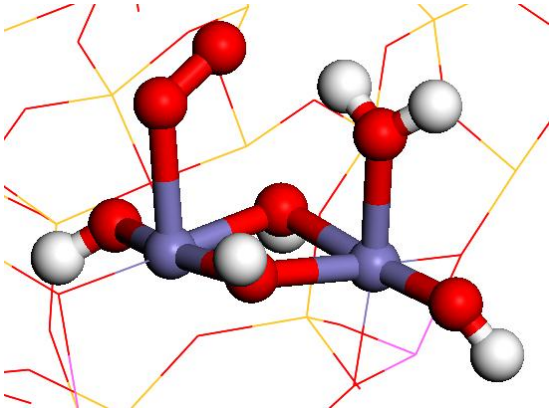

Figure 6.35. An image of $Fe_2(OH)_4.O_2.H_2O$. Si in yellow, O in red, Al in pink, Fe in blue and H in white.

Using the $Fe_2(OH)_5.OOH$ again a hydrogen atom can be transferred from the OOH to a hydroxyl group on the other Fe centre producing an O_2 and water molecule, which is shown in figure 6.35. This has a binding energy of -252 kJ mol^{-1} with respect to the addition of two H_2O_2 and replacing two water molecules from the active site based on EXAFS results and a binding energy of 47 kJ mol^{-1} with O_2 replacing water on the active site, which indicates that water would replace the O_2 once it is formed returning it to the stable active site. This structure has a Fe – O_2 distance of 2.29 Å, an O – O distance of 1.24 Å and a Fe – Fe distance of 3.04 Å.

CH_4

CH_4 does not interact with the extra-framework $Fe_2(OH)_3.OOH.2H_2O$, which is shown in figure 6.36.a) The CH_4 with the hydroxyl group on the other Fe centre to the OOH which is shown in figure 6.36.b) has a binding energy of 5 kJ mol^{-1}, CH_4 has a binding energy of 2 kJ mol^{-1} with hydroxyl group on the same Fe centre as the OOH. The shortest C – O distance is 3.25 Å in the first case and 3.40 Å in the second case. CH_4 moved in between the OOH and hydroxyl group increases the binding energy for the CH_4 to 64 kJ mol^{-1} with a C – OOH distance of 2.97 Å and a C – OH distance of 3.17 Å, which is shown in figure 6.36.c). In this last case the hydroxyl group and OOH move apart to give the CH_4 space. The lack of dispersion in DFT may account for the non-existant binding energies. CH_4 does not interact with the extra-framework $Fe_2(OH)_3.OOH.O.H_2O$, which is shown in figure 6.36.d) The CH_4 has a binding energy of 9 kJ mol^{-1} but has a shortest C – O distance of 3.03 Å.

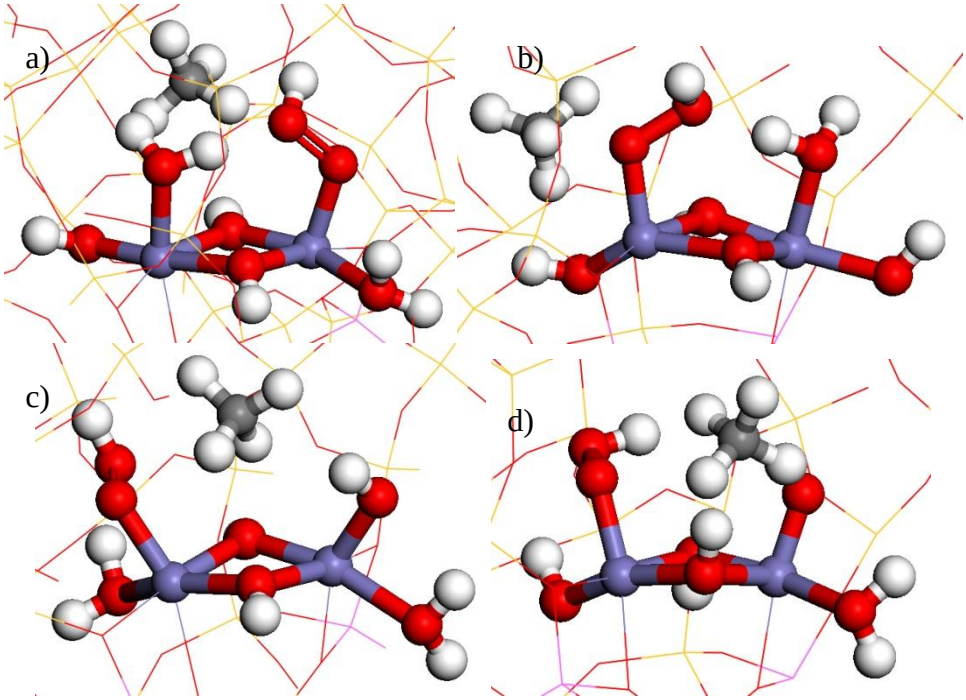

Figure 6.36. Images of CH_4 on a), b) and c) $Fe_2(OH)_5.OOH$ and d) $Fe_2(OH)_3.OOH.O.H_2O$. Si in yellow, O in red, Al in pink, Fe in blue, C in grey and H in white.

In the CHA structure radical methyl groups are produced so in the MFI structure a hydrogen atom was transferred the $Fe_2(OH)_3.OOH.2H_2O$ on to one of the terminal hydroxyl groups, which is shown in figure 6.37. The methyl and the hydrogen atom have binding energies of 104 kJ mol^{-1} and 214 kJ mol^{-1} for a) and b) respectively. These both are planar and have long C – O distances of 3.45 Å and 2.99 Å to the nearest oxygen atom with C – H distances to a hydrogen atom attached to this oxygen atom of 2.68 Å and 2.10 Å respectively. The Fe centre that the hydrogen atom transfers to changes to a 2+ formal charge. With this result it is clear in the MFI structure that free radical methyl is unfavourable and therefore unlikely.

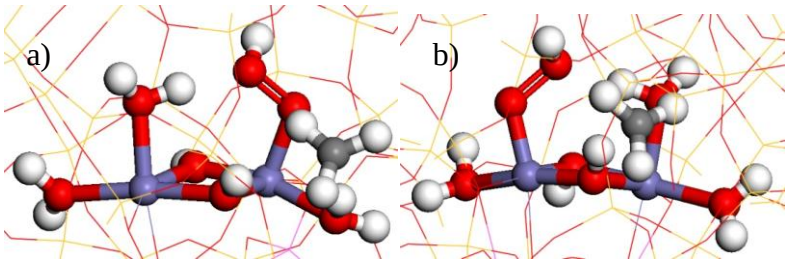

Figure 6.37. Images of CH_3 on $Fe_2(OH)_5.OOH$. Si in yellow, O in red, Al in pink, Fe in blue, C in grey and H in white.

CH_3OOH

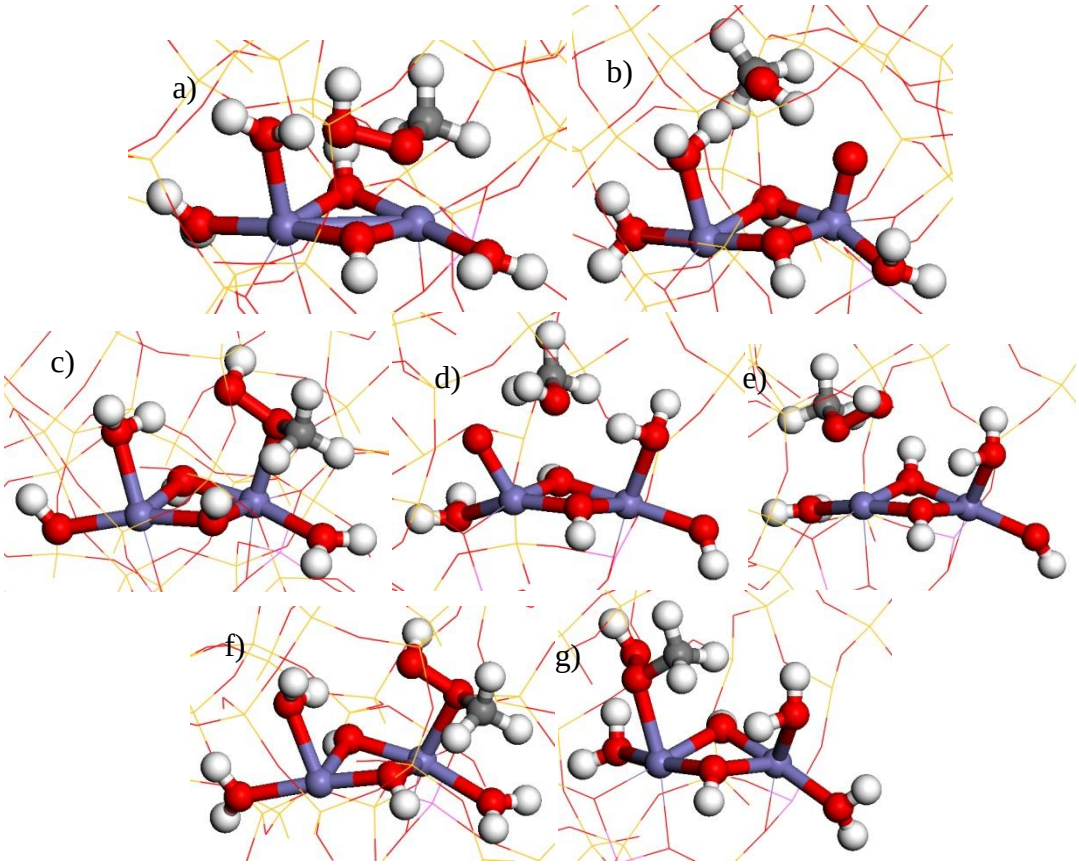

Figure 6.38. Images of CH_3OOH replacing water on $Fe_2(OH)_2.4H_2O$ in three different positions. Si in yellow, O in red, Al in pink, Fe in blue, C in grey and H in white.

CH_3OOH is formed from CH_3 and OOH and the CH_3OOH adsorbs to one the Fe centres in $Fe_2(OH)_2.4H_2O$ replacing a water molecule, which is shown in figure 6.38. and binding energies and important atomic distances are shown in table 6.10. The example labelled a) shows an unfavourable binding energy. This is due to the methyl section of the CH_3OOH being closest to the Fe centre so the oxygen atoms cannot interact. The lack of interaction with a) is also shown in the Fe – Fe distance being significantly shorter than the other cases, b) also shows this to a lesser extent. All cases show favourable formation energies from CH_4 and H_2O_2 on $Fe_2(OH)_4.2H_2O$ so would be expected to occur depending on the barrier of formation.

Structure	**Energy / kJ mol^{-1}**	**Fe – Fe distance / Å**	**Fe – O_{ef} distance / Å**	**Fe – OH_2 distance / Å**

a	-73	2.88	2.03	2.18
b	-33	2.96	1.95	2.07
c	-168	2.97	2.04	2.15
d	-128	3.07	2.02	2.17
e	-191	3.01	2.05	2.16
f	-184	2.96	2.04	2.17
g	-192	3.03	2.06	2.16

Structure	**Fe – O(CH_3)OH distance / Å**	**O – O distance / Å**	**Fe ═ O distance / Å**	**C – O distance / Å**
a	3.39	1.46	n/a	1.41
b	n/a	n/a	1.64	1.44
c	2.25	1.48	n/a	1.44
d	n/a	n/a	1.87	1.43
e	2.31	1.48	n/a	1.44
f	2.29	1.48	n/a	1.44
g	2.28	1.48	n/a	1.44

Table 6.10. Energies and important atomic distances for the structures shown in figure 6.38.

CH_3OOH adsorbs to $Fe_2(OH)_4.2H_2O$ over a Fe centre replacing a water molecule, which is shown in figure 6.39. CH_3OOH has a binding energies of -14 kJ mol^{-1} and -25 kJ mol^{-1} in a) and b) respectively. The Fe – Fe distance is 3.14 Å for a) and 3.09 Å for b).

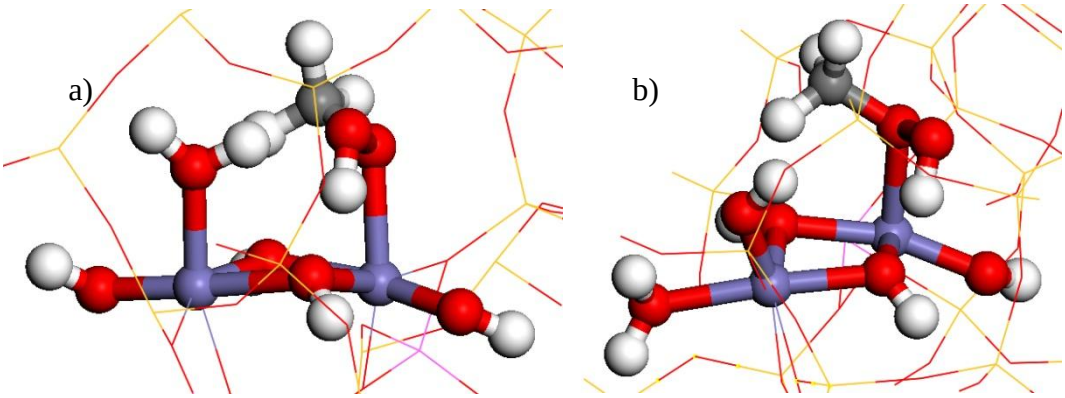

Figure 6.39. Images of CH_3OOH on $Fe_2(OH)_4.2H_2O$. Si in yellow, O in red, Al in pink, Fe in blue, C in grey and H in white.

CH_3OH

CH_3OH has no interaction with $Fe_2(OH)_4.2H_2O$ over a Fe centre replacing a water molecule, which is shown in figure 6.40.a) CH_3OH has a binding energy of 0 kJ mol^{-1}, a Fe – O distance of 2.19 Å, a C – O distance of 1.46 Å and a Fe – Fe distance of 3.09 Å.

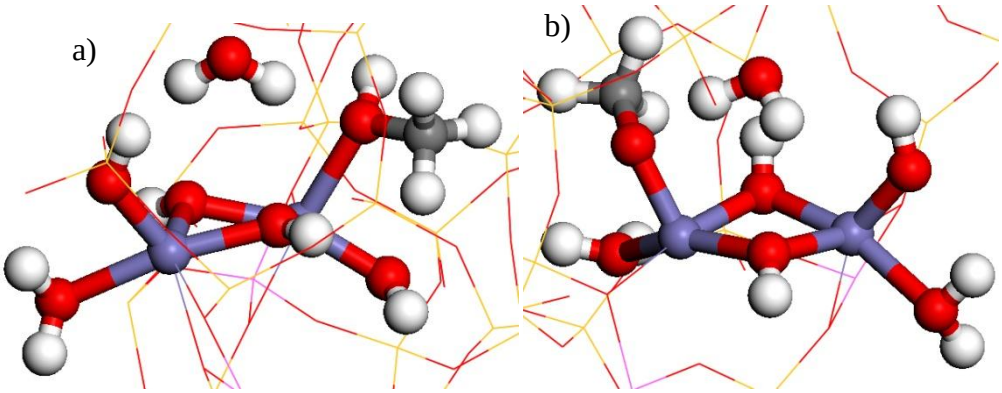

Figure 6.40. Images of CH_3OH on $Fe_2(OH)_4.2H_2O$, a) CH_3OH and b) CH_3O and H. Si in yellow, O in red, Al in pink, Fe in blue, C in grey and H in white.

CH_3OH can be formed from the decomposition of CH_3OOH via a methoxy group and the production of a water molecule. This is done by the cleavage of the O – O bond in CH_3OOH and the transfer of a hydrogen atom for a water molecule on the other Fe centre. The CH_3O and hydrogen atom bound to $Fe_2(OH)_4.2H_2O$ are shown

in figure 6.40.b) The CH_3O and a hydrogen atom have a binding energy of -26 kJ mol^{-1}, a Fe – O distance of 1.86 Å, a C – O distance of 1.42 Å and a Fe – Fe distance of 3.06 Å.

C – H bond cleavage

To produce CH_3OOH and CH_3OH, a C – H bond in CH_4 needs to be broken but the methyl has no position other than the OOH to bind to and the planar form is unfavourable. This would indicate that the path must go through a single transition state with the C – H bond breaking as the C – O to the OOH is forming. On $Fe_2(OH)_3.OOH.2H_2O$ there are very large barriers requiring 286 kJ mol^{-1} to cleave the C – H bond and form CH_3OOH, which is shown in figure 6.41. The C – H distance change from 1.14 Å to 2.05 Å and the O – H distance for the receiving oxygen atom changes from 1.66 Å to 0.98 Å, and images of this are shown in figure 6.42.

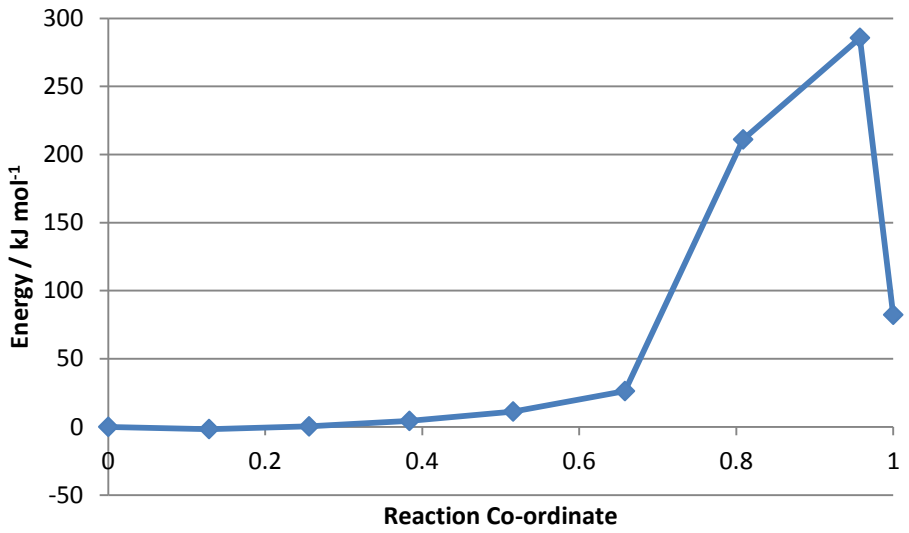

Figure 6.41. Plot of the barrier to break the CH_4, C – H bond and form CH_3OOH.

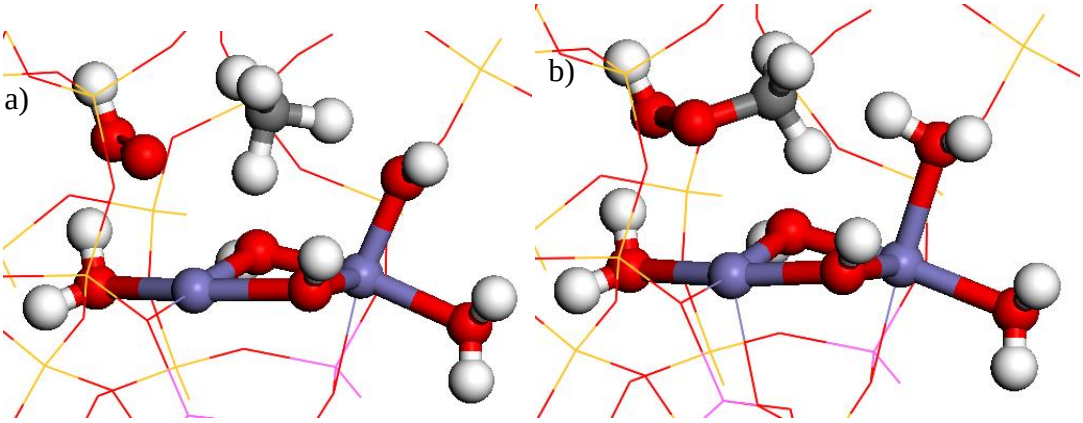

Figure 6.42. Images of a) C – H bond breaking and b) high point of the barrier in figure 6.41. Si in yellow, O in red, Al in pink, Fe in blue, C in grey and H in white.

The $Fe_2(OH)_3.OOH.O.H_2O$ has two Fe^{4+} centre with one Fe ═ O so it should be more strongly oxidising and therefore be able to remove the hydrogen atom and act as a counter charge to the methyl. The barrier for C – H bond cleavage and CH_3OOH formation is 26 kJ mol^{-1} with the reverse 388 kJ mol^{-1}, which is shown in figure 6.43. However in this barrier the C – H distance changes from 1.09 Å to 1.98 Å with the O – H distance for the receiving oxygen atom changing from 1.83 Å to 0.99 Å, and images of this are shown in figure 6.44. This would indicate that the barrier must be low for C – H bond cleavage but the NEB method has missed the transition state for the C – H bond cleavage. Image b) of figure 6.44. shows the formation of a CH_3 but this forms CH_3OOH with a geometry optimisation so there no barrier is between these species.

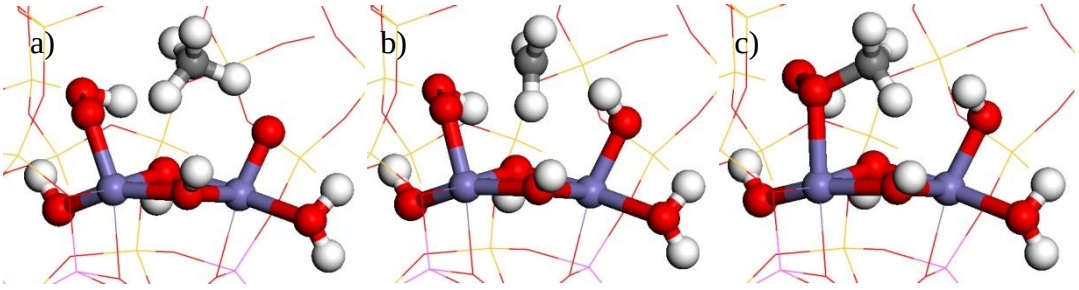

Figure 6.44. Images of a) C – H bond breaking, b) high point and c) CH_3OOH formation of the barrier in figure 6.43. Si in yellow, O in red, Al in pink, Fe in blue, C in grey and H in white.

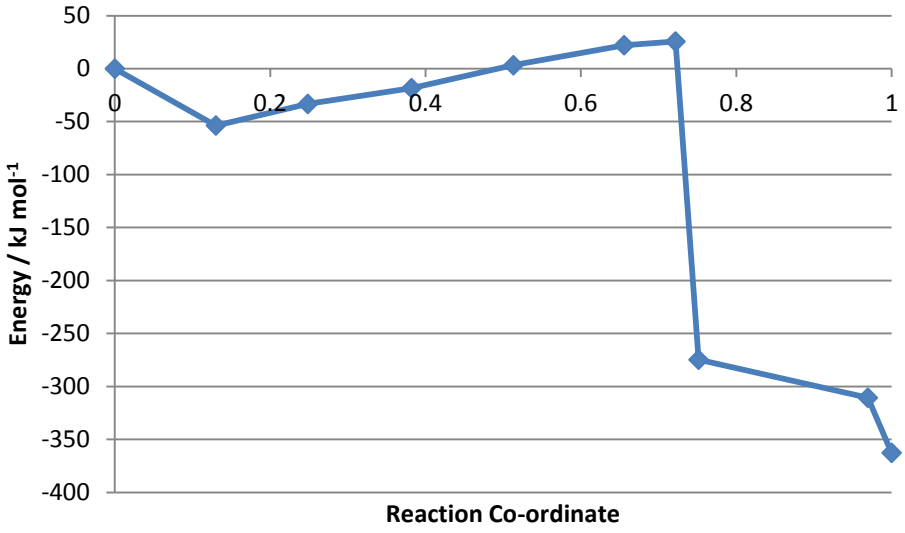

Figure 6.43. Plot of the barrier to break the CH_4, C – H bond and form CH_3OOH.

The CH_4 shows a bond stretch in the step preceding the C – H bond cleavage in that bond. One of the stretches at 2947 cm^{-1} shows a C – H bond stretch towards the Fe = O. By following the eigenvector the transfer of the hydrogen atom to the Fe = O can be investigated with a series of structures along the eigenvector, these can be geometry minimised with the C – H distance fixed. This gives a barrier of 94 kJ mol^{-1} however this shows small fluctuations in magnetisation of the C and H atoms involved in the C – H bond. The magnetisation can be set and optimised with the value set at the number of up spin minus the number of down spin with the default value of 0. For this investigation 1 and -1 were used on the carbon atom and the hydrogen atom. The plot in figure 6.45. shows how these affect the barrier.

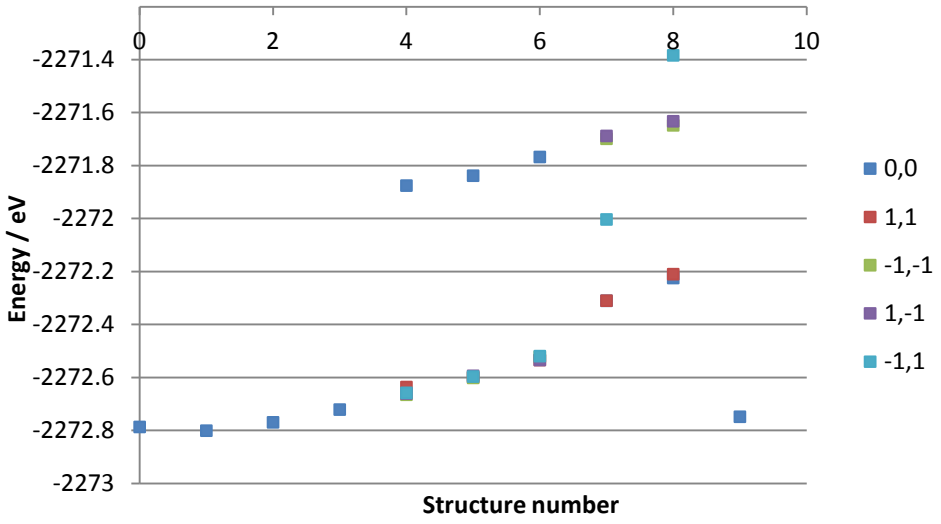

Figure 6.45. Plot of C – H stretch and cleavage at different spin states on C and H with the (a,b) representing the starting magnetisation set with the MAGMOM tag.

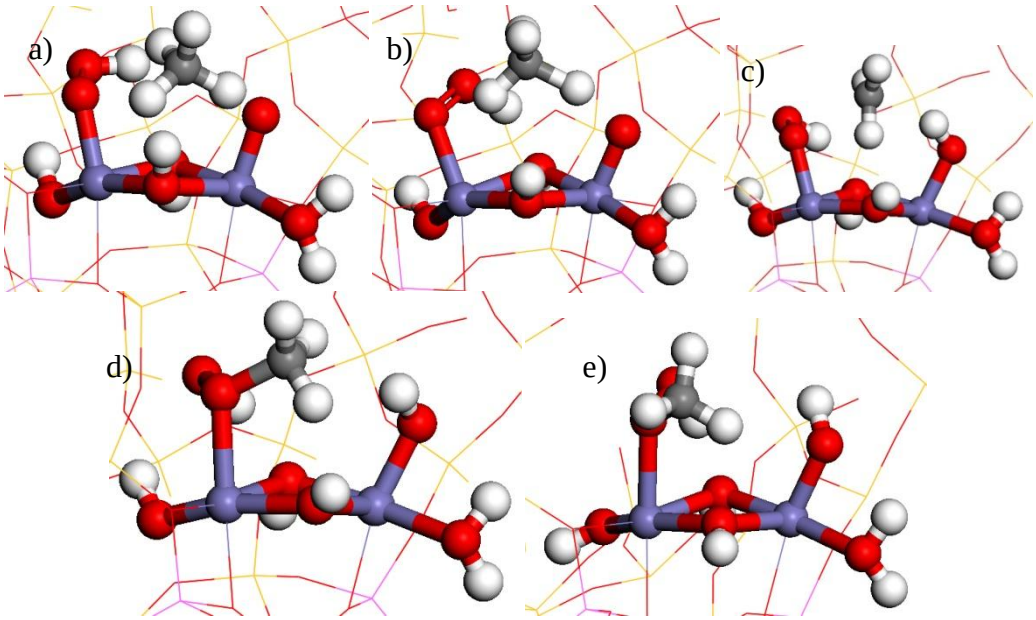

Figure 6.46. Images of different structures from the barrier in figure 6.47. a) 2, b) 14, c) 16, d) 17 and e) 19. Si in yellow, O in red, Al in pink, Fe in blue, C in grey and H in white.

This changes the structure at the transition state by creating a lower energy pathway and reducing the barrier to 50 kJ mol^{-1}, and the transition states are shown in figure 6.46. The plot with the original barrier is shown in figure 6.47. The atomic distances show the C – H distance steadily increasing until the transition state and then rapidly increasing after. At the same time the O – H bond forms and the CH_3 moves across

to form the C – O bond. The CH_3 can be considered a radical because the carbon atom has a magnetisation of -0.32 e, and it is a planar species. It would most likely not be seen as it is not a stable intermediate and would form CH_3OOH rapidly. The methyl radical can be consider trapped in the active site system and can only leave it as CH_4 and CH_3OOH.

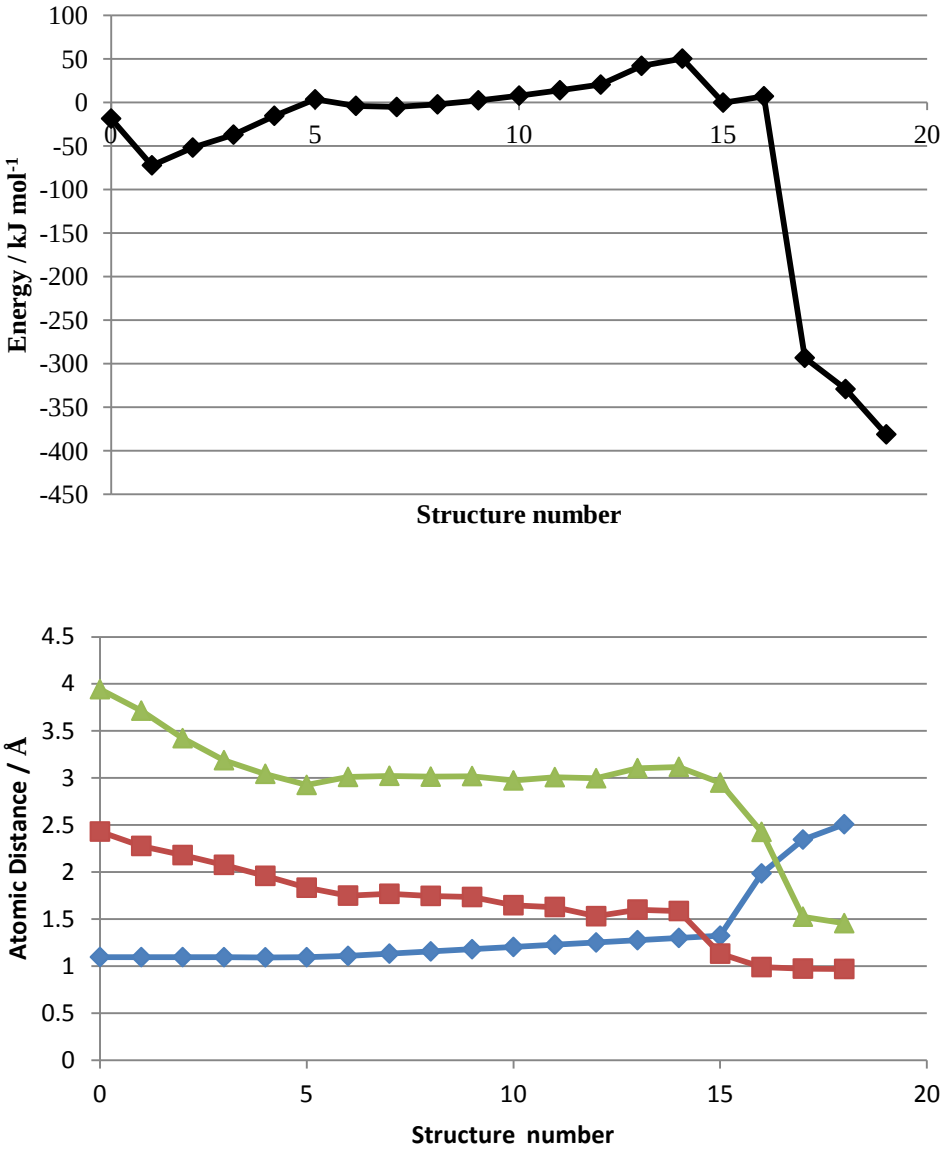

Figure 6.47. Final plot of the barrier to break the CH_4, C – H bond and form CH_3OOH. a) Energy against structure number and b) bond distances for C – OOH (green triangles), H – OFe (red squares) and C – H (blue diamonds) against structure number.

DOS plots can be used to show how the bands changing for different structures on the reaction co-ordinate and which bands are having electrons donated to them and which are losing electrons, which is shown in Figures 6.48 – 6.52. Each of the points represents the corresponding structure number in Figure 6.47. This also shows the spin changing direction clearly on the adjacent atoms. All DOS plots are shown between -10 and 5 with arbitrary units.

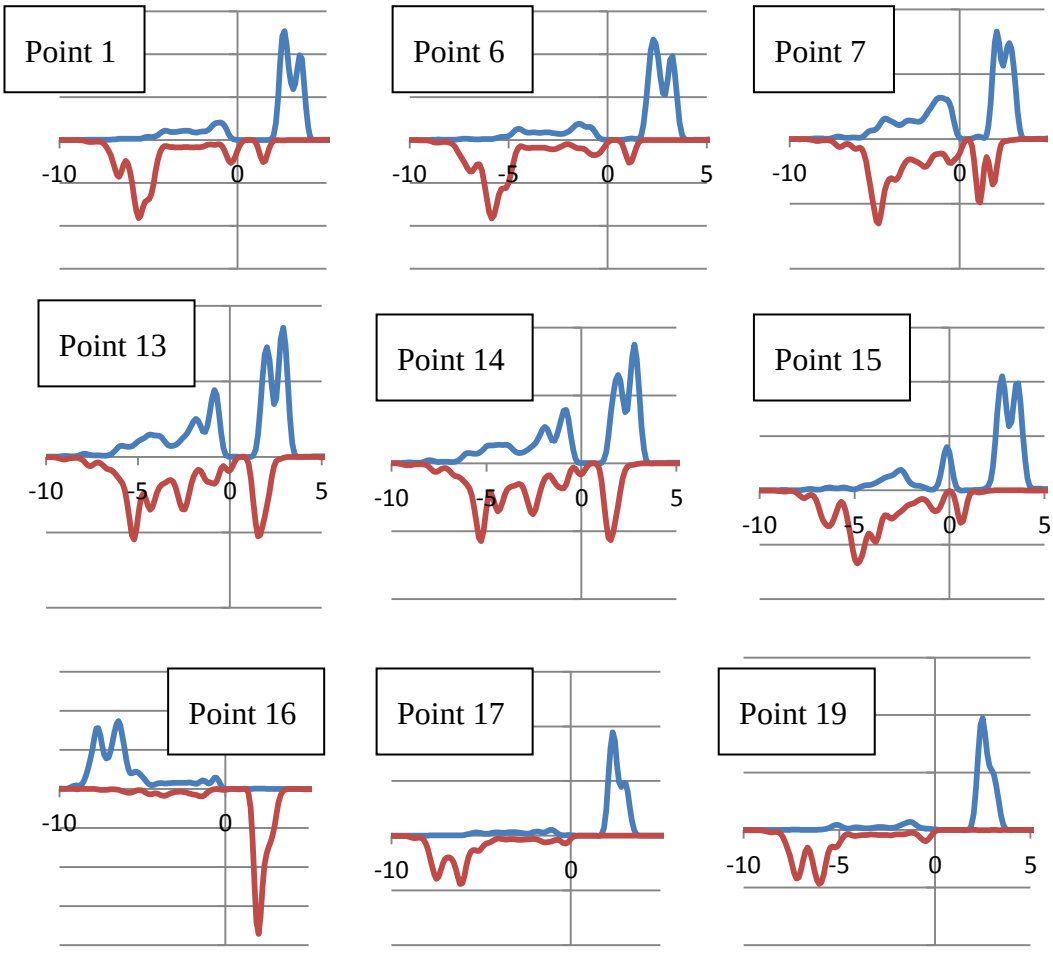

Figure 6.48. DOS of Fe centre d orbitals in Fe=O viewed over reaction co-ordinate of the reaction of between methane and the Fe-MFI active site to form methyl-hydroperoxide.

Figure 6.48 shows that in the Fe centre d orbitals in Fe=O, a move toward the Fermi level is seen and a decrease of the band gap until Point 15. This would be associated with the C-H bond cleavage and O-H bond formation. After this, the spin inversions occurring are mostly likely associated with the formation of the C-O bond.

Figure 6.49 shows that in the O centre s and p orbitals in Fe=O, an increased number of states move towards the Fermi level with a decreasing band gap until Point 16. Once the O-H bond is formed the states move back and the band gap increases again with the first spin inversion occurring between point 14 and 15. The second spin inversion occurring is mostly likely associated with the formation of the C-O bond.

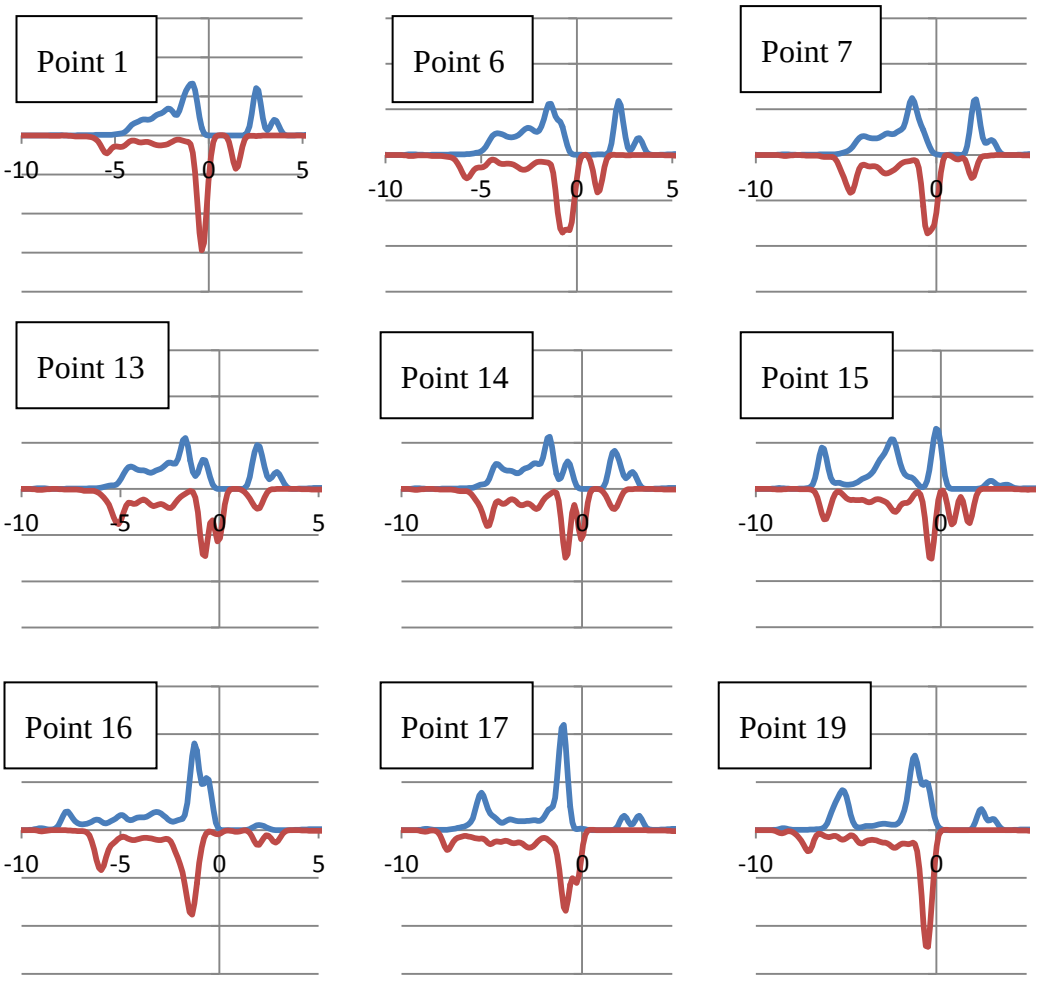

Figure 6.49. DOS of O centre s and p orbitals in Fe=O viewed over reaction co-ordinate of the reaction of between methane and the Fe-MFI active site to form methyl-hydroperoxide.

Figure 6.50 that shows in Fe centre d orbitals in Fe-O-OH, the first few points show the transfer of electrons between the up and down with the unoccupied up spin state shifting down and the down spin occupied state shifting up. This continues until Point 15, the point after the C-H bond cleavage, when the up and down spin states become equally occupied. This is followed by the same effect again with all the up spin states occupied and down states unoccupied with the loss of the band gap in Point 16. This is associated with the methyl moving between the two oxygen atoms. Point 17 and 19 have the mostly full up spin and mostly empty down spin. This change is due to the formation of the C-O bond with the attached oxygen atom.

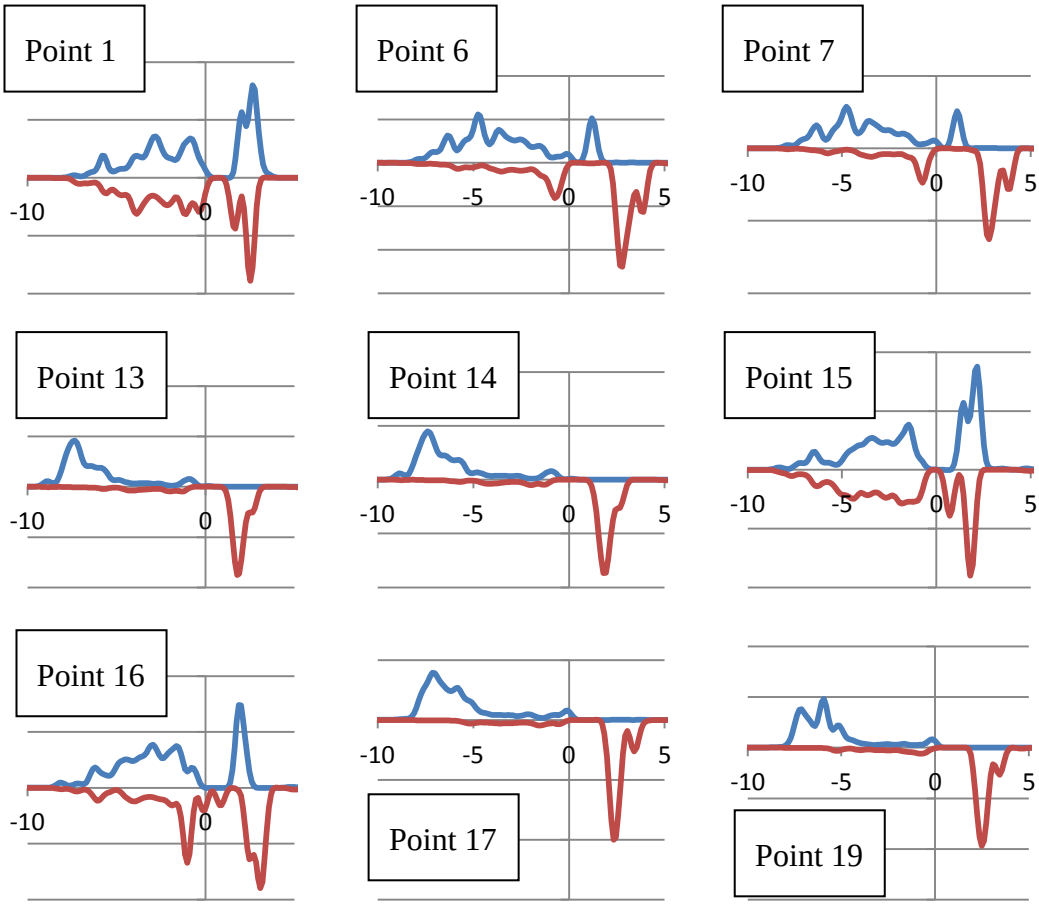

Figure 6.50. DOS of Fe centre d orbitals in Fe-O-OH viewed over reaction co-ordinate of the reaction of between methane and the Fe-MFI active site to form methyl-hydroperoxide.

Figure 6.51. shows that in the O centre s and p orbitals in Fe-O-OH, the main effect is the shift of the up spin states, shown in the first peak after the Fermi level shifting toward it and merging with the one at the Fermi level. In Point 15 this peak at the Fermi level disappears due to the formation of the O-H from the cleavage of the C-H in methane on the other oxygen atom. Other low lying unoccupied states disappear with the formation of the C-O bond.

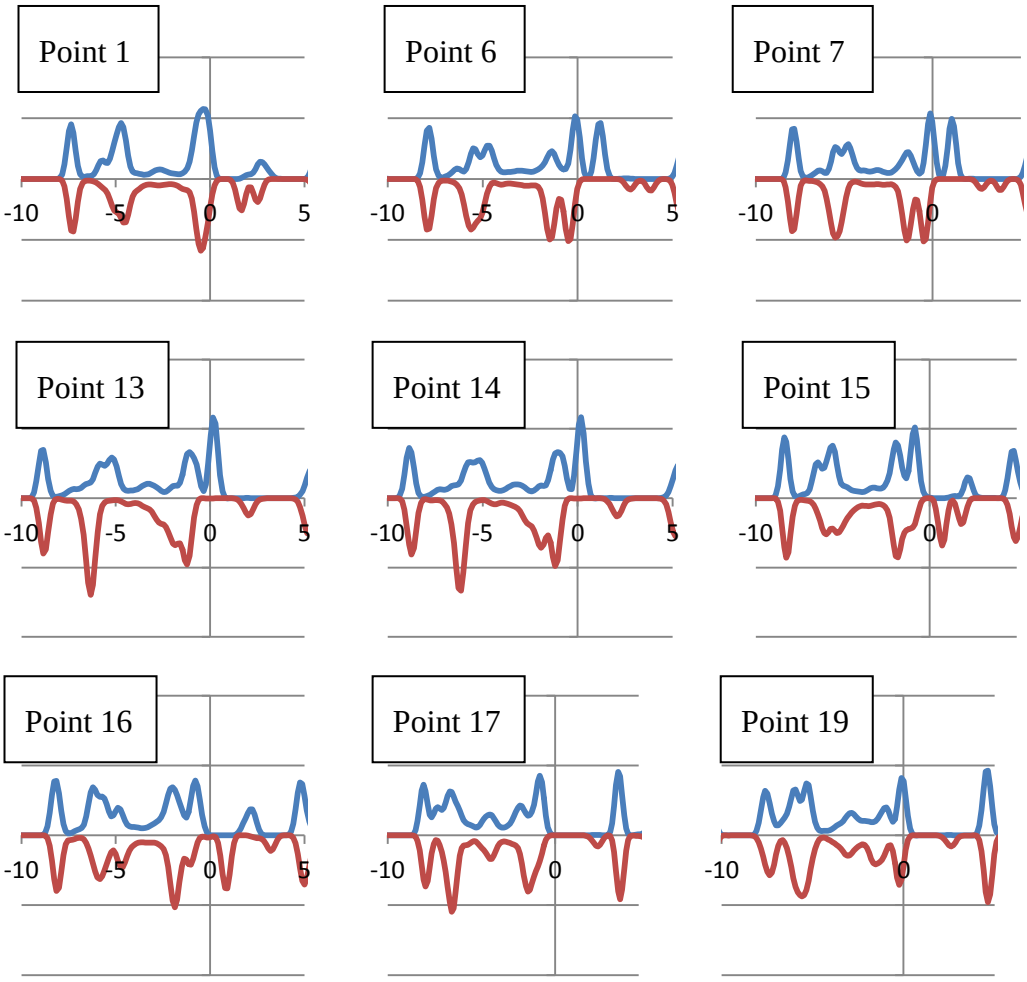

Figure 6.51. DOS of O centre s and p orbitals in Fe-O-OH on the O atom bound to the Fe centre, viewed over reaction co-ordinate of the reaction of between methane and the Fe-MFI active site to form methyl-hydroperoxide.

Figure 6.52. shows that the C centre s and p orbitals, the DOS plots are at key points along the co-ordinate. Point 1 is methane outside the active site and the plot shows very few states at the Fermi level. This however changes with an increase of states in the down spin direction through to Point 14, which is the high point on the barrier, and the cleavage of the C-H bond occurs at this point. The increase of states is shown in Points 6, 7 and 13. In Point 15 a spin inversion occurs at the Fermi level and again in Point 16 with the loss of the band gap between the HOMO and LUMO on this centre. In Point 17 the C-O bond is formed with the deactivation and loss of states at the Fermi level and the creation of a larger band gap. In Point 19 the states move towards the Fermi level but the band gap remains.

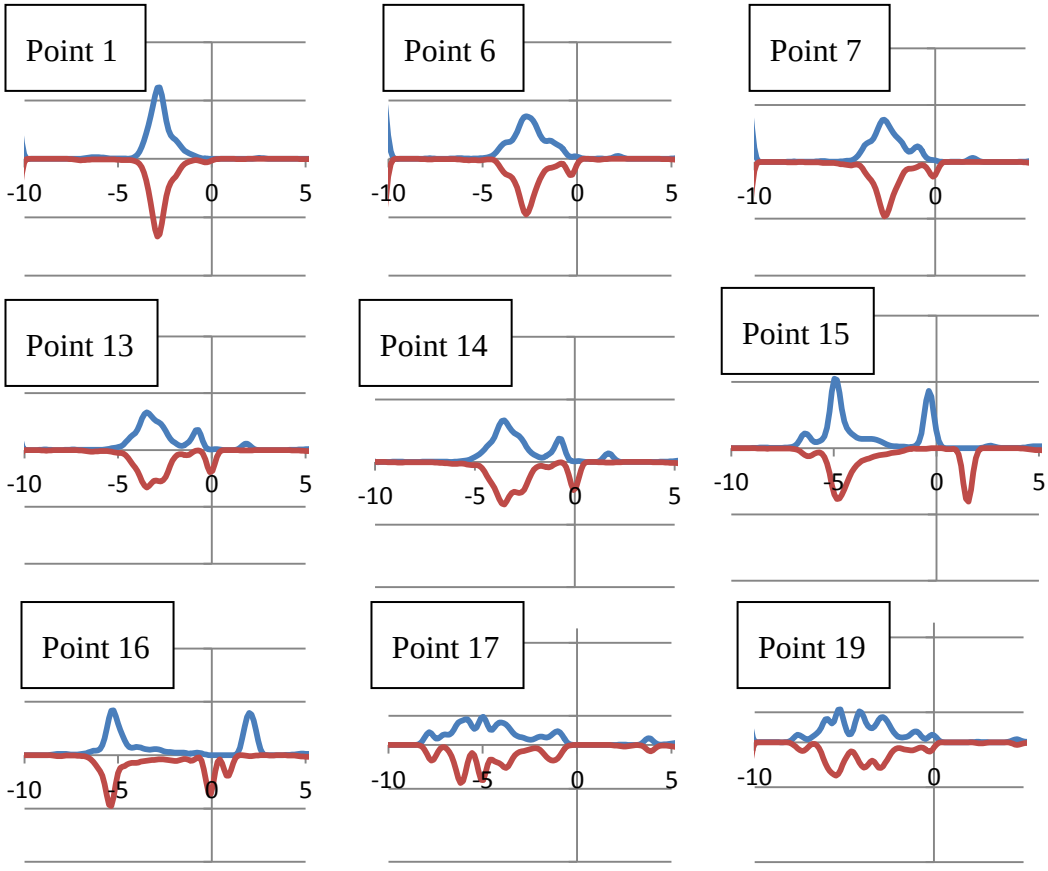

Figure 6.52. DOS of C centre s and p orbitals viewed over reaction co-ordinate of the reaction of between methane and the Fe-MFI active site to form methyl-hydroperoxide.

Mechanism

A catalytic cycle can be produced starting with the $Fe_2(OH)_4.2H_2O$ structure, which is shown in figure 6.53.

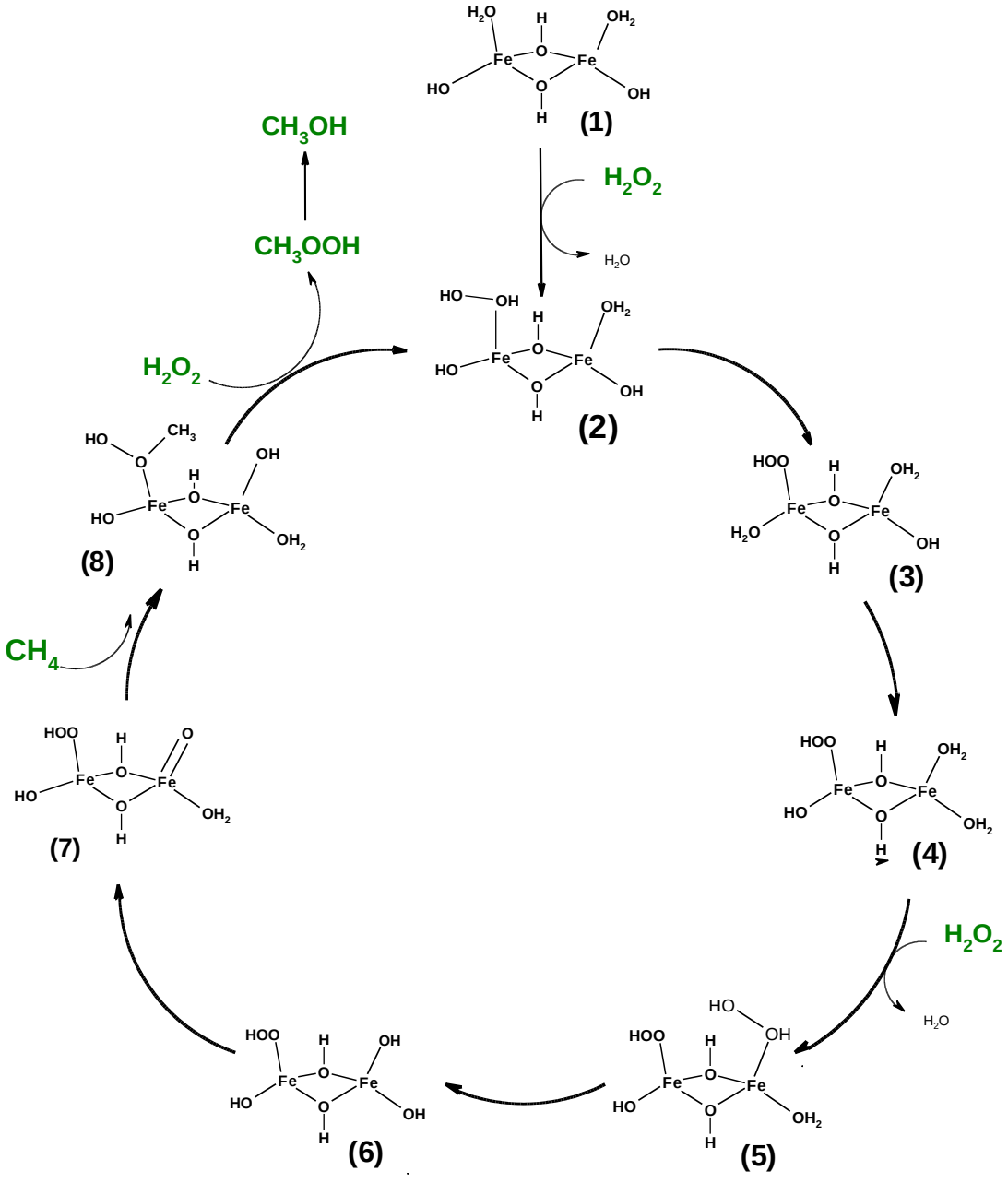

Figure 6.53. Catalytic cycle for CH_4 oxidation to CH_3OOH in Fe-ZSM-5.

This mechanism has two steps (between structures 1 and 2, and 4 and 5) with H_2O_2 replacing water which has been shown to be a favourable process. The mechanism shown keeps the hydrogen moving between ligands on the same Fe unless only a rearrangement is shown (between 2 and 3). There are a number of routes between 2

and 4 involving rapid transfers of hydrogen atoms. This mechanism proposes structure 7 as the active species with CH_4 interacting with it to directly produce CH_3OOH. Structures 1, 2 and 8 will favour the binding of H_2O_2 but H_2O is still more strongly binding than CH_3OOH so H_2O is likely to bind due to the excess of it in experimental conditions.

Conclusions

Fe_2O_2 has been found to be an active species within a CHA and MFI framework. When interacting with H_2O_2 it produces a number of different oxygen involving species including OOH, OH and Fe ═ O. These are possible due to the Fe ions having 2+, 3+ and 4+ formal charges and the interchange of charges between the two Fe ions, with the system appearing to show some delocalisation of the electrons. Most of the structures produced have favourable energies compared to the isolated molecules and Fe-zeolite. In the case of the MFI, the structures produced from $Fe_2(OH)_4.2H_2O$ are 130 kJ mol^{-1} different from this structure.

CHA and MFI appear to show different mechanisms for C – H bond breaking and C – O formation with the mechanism on CHA showing a pseudo-radical rebound mechanism. This is the formation of the CH_3 with the hydrogen atom transferring to the Fe_2O_2 but the CH_3 then moving to the OOH which is unlike a radical rebound mechanism which would move to the same oxygen than the hydrogen atom did. As the radical energy is 45 kJ mol^{-1} and the barrier 80 kJ mol^{-1} this is a possible mechanism. The radical rebound mechanism is shown not to occur as no radical is free of the $Fe_2(OH)_4.2H_2O$ and stable to rebound and form CH_3OH.

The magnetisation of different species in the barrier for the oxidation of methane has a large effect on the barrier with the spin state changing the barrier high by 40 kJ mol^{-1}. The C – O bond formation is spontaneous to form a shuttling radical species but agrees with experiment work[6] as this radical would be trapped as with enough energy to release the radical the C – O is far more likely to form. It also has to be noted that the only species to break the C – H is a highly oxidised Fe^{4+} ═ O with the Fe – OOH only acting as a receiving group for the methyl.

References

1. P.-P. H. J. . Knops-Gerrits and W. Goddard, *Catalysis Today*, 2003, **81**, 263–286.

2. B. J. Morgan and G. W. Watson, *Surface Science*, 2007, **601**, 5034–5041.

3. B. J. Morgan and G. W. Watson, *The Journal of Physical Chemistry C*, 2009, **113**, 7322–7328.

4. B. J. Morgan and G. W. Watson, *Journal of Physical Chemistry C*, 2010, **114**, 2321–2328.

5. A. Rohrbach, J. Hafner, and G. Kresse, *Phys. Rev. B*, 2004, **70**, 125426.

6. C. Hammond, M. M. Forde, M. H. Ab Rahim, A. Thetford, Q. He, R. L. Jenkins, N. Dimitratos, J. a Lopez-Sanchez, N. F. Dummer, D. M. Murphy, A. F. Carley, S. H. Taylor, D. J. Willock, E. E. Stangland, J. Kang, H. Hagen, C. J. Kiely, and G. J. Hutchings, *Angewandte Chemie (International ed. in English)*, 2012, **51**, 5129–33.

7. A. A. Battiston, J. H. Bitter, W. M. Heijboer, F. M. F. de Groot, and D. C. Koningsberger, *Journal of Catalysis*, 2003, **215**, 279–293.

8. A. A. Battiston, J. H. Bitter, and D. C. Koningsberger, *Journal of Catalysis*, 2003, **218**, 163–177.

7. Conclusions

The extended surfaces and Au_{10} clusters show the same mechanism with both the C – H bond breaking and C – O bond forming being important steps. The zeolites show a different mechanism with C – H bond breaking the more important step as C – O bond formation is a low energy step.

Au surfaces and Au_{10} clusters both break the HO – OH bond by electron donation to H_2O_2. The formation of OOH by hydrogen atom transfer from H_2O_2 on Au(111) and Pd(111) has a somewhat higher barrier but the presence of hydroxyl group reduces this, so the presence of hydroxyl groups may prove to be beneficial to the oxidation of CH_4.

The anatase TiO_2(001) and PdO(101) surfaces show a competition between the HO – OH breaking and HOO – H bond breaking, with the H – OOH bond breaking having the lower barrier in both cases, 7 kJ mol^{-1} for H – OOH and 12 kJ mol^{-1} for HO – OH on TiO_2(001) and 5 kJ mol^{-1} for H – OOH and 6 kJ mol^{-1} for HO – OH on Pd(101). However in both cases the breaking of the HO – OH requires two metal centres to co-ordinate with to break the bond whereas the H – OOH requires an oxygen and metal centre. Binding to the two metal centres is more favourable, with energies of 18 kJ mol^{-1} on the TiO_2(001) and 14 kJ mol^{-1} on the PdO(101), making the relative barriers lower for HO – OH bond breaking.

On the Fe_2O_2, HO – OH bond breaking does not occur directly. Instead, hydroxyl groups present are produced from water by transferring hydrogen atoms between other hydroxyl groups and oxygen atoms in the extra-framework Fe_2O_2. H_2O_2 decomposes by addition of a hydrogen atom to produce water and a hydroxyl group on the extra-framework Fe with the cleaving of the HO – OH or by transfer of a hydrogen atom in H_2O_2 to a nearby hydroxyl group to produce OOH and a water molecule. The direct cleavage of HO – OH would have to involve a free hydroxyl because the two Fe centres will not adsorb it in the same way as the oxide or metal surfaces.

With the mechanism on the Au(111), Pd(111) and PdO(101) surfaces, the C – O bond formation to make CH_3OOH can be considered the highest energy step. The

CH_3 forms a radical to bind to the OOH on both the Au(111) and Pd(111) surfaces, which explains why it is a high energy step.

In the CHA structure a radical methyl is formed directly from methane which is unfavourable compared to methane and the Fe_2O_2/Al-CHA, but can be considered a short lived intermediate as it can form CH_3OOH or CH_4 easily due to the low barriers. As this structure has none of the hydroxyl groups and the hydrogen atom from methane is transferred to an extra-framework oxygen atom it cannot be compared directly to the Fe_2O_2 on Al-MFI other than that the radical methyls are not as stable.

In the MFI structure, the C – H bond is broken by creating an active site with oxidisation of the Fe centre to a 4+ formal charge. With the lower oxidation state, C – H bond breaking has a high barrier to overcome and the radical methyl formed is highly unfavourable. The Fe ═ O is the species that does the C – H bond breaking and the Fe – OOH is a receiving group but both are required as the radical rebound mechanism does not work in this case. The methyl radical binds with the framework under geometry optimisation rather than existing as the radical in the MFI channel or binding spontaneously to the Fe – OH formed by the transfer of the hydrogen atom.